Imperial College London

Biomimetic Nanoscale Systems for pH-Triggered Intracellular Drug Delivery

Siyuan Chen

Thesis submitted in accordance with the requirements of

Imperial College London for the degree of

DOCTOR OF PHILOSOPHY

Department of Chemical Engineering

Imperial College London

April 2017

Declaration

This thesis is submitted for the degree of Doctor of Philosophy at Imperial College London. The research reported herein was carried out under the supervision of Dr Rongjun Chen between October 2013 and March 2017.

I can confirm that the research presented within this thesis was the result of my own work. Any results obtained in collaboration have been specifically indicated and acknowledged within the text. This thesis does not contain the material that has been previously accepted for the award of any qualification at Imperial College London or any other educational institutions.

This thesis contains 95 figures, 6 tables, and 46,369 words in length excluding the bibliography and appendix.

Parts of this work have been presented at national and international conferences, including 2nd International Conference on Nanomedicine (2016), 22nd CLSS-UK Annual Meeting (2016), 43rd Annual Meeting & Exposition of the Controlled Release Society (2016), Fundamentals and Applications of Lipid Membrane Biophysics (2015), 21st CLSS-UK Annual Meeting (2015), 42nd Annual Meeting & Exposition of the Controlled Release Society (2015), Imperial College Chemical Engineering PhD Symposium (2014 & 2015), 2D Materials and Interfaces (2015), 4th Annual Postgraduate Symposium on Nanotechnology (2014), 21st CSCST Annual Conference (2014) and Imperial College Graduate School Symposium (2014).

Parts of this work have been and will be published in the following journals and patent:

Siyuan Chen, Shiqi Wang, Michal Kopytynski, Marie Bachelet, Rongjun Chen*, Membrane Anchoring, Comb-Like Pseudopeptides for Efficient, pH-Mediated Membrane Destabilization and Intracellular Delivery. *ACS Applied Materials & Interfaces*, 2017; 9 (9), 8021–8029.

Siyuan Chen, Rongjun Chen*, A Virus-Mimicking, Endosomolytic Liposomal System for Efficient, pH-Triggered Intracellular Drug Delivery, *ACS Applied Materials & Interfaces*, 2016; 8 (34), 22457–22467.

Rongjun Chen, Siyuan Chen, Liwei Wu, Modified Peptide, *UK patent*, No. GB1612150.1, 2016/07/13, filed.

Siyuan Chen, Rongjun Chen*, Development of A Multifunctional Liposomal Delivery Platform with Membrane Anchored Pseudopeptides for Enhanced Intracellular Delivery and to Overcome Multidrug Resistance, in preparation.

Siyuan Chen, Michal Kopytynski, Rongjun Chen*, Comb-Like Pseudopeptidic Polymer-Mediated pH-Triggered Rapid Intracellular Delivery of Cargos from a Wide Size Range, in preparation.

Siyuan Chen

April 2017

The copyright of this thesis rests with the author and is made available under a Creative Commons Attribution Non-Commercial No Derivatives license. Researchers are free to copy, distribute or transmit the thesis on the condition that they attribute it, that they do not use it for commercial purposes and that they do not alter, transform or build upon it. For any reuse or redistribution, researchers must make clear to others the license terms of this work.

To my beloved family

Acknowledgements

First I would like to sincerely thank my supervisor Dr Rongjun Chen. I appreciate him very much for providing me an opportunity to join his group as a PhD student. I sincerely thank his kind guidance and support, which is of crucial importance for me not only to complete my PhD study but also enjoy doing research.

I wish to gratefully appreciate my lovely colleagues, Marie Bachelet, Shiqi Wang, Michal Kopytynski, Kira Watkins, Liwei Wu, Ruijiao Dong, Deborah Roebuck and Anna Sofia Tascini. Thanks a lot for their kind assistance and helpful discussion. I have learnt a lot from them.

I would like to acknowledge the Chemical Engineering Department at Imperial College London for the generous financial support in the past three and a half years. The precious PhD Scholarship enabled me to pursue my research at Imperial. I also own my appreciation to Imperial College Trust, United Kingdom & Ireland Controlled Release Society, the Old Centralians' Trust and Santander for providing travel funding to support me attending a number of international conferences.

I would also like to thank Patricia Carry, Stephen Rothery, David Gaboriau, Jane Srivastava and Jess Rowley for equipment training and help.

I appreciate Cher Hui Goey, Ju Zhu, Miao Guo, Zhixuan Wang and all other friends for their support along the way to help me go through my low periods.

I wish to express my gratitude to Dr Richard Rooke and Ms Julia Rooke. They not just offered me a home in London but treated me like their family. I would like to thank Nansenvillage to provide a pleasant environment and community for international students.

Finally, I would like to say a heartfelt thank you to my dearest family. I appreciate my parents a lot for their constant love and forever understanding in the past and the future. I thank my husband Dr Qi Wu who has been continuously inciting me to strive towards my goals.

My journey toward a PhD would not have been possible without the support from all those who have helped me. Words cannot express how truly grateful I am. Thank you all.

Abstract

Efficient intracellular delivery remains a major challenge for non-viral delivery systems. Insufficient endosomal escape leads to enzymatic degradation of bioactive compounds in lysosomes. This thesis presents the work involving the development of a series of biomimetic nanoscale systems for pH-triggered intracellular drug delivery.

A novel multifunctional liposomal delivery platform has been developed to resemble the structural and functional traits of an influenza virus via surface modification of cholesterol-containing liposomes with L-phenylalanine grafted poly(L-lysine isophthalamide) (PLP). Desirable pH-triggered liposomal release behavior was achieved by controlling key parameters. The pH-triggered, reversible liposomal size change was observed and the release mechanism was elucidated. The endosomal-escape ability, intracellular delivery efficiency and cytotoxicity of this system loaded with an anticancer drug, doxorubicin (DOX), were further evaluated and compared to conventional liposomes and free drugs.

A library of novel, pH-responsive, comb-like polymers were synthesized by grafting PLP with different lengthed alkyl chains which act as membrane anchors. The effects of the hydrophobic alkyl side chains on pH-responsive aqueous solution properties, cell membrane destabilization activity and in vitro cytotoxicity were investigated. The optimal polymer was almost non-hemolytic at pH 7.4, but induced nearly complete destabilization of red blood cell membrane at endosomal pH. The mechanism of membrane destabilization was investigated.

The optimal comb-like pseudopeptidic polymer displayed a superior endosomal-escape ability to release endocytosed materials into the cytoplasm of various cell lines compared to its parent polymer PLP. When the extracellular environment was mildly acidic, the intracellular delivery was considerably enhanced. The effect of side chain length, polymer concentration, treatment time, extracellular pH, serum and payload size on the delivery efficiency were systemically investigated. A variety of cell types, including stem cells and multidrug resistant cell line, were employed to explore its wide applicability in drug delivery.

The optimal membrane-anchoring, comb-like polymer was further employed to develop a novel multifunctional liposomal delivery platform. The pH-responsive hybrid liposomes were characterized and their pH-dependent drug release profiles were examined. The intracellular delivery of DOX-loaded multifunctional liposomes and their cytotoxic effects toward four different cancer cell lines were evaluated.

Table of Contents

List of Figures ..... **I**

List of Tables ..... **VIII**

List of Abbreviations ..... **IX**

Chapter 1. Introduction **1**

1.1 Drug delivery systems 1

1.1.1 Drawbacks of conventional drugs 1

1.1.2 Drug delivery systems for controlled release 2

1.2 Challenges and strategies for non-viral delivery systems to achieve efficient intracellular delivery 11

1.2.1 Intracellular barriers 11

1.2.2 Endosomal escape 15

1.3 pH-Responsive endosomolytic polymers 16

1.3.1 Polycations 17

1.3.2 Polyanions 18

1.4 Multifunctional Liposomes 24

1.4.1 Stealth liposomes 24

1.4.2 Targeting liposomes 25

1.4.3 Stimuli-responsive liposomes 25

1.5 Aims and objectives of the project 29

1.6 Novelties and impact of the research 30

1.7 Thesis outline 32

Chapter 2. Materials and methods **35**

2.1 Materials 35

2.2 Methods 36

2.2.1 Polymer synthesis 36

2.2.2 Polymer characterization 39

2.2.3 Liposomes preparation, polymer modification and characterization 41

2.2.4 Cell study 45

Chapter 3. Development of multifunctional liposomes coated with PP75 ..... **51**

3.1 Introduction 51

3.2 Results and discussion 53

3.2.1 Polymer synthesis and structure characterization 53
3.2.2 Hemolysis of PP75 55
3.2.3 Preparation of bare liposomes 56
3.2.4 Development of virus-mimicking liposomes with Phe grafted PLP 58
3.3 Conclusions 77

Chapter 4. pH-Responsive, membrane-anchoring pseudopeptides containing alkyl side chains 79
4.1 Introduction 79
4.2 Results and discussion 81
4.2.1 Structure characterization 81
4.2.2 pH-Mediated phase separation 83
4.2.3 Fluorescence characterization using pyrene as a probe 84
4.2.4 Hydrodynamic size 86
4.2.5 Membrane destabilization activity 89
4.2.6 Concentration-dependent hemolysis 92
4.2.7 Time-dependent hemolysis 93
4.2.8 Mechanism of cell membrane destabilization 94
4.3 Conclusions 99

Chapter 5. Application of the membrane-anchoring, comb-like pseudopeptides for intracellular delivery 100
5.1 Introduction 100
5.2 Results and discussion 102
5.2.1 Intracellular delivery at pH 7.4 102
5.2.2 In vitro cytotoxicity at pH 7.4 104
5.2.3 Intracellular delivery at acidic conditions 107
5.2.4 In vitro cytotoxicity 125
5.3 Conclusions 126

Chapter 6. Multifunctional liposomes coated with the membrane-anchoring, comb-like polymers 128
6.1 Introduction 128
6.2 Results and discussion 131
6.2.1. Effect of cholesterol proportion in the liposomal membrane 131
6.3.2 Effect of NDA grafting degree 132
6.2.3 Effect of polymer concentration 134

6.2.4 Dilution effect 136
6.2.5. pH-Triggered liposomal size change 137
6.2.6 Mechanism of inter-vesicular interaction 138
6.2.7 Hemolysis assay 140
6.2.8 Cellular uptake 141
6.2.9 Intracellular delivery 143
6.2.10 In vitro cytotoxicity of the liposomal carrier 146
6.2.11 In vitro cytotoxicity of the DOX-loaded liposomes 148
6.3 Conclusions 150

Chapter 7. Conclusions and future work 152

7.1 Conclusions 152
7.1.1 Virus-mimicking liposomes coated with PP75 bearing hydrophobic amino acids 153
7.1.2 pH-Responsive pseudopeptidic polymers bearing hydrophobic relatively long alkyl side chains as membrane anchors 153
7.1.3 Efficient intracellular delivery of a wide size range of payload into a wide range of cell types using the pH-responsive, comb-like pseudopeptidic polymer 154
7.1.4 Virus-mimicking liposomes coated with pH-responsive, comb-like, membrane-anchoring pseudopeptides containing relatively long hydrophobic alkyl side chains 155
7.2 Future work 155
7.2.1 Investigation of the mechanism of polymer-mediated intracellular delivery at acidic extracellular pH 155
7.2.2 Subcellular fate and biodegradability 156
7.2.3 Further modification of polymer structure 156
7.2.4 Intracellular delivery of genetic therapeutic agents 157
7.2.5 Co-delivery mediated by the virus-mimicking liposomes 158
7.3 Closing remarks 158

References 160

Appendix 190

List of Figures

Figure 1-1. Ringsdorf model of a polymer-drug conjugate, containing a soluble polymer backbone, a biodegradable linker and a covalently linked drug……..……....4

Figure 1-2. Polymeric micelles are formed by amphiphilic block copolymers…….…....5

Figure 1-3. (A) Solid lipid nanoparticles and (B) nanostructured lipid carriers…….…...7

Figure 1-4. Schematic of a liposome which presents a bilayer structure…….……....8

Figure 1-5. Liposome-cell interaction……...…….10

Figure 1-6. Extracellular uptake by endocytosis in a typical eukaryotic cell…….…….14

Figure 1-7. Different types of endosomal escape……..……..……...16

Figure 1-8. Schematic illustration of the "proton-sponge" effect hypothesis…….....18

Figure 1-9. Schematic illustration of coil-to-globule conformational change of polyanions using poly(acrylic acid) as an example……...……..….20

Figure 1-10. The unit structures of (A) PMAA, (B) PEAA, (C) PPAA and (D) PBAA..……....21

Figure 1-11. The unit structures of PLP and PP75…….24

Figure 1-12. Destabilization of the endosomal membrane…….26

Figure 1-13. Schematic of the liposomes prepared by using the (A) pre-insertion method and the (B) post-insertion method…….……..…....28

Figure 1-14. Scheme of the thesis outline, summarizing the research gap, aim and novelty for each sub-project……..34

Figure 2-1 Schematic of PLP synthesis…….....37

Figure 2-2. Schematic of PLP grafted with L-phenylalanine synthesis……..38

Figure 3-1. Schematic of the virus-mimicking, endosomolytic liposome and its endosomal escape……53

Figure 3-2. FT-IR spectra of PLP, PP25, PP50 and PP75 in their acid forms……54

Figure 3-3. ^{1}H-NMR spectra of PLP, PP25, PP50 and PP75 in their acid forms in d_6-DMSO at room temperature…….....55

Figure 3-4. pH-Dependent relative hemolysis of PP75 at 1 (■), 0.5 (●), 0.1 (▲), 0.05 (▼) and 0.025 (◆) mg mL^{-1} …….…….56

Figure 3-5. Effect of different sonication modes on sample temperature……...57

Figure 3-6. Effect of sonication time on liposomal size……..……..57

Figure 3-7. Effect of cholesterol proportion on the calcein release from the virus-mimicking liposomes……..…….....59

Figure 3-8. Schematic of the polymer-liposome interaction in the (A) absence and (B) presence of cholesterol……..…….....60

Figure 3-9. pH-Dependent calcein release from the bare liposomes (◆), and the virus-mimicking liposomes coated with PLP (▼), PP25 (▲), PP50 (●), and PP75 (■) respectively……...……...61

Figure 3-10. Effect of PP75 adsorbed on the liposomal membrane……..63

Figure 3-11. Effect of modification time on the concentration of PP75 adsorbed on the virus-mimicking liposomes……64

Figure 3-12. Effect of modification time on the pH-dependent calcein release from the virus-mimicking liposomes modified with PP75 for overnight (●) or 5 min (■)……...64

Figure 3-13. Size distributions of (A) the bare liposomes and (B) the PP75-coated, virus-mimicking liposomes……65

Figure 3-14. (A) pH-Dependent hydrodynamic size change of the bare liposomes (Bare-LP), PLP-coated liposomes (PLP-LP), PP25-coated liposomes (PP25-LP), PP50-coated liposomes (PP50-LP) and PP75-coated liposomes (PP75-LP). (B) Reversible size change of the PP75-coated liposomes between pH 7.4 and 4.5, imaged by confocal microscopy and measured by DLS…….……..66

Figure 3-15. Lipid mixing assay of the bare liposomes and PP75-coated liposomes at pH 7.4 and 4.5 through the detection of NBD-Rh FRET…….……...67

Figure 3-16. Schematic representation of the mechanism of the revisable size change between pH 7.4 and 4.5 for the PP75-coated, virus-mimicking liposomes…….……....68

Figure 3-17. Relative hemolysis of the PP75-coated, virus-mimicking liposomes with a fixed polymer-to-lipid molar ratio at 1.9:100……..……70

Figure 3-18. Laser scanning confocal microscopy images of HeLa cells demonstrating the escape of the endocytosed free calcein from intracellular vesicles into the cytoplasm facilitated by (A) the bare liposomes and (B) the PP75-coated, virus-mimicking liposomes…….……71

Figure 3-19. Laser scanning confocal microscopy images of HeLa cells showing the subcellular localization of the anticancer drug DOX……..……...72

Figure 3-20. Cellular uptake of DOX was quantitatively analyzed by flow cytometry and presented as relative MFI (A) and representative histogram plots (B)…….……73

Figure 3-21. Confocal microscopy image shows subcellular localization of rhodamine B (red channel) labelled liposomes……..…..74

Figure 3-22. (A) MFI and (B) the representative histogram plots of the HeLa cell treated with the bare liposomes (Bare-LP) and the PP75-coated liposomes (PP75-LP)……..…..74

Figure 3-23. Relative viability of HeLa cells treated with the liposomes with (close columns) or without (open columns) PP75 coating at various lipid concentrations for 24 h, as determined by (A) Alamar Blue assay and (B) LDH assay…….……76

Figure 3-24. In vitro cytotoxicity of free DOX (open columns), DOX-loaded bare liposomes (gray columns), and DOX-loaded virus-mimicking liposomes (dark columns) toward HeLa cells after treatment for 24 h and further incubated for 24 h……..77

Figure 4-1. FT-IR spectra of PLP, PLP-HDA 18%, PLP-NDA 18%, PLP-TDA 18% and PLP-ODA 18% in their acid forms……...82

Figure 4-2. ^{1}H-NMR spectra of PLP, PLP-HDA 18%, PLP-NDA 18%, PLP-TDA 18% and PLP-ODA 18% in their acid forms in d_6-DMSO at room temperature……....82

Figure 4-3. pH-Dependent transmittance of the aqueous solutions of (A) PLP, (B) PLP-NDA 3%, (C) PLP-NDA 10% and (D) PLP-NDA 18% at 1.0 mg mL^{-1} in 100 mM phosphate or citrate buffer……83

Figure 4-4. pH-Dependent I_{338}/I_{333} in the excitation spectra of pyrene dissolved in aqueous solutions of PLP (■), PLP-NDA 3% (●), PLP-NDA 10% (▲) and PLP-NDA 18% (▼) at 0.5 mg mL^{-1}…….……85

Figure 4-5. Concentration-dependent I_{338}/I_{333} in the excitation spectra of pyrene dissolved in aqueous solutions of PLP (■), PLP-NDA 3% (●), PLP-NDA 10% (▲) and PLP-NDA 18% (▼) at pH 7.4……..……..86

Figure 4-6. Particle size distributions of PLP, PLP-NDA 3%, PLP-NDA 10% and PLP-NDA 18% at the concentration of 0.5 mg mL^{-1} at pH 7.4……...…….87

Figure 4-7. Particle size distributions of PLP (A) and PLP-NDA 18% (B) at a concentration of 0.5 mg mL^{-1} at pH 7.4 (solid) and pH 5.5 (dash)……..…….……88

Figure 4-8. Particle size distributions of PLP-NDA 18% at different polymer concentrations at pH 7.4……...……...89

Figure 4-9. Relative hemolysis of RBCs incubated with PLP (■), PLP-HDA 18% (◆), PLP-NDA 18% (▲), PLP-TDA 18% (▼) and PLP-ODA 18% (●) at 0.5 mg mL^{-1}for 1h……91

Figure 4-10. pH-Dependent hemolysis of RBCs incubated with PLP (■), PLP-NDA 3% (●), PLP-NDA 10% (▲) and PLP-NDA 18% (▼) at 0.5 mg mL^{-1} for 1h……....92

Figure 4-11. Concentration-dependent hemolysis of RBCs incubated with PLP-NDA 18% (A) and PLP (B) at pH 7.4 (open columns) and 5.5 (close columns)……...93

Figure 4-12. Time-dependent hemolysis of RBC incubated with PLP (■), PLP-NDA 3% (●), PLP-NDA 10% (▲), PLP-NDA 18% (▼) at 0.5 mg mL^{-1} at pH 5.5…....……..94

Figure 4-13. Relative hemolysis of RBCs incubated with 0.5 mg mL^{-1} PLP-NDA 18% with or without the presence of 10 mM sucrose or 10 mM PEG with different molecular weights at pH 5.5 for 1 h…….....95

Figure 4-14. Confocal microscopy images of RBCs incubated with FITC-dextran (4 kDa) and Texas Red® with or without polymers (0.5 mg mL^{-1}) for 30 min at pH 5.5…….96

Figure 4-15. Confocal microscopy images of RBCs incubated with FITC-dextran (4 kDa) and Texas Red® with or without polymers (0.5 mg mL^{-1}) for 30 min at pH 7.4…….97

Figure 4-16. Confocal microscopy images of RBCs incubated with Texas Red® and different molecular weight of FITC-dextran with the presence of 0.5 mg mL^{-1} PLP-NDA 18% for 30 min at pH 5.5…….98

Figure 5-1. Confocal microscopy images of Hela (A), A549 (B) and CHO (C) cells showing the subcellular distribution of calcein fluorescence……...…...……...103

Figure 5-2. Confocal microscopy images of Hela (A), A549 (B) and CHO (C) cells showing the subcellular distribution of calcein fluorescence……..……...104

Figure 5-3. Viabilities of HeLa cells incubated with PLP (open columns) and PLP-NDA 18% (close columns) at various concentrations for 4 h (A), 12 h (B), 24 h (C) and 48 h (D), as determined by Alamar Blue assay……...……..105

Figure 5-4. Viabilities of CHO cells incubated with PLP (open columns) and PLP-NDA 18% (close columns) at various concentrations for 4 h (A), 12 h (B), 24 h (C) and 48 h (D), as measured by Alamar Blue assay……106

Figure 5-5. Viabilities of A549 cells incubated with PLP (open columns) and PLP-NDA 18% (close columns) at various concentrations for 4 h (A), 12 h (B), 24 h (C) and 48 h (D), as measured by Alamar Blue assay……..……..……106

Figure 5-6. (A) Confocal microscopy images and (B) MFI of the polymer-mediated delivery analyzed by flow cytometry. HeLa cells were incubated with 200 μM FITC-dextran (4 kDa) and the comb-like polymer containing alkyl chains with different lengths at pH 6.5 for 30 min...108

Figure 5-7. Confocal microscopy images of HeLa cells treated with PLP-NDA 18% at various concentrations and 200 μM FITC-dextran (4 kDa) at pH 6.5 for 30 min..109

Figure 5-8. Relative MFI of HeLa cells treated with 200 μM FITC-dextran (4 kDa) in the absence (control) or presence of PLP-NDA 18% at various concentration at pH 6.5 for 30 min..110

Figure 5-9. Confocal microscopy images of pH-dependent polymer-mediated intracellular delivery..111

Figure 5-10. (A) Relative MFI and (B) representative histogram plots of the polymer-mediated delivery of 200 μM FITC-dextran (4 kDa) at different extracellular pHs analyzed by flow cytometry...113

Figure 5-11. Confocal microscopy images of polymer-mediated delivery kinetics.....114

Figure 5-12. Relative MFI of polymer-mediated delivery kinetics analyzed by flow cytometry..115

Figure 5-13. Confocal microscopy images of polymer-mediated intracellular delivery of different sized FITC-dextran at acidic external pH.....117

Figure 5-14. Confocal microscopy images of HeLa cells co-incubated with different sized FITC-dextran alone at pH 6.5 for 30 min.....118

Figure 5-15. Confocal microscopy images of polymer-mediated intracellular delivery of different sized FITC-dextran at physiological pH..119

Figure 5-16. Confocal microscopy images of polymer-mediated intracellular delivery with or without the presence of serum..120

Figure 5-17. Confocal microscopy images of polymer-mediated delivery of FITC-dextran (4 kDa) into difference cell types.....122

Figure 5-18. (A) Relative MFI and (B) representative histogram plots showing the polymer-mediated delivery of FITC-dextran into difference cell types..124

Figure 5-19. In vitro cytotoxicity of PLP-NDA 18%.....126

Figure 6-1. Calcein leakage from the liposomes containing different proportions of cholesterol during surface functionalization with 10 mg mL^{-1} various PLP-NDA polymers for overnight at pH 7.4……132

Figure 6-2. pH-Dependent calcein release from the virus-mimicking liposomes coated with PLP (■), PLP-NDA 3% (●), PLP-NDA 10% (▲), and PLP-NDA 18% (▼) respectively……134

Figure 6-3. pH-Dependent calcein release from the cholesterol (40 mol%)-containing liposomes treated with PLP-NDA 18% at 10 mg mL^{-1} (■), 1 mg mL^{-1} (●) and 0.1 mg mL^{-1} (▲) followed by the removal of unadsorbed polymer……135

Figure 6-4. Calcein release from the PLP-NDA 18%-coated liposomes (with a fixed polymer-to-lipid molar ratio at 2.85:100 upon 5-, 10-, 50- and 100-fold dilution) at pH 4.5……..137

Figure 6-5. Size distributions of (A) the bare liposomes and (B) the PLP-NDA 18%-coated liposomes……...138

Figure 6-6 The mean hydrodynamic size of the bare liposomes (Bare-LP), PLP-coated liposomes (PLP-LP), PLP-NDA 3%-coated liposomes (PLP-NDA 3%-LP), PLP-NDA 10%-coated liposomes (PLP-NDA 10%-LP) and PLP-NDA 18%-coated liposomes (PLP-NDA 18%-LP) at different pHs…….…….…….138

Figure 6-7. Lipid mixing assay of the bare and PLP-NDA 18%-coated liposomes at pH 7.4 and 4.5……139

Figure 6-8. Reversible size change of the PLP-NDA 18%-coated liposomes, as measured by DLS……...140

Figure 6-9. pH-Dependent relative hemolysis of the bare liposomes (■), PLP-coated liposomes (●) and PLP-NDA 18%-coated liposomes (▲)……..……141

Figure 6-10. (A) Confocal microscopy images of HeLa cells showing the subcellular localization of the bare liposomes (B-LP) and the PLP-NDA 18%-coated liposomes (PLP-NDA 18%-LP) labeled with 1 mol% Rh-PE. Cellular uptake of the fluorescent liposomes was further analyzed by flow cytometry and presented as (B) relative MFI and (C) representative histogram plots…….…….…….143

Figure 6-11. (A) Confocal microscopy images, (B) MFI and (C) representative histogram plots showing the subcellular distribution and cellular uptake of free DOX, DOX-loaded bare liposomes, and DOX-loaded, PLP-NDA 18%-coated liposomes in HeLa cells……144

Figure 6-12. (A) Confocal microscopy images, (B) MFI and (C) representative histogram plots showing the subcellular distribution and cellular uptake of free DOX, DOX-loaded bare liposomes, and DOX-loaded, PLP-NDA 18%-coated liposomes in A549 cells……145

Figure 6-13. (A) Confocal microscopy images, (B) MFI and (C) representative histogram plots showing the subcellular distribution and cellular uptake of free DOX, DOX-loaded bare liposomes, and DOX-loaded, PLP-NDA 18%-coated liposomes in MES-SA cells…….……...145

Figure 6-14. (A) Confocal microscopy images, (B) MFI and (C) representative histogram plots showing the subcellular distribution and cellular uptake of free DOX, DOX-loaded bare liposomes, and DOX-loaded, PLP-NDA 18%-coated liposomes in MES-SA/DX5 cells……...……..146

Figure 6-15. Concentration-dependent relative viabilities of HeLa cells treated with the liposomes with (close columns) or without (open columns) PLP-NDA 18% for (A) 24 h and (B) 48 h as determined by Alamar Blue assay……...……147

Figure 6-16. Concentration-dependent relative viabilities of A549 cells treated with the liposomes with (close columns) or without (open columns) PLP-NDA 18% for (A) 24 h and (B) 48 h as determined by Alamar Blue assay……..……147

Figure 6-17. Concentration-dependent relative viabilities of MES-SA cells treated with the liposomes with (close columns) or without (open columns) PLP-NDA 18% for (A) 24 h and (B) 48 h as determined by Alamar Blue assay……..…...……148

Figure 6-18. Concentration-dependent relative viabilities of MES-SA/DX5 cells treated with the liposomes with (close columns) or without (open columns) PLP-NDA 18% for (A) 24 h and (B) 48 h as determined by Alamar Blue assay……...……...……148

Figure 6-19. Potency of free DOX (open columns), DOX-loaded bare liposomes (gray columns), and DOX-loaded, PLP-NDA 18%-coated liposomes (dark columns) against (A) HeLa, (B) A549, (C) MES-SA and (D) MES-SA/DX5 cells after 24 h of treatment and 24 h of further incubation……...…….150

Figure 7-1. Summary of the major achievements arising from this project and recommended future work…….……...159

List of Tables

Table 1-1. Comparison of different liposomal preparation methods……...9

Table 1-2. Marketed liposomal and lipid-based anticancer products, plus a selection of products in clinical development…….12

Table 3-1. Mean hydrodynamic diameters of the liposomes before and after surface modification with PP75……60

Table 4-1. pH Values at the onset of precipitation (pH_p), pH values at the onset of hydrophobic association (pH_h), and pH ranges for hydrophobic association of PLP and the comb-like polymers at 0.5 mg mL^{-1} and their CACs at pH 7.4…...86

Table 4-2. The mean hydrodynamic diameters of PLP and its derivatives at a concentration of 0.5 mg mL^{-1} at pH 7.4……..87

Table 4-3. The mean hydrodynamic diameters of PLP-NDA 18% with various concentrations at pH 7.4…….……...89

List of Abbreviations

C

CAC	Critical association concentration
CHEMS	Cholesteryl hemisuccinate
CIE	Clathrin-independent endocytosis
CME	Clathrin-mediated endocytosis
CPP	Cell-penetrating peptide

D

DCC	*N*,*N'*-dicyclohexylcarbodiimide
DC-Chol	3β-[*N*-(*N*',*N*'-dimethylaminoethane)-carbamoyl] cholesterol
DDS	Drug delivery system
DLS	Dynamic light scattering
DMAP	4-dimethylaminopyridine
DMEM	Dulbecco's modified Eagle's medium
DMF	*N,N*-dimethylformamide
DMPC	1,2-dimyristoyl-sn-glycero-3-phosphocholine
DMSO	Dimethyl sulfoxide
DOPC	1,2-dioleoyl-sn-glycero-3-phosphocholine
DOPE	1,2-dioleoyl-sn-3-phosphatidylethanolamine
DOX	Doxorubicin
DSPC	1,2-distearoyl-sn-glycero-3-phosphocholine
DOTAP	1,2-dioleoyl-3-trimethylammonium-propane
DOTMA	1,2-di-o-octadecenyl-3-trimethylammonium propane
D-PBS	Dulbecco’s phosphate buffered saline
DPPC	1,2-dipalmitoyl-sn-glycero-3-phosphocholine

E

EPC	L-α-phosphatidylcholine from soy bean or egg yolk
EPR	Enhanced permeability and retention

F

FBS	Fetal bovine serum
FITC-dextran	Fluorescein isothiocyanate–dextran
FRET	Fluorescence resonance energy transfer
FT-IR	Fourier Transform Infrared

G

GPI	Glycosyl phosphatidyl inositol
GUVs	Giant unilamellar vesicles

H

HA	Haemagglutinin
HA2	Subunit of haemagglutinin of the influenza virus
HDA	Heptylamine
HEPES	*N*-(2-hydroxyethyl) piperazine-*N'*-(2-ethanesulfonic acid)
hMSC	Mesenchymal stem cells
HPMA	Poly *N*-(2-hydroxypropyl) methacrylamide

I

IC_{50}	Half inhibition concentration
INT	Tetrazolium salt

L

LDH	Lactate dehydrogenase
LUVs	Large unilamellar vesicles
L2 peptide	C terminus of the capsid protein of Papillomavirus

M

MβCD	Methyl-β-cyclodextrin
MDR	Multidrug resistance
MFI	Mean fluorescence intensity
MLVs	Multilamellar vesicles
MoMLV	Moloney Murine Leukemia Virus
MRP	Multidrug resistance protein

MVB	Multivesicular bodies
MVL	Multivesicular liposomes

N

NBD-PE	*N*-(7-nitrobenz-2-oxa-1,3-diazol-4-yl)-1,2-dihexadecanoyl-*sn*-glycero-3-phosphoethanolamine
NDA	Decylamine
NIPAM	*N*-isopropylacrylamide
NLCs	Nanostructured lipid carriers
NMR	Nuclear magnetic resonance

O

ODA	Octadecylamine

P

PAA	Poly(aspartic acid)
PBAA	Poly(butylacrylic acid)
PC	Phosphatidylcholine
PCI	Photochemical internalization
PDMAEMA	P oly(2-(dimethylamino)ethyl methacrylate)
PE	Phosphatidylethanolamine
PEAA	Poly(α-ethylacrylic acid)
PEG	Polyethylene glycol
PEI	Poly(ethylene imine)
Pgp	P-glycoprotein
pH_p	pH value at the onset of precipitation
pH_h	pH at the onset of hydrophobic association
Phe	Phenylalanine
PGA	Poly(glutamic acid)
PLL	Poly(L-lysine)
PLP	Poly(L-lysine isophthalamide)
PMAA	Poly(α-methylacrylic acid)
PPAA	Poly(propylacrylic acid)

PP75	PLP side chain grafted with L-phenylalanine at a stoichiometric ratio of 75%
PS	Phosphatidylserine

R

RES	Reticulo-endothelial system
RBC	Red blood cell
Rh	Rhodamine
Rh-PE	Lissamine™ rhodamine B 1,2-dihexadecanoyl-*sn*-glycero-3-phosphoethanolamine

S

SLNs	Solid lipid nanoparticles
SUVs	Small unilamellar vesicles

T

TAT	HIV-1 Trans-activator gene product
TDA	Tetradecylamine
Topo II	Topisomerase II

Chapter 1

Introduction

This chapter presents an introduction to the basic concepts, advances and current status of polymer- and lipid-based drug delivery systems, with a particular focus on pH-responsive polymers and liposomes. The drawbacks of conventional chemotherapy, the barriers to intracellular delivery and the limitations of viral vectors are described. The relevant work on pH-responsive polymers and liposomes, in particular synthetic polyanions and polymer-modified liposomes, for drug delivery is then summarized. The project objectives, originality and thesis outline are included in the latter part of this chapter to give a general idea of the research included in the thesis.

1.1 Drug delivery systems

1.1.1 Drawbacks of conventional drugs

Cancer is one of the most devastating diseases in the world. The outcome for cancer treatment remains unsatisfactory as 8.8 million people died of cancer in 2015 according to the statistic from the World Health Organization (WHO). Therefore, efficient cancer therapy is in an urgent need. Cancer treatment strategies include surgery, chemotherapy, radiotherapy, hormone therapy, gene therapy and so on, among which chemotherapy is most commonly used (Shi et al., 2017). Chemotherapeutic drugs are traditionally administered in the form of free drug solutions or tablets. However, they have many issues as described below and their clinical outcomes are usually below expectation.

The specificity of free cytotoxic drug solutions is usually poor (Liboiron & Mayer, 2014). Administered cytotoxic agents, especially macromolecules, often bind to body tissues and serum protein leading to only a small amount of effective drugs reaching the tumor site (Barreto et al., 2011; Chen, 2013). High dosage is often required to ensure a therapeutic success which leads to systemic drug toxicity (Eldar-Boock et al., 2013). Moreover, cytotoxic drugs are toxic to both cancer and healthy cells. Side effects, some of which are cumulative and life-threatening, are commonly caused by almost all cytotoxic drugs. The poor biodistibution and lack of targeting effect substantially diminish the therapeutic value of the drugs (Coelho et al., 2010; Hu & Zhang, 2012). Dosing schedule should be optimized extremely carefully because

high dose would mean a high risk to normal cells and tissues while low dosage may be not enough for a therapeutic success (Parhi et al., 2012).

1.1.2 Drug delivery systems for controlled release

In order to overcome the major drawbacks of conventional chemotherapeutic drugs, drug delivery systems (DDSs) have emerged since 1970s to enhance the efficacy of therapeutic agents (Robinson, 1978; Park, 2014; Safari & Zarnegar, 2014). DDSs can enhance the solubility of the drugs by providing hydrophobic/hydrophilic environments and protect the drugs from degradation before they reach the disease tissue (Allen & Cullis, 2004a). DDSs can release drugs at predetermined rates and predefined periods of time, alter the pKa of the drugs and substantially reduce rapid renal clearance (Shi et al., 2017). Therefore, lower dosage is required and the unwanted side effects will be minimized. In recent years, numerous DDSs have been developed, which can be categorized into viral and non-viral vectors (Allen & Cullis, 2004b; Park, 2014; Safari & Zarnegar, 2014).

1.1.2.1 Viral vectors

As nature's own infecting vehicles, viruses are thought to be smart organisms due to their superior ability to efficiently invade intracellular organelles and infect host cells (Wysocki et al., 2002). In order to replicate in living host cells, viruses must successfully deliver their genomes into the nucleus of the host cell (Mudhakir & Harashima, 2009). Viruses usually enter the cell by endocytosis. In order to escape from the endocytic vesicles after internalization, viruses have developed fusogenic peptides to escape from the endosomes and release the endocytosed viral genome. Viral fusogenic peptides are frequently found at amino terminus of the fusogenic proteins, and usually displayed a pH-dependent conformational change in response to the relatively low pH in the endosomes to reach the fusogenic-state (Epand, 2003). The viral fusogenic peptides facilitate the endosomal escape by fusion with endosomal membranes (enveloped viruses) or lysing or forming pores on the endosomal membrane (non-enveloped viruses), depending on the viral type (White, 1990).

Retrovirus, adenovirus, adeno-associated virus, lentivirus, and herpes simplex virus are commonly used virus vectors for nucleic acid delivery (Lundstrom, 2003). Recombinant retroviral vectors were first used for gene therapy by Rosenberg et al., 1990. The most widely used viral gene delivery vector is the Moloney Murine Leukemia Virus (MoMLV)-based retroviral vector (McTaggart & Al-Rubeai, 2002). Recombinant retrovirus is another popular

viral vector for the production of cancer vaccines (Wysocki et al., 2002). However, it is not the best tool for in vivo application due to its low transfection efficiency. The Adenoviral vector is becoming more widely used due to its high transfection efficiency (Kaliberov & Buchsbaum, 2012). But those viral vectors are still not ideal tools for drug delivery due to their high immunogenicity and inflammatory responses, toxicity and difficulty for large-scale production even the viruses are modified or inactivated (Mhashilkar et al., 2001; Wang et al., 2012).

1.1.2.2 Non-viral delivery systems

Considering the safety concerns of viral vectors, non-viral delivery systems have become increasingly important. The application of nanotechnology to drug delivery is widely expected to change the landscape of healthcare, pharmaceutical and biotechnology industries in the foreseeable future through improving the pharmacological and therapeutic properties of drugs (Park, 2007). The efficacy of nanoscale DDSs is dependent on their size and shape. The size of the DDS impacts their movement in and out of the vasculature, while the margination to the vessel wall is affected by their shape (Farokhzad & Langer, 2009). Nano DDSs could increase drug concentrations in the tumor tissues through the enhanced permeability and retention (EPR) effect (passive targeting) (Wang & Thanou, 2010). A wide variety of nanoscale DDSs have been extensively investigated, e.g. gold nanoparticles, polymer micelles, liposomes, nanogels, magnetic nanoparticles (Barreto et al., 2011; Kedar et al., 2010; Motornov et al., 2010; Torchilin, 2006, 2005). The majority of the nanoscale DDSs currently approved for parenteral administration is based on polymers or lipids (Venditto & Szoka Jr, 2013). Therefore, polymer and lipid-based DDSs are believed to be the two most promising delivery systems (Farokhzad & Langer, 2009; Shi et al., 2017).

1.1.2.2.1 Polymer-based DDSs

- **Polymer-drug conjugates**

Covalently attaching therapeutic agents to a polymer was first introduced by Ringsdorf in 1975. In the Ringsdorf model of a polymer-drug conjugate (Figure 1-1), there are at least three parts: a soluble polymer backbone, a biodegradable linker and a covalently linked drug (Ringsdorf, 1975). Conjugation of drugs to a polymer can significantly enhance the blood circulation time, especially for protein or peptide drugs (Khandare & Minko, 2006; Kim et al., 2009). The drug remains inactive during delivery and will be activated at the target site (Duncan, 2006). Another advantage is to increase the solubility of poorly soluble drugs by conjugating onto water-soluble polymers (Li & Wallace, 2008). Several polymer-drug conjugates, such as

PEG-L-asparaginase (Oncaspar/pegaspargase®) and PEG-Interferon α-2b (PEG-Intron®), were approved in 1997 and 2001 respectively (Khandare & Minko, 2006). Other polymer-drug conjugates, such as poly *N*-(2-hydroxypropyl) methacrylamide (HMPA) copolymer-doxorubicin, HMPA copolymer-doxorubicin-galactosamine, PEG-poly(glutamate)-paclitaxel, PEG-poly(aspartic acid)-doxorubicin micelles are in clinical trials (Venditto & Szoka Jr, 2013). However, clinical trials for some polymer-drug conjugates (e.g. PEG-camptothecin, HMPA copolymer-camptothecin) have been discontinued or suspended due to their significant toxicity (Shi et al., 2017).

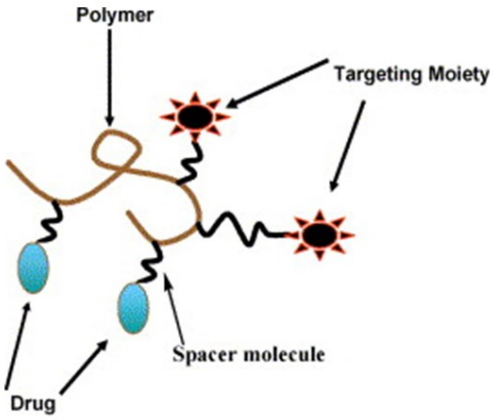

Figure 1-1. Ringsdorf model of a polymer-drug conjugate, containing a soluble polymer backbone, a biodegradable linker and a covalently linked drug. Targeting ligand could be further conjugated to the polymer-drug conjugate to improve the targeting effect (Khandare & Minko, 2006).

- **Polymer micelles**

Polymer micelles (Figure 1-2) are spontaneously formed in aqueous solution by self-assembly of amphiphilic block copolymers (de Las Heras Alarcon et al., 2005; Joglekar & Trewyn, 2013). Polymer micelles typically consist of a hydrophilic shell and a hydrophobic core, which acts as a reservoir for hydrophobic drugs (Nishiyama & Kataoka, 2006). Polymer micelles were first introduced by Bader as DDSs in 1984 (Bader et al., 1984). Drugs can be incorporated into the inner core of micelles by conjugation or entrapment. Polymer micelles can solubilize extremely hydrophobic drugs, prolong the circulation time and increase the drug stability (Yokoyama, 2010). In addition, the functionalities of the outer shell and the inner core are separated. The outer shell of polymer micelles can be conjugated with a variety of ligands for targeted delivery while the inner core plays a role for drug loading (Nishiyama & Kataoka,

2006). Smart micelles which are prepared by stimuli responsive copolymers are the new generation of polymeric micelles (Bae et al., 2003; Younsoo Bae et al., 2005).

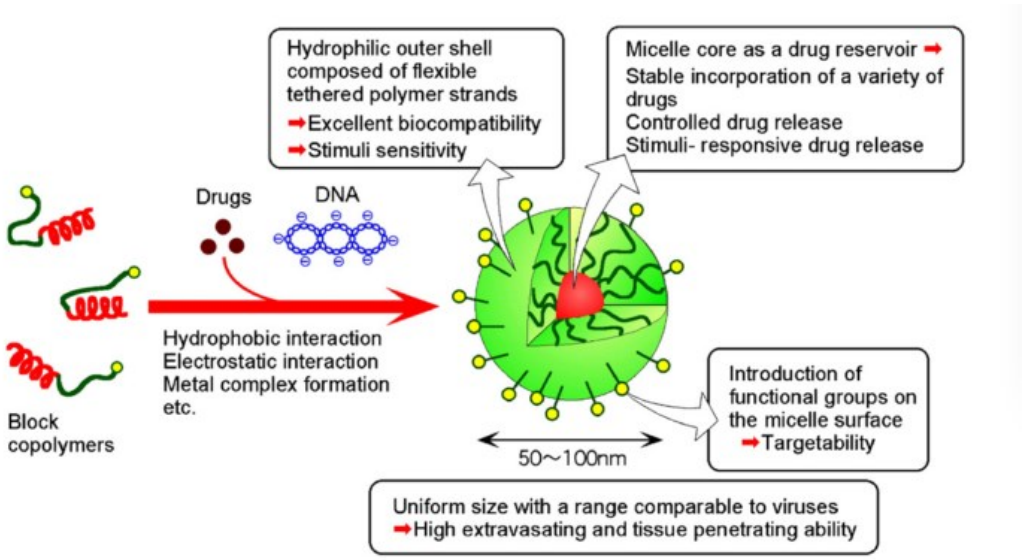

Figure 1-2. Polymeric micelles are formed by amphiphilic block copolymers. They have a hydrophobic core as a drug reservoir and hydrophilic shell which improve the biocompatibility of the polymeric micelles. The micelle surface could be further modified with targeting ligand. Drugs and genes could be loaded due to the hydrophobic interaction, electrostatic interaction and metal complex formation etc. (Nishiyama & Kataoka, 2006).

Several polymeric micelles have been launched in clinical trials, e.g. NK-105 (PTX-loaded micelles formed by PEG and polyaspartate), SP-1049C (doxorubicin-loaded micelles formed by poly(ethylene oxide)-b-poly(propylene oxide)-b-poly(ethylene oxide)), NC-6004 (cisplatin-loaded micelles prepared by PEG and poly(glutamic acid)), Genexol-PM (paclitaxel-loaded micelles formed by poly(ethylene glycol)-b-poly(DL-lactide)) and SN-38 (Irinotecan hydrochloride loaded micelles prepared by PEG-PGlu(SN-38)) (Cabral & Kataoka, 2014).

However, polymeric micelles are still waiting for clinical approval. According to the results obtained from clinical studies, one major problem associated with micelles is their toxic side effects (Kataoka et al., 1993). More clinical trials are needed to confirm the safety of synthetic block copolymers. Besides, unsuitability for large-scale production and the immature drug-incorporation technology are other drawbacks that limit the clinical application of polymeric micelles (Cabral & Kataoka, 2014).

1.1.2.2.2 Lipid-based DDSs

- **Solid lipid nanoparticles (SLNs)**

SLNs (Figure 1-3A) are produced by a solid lipid or a blend of solid lipids (mono-, di- and triglycerides, fatty acids, waxes) that should be solid at both room and body temperature (Müller et al., 2000; Wissing et al., 2004). Surfactants must be used in the formulation to stabilize the emulsions. SLNs are biocompatible, biodegradable and have low toxicity (Schubert & Müller-Goymann, 2005). The solid lipid matrix can effectively protect the encapsulated active ingredients against chemical degradation or oxidation (Harde et al., 2011). In addition, SLNs have high drug-loading capacity and encapsulation efficiency for hydrophobic drugs, possibility to achieve sustained/controlled drug release and drug targeting, as well as ease-to-manufacture at a large scale (Severino et al., 2011; Wong et al., 2007). However, it remains a major issue to load hydrophilic drugs into SLNs (Das & Chaudhury, 2011).

- **Nanostructured lipid carriers (NLCs)**

NLCs (Figure 1-3B) have been developed on the basis of SLNs by adding liquid lipids in solid lipids (Iqbal et al., 2012). The addition of liquid lipids distorts the formation of a perfect crystal, thus, a less ordered matrix containing many imperfections can provide much space to accommodate more drugs. Therefore, compared to SLNs, NLCs show a higher drug-loading capacity, a lower water content in the particle suspension and the minimized potential drug expulsion during storage (Severino et al., 2011). NLCs are attractive carriers for topical application due to their occlusive effects on skin. Some commercial cosmetics containing NLCs have already been launched on the market, e.g. Cutanova Cream NanoRepair Q10 (Müller et al., 2007). Besides topical application, they have also been reported for oral, parenteral, inhalational and ocular administration (Martins et al., 2007). Although NLCs have several advantages compared to SLNs, the limited loading capacity for hydrophilic drugs remains a problem for NLCs (Severino et al., 2011).

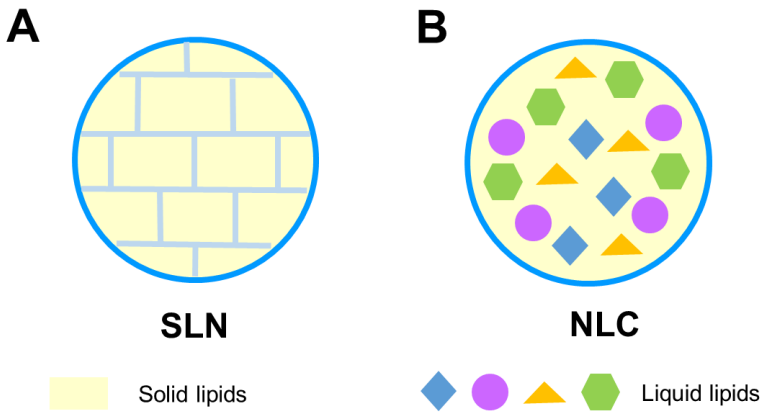

Figure 1-3. (A) SLNs and (B) NLCs. The solid lipids tend to form a perfect crystal structure in SLNs, which may lead to drug leakage during storage. While in NLCs, the addition of various types of liquid lipids distorts the perfect crystal and forms an "imperfect" less ordered matrix which can provide more space for drug loading and improve the storage stability. Reproduced from Das, 2011.

- **Liposomes**

Liposomes were first formulated by Alec Bangham in 1965 and soon proposed as DDSs (Bangham et al., 1965). Liposomes (Figure 1-4) are closed spherical vesicles formed by one or several concentric lipid bilayers with an aqueous phase inside (Jesorka & Orwar, 2008; Torchilin & Weissig, 2003). There are several different types of liposomes according to the size and the number of bilayer, such as small unilamellar vesicles (SUVs), large unilamellar vesicles (LUVs), multilamellar vesicles (MLVs) and multivesicular liposomes (MVLs) (Brandl, 2001; Sharma & Sharma, 1997).

Liposomes can be made from either synthetic or natural phospholipids (Mallick & Choi, 2014). The physical and chemical properties of liposomes are mainly based on the properties of the constituent phospholipids (Fenske & Cullis, 2008). Commonly used neutral lipids are L-α-phosphatidylcholine from soy bean or egg yolk (EPC), 1,2-distearoyl-sn-glycero-3-phosphocholine (DSPC), 1,2-dimyristoyl-sn-glycero-3-phosphocholine (DMPC), 1,2-dipalmitoyl-sn-glycero-3-phosphocholine (DPPC) and so on (van der Meel et al., 2014). Liposomes can be administered by a variety of routes, e.g. oral, parenteral, topical and so on (Al-Jamal & Kostarelos, 2011; Barenholz, 2001; Etheridge et al., 2013).

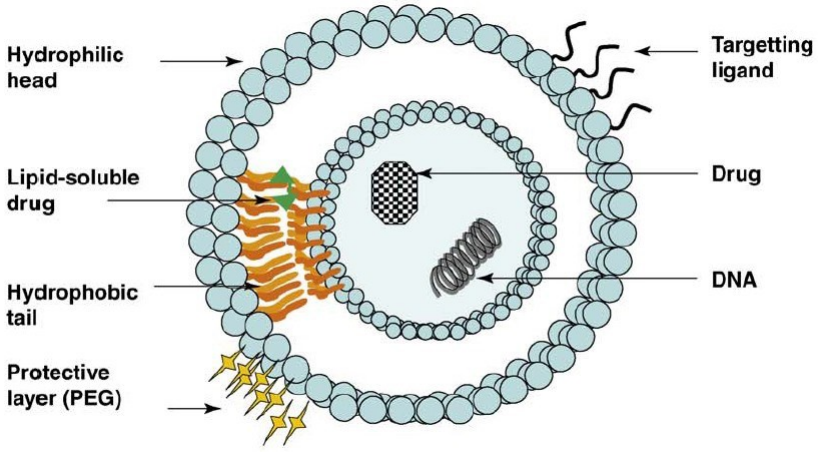

Figure 1-4. Schematic of a liposome which presents a bilayer structure. Hydrophilic drugs or genes can be encapsulated in the aqueous core, while hydrophobic drugs can be incorporated into the bilayer. The liposomal surface can be modified with targeting ligands and polymers, such as PEG as a protective layer (Malam et al., 2009).

Liposomes display a variety of attractive properties. First, liposomes are usually biocompatible (Malam et al., 2009). Secondly, compared to SLNs and NLCs, liposomes can encapsulate both water-soluble and water-insoluble drugs (Sharma & Sharma, 1997). Lipophilic drugs can be loaded within the bilayers whilst hydrophilic drugs can be encapsulated in the aqueous phase (Coelho et al., 2010). Size, charge and surface properties of liposomes can be changed by using different lipids or preparation methods (Table 1-1). In addition, these incorporated pharmaceuticals can be protected from being inactivated by external environments, thus avoiding undesirable side effects (Allen & Cullis, 2004a). Furthermore, liposomes can provide different ways of drug delivery into cells or even inside cellular compartments (Brandl, 2001), as shown in Figure 1-5. Liposomes can adsorb onto the cell surface or fuse with the cell membrane to release drugs. Alternatively, liposomes can be destabilized by certain cell membrane components when being adsorbed on the cell surface, leading to the release of drug payload and its consequent internalization into the cell interior via micropinocytosis. In addition, drugs can be delivered from endosomes into lysosomes or liposomes can provoke destabilization of the endosomal membrane and liberate drugs into the cell cytoplasm (Barreto et al., 2011; Mitragotri et al., 2014; Torchilin, 2005).

Table 1-1. Comparison of different liposomal preparation methods.

Preparation method	Advantages	Disadvantages	References
Lipid film hydration	Commonly used in laboratory or large scale production, easy and simple, low cost	Low level of aqueous components encapsulation	(Sharma & Sharma, 1997; Woodle & Papahadjopoulos, 1989)
French pressure cell	Low damage to liposomes, more stable	Large size and greater heterogeneity, poor reproducibility	(Hamilton et al., 1980; Sahoo et al., 2003)
Sonication	Smaller average size than French pressure cell	May case lipid damage	(Jesorka & Orwar, 2008)
High pressure homogenization	Smaller average size, suitable for large scale production	May case lipid damage	(Brandl, 2001; Woodle & Papahadjopoulos, 1989)
Dehydration-rehydration	Useful for entrapping a wide variety of aqueous components; especially proteins	Rehydration must be done extremely carefully	(Jesorka & Orwar, 2008; Kirby & Gregoriadis, 1984)
Freeze thaw	Low damage, without the need for exposure of aqueous solutes to organic solvents or detergents	Greater heterogeneity	(Castile & Taylor, 1999; Pick, 1981)
Ethanol injection	Simple and quick, mild treatment	Difficult to remove all ethanol	(Pons et al., 1993; Yu et al., 2004)
Ether injection	High aqueous entrapment	Compounds exposure to organic solvents, not suitable for proteins	(Deamer, 1978; Samad et al., 2007)
Detergent removal	Mild treatment, even sensitive proteins can survive	The retention of traces detergent Only a few detergents are suitable	(Jiskoot et al., 1986; Sahoo et al., 2003)
Reverse phase evaporation	High aqueous space and high entrapment efficiencies	Exposure to organic solvent may lead to denaturation of proteins	(Düzgüneş et al., 1983; Szoka & Papahadjopoulos, 1978)

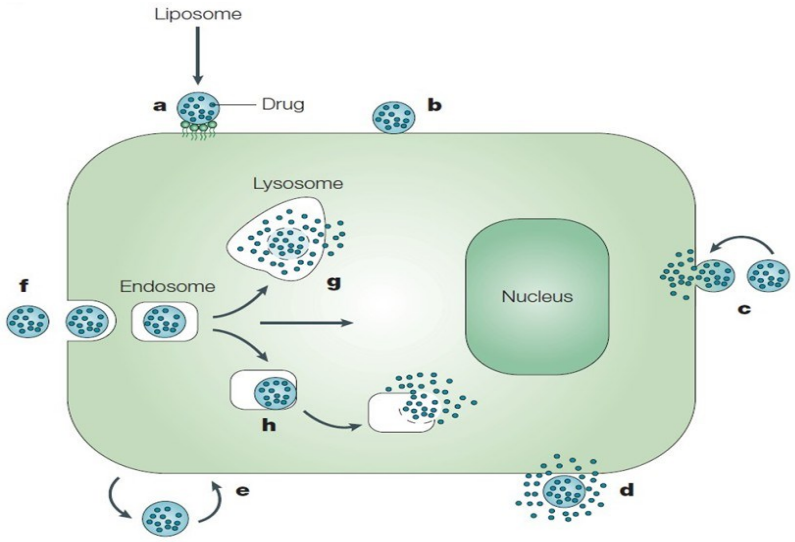

Figure 1-5. Liposome-cell interaction. Liposomes can specifically (a) or non-specifically (b) adsorb on the cell surface. Fusion can also occur between liposomes and cell membrane (c). Liposomes destabilization can be caused by certain cell membrane components when adsorbed on the surface (d). Lipid components can be exchanged with cell membrane mediated by transfer protein (e). Liposomes can also be delivered by endosomes (f) into lysosomes (g) or provoke endosome destabilization and release drugs into cytoplasm (h) (Torchilin, 2005).

Another interesting characteristics is that liposomes can be designed to mimic virus (Chen & Chen, 2016; Martin & MacDonald, 1974). All viruses consist of two parts: i) the genetic material made from either DNA or RNA carrying genetic information; ii) a protein coat which encases the nucleic acid. In some cases, viruses also contain an envelope of lipids that surrounds the protein coat when they are outside a cell (Lundstrom, 2003). A virus mimic can be developed by incorporating DNA or RNA inside the liposome which is surface modified by the material mimicking viral protein coatings or viral peptides. After surface modification with viral (or viral-mimicking) components, liposomes can efficiently deliver drugs into the cytoplasm by specifically interacting with cells and provoking endocytosis (Fattal et al., 2004; Ferreira et al., 2013).

The considerable clinical acceptance of liposomes makes them extremely attractive for drug delivery. The first non-viral nanomedicine (Doxil®) approved by FDA in 1995 is a doxorubicin (DOX)-loaded liposomal system (Barenholz, 2012). Until now, more than 13 liposomes-based nanomedicines have been launched on the market (7 for anticancer therapy) and more are currently in different clinical phases (Table 1-2) (Allen & Cullis, 2013; Etheridge et al., 2013; Venditto & Szoka, 2013). DOX is a hydrophilic anticancer compound which can bind to DNA-

associated enzymes, intercalate with DNA base pairs and produce stabilized DNA strand breaks to trigger cell death (Gaitanis & Staal, 2010). DOX can be passively or actively loaded into liposomes to eliminate its side effects and increase half-life (Fritze et al., 2006; Lasic et al., 1995). Although the success of Doxil® is encouraging, it may also induce palmar plantar erythrodysthesia (foot and hand syndrome) and shortness of breath (Abraham et al., 2005). Therefore, more research is needed to improve the DOX-loaded liposomal formulations.

1.2 Challenges and strategies for non-viral delivery systems to achieve efficient intracellular delivery

1.2.1 Intracellular barriers

Although incorporation of free drugs into DDSs could improve their stability within the bloodstream and prevent rapid elimination by the reticulo-endothelial system (RES) and renal clearance, cytoplasmic delivery remains an inefficient process for most non-viral delivery systems. The plasma membrane is a significant barrier to intracellular delivery (Iversen et al., 2011). Due to the relatively large particle size, most DDSs cannot enter cells by direct diffusion. Endocytosis is a primary route in which cells internalize viral and non-viral DDSs (Mudhakir & Harashima, 2009).

Endocytosis is usually divided into two categories dependent on the particle size: phagocytosis (cell eating) and pinocytosis (cell drinking) as shown in Figure 1-6 (Belting et al., 2005). Phagocytosis, which was discovered by Metchnikoff in 1882, is used by few specialized cells such as macrophages, neutrophils, monocytes and dendritic cells to internalize particles larger than 0.5 μm (Kaufmann, 2008). Pinocytosis, in contrast, is present in nearly all mammalian cell types and has multiple pathways depending on the cell origin and function (Platta & Stenmark, 2011). Several classifications of pinocytosis have been proposed. Among these, the most widely used approach is to categorize pinocytosis according to the types of protein involved, such as clathrin-mediated endocytosis (CME, most widely studied, also known as “classic endocytosis”) and clathrin-independent endocytosis (CIE, including caveolae-mediated endocytosis, clathrin- and caveolae-independent endocytosis, and micropinocytosis) (Conner & Schmid, 2003).

Table 1-2. Marketed liposomal and lipid–based anticancer products, plus a selection of products in clinical development (Allen et al., 2013).

Product	**Drug**	**Indications**	**Year approved / Clinical stage**
Approved products			
Doxil/Caelyx	DOX	Kaposi's sarcoma	1995
(Johnson & Johnson)		Ovarian cancer	1999
		Breast Cancer	2003
		Multiple myeloma and Velcade	2007 (Europe, Canada)
DaunoXome (Galen)	Daunorubicin	Kaposi's sarcoma	1996 (Europe) 1996 (USA)
Myocet (Cephalon)	DOX	Breast cancer and cyclophosphamide	2000 (Europe)
DepoCyt (Pacira)	Cytosine	Lymphomatous	1999
	Arabinoside	Neoplastic	
Lipo-Dox (Taiwan Liposome)	DOX	Kaposi's sarcoma, breast and ovarian cancer	2001 (Taiwan)
Marqibl (Talon)	Vincristine	Acute lymphoblastic leukemia	2012
Lipusu (Luye Pharma Group)	Paclitaxel	Solid tumors	2006 (China)
Products in clinical trials			
CPX-351 (Celator)	Cytarabine:daunorubicin	Acute myeloid leukemia	Phase II
CPX-1 (Celator)	Irinotecan HCI:floxuridine	Colorectal cancer	Phase II
MM-398 (Merrimack)	CPT-11	Gastric and pancreatic cancer	Phase II
		Glioma and colon cancer	Phase I
MM-302 (Merrimack)	ErbB2/ErbB3-targeted DOX	ErbB2-positive breast cancer	Phase I
MBP-436 (Mebiopharm)	Transferrin-targeted oxaliplatin	Gastric cancer and gastro-esophageal junction	Phase II

Product	**Drug**	**Indications**	**Year approved / Clinical stage**
Brakiva (Talon)	Topotecan	Relapsed solid tumors	Phase I
Alocrest (Talon)	Vinorelbine	Newly diagnosed or relapsed solid tumors	Phase I
Lipoplatin (Regulon)	cisplatin	Non-small cell lung cancer	Phase III
L-annamycin (Callisto)	Annamycin	myelogenous leukemia	Phase I
ThermoDox (Celsion)	Thermosensitive DOX	Primary hepatocellular carcinoma	Phase III
		Refractory chest wall breast cancer	Phase II
		Colorectal liver metastases	Phase II
Endo-Tag-1 (Medigene)	Cationic liposomal paclitaxel	Pancreatic cancer	Phase II
		Triple negative breast cancer	Phase II
ALN-VSP (Alnylam)	siRNA targeting VEGF, KSP	Liver cancer	Phase I
TKM-PLK1(Tekmira)	RNAi targeting polo-like kinase 1 (POLO)	Liver tumors	Phase I
Stimuvax (Oncothyreon/Merck)	Anti-MUC1 cancer vaccine	Non-small cell lung cancer	Phase III

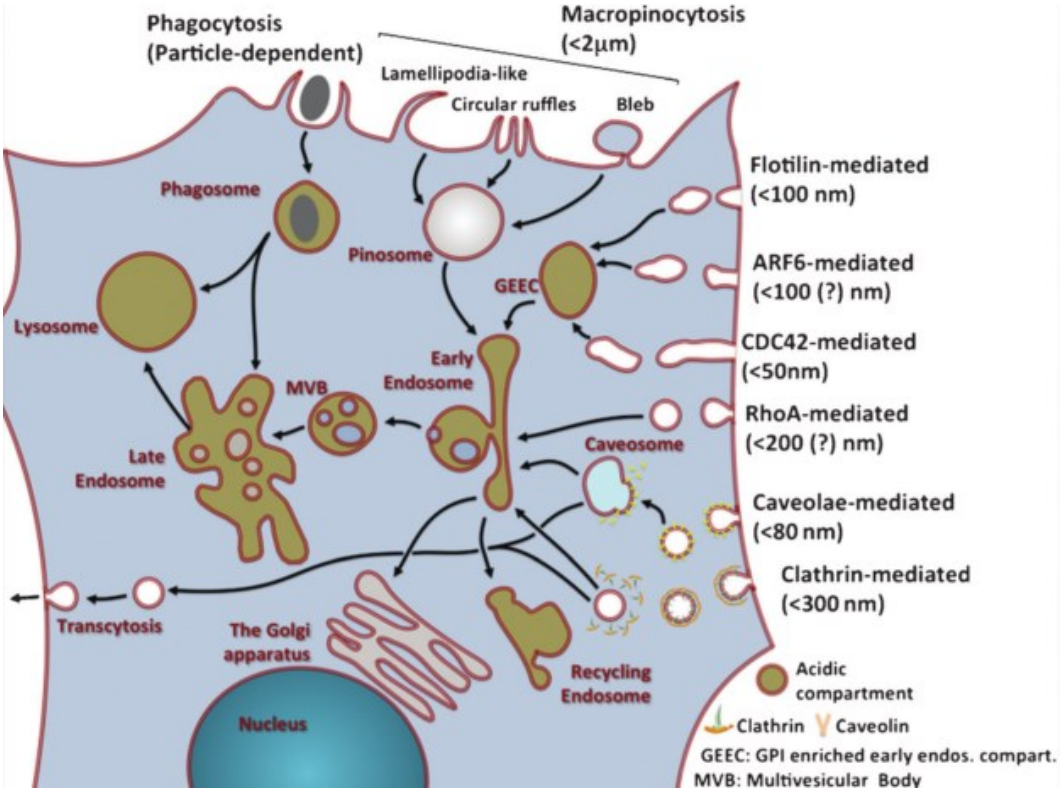

Figure 1-6. Extracellular uptake by endocytosis in a typical eukaryotic cell. Contents uptake by endocytosis first bind at cellular surface and then are enclosed within the early endosomes or phagosomes depending on the endocytosis type. These vesicles then mature down the degradative pathway and become multivesicular bodies (MVB) and late endosomes which fuse with lysosomes. The proteases and other enzymes present in the lysosomes degrade most biological substances. Alternatively, the endocytosed contents may be released to the cytoplasm from the endosomes, or transported back to the cell surface through the recycling endosomes or transcytosis (Canton & Battaglia, 2012).

All types of endocytosis include four essential steps: (i) binding to the cell surface; (ii) plasma membrane budding and pinching off (cargos engulfed in endosomes or phagosomes); (iii) tethering of the resulting trafficking vesicle; (iv) the trafficking vesicle delivering cargos to different intracellular compartments (Canton & Battaglia, 2012). After internalization, the pH inside early endosomes rapidly decreases to pH 6.0 – 6.8 within only 2 – 3 minutes due to ATP-driven proton pumps (Mellman & Warren, 2000; Mukherjee et al., 1997; Pack et al., 2005). The maturation of early endosomes to later endosomes is coupled with a further decrease of the luminal pH to 5.0 – 6.0 (El-Sayed et al., 2015). Further acidification promotes fusion with lysosomes, leading to degradation of endocytosed materials by lysosomal enzymes (Ganta et al., 2008; Martens et al., 2014). The endo-lysosomal trafficking time could vary from 30 –

60 minutes (Mellman, 1996) to several hours (Pack et al., 2005). The loss of therapeutic effectiveness of many drugs due to the enzymatic degradation inside lysosomes has become a significant challenge to efficient intracellular delivery. Alternatively, the endocytosed contents may be transported back to the cell surface through the recycling endosomes or transcytosis (Iversen et al., 2011).

1.2.2 Endosomal escape

In order to overcome endo-lysosomal sequestration and avoid enzymatic degradation, it is of importance to facilitate the endosomal escape in a timely manner. This can be achieved by pore formation, endosomal membrane rupture or endosomal membrane fusion, as shown in Figure 1-7 (Martens et al., 2014). There are several models of pore-formation, such as barrel-stave pore model and carpet model (Binder, 2008). Endosomal rupture is usually resulted from the "proton sponge effect" mediated by cationic polymers (such as PEI, poly(amido amines) and imidazole-containing polymers) with high buffering capacity (Iversen et al., 2011). Also, "osmolytic shock" and photochemical internalization (PCI) could also induce endosomal rupture (Hornung et al., 2008; Lu et al., 2011). Membrane fusion is usually mediated by fusion proteins/peptides or fusogenic "helper" lipids such as 1,2-dioleoyl-sn-3-phosphatidylethanolamine (DOPE). The fusion of the vesicular membrane with the endosomal membrane leads to cargo release into the cytoplasm (Epand, 2003).

Several viruses and pathogenic organisms, such as influenza virus and corynebacterium diphtheriae, have developed fusogenic proteins that can facilitate endosomal escape and the release of the viral genome into the cell cytoplasm (Epand, 2003). HA2 (subunit of haemagglutinin of the influenza virus), TAT (HIV-1 Trans-activator gene product) and L2 peptide (C terminus of the capsid protein of Papillomavirus) have been employed as delivery vehicles for cytoplasmic delivery (Varkouhi et al., 2011). However, their clinical applications are limited due to the safety concerns as discussed in details in Section 1.1.2.1. Synthetic peptides have been developed (Nakase et al., 2010), but they usually have low stability, high immunogenicity and low efficiency in membrane destabilization (Plank et al., 1998). Therefore, synthetic pH-responsive polymers have been designed to mimic the viral functions for the enhanced endosomal escape (Shim & Kwon, 2012).

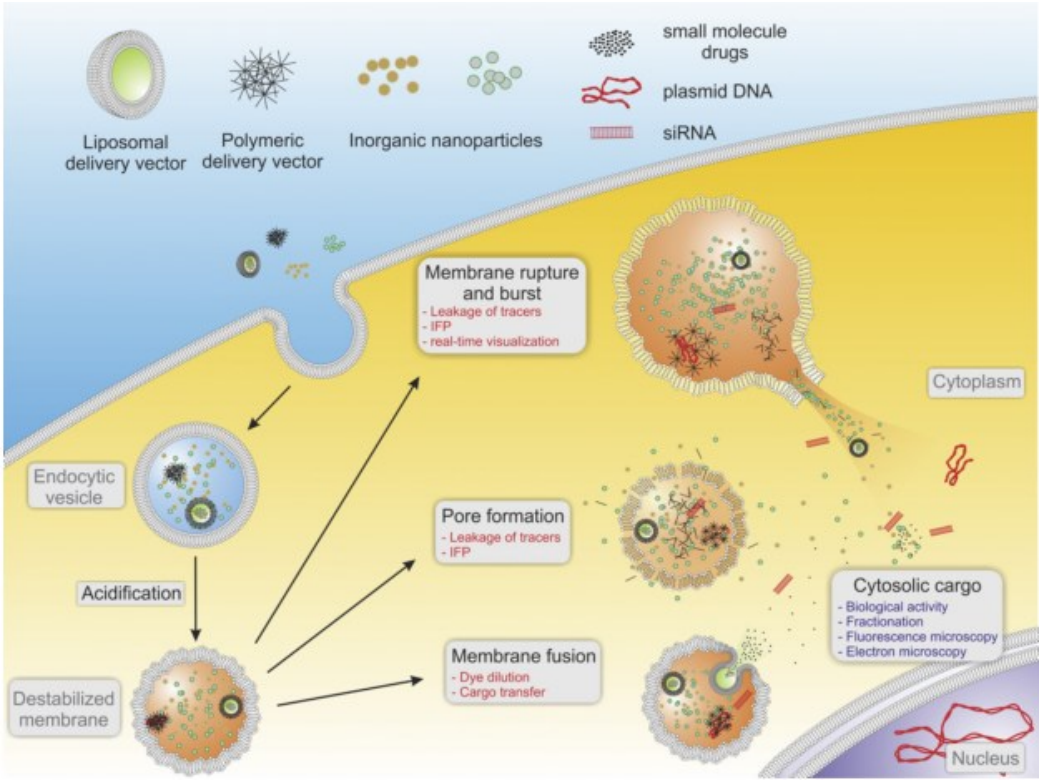

Figure 1-7. Different types of endosomal escape. Most DDSs are usually uptaken by cells via endocytosis, leading to sequestration of the cargo in the endosomes. The endosomal membrane can be destabilized by the endosomolytic delivery vectors and lead to cargo release through membrane rupture and burst, or by pore formation or membrane fusion, depending on the type of delivery vectors (Martens et al., 2014).

1.3 pH-Responsive endosomolytic polymers

The pH value varies in different tissues and cellular compartments. The pH at systemic sites of infections and tumors (pH ranging from 6.5 – 7.2) is lower compared to the pH of normal tissues (pH 7.35 – 7.45) due to the "Warburg Effect'" (Warburg et al., 1927). The mildly acidic pH at the tumor microenvironment can cause protonation of chemotherapeutic drugs such as doxorubicin and subsequently decrease the drug uptake (Gerweck & Seetharaman, 1996). Furthermore, the intracellular compartments, such as endosomes and lysosomes, undergo gradual acidification during the endocytic pathway, as discussed in Section 1.2.1. Thus, it is required to develop pH-sensitive polymers for efficient intracellular delivery (Ganta et al., 2008).

Ideally pH-responsive polymers should be non-lytic at neutral pH, but can rapidly destabilize the lipid membrane upon acidification in the tumor microenvironment or during endo-lysosomal trafficking. pH-Responsive polymers typically contain ionizable functional groups, such as amino, carboxylic and sulfonic acid groups (de Las Heras Alarcon, Pennadam & Alexander, 2005), and their protonation can result in either a conformational swelling (for polycations) or a coil-to-globule conformational change (for polyanions), leading to the membrane destabilization (Schmaljohann, 2006). Efforts have been made to enhance the polymer-membrane interaction, such as conjugation of hydrophobic groups or chains to enhance the hydrophobicity of the polymer, and alternatively incorporation of cationic components to enhance the electrostatic attraction between the polymer and the negatively charged cell surface (Tribet & Vial, 2008).

1.3.1 Polycations

Polycations were firstly developed as non-viral gene vectors. Cationic polymers are able to form complexes with nucleic acids and deliver genetic agents into a subcellular target site (Kim et al., 2009). Their binding with the lipid membrane is facilitated by the electrostatic attractions between the positively charged polymer and the negatively charged lipid bilayer, leading to pronounced adsorption at the plasma membrane and consequent rapid internalization (Chen, 2013). There are several hypotheses about the cationic polymer mediated endosomal escape and cytoplasmic delivery (Morille et al., 2008). The most accepted one is the so-called “proton-sponge” effect (Figure 1-8). This hypothesis assumes that cationic polymers containing a large number of secondary and tertiary amines can provide buffering capacity at endosomal pH, and cause the ATPase to pump more protons into endosomes to reach the desired pH. The accumulation of protons in the vesicle results in an increased influx of counter ions and water, leading to osmotic swelling and rupture of the endosomal membrane, which in turn facilitates the release of the cargo from endosomes into the cytoplasm (Akhtar, 2010; Chou et al., 2011; David et al., 2010; Miele et al., 2012).

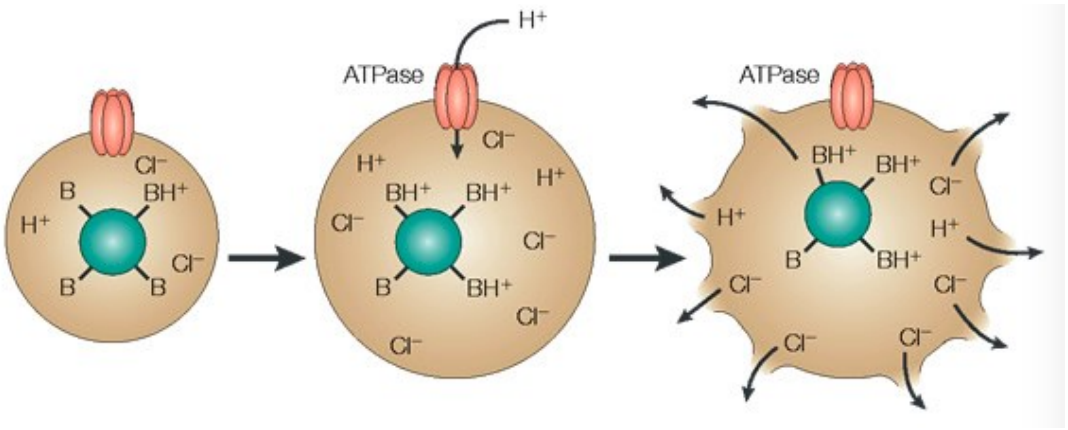

Figure 1-8. Schematic illustration of the "proton-sponge" effect hypothesis (Pack et al., 2005).

A variety of cationic endosomolytic polymers, such as poly(ethylene imine) (PEI), poly(L-lysine) (PLL), poly (L-histidine), poly(2-(dimethylamino)ethyl methacrylate) (PDMAEMA) and modified chitosan, have been developed to destabilize endosomal membranes at acidic pH (Schmaljohann, 2006). Among these polymers, PEI is still the gold standard for gene delivery (Yin et al., 2014). It can balance out the charge and condense DNA to nanoparticles (around 100 nm in size) (Morille et al., 2008). Although cationic polymers have shown potential for gene delivery, their high cytotoxicity limits their clinical application. Polycations can induce cellular membrane damage or apoptosis, due to their non cell-specific interaction and non-biodegradable nature. Off-target adsorption with serum proteins and other anionic molecules further lead to undesirable aggregations or premature release of nucleic acids and enhance their immunogenicity (Zhang et al., 2007). In addition, the transfection efficiency of cationic polymers is still relatively low compared to viral vectors (Wang et al., 2012). Therefore, the application of cationic polymers for systemic gene delivery may be problematic unless their serum stability are improved. Conjugating with PEG or masking the charge group can reduce their cytotoxicity and improve serum stability, but in turn may lead to reduced transfection efficiency, which is called "polycation dilemma" (Wang et al., 2012).

1.3.2 Polyanions

Anionic polymers can display lower cytotoxicity, higher serum stability, reduced renal clearance and longer circulation time as compared with cationic polymers, probably due to the reduced binding with serum proteins and decreased non-specific interaction with cell

membrane (Yessine & Leroux, 2004). Therefore, particular research interest has been paid to the development of anionic pH-responsive polymers for drug delivery.

Anionic polymers contain ionizable carboxyl groups for pH-sensitive functionalities (Hoffman, 2013). In order to enhance their hydrophobic interaction with the lipid membrane, anionic pH-responsive polymers are usually designed to include hydrophobic segments (Fleige et al., 2012; Jeong & Gutowska, 2002). As shown in Figure 1-9, at neutral pH, the polymer displays an extended coil confirmation, due to the electrostatic repulsion between the negatively charged carboxylate groups outweighing the hydrophobic interaction. With protonation of carboxylate groups at acidic pH, the polymer confirmation changes from an extended coil to a compact globule structure (Chen & Chen, 2016; El-Sayed et al., 2015; Thomas & Tirrell, 1992). Accordingly, the pH-responsive polymer can destabilize the endosomal membrane and release the endocytosed cargos into the cell cytoplasm in response to the pH decrease in the endosomes (Plank et al., 1994). The membrane activity and transition pH can be manipulated by controlling the hydrophobic/hydrophilic balance of the polymers (Schulz et al., 2012). This endosomolytic activity is similar to the pH-responsive membrane disruptive behavior of the anionic fusogenic peptide present in the HA2 subunit of haemagglutinin (HA) protein of the influenza virus. At acidic pH, the protonation of aspartic acid and glutamic acid residues in the fusogenic peptide facilitates the change of its conformation to an α-helical structure, which leads to destabilization of the endosomal membrane (Cheng et al., 2016; Skehel & Wiley, 2000).

So far, a variety of pH-responsive anionic polymers have been developed as smart drug carriers, including pH-responsive polymeric micelles, polymeric nanoparticles, polymer-drug conjugates and hydrogels. They have been demonstrated to enhance the cytoplasmic delivery of therapeutic molecules, e.g. small molecular drugs, siRNA, proteins (Joglekar & Trewyn, 2013; Motornov et al., 2010; Mura et al., 2013; Stuart et al., 2010; Yoo et al., 2011).

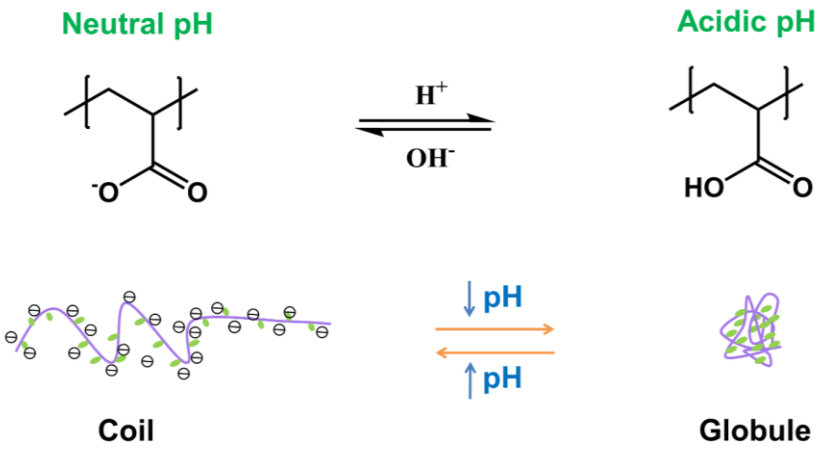

Figure 1-9. Schematic illustration of coil-to-globule conformational change of polyanions using poly(acrylic acid) as an example. At neutral pH, the polymer forms extended coil confirmation, due to the electrostatic repulsion between the negatively charged carboxylic groups. At acidic pH, because of the protonation of carboxylic group and the domination of hydrophobic interaction, the polymer displays compact globule structure. Reproduced from Chen & Chen, 2016.

1.3.2.1 Non-biodegradable anionic pH-responsive polymers

Tirrell and co-workers have initiated the work on anionic, pH-responsive, vinyl-based polymers, such as poly(α-methylacrylic acid) (PMAA, Figure 1-10A) and poly(α-ethylacrylic acid) (PEAA, Figure 1-10B). PEAA disrupted the membrane of lipid vesicles at endosomal pH, but was not membrane-lytic at physiological pH, which is ideal for drug delivery application (Linhardt & Tirrell, 2000; Seki & Tirrell, 1984; Thomas et al., 1996; Thomas et al., 1994; Thomas & Tirrell, 1992; Tirrell et al., 1985). Hoffman and co-workers further investigated the membrane activity of PEAA and then designed other vinyl-based polymers, including poly(propylacrylic acid) (PPAA, Figure 1-10C) and poly(butylacrylic acid) (PBAA, Figure 1-10D) (Murthy et al., 2001, 1999). Increasing the length of short hydrophobic α-alkyl side groups could significantly increase the membrane destabilization activity and shift the transition of pH to higher values (Murthy et al., 1999). By increasing just one methylene unit in the pendant α-alkyl group, PPAA was approximately 15 times more efficient at hemolysis than PEAA at pH 6.1. A further increase of one methylene unit in the pendent alkyl chain led to the resulting PBAA showing 100% hemolysis at pH 7.4 (Murthy et al., 1999). The significant shift of pH profile and the enhanced membrane destabilization activity indicate that the length

of the pendent hydrophobic alkyl group is of critical importance in determining the pH-dependent membrane activity (El-Sayed et al., 2015).

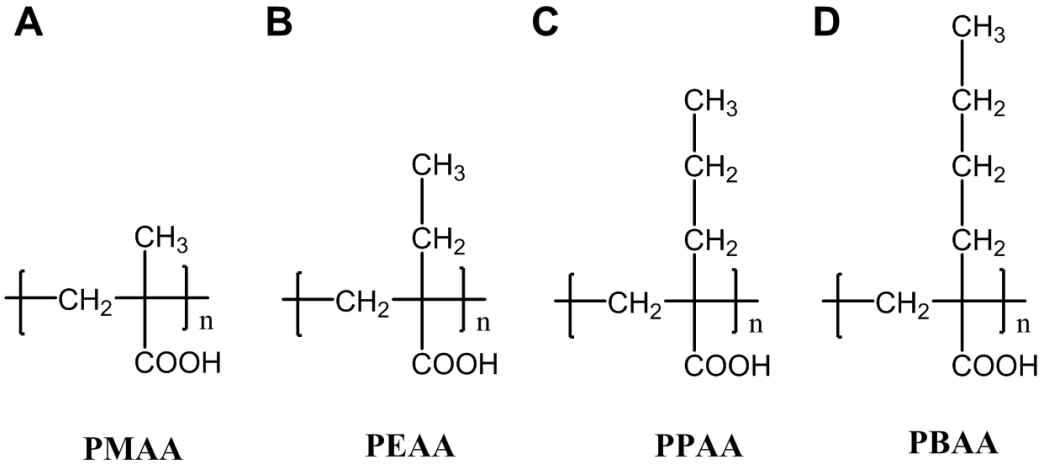

Figure 1-10. The unit structures of (A) PMAA, (B) PEAA, (C) PPAA and (D) PBAA.

Poly(acrylic acid-*co*-alkylacrylate) copolymers have been further developed to evaluate the effect of the hydrophobicity/hydrophilicity balance on membrane disruption (Henry et al., 2006; Murthy et al., 2001). The hydrophobic/hydrophilic balance can be easily manipulated by varying the acrylic acid/alkyl acrylate ratio or the chain length of alkyl acrylate. It has been reported that increasing the alkylacrylate content or increasing the hydrophobic alkyl chain length led to the enhanced hemolytic activity (Murthy et al., 2001). This opens an avenue towards designing more efficient endosomolytic pH-responsive polymers by carefully tuning the hydrophilic/hydrophobic balance.

Besides the poly(acrylic acid) family, other polymers have also been developed and displayed pH-dependent hemolytic activity, such as maleic acid/alkyl vinyl ether copolymers, maleic acid/styrene copolymers, *N*-isopropylacrylamide (NIPAM)/MAA copolymers (both pH- and thermo-responsive) (Jeong & Gutowska, 2002; Joglekar & Trewyn, 2013; Yessine & Leroux, 2004). Further research has been carried out to investigate the potential of these non-biodegradable anionic pH-responsive polymers for biomedical application. The excellent pH-dependent membrane destabilization activity of PPAA has motivated the investigation of its ability in gene delivery. Mixture of PPAA, cationic lipid DOTAP and pCMVbeta plasmid DNA showed higher serum stability, enhanced cellular uptake and transfection of NIH3T3 fibroblasts than the lipoplex without PPAA (Cheung et al., 2001). The successful transfection

results further encouraged the in vivo study. With the addition of PPAA, the lipoplex formulation greatly enhanced the transfection in the TPS2-null knockout mice and localized modulation of the wound healing response (Kyriakides et al., 2002). PPAA also displayed an ability to enhance antibody and protein delivery by direct conjugation or mixing (Foster et al., 2010; Lackey et al., 2002). pH-Responsive micelles based on PEG-b-poly(alkyl acrylate-co-methacrylic acid) were developed for oral delivery. Once the pH increased from 1.2 to 7.2, the micelle was disrupted by the ionization of the carboxylic acid groups and rapid drug release was observed (Sant et al., 2004). pH-Responsive polymeric nanoparticles prepared by the poly(methacrylic acid and methacrylate) copolymer enhanced the oral bioavailability of cyclosporine A, which was prevented from acidic degradation in stomach and released only at pH > 6 (Dai et al., 2004). The copolymer of NIPAM and acrylic acid (AAc) displayed both pH and temperature sensitivity and could provide triggered release of biotin (Bulmus et al., 2000).

1.3.2.2 Biodegradable anionic pH-responsive polymers

The molecular weights of those non-biodegradable polymers must be below the renal excretion threshold to avoid unfavorable bioaccumulation, which consequently limits their clinical application (Duncan, 2006). The development of biodegradable anionic pH-responsive polymers with desirable membrane-activity has therefore become increasingly important. Hydrolytically or enzymatically cleavable linkages, e.g. amides, esters and anhydrides, can be incorporated within the polymer backbone (Eccleston et al., 1999). Biodegradable anionic poly (amino acid)s, such as poly(aspartic acid) (PAA), poly(glutamic acid) (PGA) and their derivatives, have been utilized as delivery agents (Mallakpour & Dinari, 2011). These anionic polymers consist of repeating amino acid units with pendant ionizable groups and can destabilize the lipid membrane at acidic conditions (Ito et al., 1997). These biocompatible and biodegradable polymers have been employed for drug delivery and causing limited cytotoxicity (Guan et al., 2008; Kurosaki et al., 2012, 2009).

Eccleston *et al.* have developed a biodegradable, pH-responsive amphiphilic pseudopeptide, poly(L-lysine isophthalamide) (PLP, Figure 1-11) via polycondenzation of natural metabolite L-lysine with diacyl chlorides through amide bonding (Eccleston et al., 1999). PLP contain a hydrophobic backbone and pendant ionizable carboxyl groups, displaying a pH-dependent coil-to-globule conformational change (Eccleston et al., 2000). PLP disrupted the erythrocyte membrane within a narrow pH range (pH 4.6 – 5.0) (Eccleston *et al.*, 2000). The application of PLP in clinical use is not ideal due to its low membrane lytic capacity (~15% hemolysis)

and the low pH (below the endosomal pH range) when membrane disruption occurred (Eccleston et al., 2005).

The lack of pendant hydrophobic groups was thought to be the main reason for the limited membrane destabilization activity (Chen et al., 2009b). In order to overcome the drawbacks of PLP, different hydrophobic amino acids (L-valine, L-leucine and L-phenylalanine) have been grafted on the pendant carboxylic acid groups of the PLP backbone at various substitutions to enhance the membrane disruptive activity within the pH range typical of endosomes, ideally early endosomes. Compared to the PLP derivatives grafted with valine and leucine, PLP grafted with phenylalanine (Phe) displayed much higher membrane lytic activity, indicating that grafting PLP with more hydrophobic amino acids would lead to the enhanced membrane destabilization activity (Chen et al., 2009c). PP75 (Figure 1-11), which is the PLP grafted with Phe at a stoichiometric ratio of 75% relative to the available carboxylic acid groups on the backbone, showed optimal membrane lytic activity (Chen et al., 2009b). PP75 displayed extremely high membrane-lytic efficiency at early endosomal pH 6.0 – 7.0, 35-fold more efficient than the antimicrobial peptide melittin, but essentially non-lytic at neutral pH (Chen et al., 2009b). The efficient membrane destabilization was due to the significantly enhanced hydrophobic interaction of PP75 with the cell membrane, which resulted from the increased polymer hydrophobicity and also the presence of an aromatic ring in each Phe (Zhang et al., 2011).

These novel pseudopeptidic polymers have shown promising potential for drug delivery application. PP75 has been successfully used for efficient intracellular delivery of small molecules and therapeutic proteins into a variety of cells (Chen et al., 2009c; Liechty et al., 2009). Furthermore, PP75 efficiently traversed across the extracellular barrier in three-dimensional multicellular spheroid tumor models to reach individual cells and facilitate endosomal release of the endocytosed cargos into the cytoplasm (Ho et al., 2011). PP75 has also been used for cytoplasmic delivery of stathmin siRNA via conjugation with a cleavable disulfide bond, which led to successful silencing of stathmin gene expression and the consequent inhibition of tumor growth upon combination with carmustine (Khormaee et al., 2013). In addition, PP50, the PLP grafted with Phe at a stoichiometric ratio of 50%, has been utilized for cell cryopreservation and desiccation through temporarily permeabilizing the cell membrane at mildly acidic pH and delivering the preservative agents (*e.g.* trehalose) into the cell interior without significant cell damage (Lynch et al., 2010, 2011).

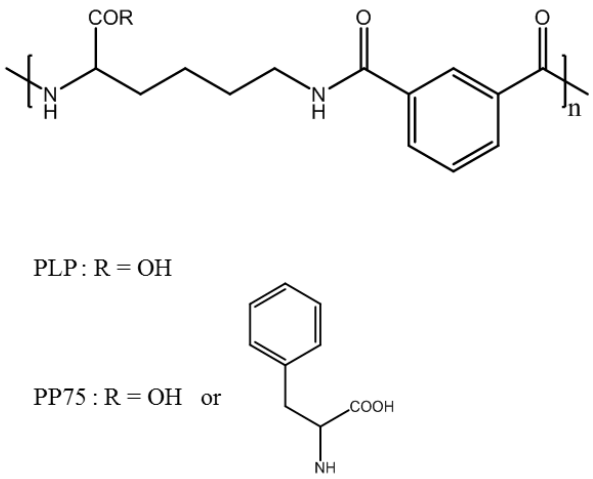

Figure 1-11. The unit structures of PLP and PP75.

1.4 Multifunctional Liposomes

Although liposomal drug delivery systems have shown great clinical potential, they still have some problems which cannot be neglected, such as poor stability, inability to achieve sustained drug delivery over a prolonged period of time, and fast elimination by the mononuclear phagocyte system (van der Meel et al., 2014). In addition, liposomes without tumor targeting ligands have to rely solely on passive targeting by the EPR effect, which is not effective enough compared to active targeting (Wang & Thanou, 2010). Thus, research has been focused on developing multifunctional liposomes as new generations of liposomes with stimuli-responsive, long-circulating, controlled-release and targeting functionalities (Ganta et al., 2008; Kale & Torchilin, 2010; Torchilin, 2014).

1.4.1 Stealth liposomes

A number of polymers have been employed to prepare liposomes with "stealth" properties, such as poly[*N*-(2-hydroxypropyl) methacrylamide]], poly-*N*-vinylpyrrolidones, L-amino-acid-based biodegradable polymer-lipid conjugates and polyvinyl alcohol (Immordino et al., 2006; Nag & Awasthi, 2013). The most common strategy is to coat the liposomal surface with polyethylene glycol (PEG) as a protective layer. The PEG coating layer with a thickness of around 10% of the particle diameter can reduce the recognition of the PEGylated liposomes by the mononuclear phagocytic system and therefore prolong their circulation time in the blood stream (C˘eh et al., 1997). Stealth liposomes have demonstrated several advantages, such as

improved stability, increased blood circulation half-life and enhanced bioavailability, and are currently being used in clinical practice (e.g. Doxil®, Caelyx®) (Suk et al., 2016). Although PEG could provide steric protection of liposomes, PEGylation can decrease the intracellular trafficking of liposomes (Wang et al., 2012). Several detachable PEG conjugation after arrival at tumor tissue have been reported, such as conjugating PEG onto the liposomal surface via pH sensitive (Zhang et al., 2015), esterase sensitive (Xu et al., 2008) and reductive potential sensitive (McNeeley et al., 2009) bonds.

1.4.2 Targeting liposomes

Conventional liposomes have been reported to passively accumulate at the tumor site due to the EPR effect (Fang et al., 2011). The leaky vasculature characteristic of the tumor site enables nano vehicles to accumulate in tumor tissue more than they do in normal tissues (Fang et al., 2011; Farokhzad & Langer, 2009). However, the undesirable cellular uptake without targeting ligands remains a barrier (Farokhzad & Langer, 2009). Besides, there are arguments that the EPR effect could not significantly increase the accumulation of nano DDSs at the tumor site which would result in the local drug concentration not sufficiently high for the treatment of most cancers (Nakamura et al., 2016). Improved accumulation efficiency can be achieved through active targeting (Noble et al., 2004). Active targeting of liposomes can considerably increase the amount of drug delivered to the target cell (Torchilin, 2009). Furthermore, targeting liposomes could selectively bind to the cell surface and be internalized via receptor-mediated endocytosis, thus leading to improved therapeutic outcomes and reduced systemic toxicity (Noble et al., 2004; Sapra & Allen, 2003). The selection of targeting ligand type is of crucial importance. Ideally target receptors are over-expressed homogenously at a high level by the tumor cells but show a negligible or low expression in healthy tissues (Noble et al., 2014). The most frequently used targeting ligands include monocolnal antibodies, antibody fragments, proteins, peptides, vitamins, carbohydrates and glycoproteins (Kamaly et al., 2012; Marqués-Gallego & de Kroon, 2014; Pradhan et al., 2010; Sawant & Torchilin, 2012). Strategies for development of targeting liposomes include synthesis of ligand-lipid conjugates prior to the liposome preparation and surface modification of the formulated liposomes (Marqués-Gallego & de Kroon, 2014).

1.4.3 Stimuli-responsive liposomes

The stimuli-responsive liposomes are “smart” DDSs and have become increasingly important in drug delivery, in particular when the stimuli are unique to the diseased tissues.

The specific response to the pathological "triggers" will allow the liposomes to deliver and release the drug payloads only to the diseased sites, therefore reduce systemic toxicity in anticancer therapy. External stimuli include biological stimuli such as pH, temperature and redox as well as physical stimuli such as ultrasound, light, heat and magnetic field (Mura et al., 2013; Stuart et al., 2010; Torchilin, 2014).

Particular attention has been given to pH-responsive liposomes, due to the pH-gradient between the tumor site and healthy tissues and the acidification during the endo/lysosomal trafficking pathway (Gerweck & Seetharaman, 1996; Mukherjee et al., 1997). pH-Responsive liposomes are stable at neutral pH, which will allow them to retain payloads during the blood circulation and reach the target site. At acidic pHs, the pH-sensitive liposomes become destabilized and release the encapsulated drugs (Chiang & Lo, 2014; Torchilin, 2005). They can fuse with the endovascular membrane at low pH conditions and enhance cytoplasmic drug delivery after being endocytosed in the intact form (Kale & Torchilin, 2010), as shown in Figure 1-12. There are several strategies to prepare pH-sensitive liposomes, including the use of pH-sensitive lipids, surface conjugation of pH-sensitive polymers, surface complexation of oppositely charged fusogenic peptides/proteins and encapsulation of synthetic fusogenic peptides inside liposomes (Jølck et al., 2011; Karanth & Murthy, 2007).

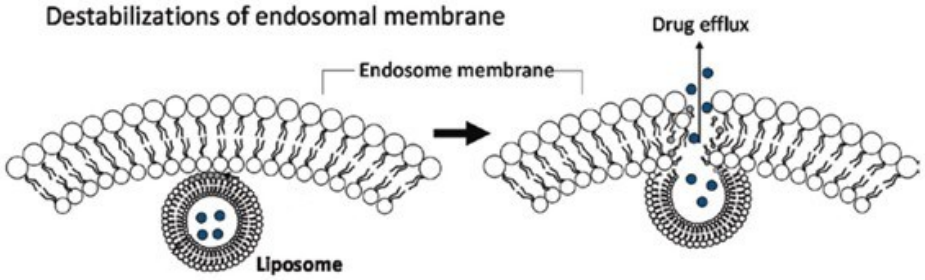

Figure 1-12. Destabilization of the endosomal membrane. After being endocytosed into the endosome, pH-responsive liposomes can undergo membrane destabilization in response to pH reduction and fusion with the lysosomal membrane to allow drug release into the cell cytoplasm (Torchilin, 2005).

PE or its derivatives are commonly used for preparing pH-sensitive liposomes (Mallick & Choi, 2014).The PE-containing liposomes are stable at physiological pH, but undergo phase transition at acidic conditions and thereby release the cargos into the cytoplasm (Torchilin, 2006). The pH-responsive lipid, DOPE was first used to prepare pH-responsive liposomes

(Simões et al., 2004). DOPE has also been combined with other lipids such as phosphatidylglycerol (PG), phosphatidylserine (PS), phosphatidylcholine (PC) and cholesteryl hemisuccinate (CHEMS), to prepare pH-responsive liposomes (Drummond et al., 2000). One major problem associated with the PE-containing pH-sensitive liposomes is their instability in plasma or serum, which could lead to premature drug leakage (Karanth & Murthy, 2007). An improvement can be made by adding dihydrocholesterol, but it might lead to a compromised pH-sensitivity (Roux et al., 2003).

Incorporation of fusogenic peptides inside liposomes could facilitate membrane destabilization at acidic conditions, leading to cargo release into the cytoplasm. A pH-dependent fusogenic peptide (diINF-7) was co-encapsulated with diphtheria toxin A chain inside liposomes and promoted cytoplasmic delivery (Mastrobattista et al., 2002). Another way is complexing synthetic fusogenic peptides/proteins with cationic liposomes to facilitate the association of peptides/proteins on the liposomal surface. It has been demonstrated that pH-sensitive peptide GALA complexed on the surface of the DOTAP/DOPE (1:1) cationic liposomes could enhance intracellular delivery of plasmid DNA through destabilization of the endosomal membrane and as a result improve transfection efficiency (Simões et al., 2004). However, one of the major issues for using the fusogenic proteins/peptides containing liposomal formulations is immunogenicity (Morille et al., 2008; Shim et al., 2013).

Surface modification of liposomes with synthetic pH-responsive polymers could diminish the safety concern (Chen, 2013; Chen & Chen, 2016). Typically, there are three ways to modify the liposomal surface: (i) adding polymers to lipids before liposomes are formed (pre-insertion); (ii) physically inserting polymers into the out layer of pre-formed liposomes (post-insertion); and (iii) chemical conjugation of polymers onto the liposomal surface (post-modification) (Mallick & Choi, 2014; Torchilin, 2005). For the pre-insertion method, the polymers may occupy the interior space of the liposomes which is designed for drug loading (Figure 1-13A) (Nag & Awasthi, 2013). This problem can be addressed by using the post-insertion method, whereby polymers can be spontaneously inserted into the outer surface of the liposomes via hydrophobic interaction, hydrogen bonding or electrostatic attractions (Figure 1-13B). High colloidal stability can be achieved by reducing polymer-lipid interactions and prolonged blood circulation has been reported compared to liposomes prepared using the pre-insertion method (Nakamura et al., 2012). Moreover, the post-insertion method is more favorable in manufacturing, since it only requires a simple incubation step. For the post-modification, it

needs extra reagent for chemical conjugation and aggregation of liposomes might occur during the reaction (Nag & Awasthi, 2013).

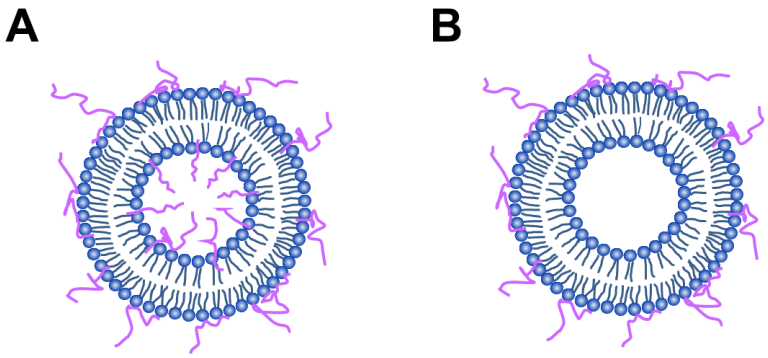

Figure 1-13. Schematic of the liposomes prepared by using the (A) pre-insertion method; and the (B) post-insertion method.

A number of cationic and anionic pH-responsive polymers have been applied to develop pH-responsive liposomes by post-insertion (Joglekar & Trewyn, 2013; Yessine & Leroux, 2004). Due to the electrostatic attraction, polycations could adsorb on the anionic liposomal surface, and vice versa. Polycations, such as PEI, PLL and poly(diallyldimethylammonium chloride) have been employed for surface modification of anionic phospholipid vesicles and the resulting pH-responsive liposomes showed the enhanced intracellular delivery (Cheung et al., 2001; Chieng & Chen, 2011; Zhao et al., 2012). However, the overall cytotoxicity remains a big issue for the application of the liposomes surface-modified with polycations (Wang et al., 2012; Zhang et al., 2007). In contrast, polyanions have attracted an increasing attention to confer their pH-sensitivity on liposomes because of their low toxicity. Polyanions can not only adsorb on the cationic liposomal surface due to electrostatic interaction, but also can bind on the neutral or even negatively charged liposome surface through hydrophobic interaction and/or hydrogen bonding (Yessine & Leroux, 2004). It has been reported that PEAA can bind to a variety of liposomes through hydrogen bonding between carboxyl groups of the PEAA polymer and the phosphodiester groups of the lipids (Seki & Tirrell, 1984; Tirrell et al., 1985). Research has also shown that PEAA at a low concentration could generate pores in the bilayer at acidic pH, through which the drug release process could be well controlled (Binder, 2008; Thomas & Tirrell, 1992; Torchilin et al., 1993; Yessine & Leroux, 2004). Anionic succinylated poly(glycidol)-coated liposomes have been shown to successfully fuse with the

endosomal/lysosomal membrane and efficiently deliver calcein into the cell cytoplasm (Kono et al., 1997; Sakaguchi et al., 2008; Yuba et al., 2008). In addition, dual responsive liposomes can be developed based on NIPAM copolymers that are sensitive to both pH and temperature (Bertrand et al., 2009; Kaiden et al., 2011; Meyer et al., 1998; Polozova et al., 1999; Polozova & Winnik, 1997). At acidic pH and below their critical solution temperature, the alkyl chains in NIPAMs become more hydrophobic, stimulating the lipid flip-flop (Felber et al., 2012). NIPAMs copolymers are able to destabilize the phospholipid vesicles prepared by lipids with high-temperature phase transition at acidic pHs, such as the liposomes prepared from DSPC (Kono et al., 1999).

However, to date, most reported work focused on modification of the liposomal surface with non-biodegradable synthetic pH-responsive polymers (Drummond et al., 2000; Ferreira et al., 2013; Ganta et al., 2008; Leroux, 2004). This limits their potential clinical application. Development of pH-responsive liposomes coated with biodegradable polymers represents a strategy to solve this problem.

1.5 Aims and objectives of the project

In order to overcome the low cytoplasmic delivery efficiency of most non-viral DDSs, this project aims to develop novel biomimetic nanoscale systems including biodegradable endosomolytic pseudopeptidic polymers and virus-mimicking liposomes for pH-triggered intracellular drug delivery. The specific objectives of this project include:

1) Design and development of pH-responsive, comb-like pseudopeptidic polymers containing relatively long alkyl side chain

Inspired by natural existing membrane proteins which contain long-chain fatty acids, the work presented in this thesis aims to modify PLP by grafting relatively long alkyl side chains to enhance its membrane destabilization activity. Alkyl chains with different lengths will be grafted on the pendent carboxylic groups of PLP at different degrees of substitution to modulate the pH-dependent endosomolytic activity.

2) Systematic study of the physicochemical properties and membrane activity of the comb-like pseudopeptidic polymers

A detailed study was carried out to evaluate the impact of grafted side chains on the physicochemical properties of the polymers. The erythrocyte membrane was applied as a model

membrane to evaluate their pH-dependent membrane destabilization ability. The possible polymer-membrane interaction mechanism was examined.

3) Evaluation of the optimal pH-responsive, comb-like pseudopeptidic polymer for intracellular delivery

The potential of the optimal endosomolytic comb-like pseudopeptidic polymer for intracellular delivery was further explored. Its delivery capacity was evaluated at physiological and tumor pHs. The impact of polymer concentration, treatment time, pHs and the presence of serum on intracellular delivery were studied. Delivery of a wide size range of payloads into 7 different cell types was examined to fully explore the delivery potential of the optimal pseudopepetidic polymer. The cytotoxicity assay was then performed to assess the in vitro toxicity.

4) Development of novel virus-mimicking, endosomolytic liposomes for efficient intracellular delivery

Two types of multifunctional liposomes were developed to mimic the structural and functional traits of influenza virus for efficient intracellular delivery, with the endosomolytic pseudopeptides mimicking the fusogenic peptides present in the viral spikes, the liposomal bilayer structure mimicking the viral envelope, and the drug payload mimicking the viral genome. PP75, which bears hydrophobic amino acid L-phenylalanine as side groups, and PLP-NDA 18%, which bears decylamine as hydrophobic relatively long side chains, displayed vastly superior membrane activity and were employed for liposomal surface modification. Key parameters affecting the pH-responsiveness of the virus-mimicking nanosystems were studied. The mechanism of polymer-liposome interaction was elucidated. The cytotoxicity and intracellular delivery ability of these virus-mimicking liposomal delivery systems loaded with anticancer drug were further evaluated in various types of mammalian cells.

1.6 Novelties and impact of the research

The key novelties of the research are listed below:

- The development of novel virus-mimicking, endosomolytic liposomes through surface modification with PP75 further extended the polymer's application in drug delivery. The published work introduces PP75 as a promising polymeric drug delivery system. The work presented in this thesis is the first report on surface modification of a cholesterol-

containing liposomal system with PP75 to mimic the viral structure and functionality for efficient intracellular drug delivery.

- This project is the first report on development of bio-inspired, membrane-anchoring, comb-like pseudopeptidic polymers. Inspired by membrane proteins containing one or more relatively long fatty chains, which act as membrane anchors to facilitate membrane binding, the research presented here aims to develop a series of novel pH-responsive, membrane-active polymers by grafting PLP with hydrophobic relatively long alkyl side chains at different degrees of substitutions to improve the membrane binding and destabilization activity. A patent has been filed partly based on this work.

- This project also enables the development of a novel simple method for non-toxic, rapid and efficient intracellular delivery of a wide size range payloads into a variety of cell types using the membrane-anchoring, comb-like polymers at mildly acidic pH.

- Another novel virus-mimicking liposomal platform arising from this project is based on surface modification of a cholesterol-containing liposomal system using the novel membrane-anchoring, comb-like polymer. The integrated synergy of pH-triggered liposomal drug release and efficient endosomal escape can facilitate enhanced intracellular drug delivery into a variety of cancer cell lines and overcome multidrug resistance.

The work undertaken in this project will provide a better understanding of key parameters controlling polymer-membrane interaction and intracellular delivery mechanisms. Results generated from the work can be used to enhance the design and development of the novel come-like polymers and virus-mimicking liposomal systems to optimize the delivery of a wide range of therapeutic payloads, including small molecules and macromolecules, to a variety of intracellular target sites. The applicability of these biomimetic delivery systems in various cell types confirms their wide application in disease therapy. The results arising from this project may also provide the basis for more effective treatment to overcome multidrug resistance. This research will also contribute to development of other delivery platforms and biomedical applications. For example, the membrane-anchoring, comb-like polymers are used by other researchers in the same research group on the development of novel nanogels for oral drug delivery and on the intracellular loading of bioprotectants for mammalian cell preservation and cell therapy. In addition, the viral-mimicking liposomal systems are further developed in the same group for targeted thrombolytic therapy. The research is of interest to biopharmaceutical

and healthcare industrial sectors. The delivery platform technologies and knowledge developed from this research are promising to enhance the efficiency of current treatments, therefore improving patients' longevity and life quality.

1.7 Thesis outline

This thesis comprises of 7 chapters, outlined as follows and summarized in Figure 1-14:

Chapter 1 provides an introduction to the field of intracellular delivery, including the barriers to intracellular delivery, historical development and current status of viral and non-viral delivery systems. In particular pH-responsive polymers and pH-sensitive liposomes are discussed, which provides the focus of the research presented within this thesis.

Chapter 2 summarizes the materials and methods used in this project, covering synthesis and characterization of pseduopeptidic polymers, optimized methods for preparing liposomes, and cell assays for evaluation of cytotoxicity and intracellular delivery.

Chapter 3 describes the development and characterization of virus-mimicking liposomes through surface modification with PP75. The key parameters controlling the size and pH-responsiveness of the multifunctional liposomes were systematically examined and the mechanism of polymer-liposome interaction was elucidated. The cellular uptake, subcellular localization and cytotoxicity of drug-loaded multifunctional liposomes were investigated.

Chapter 4 describes the design, synthesis and characterization of a series of pH-responsive, comb-like pseudopeptides for efficient intracellular delivery. PLP was grafted with various hydrophobic relatively long alkyl chains (with different lengths and at various degrees of grafting) as membrane anchors. The effects of polymer structure on pH-responsive aqueous solution properties and membrane destabilizing activity were investigated. The mechanism of polymer-lipid interaction was elucidated.

Chapter 5 describes the method for intracellular delivery of a wide size range of payloads into a variety of cell types, including stem cells and multidrug resistant cells, using the comb-like pseudopeptidic polymers. The effects of polymer concentration, pH, serum, side chain length, and incubation time on the intracellular delivery efficiency were examined. The cytotoxicity and IC_{50} of the polymers were also investigated.

Chapter 6 describes the development of another type of virus-mimicking liposomes through surface coating with the optimal comb-like polymer for an effective intracellular delivery. The

effects of key parameters, e.g. cholesterol proportion, hydrophobicity of the polymer, polymer coating density and dilution effect on the pH-responsiveness of the multifunctional liposomes were investigated. pH-Triggered size change and its mechanism were further explored. Furthermore, intracellular drug delivery and cell-killing activity of the drug-loaded virus-mimicking system were tested using four different cancer cell lines (including drug-resistant cell line).

Chapter 7 presents general conclusions and major achievements of this project based on the preceding results chapters, and also the recommendations for future work.

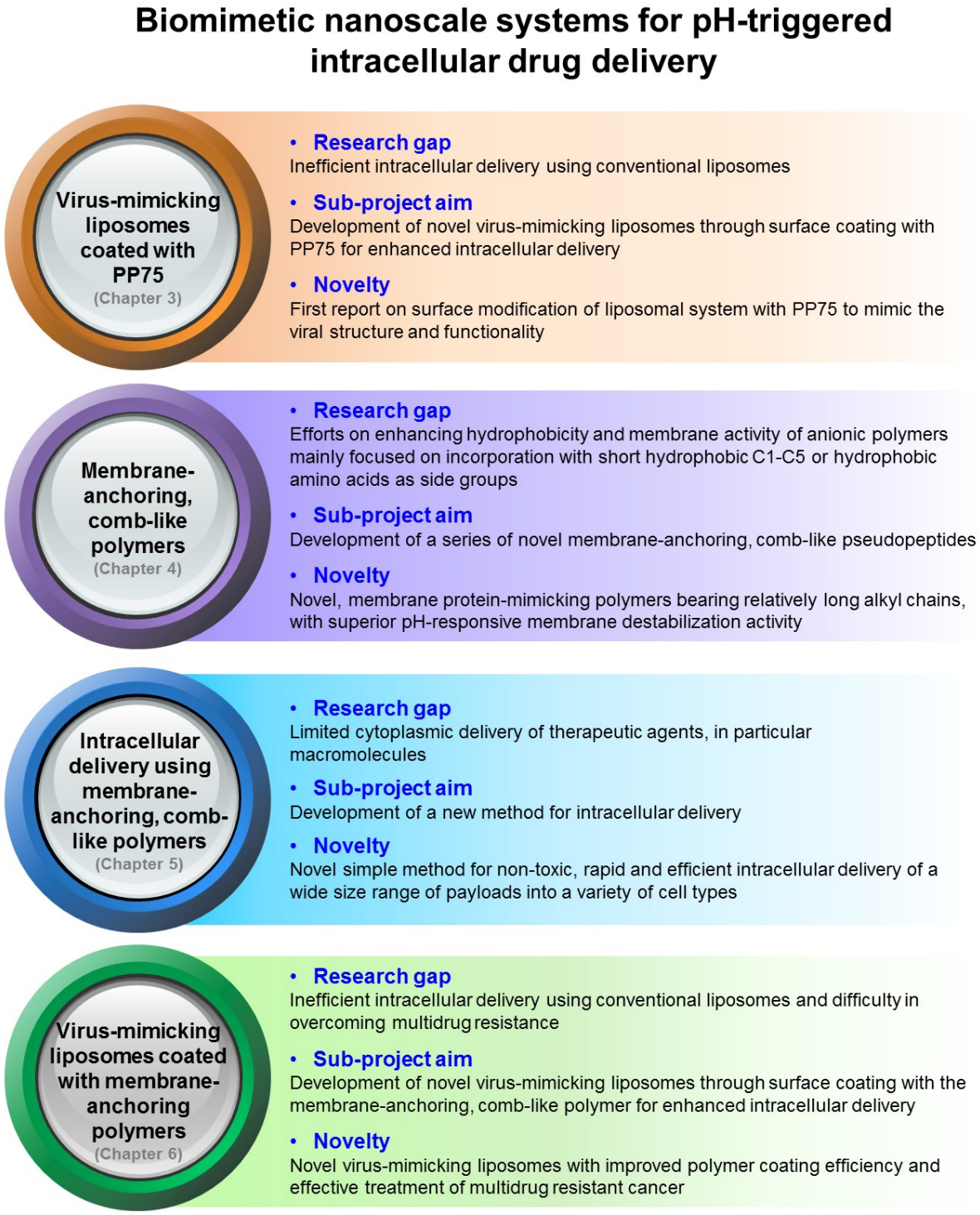

Figure 1-14. Scheme of the thesis outline, summarizing the research gap, aim and novelty for each sub-project.

Chapter 2

Materials and methods

This chapter covers detailed information about the materials and methods used to complete the research contained in this thesis. The materials listed include chemicals, solvents, reagents, cell lines, cell culture media, assay kits and instruments. The methods include synthesis and characterization of a variety of pseudopeptidic polymers, liposomal preparation and modification, and cell assays determining the drug delivery potential and cytotoxicity of these delivery vesicles.

2.1 Materials

EPC, cholesterol, *iso*-phthaloyl chloride, 6-aminofluorescein, Dulbecco's modified Eagle's medium (DMEM), McCoy's 5A modified medium, MEM non-essential amino acid solution (100×), fetal bovine serum (FBS), Dulbecco's phosphate buffered saline (D-PBS), RPMI-1640 medium, minimum essential medium Eagle, penicillin, calcein, pyrene, decylamine (NDA), heptylamine (HDA), tetradecylamine (TDA), octadecylamine (ODA), fluorescein isothiocyanate-dextran (FITC-dextran, average M_w = 4 k, 10 k, 70 k, 150 k and 2000 kDa) and doxorubicin (DOX) were purchased from Sigma-Aldrich (Dorset, UK).

Dimethyl sulfoxide (DMSO), triethylamine, *N,N*-dimethylformamide (DMF), 4-dimethylaminopyridine (DMAP), sodium chloride, hoechst 33342, alamar blue, Texas Red® hydrazide and Pierce™ LDH cytotoxicity assay kit, LysoTracker® red DND-99, *N*-(7-nitrobenz-2-oxa-1,3-diazol-4-yl)-1,2-dihexadecanoyl-*sn*-glycero-3-phosphoethanolamine (NBD-PE) and Lissamine™ rhodamine B 1,2-dihexadecanoyl-*sn*-glycero-3-phosphoethanolamine (Rh-PE) were purchased from Fisher Scientific (Loughborough, UK).

Anhydrous ethanol, acetone, hydrochloric acid, d_6-DMSO, potassium carbonate, sodium hydroxide, chloroform, methanol, diethyl ether, trithylamine, sodium citrate dehydrate and sodium phosphate were obtained from VWR (Lutterworth, UK).

N-(2-hydroxyethyl) piperazine-*N'*-(2-ethanesulfonic acid) (HEPES), ninhydrin, L-lysine methyl ester dihydrochloride, L-phenylalanine methyl ester hydrochloride, *N,N'*-dicyclohexylcarbodiimide (DCC) and triton® X-100 were purchased from Alfa Aesar (Heysham, UK).

Defibrinated sheep red blood cells (RBCs) were obtained from TCS Biosciences Ltd (Buckingham, UK).

2.2 Methods

2.2.1 Polymer synthesis

2.2.1.1 PLP synthesis

PLP was synthesized in house using the single phase polymerization technique according to the method published by Eccleston (Eccleston et al., 1999).

2.2.1.1.1 Polycondenzation

L-lysine methyl ester·2 HCl (0.15 mole) and potassium carbonate (0.6 mole) were dissolved in 750 mL of deionized water and stirred in an ice bath. Anhydrous *iso*-phthaloyl chloride (0.2 M) was dissolved in 750 mL pre-cooled dried acetone and rapidly poured into the aqueous solution and stirred at the maximum speed. The reaction was allowed to proceed until precipitation of poly(L-lysine methyl ester *iso*-phthalamide) (PLP methyl ester). The polymer was washed several times with deionized water to remove excess solvent, and dried overnight in the oven at 70 °C. After the polymer was totally dried, the polymer was blended into white powder.

2.2.1.1.2 Ester hydrolysis

NaOH (2.5 molar equivalents to PLP methyl ester) was dissolved in anhydrous ethanol to a final concentration of 5 wt% and added to a solution of PLP methyl ester in dry DMSO (0.5 M). The hydrolyzed product precipitated out in 5-10 minutes, and was collected by vacuum filtration and re-dissolved in deionized water.

2.2.1.1.3 Purification

0.2 M HCl solution was added to the solution to precipitate the polymer. The precipitation was collected by vacuum filtration and re-dissolved in deionized water with 0.2 M NaOH. The precipitation-filtration-re-dissolution process was carried out at least three times.

Dialysis was performed to remove inorganic salts, residual organic solvents and low molecular weight oligomers for purification. The crude polymer solution was dialyzed in Visking tubing membrane (Medicell, MWCO 12-14 kDa) against deionized water for 5 days.

The deionized water was frequently changed to maintain the concentration gradient. After dialysis, the clear polymer solution was adjusted to pH 7.4 using NaOH aqueous solution, and lyophilized to produce PLP in the sodium salt form. In order to prepare PLP in acidic form for structure characterization and side chain modification, the dialyzed polymer solution was acidified to pH ~ 3.0 with 0.2 M HCl solution. The precipitate was collected by vacuum filtration, washed with deionized water to remove HCl, and lyophilized to fine white powder.

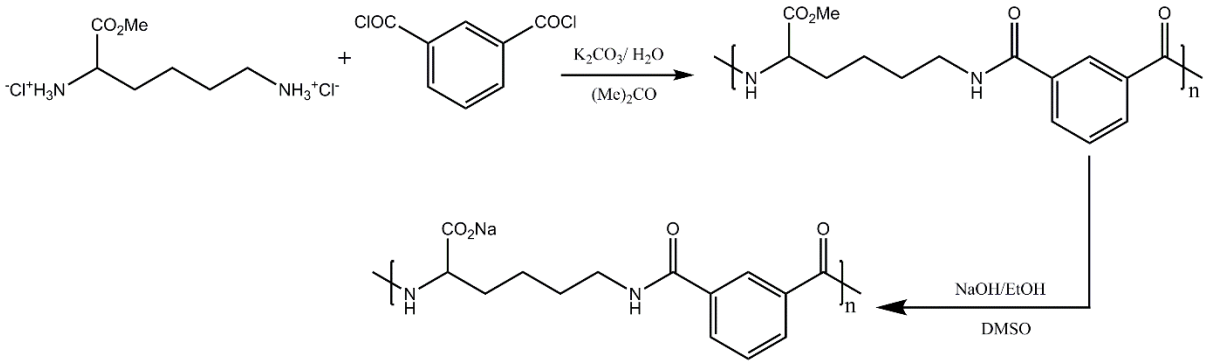

Figure 2-1. Schematic of PLP synthesis.

2.2.1.2 PLP grafted with phenylalanine

Phe was grafted onto the carboxylic acid groups of PLP via DCC/DMAP coupling to synthesize PP25, PP50 and PP75 as reported by Chen et al. 2009a. The number (25, 50, or 75) indicates the stoichiometric ratio of Phe relative to carboxylic acid used for grafting during synthesis.

PLP (3.0 g), L-phenylalanine methyl ester hydrochloride (0.58 g for PP25, 1.17 g for PP50 and 1.76 g for PP75), triethylamine (2.4 molar equivalents of Phe) and DMAP (0.6 g) were dissolved in 60 mL anhydrous DMSO/DMF (1:3 v:v). DCC (3 molar equivalents of Phe) was dissolved in 20 mL anhydrous DMF and added dropwise to the previous solution. The reaction was proceeded at room temperature for around 60 h.

After 60 h of reaction, solid impurities and the side product dicyclohexylurea were removed by vacuum filtration. Sodium hydroxide in anhydrous ethanol (5 wt%, 28 mL) was added to the filter to hydrolyze for 3 h. PP25 was precipitated directly out in 5 min, the precipitation was collected by vacuum filtration and re-dissolved in deionized water. PP50 and PP75 remained in solution after hydrolysis. Five volumes of diethyl ether was rapidly poured into

the remaining solution to precipitate PP50 and PP75. The precipitation was collected and re-dissolved in deionized water. Dialysis was performed to purify the polymers. Salt and acidic form of the polymers was prepared as described before.

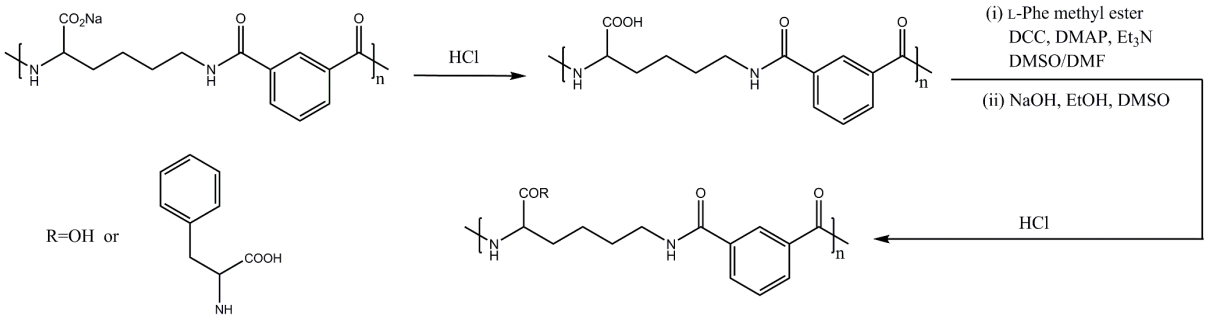

Figure 2-2. Schematic of PLP grafted with L-phenylalanine synthesis.

2.2.1.3 PP75 grafted with 6-aminofluorescein

Fluorophore-labelled PP75 was prepared by conjugating 6-aminofluorescein to its pendant carboxylic acid groups by DCC/DMAP coupling. A low level of labeling at 2 mol% was chosen to avoid a significant change to the properties of the pseudopeptide. Briefly, PP75 (200 mg), 6-aminofluorescein (38 mg) and DMAP (40 mg) were dissolved in anhydrous DMF (5 mL). DCC (3 molar equivalents to 6-aminofluorescein) dissolved in anhydrous DMF (200 μL) was added dropwise to the reaction solution and the reaction was carried out in room temperature for overnight. The reaction solution was centrifuged at 10,000 rpm to remove the solid impurities, and supernatant was then collect and added into five volumes of diethyl ether. The precipitation was collected and re-dissolved in deionized water by adding 0.2 M NaOH. After filtration, the polymer solution was dialyzed against deionized water in a Visking dialysis tubing (Medicell, MWCO 12-14 kDa). After dialysis, the pH of the polymer solution was adjusted to pH 7.4 and lyophilization was carried out.

2.2.1.4 PLP grafted with hydrophobic anchors

HDA, NDA, TDA or ODA was conjugated onto the PLP backbone at various degrees of substitution via DCC/DMAP coupling. PLP (3 g) and DMAP (0.6 g, 20 wt% of PLP) were dissolved in anhydrous DMSO/DMF (1:3 v:v). HDA, NDA, TDA or ODA was dissolved in chloroform and then transferred to the reaction solution. DCC (3 molar equivalents of NDA, HDA, TDA or ODA) in anhydrous DMF was added dropwise. The progress of the reaction

was monitored by thin-layer chromatography ($CHCl_3$:MeOH:trithylamine= 8:2:0.2, ninhydrin was applied to detect amine). In the end of the reaction, solid impurities were removed by vacuum filtration and the reaction solution was added with 5 wt% NaOH in anhydrous ethanol and precipitated rapidly into five volumes of diethyl ether. The precipitate was collected by vacuum filtration and re-dissolved in deionized water. 0.2 M HCl solution was added to the solution to precipitate the polymer out. The precipitated polymer was collected and re-dissolved in deionized water with 0.2 M NaOH. The polymer was further purified by dialysis against deionized water in a Visking dialysis tubing (Medicell, MWCO 12-14 kDa). After dialysis, the polymer solution was titrated to pH 7.4 using 0.2 M NaOH, filtrated and then lyophilized. To prepare acidic form, the dialyzed polymer solution was acidified to around pH 3.0 using 0.2 M HCl. The precipitate was washed with deionized water three times, collected by vacuum filtration and lyophilized.

2.2.1.5 PLP-NDA 18% grafted with 6-aminofluorescein

Fluorophore-labelled PLP-NDA 18% was prepared by conjugating 6-aminofluorescein to its pendant carboxylic acid groups by DCC/DMAP coupling. The labeling percentage was the same as fluorophore labelled PP75 (2 mol%) to minimize the change of polymer properties. The DCC/DMAP reaction process was similar as conjugating 6-aminofluorescein to PP75 as described before.

2.2.2 Polymer characterization

The compositions, polymer structure, conformational behavior, critical association concentration (CAC), optical density, hydrodynamic size and membrane disruption activity of the polymers were characterized by Fourier Transform Infrared (FT-IR) spectroscopy, nuclear magnetic resonance (NMR) spectroscopy, fluorescence spectroscopy using pyrene as a probe, transmittance measurement, dynamic light scattering (DLS) and hemolysis assay. The detail for the measurements is described as below.

2.2.2.1 Fourier Transform Infrared (FT-IR) Spectroscopy

Fine acidic polymer powder was pressed into a pellet and FT-IR spectra were recorded on a Spectrum 100 FT-IR Spectrometer (Perkin Elmer, USA).

2.2.2.2 Nuclear Magnetic Resonance (NMR) Spectroscopy

Acidic polymers powder was dissolved in d_6-DMSO and ^{1}H-NMR spectra were obtained using a 400 MHz NMR spectrometer (Bruker, Germany) at room temperature.

The degree of substitution of each polymer was determined by ^{1}H-NMR spectroscopy in d_6-DMSO. The ratio of the integral 7.11-7.33 ppm to the integral 7.45-7.64 ppm was used to calculate the degree of substitution for the PLP polymer grafted with Phe. The number (25, 50, or 75) indicates the stoichiometric degree of substitution.

The ratio of the integral 0.77-0.91 ppm to the integral 7.45-7.64 ppm was used to calculate the degree of substitution for the PLP polymer grafted with hydrophobic relatively long alkyl chains (HDA, NDA, TDA or ODA). PLP-NDA 3%, 10% and 18% are expressed as the numbers of NDA grafts per 100 carboxylic acid groups along the parent backbone (mol%). The degree of substitution and the M_w of PLP were then used to calculate the molecular weight of the PLP derivatives.

2.2.2.3 Fluorescence spectroscopy

Pyrene, a microenvironmental-polarity-sensitive probe, was used to investigate the conformational behavior of polymers in aqueous solution (Aguiar et al., 2003). 1.0 mM pyrene solution was freshly prepared in absolute methanol and was added to each polymer sample to give a final pyrene concentration of 600 nM. The polymer samples were wrapped with foil to protect from light and equilibrated for 48 h before measurement. The excitation intensities at wavelengths of 338 and 333 nm (with an emission wavelength of 390 nm) of the polymer solution containing pyrene were measured and recorded on a spectrofluorometer (FluoroMax, HORIBA, Japan). The fluorescence intensity ratio of I_{338}/I_{333} was calculated.

The CAC was also calculated based on fluorescence excitation spectra of pyrene. Pyrene was added to polymer solutions to give a final pyrene concentration of 600 nM and I_{338}/I_{333} was measured as described previously. The CAC was calculated as the intersection point of the slopes of a flat region and a dramatic rising region in the plot of I_{338}/I_{333} against the concentration of polymer.

2.2.2.4 Transmittance

The optical densities of polymer solutions at different pHs were investigated on a UV-Vis spectrophotometer (Genesys 10s UV-Vis, Thermo Scientific, UK) at 480 nm. Polymer

solutions were prepared with buffers at different pHs and equilibrated for 48h before measurement.

2.2.2.5 Dynamic light scattering

The hydrodynamic size and polymer size distribution were explored based on a dynamic light scattering platform (Zetasizer Nano S, Malvern, UK). The polymer aqueous solutions were prepared in the buffers at specific pHs, filtrated through 0.45 μm filter (Milipore) and equilibrate for 48 h before measurement. The size measurement was conducted in a 10 mm diameter cell with scattering angle of 137°, repeated for 11 times for each run.

2.2.2.6 Hemolysis assay

Hemolysis assay was applied to exam the membrane disruptive activity of polymers (Chen et al., 2009c). The polymer stock solution was added into 0.1 M phosphate buffer or 0.1 M citric buffer to achieve polymer buffer solution at different polymeric concentrations and pHs. Sheep RBCs were washed at least three times with 150 mM NaCl solution and the polymer buffer solution was used to resuspend the RBCs pellet. The final cell concentration was controlled within the range of $1 - 2 \times 10^8$ RBCs mL^{-1}. Negative control (RBCs in buffer only, without the present of polymer) and positive control (RBCs lysed with deionized water) were prepared with the same cell density. The samples were incubated at 37 °C in a shaking water bath (120 rpm) for 1 h, and then centrifuged at 4000 rpm for 4 min. The supernatant was collect and measured the absorbance at 540 nm using UV-Vis spectrophotometer to evaluate the hemoglobin release. The relative hemolysis percentage was calculated using Equation 2-1:

$$\text{Relative hemolysis (\%)} = \frac{\text{Experimental absorbance} - \text{negative control absorbance}}{\text{Experimental absorbance} - \text{positive control absorbance}} \times 100\%$$

(Equation 2-1)

2.2.3 Liposomes preparation, polymer modification and characterization

2.2.3.1 Conventional liposome preparation

Conventional liposomes were prepared using the lipid film hydration method (Guo et al., 2015). Briefly, cholesterol and EPC with required ratios were mixed and dissolved in chloroform containing 1% (v/v) ethanol. The organic solvent was removed by rotary evaporation for overnight and a lipid film was formed. The lipid film was hydrated with 5 mL

of HBS buffer (20 mM HEPES, 150 mM NaCl, titrated to pH 7.4) at 40 ºC for 1 h. The size of the liposomes was further decreased by sonication (Sonicator, 120 watt, Fisher Scientific) for certain time. After filtration through a 0.22 μm filter, the sample was stored at 4 °C.

2.2.3.2 Drug loading

To encapsulate the model drug calcein into the liposomes, a lipid film was prepared and hydrated with HBS buffer containing 100 mM calcein. After sonication and filtration, free calcein was removed by gel filtration chromatography using sephadex G-50.

DOX-loaded liposomes were prepared using the same method. The lipid film was hydrated with HBS buffer containing 1 mg mL^{-1} DOX. After sonication and filtration, free DOX was removed by dialysis against HBS buffer at pH 7.4 at 4 °C for 3 h.

2.2.3.3 Virus-mimicking liposomes preparation

Virus-mimicking liposomes were prepared by incubation of the conventional liposomes with an aqueous solution of a specific pseudopeptidic polymer (in HBS buffer at pH 7.4) at a desired concentration for overnight at room temperature. Multifunctional liposomes were further purified through dialysis (Float-A-Lyzer®, MWCO 300 kDa, Spectrumlabs, USA) against the HBS buffer (pH 7.4) for 7 h to remove excess pseudopeptides. Buffer was frequently refreshed to ensure the efficiency of dialysis.

In order to quantitatively determine the polymer adsorption on the liposomal membrane, the fluorophore-labelled pseudopeptidic polymers were used to modify the liposomes following the step described in the Section 2.2.3.3. The fluorescence intensity of the fluorescent polymer adsorbed on liposomes surface was measured by a spectrofluorometer (GloMax®-Multi Detection System, Promega, USA) at an excitation wavelength of 490 nm and emission wavelength from 510 to 570 nm. The polymer adsorption amount was calculated based on the standard linear curve of fluorescence intensity versus the fluorescent polymer concentration.

2.2.3.4 Measurement of pH-responsive liposomal drug release

The content release from the virus-mimicking liposomes mediated by the polymer coating layer at different pHs was explored by a fluorescence dequenching assay (Guo et al., 2002). The membrane-impermeable dye calcein was applied as a model drug and was incorporated into the liposomes at a self-quenching concentration (100 mM). The pH of virus-mimicking liposomes was controlled to the desired value by acidification with 1 wt% HCl. An aliquot was

withdrawn and equilibrated at 37 ºC for 1 h. Then the pH was adjusted back to 6.5 – 7.5 in order to minimize the effect of pH on calcein fluorescence. The fluorescence intensity was determined by the spectrofluorometer (GloMax®-Multi Detection System, Promega, USA) with excitation wavelength of 490 nm and emission at 510 – 570 nm. The release percentage was calculated using Equation 2-2:

$$\% \text{ Release} = \frac{F_t - F_0}{F_{max} - F_0} \times 100\% \qquad \text{(Equation 2-2)}$$

Where F_0 is the initial fluorescence, F_t is the fluorescence intensity at time t and F_{max} represents the fluorescence upon addition of triton® X-100 to completely lyse liposomal membranes.

For the measurement of calcein release from liposomes upon dilution, the calcein-loaded virus mimicking liposomes were diluted for different folds with HBS buffer at pH 7.4 and then the pH was acidified to 4.5 with 1 wt% HCl. The release percentage was determined using the method described before.

2.2.3.5 Encapsulation efficacy and loading capacity

The encapsulation efficacy of DOX into the liposomes was analyzed by measuring DOX concentration before and after purification. The liposomes were lysed with ethanol and further processed by sonication 10 min to totally dissolve the lipids and DOX. The concentration of DOX before and after purification was determined by absorbance measurement at a wavelength of 495 nm with a UV-Vis spectrophotometer (Genesys 10s UV-Vis, Thermo Scientific). The encapsulation efficacy was calculated using Equation 2-3.

$$\text{Encapsulation efficacy (\%)} = \frac{\text{DOX concentration of the liposomes sample after purification}}{\text{DOX concentration of the liposomes sample before purification}} \times 100\% \qquad \text{(Equation 2-3)}$$

2.2.3.6 pH-Dependent change of liposomal size

DLS was applied to investigate the hydrodynamic size change of the conventional and virus-mimicking liposomes at different pHs. The liposomes were diluted with specific HBS or citrate buffer and equilibrated for 5 min to yield an appropriate counting rate and then analyzed by DLS (Zetasizer Nano S, Malvern, UK) at an angle of 137º in 10 mm diameter cells at 25 ˚C, repeated for 11 times.

To measure the reversibility of the liposomal size change in response to pH, the virus-mimicking liposomes at pH 7.4 were titrated to pH 4.5 using 1% HCl and back to pH 7.4 using 0.1 M NaOH, and then repeated for several cycles. The size was measure by DLS after 5 min of each titration. In order to visualize the change of liposomal size, the fluorescent polymer-modified liposomes were imaged by laser scanning confocal microscopy (Zeiss LSM-510 inverted laser scanning confocal microscope, Germany) at the excitation wavelength of 488 nm and the emission wavelength of 535 nm.

2.2.3.7 Lipid mixing assay

In order to study whether membrane fusion occurred with the size increase, the lipid mixing assay by monitoring NBD-Rh energy transfer was carried out. Labelled conventional liposomes were prepared with 1 mol% of donor lipid probe (NBD-PE) and 1 mol% of acceptor lipid probe (Rh-PE) and then coated with the pseudopeptide to prepare virus mimicking liposomes. Unlabeled liposomes were mixed with the labelled liposomes at a ratio of 9:1 (v/v) for certain time and the membrane fusion would occur only if there was an increase in NBD fluorescence (excitation 490 nm, emission 510-570 nm) caused by the reduced amount of fluorescence energy transfer from NBD to rhodamine (Rh). The lipid mixing percentage was calculated using Equation 2-4.

$$\text{Lipid mixing } \% = \frac{F_t - F_0}{F_{max} - F_0} \times 100\% \qquad \text{(Equation 2-4)}$$

F_t is the fluorescence intensity at each time point, F_0 is the initial fluorescence intensity and F_{max} is the fluorescence intensity of the sample solubilized with triton® X-100.

2.2.3.8. Hemolysis assay of virus-mimicking liposomes

The membrane disruptive activity of the virus-mimicking liposomes was examined by hemolysis assay to verify if the polymer adsorbed on the liposomal membrane still retains its membrane functionality. Liposomal samples were prepared at required concentrations in the phosphate or citrate buffer at specific pHs. Defibrinated sheep red blood cells (RBCs) were washed three times with NaCl aqueous solution (150 mM) to achieve a pellet, and resuspended in the liposomal solutions to a final RBC concentration of $1 - 2 \times 10^8$ RBC mL^{-1}. The samples were incubated at 37 ˚C for 1 h with shaking, and then centrifuged at 4000 rpm for 4 min. The absorbance of the supernatant was measured at 541 nm with a UV-Vis spectrophotometer

(GENESYS™ 10S UV-Vis, Thermo Scientific, USA), and the hemolysis percentages were calculated.

2.2.4 Cell study

2.2.4.1 Cell culture

HeLa adherent epithelial cells (human cervical cells) and A549 adherent epithelial cells (human lung cells) were grown in DMEM supplemented with 10% (v/v) FBS and 100 U mL^{-1} penicillin unless specified otherwise. CHO adherent epithelial cells (Chinese hamster ovary cells) were cultured in DMEM supplemented with 1% (v/v) non-essential amino acids, 10% (v/v) FBS and 100 U mL^{-1} penicillin unless specified otherwise. The HeLa, A549 and CHO cells were trypsinized using trypsin-EDTA and maintained in a humidified incubator with 5% CO_2 at 37 ºC.

MES-SA adherent epithelial cells (human uterus cells) and the corresponding multi-drug resistant cells MES-SA/DX5 were cultured in McCoy's 5a medium containing 10% (v/v) FBS and 100 U mL^{-1} penicillin unless specified otherwise. The MES-SA and MES-SA/DX5 cells were subcultured with EDTA solution (0.8 mM disodium EDTA, 68.5 mM NaCl, 6.7 mM sodium bicarbonate, 5.6 mM glucose and 5.4 mM KCl) and maintained in a humidified incubator with 5% CO_2 at 37 ºC.

SU-DHL-8 suspension B lymphocyte cells (human lymph node cells) were grown in RPMI-1640 medium supplemented with 10% (v/v) FBS and 100 U mL^{-1} penicillin and kept in a humidified incubator with 5% CO_2 at 37 ºC.

Mesenchymal stem cells (hMSC) (human bone marrow derived) were cultured in minimum essential medium Eagle containing 10% FBS and 100 U mL^{-1} penicillin. The cells were trypsinized using trypsin-EDTA and maintained in a humidified incubator with 5% CO_2 at 37 ºC.

2.2.4.2 Laser scanning confocal microscopy

2.2.4.2.1 Laser scanning confocal microscopy of RBCs

To investigate the mechanism of cell membrane destabilization, laser scanning confocal microscopy of RBC was performed. RBCs were washed three times with 150 mM NaCl, and then resuspended with buffers at specific pHs with 10 μM FITC-dextran and 1 μM Texas Red®

hydrazide with or without the presence of polymer at a cell concentration of 10^7 RBCs mL^{-1}. The RBCs were then imaged using a laser scanning confocal microscope (LSM-510 inverted, Zeiss, Germany) at 37 ºC. FITC and Texas red were excited at 488 and 543 nm respectively.

2.2.4.2.2 Endosomal escape of calcein co-treated with virus-mimicking liposomes

In order to verify whether the virus-mimicking liposomes can induce endosomal escape, calcein, a membrane-impermeable dye was used as a tracer molecule. 2 mL of HeLa cells (1×10^5 cells mL^{-1}) were cultured in a glass-bottom dish (35 mm, MatTek, USA) for overnight followed by the treatment with 2 mL of the serum free DMEM containing 3.2 mM calcein and the virus-mimicking liposomes or bare liposomes (with a fixed polymer-to-lipid molar ratio at 1.9:100). After incubation at 37 ºC for 2 h, the cells were washed with D-PBS for three times and replaced with fresh DMEM serum free medium for 2 h of further incubation. Hoechst 33342 (1 μg mL^{-1}) and LysoTracker (50 nM) were used to stain nuclei and endosomes/lysosomes respectively. The cells were then imaged using a laser scanning confocal microscope as described above. Calcein was excited at 488 nm and the emission at 535 nm was collected.

2.2.4.2.3 Intracellular delivery of DOX using the virus-mimicking liposomes

The intracellular delivery of DOX to a variety of cell lines was examined by confocal microscopy. 2 mL of cells (1×10^5 cells mL^{-1}) were seeded into a 35 mm glass-bottom dish and cultured for overnight. The spent medium was replaced with 1 mL of serum free medium containing 0.22 μm filter-sterilized, free DOX or DOX-loaded liposomal samples with or without polymer coating at the fixed DOX concentration of 2.5 μM. After 1 h incubation, the cells were washed with D-PBS buffer and stained by Hoechst 33342 at 1 μg mL^{-1}. The cells were imaged using the laser scanning confocal microscope. DOX was excited at 480 nm and the emission at 560 nm was collected.

2.2.4.2.4 Subcellular localization of virus-mimicking liposomes

The virus-mimicking liposomes were incorporated with 1 mol% Rh-PE to visualize their subcellular localization. 2 mL of HeLa cells (1×10^5 cells mL^{-1}) were seeded into a glass-bottom dish and cultured for overnight. The cells were treated with serum free DMEM containing the virus-mimicking liposomes with 1 mol% Rh-PE in the lipid membrane in the presence or absence of polymer coating. After 1 h of treatment, the cells were washed with D-PBS for three times and incubated with fresh serum free DMEM for further incubation of 3 h.

Afterwards, the cells were stained with Hoechst 33342 at 1 μg mL^{-1} and imaged by laser scanning confocal microscopy. Rh was excited at 543nm and emission at 580 nm was collected. Hoechst was excited at 405 nm and emission at 505 nm was collected.

2.2.4.2.5 Endosomal escape of PLP-NDA 18%

The endosomal escape ability of PLP-NDA 18% in HeLa, CHO and A549 cell lines was determined using calein as a tracer molecular. Briefly, 2 mL of cells (1×10^5 cells mL^{-1}) were cultured into a glass-bottom dish for overnight. The cells with 1 mL of the serum free culture medium containing 3.2 mM calcein and 0.5 mg mL^{-1} PLP-NDA 18% or PLP. After incubation at 37 °C for a certain period of time depending on the types of cell lines, the cells were washed with D-PBS for three times and replaced with fresh serum free medium for further incubation. The cells were then stained with LysoTracker (50 nM) and Hoechst 33342 (1 μg mL^{-1}) and then imaged as described above.

2.2.4.2.6 Intracellular delivery of payloads by the pseudopeptidic polymer

The ability of the pseudopeptidic polymers to deliver a wide size range of FITC-labelled dextran (4 – 2000 kDa) was tested in 7 different cell liens. Adherent cells were cultured in a glass-bottom dish at a total cell number of 2×10^5 cells for overnight followed by treatment with PBS containing the pseudopeptidic polymer and FITC-dextran at specific concentrations and pHs for a certain period of time. The cells were then washed with D-PBS and stained with LysoTracker and Hoechst and imaged as described above. For the suspension cell (SU-DHL-8), the cells were centrifuged and resuspended with 1 mL of PBS buffer containing the pseudopeptidic polymer and FITC-dextran to reach a final cell concentration of 4×10^5 cells mL^{-1}. After 30 min of incubation, the cells were centrifuged to remove the supernatant and resuspended with D-PBS for three times and stained with LysoTracker and Hoechst before imaging.

2.2.4.3 Flow cytometry

2.2.4.3.1 Cellular uptake of Rh-PE-labelled liposomes

Flow cytometry was employed to quantitatively evaluate the cellular uptake of the Rh-PE-labelled liposomes with or without polymer coating. HeLa cells were cultured in a 6-well plate (3×10^5 cells per well) for overnight and treated with 1 mL of serum free DMEM containing the liposomes labelled with 1 mol% Rh-PE in the presence of absence of polymer coating.

After 1 h of incubation, the cells were washed with D-PBS for three times and further incubated with serum free DMEM for 3 h. The cells were then detached using trypsin and centrifuged at 1000 rpm. The cell pellet was resuspended in serum free DMEM and filtered through 40 μm FlowmiTM tip strainers (Bel-Art, USA) to remove cell aggregates. The flow cytometry measurements were carried out using an LSRFortessa cell analyzer (BD, USA) with an excitation wavelength of 543 nm.

2.2.4.3.2 Cellular uptake of DOX-loaded liposomes

Cells were cultured in a 6-well plate (5×10^5 cells per well) for overnight followed by 1 h of treatment with 1 mL of serum free cell culture medium containing free DOX, DOX-loaded bare liposomes or DOX-loaded, virus-mimicking liposomes. The DOX concentration for all the samples was fixed at 2.5 μM. Afterwards, the cells were washed with D-PBS for three times, detached by trypsin or EDTA and then centrifuged. The cell pellet was resuspended in serum culture medium and filtered before measurement by flow cytometry with an excitation wavelength of 488 nm.

2.2.4.3.3 Intracellular delivery of FITC-dextran by the pseudopeptidic polymer

Adherent cells were cultured in a 6-well plate (3×10^5 cells per well) for overnight and treated with 1 mL PBS containing the pseudopeptides and FITC-dextran at specific concentrations for a certain period of time. Afterwards, the cells were washed with D-PBS for three times, detached using trypsin and then centrifuged at 1000 rpm. The cell pellet was resuspended in serum free culture medium and filtered through 40 μm Flowmi^{TM} tip strainers (Bel-Art, USA) to remove cell aggregates. SU-DHL-8 suspension cells (8×10^5 cell mL^{-1}) were treated with PBS containing the polymers and FITC-dextran for 30 min. The cells were then centrifuged to remove the supernatant and filtered. The flow cytometry was carried out with an LSRFortessa cell analyzer at excitation wavelength of 488 nm.

2.2.4.4 Alamar Blue assay

2.2.4.4.1 In vitro cytotoxicity of the virus-mimicking liposomes

The cytotoxicity of the virus-mimicking liposomes was studied by Alamar Blue assay. Cells were cultured in a 96-well plate (Corning, USA) at a density of 10^4 cells per well for overnight. The spent medium was replaced with 0.1 mL of liposomes (with or without polymer coating) in serum free culture medium. Negative and positive controls were performed by incubating

cells with 0.1 mL serum free DMEM or totally lysed by 1% triton® X-100 respectively. After incubation for a certain period of time, the cells were washed three times with D-PBS and incubated with culture medium containing 10% (v/v) Alamar Blue for 4 h. The fluorescence in each well was measured by the spectrofluorometer at excitation of 525 nm and emission of 580-640 nm. The cytotoxic effect was determined from the fluorescence readings. The cell viability was calculated according to equation 2-5.

$$\text{Cell viability (\%)} = \frac{F_t - F_0}{F_{max} - F_0} \times 100\% \qquad \text{(Equation 2-5)}$$

F_t is the fluorescence intensity of the cells treated with sample, F_{max} is the fluorescence intensity of the cells treated with culture medium without sample and F_0 is the fluorescence intensity of the cells lysed with triton® X-100.

2.2.4.4.2 In vitro cytotoxicity of the DOX-loaded, virus-mimicking liposomes

The potency of the DOX-loaded, virus-mimicking liposomes compared to free DOX or DOX-loaded bare liposomes was investigated by Alamar Blue assay. Various types of cells (10^4 cells per well) were seeded into a 96-well plate (Corning, USA) and cultured for overnight. The spent medium was removed and replaced with 0.1 mL of serum free medium with free DOX, DOX-loaded bare liposomes or DOX-loaded virus-mimicking liposomes. After 24 h of incubation, the cells were washed three times with D-PBS and further incubated with fresh serum free culture medium for 24 h. The cells were then treated with complete culture medium containing 10% (v/v) Alamar Blue and the fluorescence was measured as described above. The concentrations leading to half inhibition, IC_{50}, were calculated from the concentration-dependent cell viability curves.

2.2.4.4.3 In vitro cytotoxicity of the pseudopeptidic polymers

The cytotoxicity of the pseudopeptidic polymers was studied by Alamar Blue assay. 10^4 cells per well were seeded in a 96-well plate with complete culture medium for overnight followed by treatment with 0.1 mL serum free culture medium or PBS containing the pseudopeptidic polymer at specific concentrations at pH 7.4 or 6.5. After a certain period of time, the cells were washed three times with D-PBS and incubated with DMEM with 10% (v/v) Alamar Blue for 4 h. The fluorescence was determined and cell viability was calculated as described above.

2.2.4.5 Lactate dehydrogenase (LDH) assay

The cell membrane integrity was investigated by LDH assay. HeLa cells (10^4 cells per well) were seeded into a 96-well plate (Corning, USA) and cultured for overnight. The cells were then treated with 0.1 mL of serum free DMEM containing the virus-mimicking liposomes or bare liposomes at various lipid concentrations. Negative and positive controls were carried out by incubating cells with 0.1 mL serum free DMEM or totally lysed by 1% triton® X-100 respectively. After 24 h of incubation, 50 μL of supernatant in each well was transferred to a new plate and mixed with the reaction mixture from the LDH Cytotoxicity Assay Kit. After 30 min of incubation, the stop solution was added to stop the reaction and the absorbance at 490 nm was measured by the spectrofluorometer (GloMax-Multi Detection System, Promega, USA) using 680 nm as reference. The cell viability was calculated using the equation 2-6.

$$\text{Cell viability (\%)} = \frac{A_t - A_0}{A_{max} - A_0} \times 100\% \qquad \text{(Equation 2-6)}$$

A_t is the absorbance of the cells treated with sample, A_{max} is the absorbance of the cells treated with culture medium without sample and A_0 is the absorbance of the cells lysed with triton® X-100.

Chapter 3

Development of multifunctional liposomes coated with PP75

This chapter describes the development of novel, multifunctional liposomes coated with the bio-inspired, fusogenic pseudopeptides to mimic the structural and functional traits of an influenza virus for controllable and efficient intracellular drug delivery. The preparation of liposomes was optimized by using different sonication types and different fabrication times. A library of pH responsive pseudopeptides were synthesized to mimic the endosomolytic behavior of influenza viral peptides via grafting a hydrophobic amino acid, L-phenylalanine, onto the backbone of a polyamide, PLP, at different degrees of substitution. The pseudopeptidic polymers were used to modify the surface of cholesterol-containing liposomes that mimics the viral envelope. The effects of cholesterol, polymer hydrophobicity, polymer concentration, dilution and modification time on the pH-dependent release behavior were systematically examined. The mechanism of polymer-liposome interaction was proposed. Furthermore, DOX, a widely used anticancer drug, was encapsulated into the virus-mimicking liposomes, and the subcellular localization and cytotoxicity of the DOX-loaded liposomes were investigated.

3.1 Introduction

Efficient intracellular delivery of therapeutic agents remains a major challenge to most of the drug delivery systems (Hubbell & Chilkoti, 2012). Although viral vectors displayed high transfection efficiency, the serious safety concerns and difficulties in large-scale production largely limit their clinical applications (Chen, 2013; Chen et al., 2010). There is an increasing need to rationally design non-viral drug delivery systems with high efficiency, improved safety and easy to large-scale production (Andrade et al., 2015; Farokhzad & Langer, 2009; Torchilin, 2014). Liposomes are regarded as one of the most promising non-viral delivery systems for clinical application since the first nanomedicine (Doxil®) approved by FDA is based on the use of liposomal systems (Barenholz, 2012). However, the disadvantages of conventional liposomes including low colloidal stability, fast elimination from the blood circulation, no or low controlled release and a lack of targeting effect have greatly limited their clinical applications (Torchilin, 2005).

Therefore, it is in high demand to develop multifunctional liposomes for targeted, controllable and efficient intracellular drug delivery. One strategy is to develop pH-responsive

liposomes via coating the liposomal surface with viral fusogenic peptides, which can be transformed to destabilize membrane upon acidification in endosomes and release cargos into the cytoplasm (Mura et al., 2013). However, their application is limited due to the safety concerns and high production costs of the naturally derived peptides (McTaggart & Al-Rubeai, 2002). Although synthetic peptides have been developed, they are far less efficient in destabilizing the lipid membrane and are difficult to manufacture (Plank et al., 1998).

A class of novel biocompatible and biodegradable pseudopeptides has been recently developed to mimic the pH-dependent membrane destabilization activity of influenza viral fusogenic peptides. The parent pseudopeptide, PLP, is a metabolite-derived linear polyamide (Eccleston et al., 2000, 1999). Its derivatives have been developed by grafting hydrophobic amino acids present in influenza viral peptides onto its pendant carboxylic groups to increase its hydrophobicity and as a result its membrane activity (Chen et al., 2009a, 2009b). These anionic pH-responsive polymers can undergo a coil-to-globule conformation change upon pH decrease, resulting in efficient membrane disruption at endosomal pHs (Chen et al., 2009c, 2005). PP75 (75% stoichiometric degree of substitution with L-phenylalanine on the PLP backbone), one of the derivatives of PLP, was non-lytic at neutral pH, but can display vastly superior membrane destabilization activity at early endosomal pH, 35-fold more efficient than melittin that is a highly membrane-lytic bee venom peptide (Chen et al., 2009c). PP75 has also been demonstrated to efficiently traverse across extracellular matrix to reach individual cells in three dimensional (3D) spheroid tumor models (Ho et al., 2011). It has been applied for successful intracellular delivery of small-molecule model drugs (Chen et al., 2009c; Eccleston et al., 2005) and biomacromolecules (e.g. therapeutic protein and siRNA) (Khormaee et al., 2013; Liechty et al., 2009) for efficient cancer treatment in vitro and in vivo. All of these characteristics suggest PP75 an ideal candidate for the liposomal surface modification to develop novel multifunctional liposomes.

This chapter reports the development of a novel multifunctional liposomal drug-delivery platform that mimics the structural and functional traits of an influenza virus for efficient, safe and controllable intracellular delivery (Figure 3-1). In this virus-mimicking liposomal system, the endosomolytic pseudopeptides mimic the fusogenic peptides present in the viral spikes, the liposome bilayer structure mimics the viral envelope, and the drug payload mimics the viral genome. The pH-dependent drug release profiles were examined by varying key parameters such as polymer amphiphilicity and concentration, cholesterol proportion, modification time

and dilution. The liposomal size was investigated at different pHs to elucidate the mechanism of polymer-liposome interaction. The cytotoxicity and endosomal escape ability of the multifunctional liposomes were further explored. The potency of the DOX-loaded virus-mimicking liposomes against HeLa cancer cells was assessed and compared to free DOX and DOX-loaded bare liposomes.

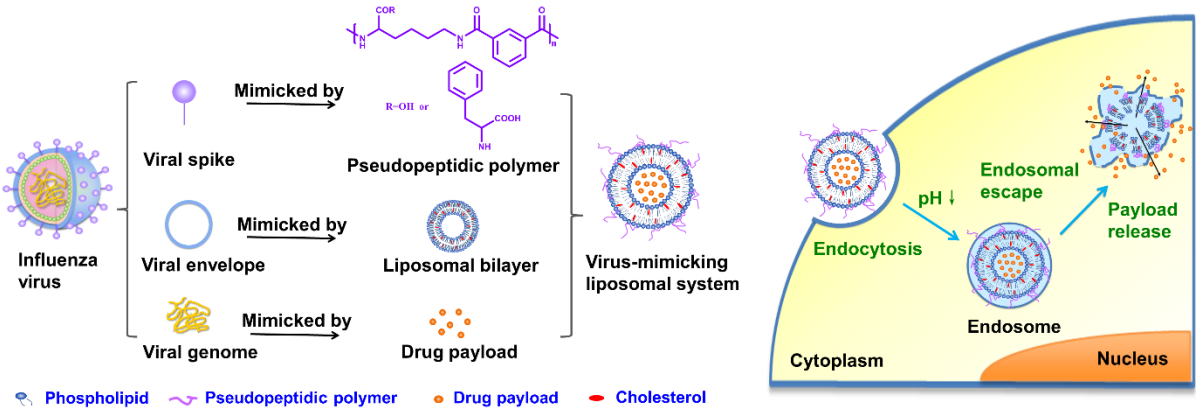

Figure 3-1. Schematic of the virus-mimicking, endosomolytic liposome and its endosomal escape. The multifunctional liposome consists of the pH-responsive, endosomolytic pseudopeptidic polymer mimicking the viral fusogenic peptide present in the vial spikes, the liposomal bilayer mimicking the viral envelope, and the drug payload mimicking the viral genome.

3.2 Results and discussion

3.2.1 Polymer synthesis and structure characterization

PLP and its derivatives were synthesized and characterized according to the previous publications (Chen et al., 2009a; Eccleston et al., 2000, 1999). The numbers in PP25, PP50 and PP75 denote to the stoichiometrical degrees of substitution of Phe on the polymer backbone. The FT-IR spectra (Figure 3-2) showed the characteristic peaks located at 3301 cm^{-1} (N−H str and O−H str), 1722 cm^{-1} (C=O acid str), 1619 cm^{-1} (amide band I) and 1520 cm^{-1} (amide band II). These confirm the successful amide bond formation during polycondenzation and successful ester hydrolysis into carboxylic acid.

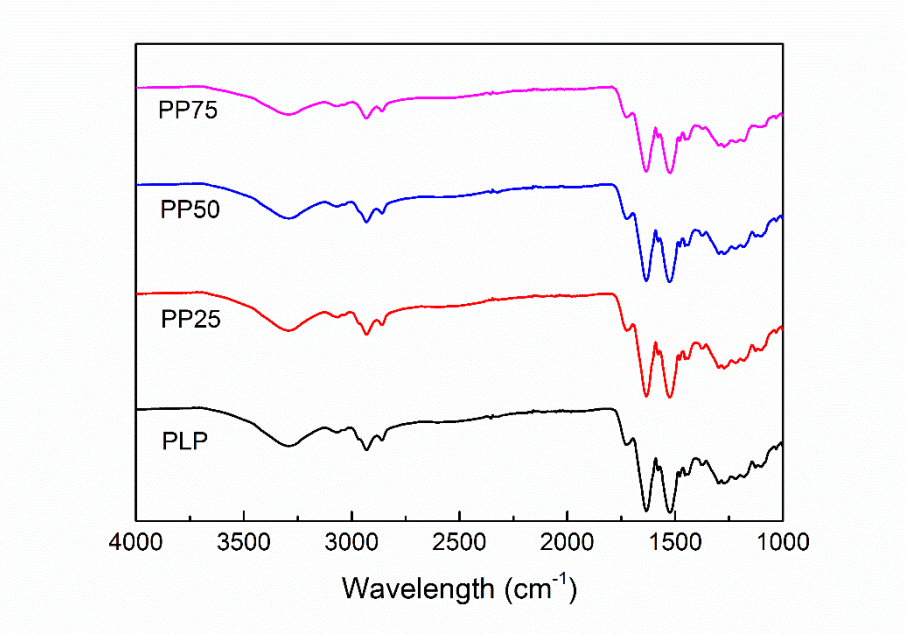

Figure 3-2. FT-IR spectra of PLP, PP25, PP50 and PP75 in their acid forms.

^{1}H-NMR spectroscopy was applied to further characterize the structures of the PLP and its derivatives. The ^{1}H-NMR spectrum of PLP in its acidic form (Figure 3-3) shows the characteristic peaks as follows: δ (ppm) 1.436 – 1.582 (c,d-CH_2-), 1.855 – 1.959 (e-CH_2-), 3.274 – 3.360 (b-CH_2-), 4.327 – 4.464 (f-CH-), 7.479 – 7.617 (H_5-H), 7.922 – 8.395 (complex multiplet aromatic H_6-H, H_4-H, H_2-H), 8.604 – 8,794 (complex series of peaks amide a-NH and g-NH).

The ^{1}H-NMR spectra of PP25, PP50 and PP75 in their acidic forms (Figure 3-3) show the characteristic peaks as follows: δ (ppm) 1.093 – 1.746 (e-CH_2-, c-CH_2-, d-CH_2-), 3.134 – 3.426 (b-CH_2, j-CH_2), 4.358 – 4.517 (f-CH-, i-CH-), 7.107 – 7.280 (H_{Ar2}-H), 7.447 – 7.693 (H_5-H), 7.985 – 8.647 (complex multiplet aromatic H_6-H, H_4-H, H_2-H), 7.860 – 8.647 (a-NH, g-NH, h-NH).

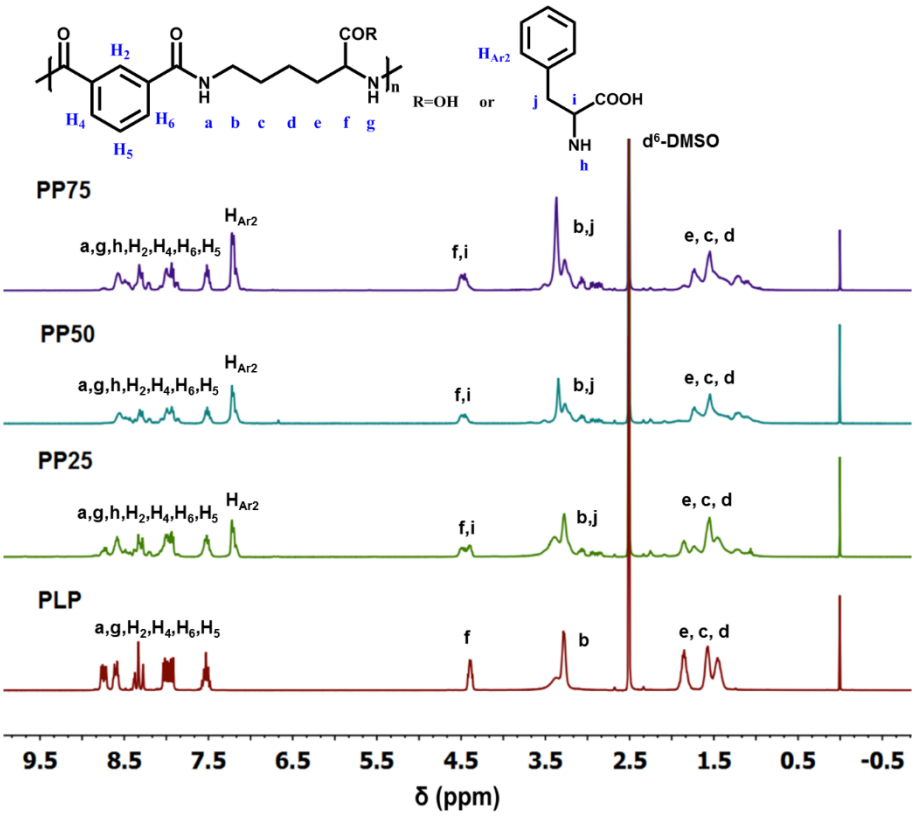

Figure 3-3. ^{1}H-NMR spectra of PLP, PP25, PP50 and PP75 in their acid forms in d_6-DMSO at room temperature.

3.2.2 Hemolysis of PP75

The membrane destabilization activity of the pseudopeptidic polymer was assessed by hemolysis assay, using the RBC membrane as a model of the endosomal membrane. As shown in Figure 3-4, at the concentration ranging from 0.05 to 0.1 mg mL^{-1}, PP75 displayed pH-dependent membrane destabilization activity, with maximum hemolysis at the typical early endosomal pH 6.5 while relatively low hemolysis at pH 7.4. Almost no hemolysis was shown at pH below 5.5 due to the precipitation of the polymer (Chen et al., 2009a). Complete disruption of the RBC membrane (from pH 6.5 to 7.4) was achieved by increasing the PP75 concentration to higher than 0.5 mg mL^{-1}, while the polymer was almost no hemolytic at a low concentration of 0.025 mg mL^{-1}, indicating that the hemolytic activity of PP75 was strongly influenced by the polymer concentration and pH (Chen et al., 2009c).

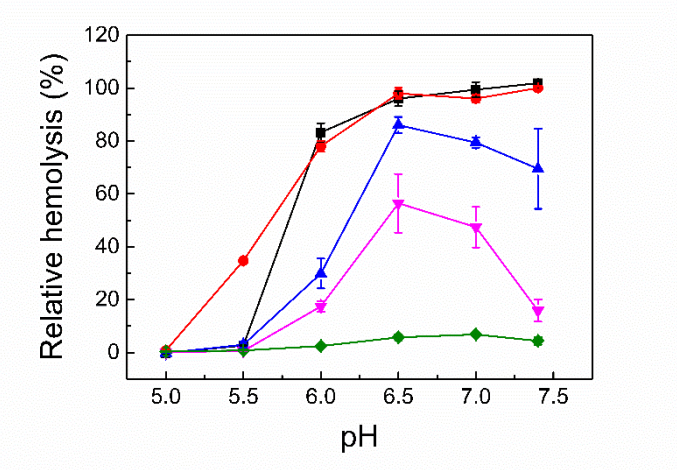

Figure 3-4. pH-Dependent relative hemolysis of PP75 at 1 (■), 0.5 (●), 0.1 (▲), 0.05 (▼) and 0.025 (◆) mg mL^{-1}. Mean ± S.D. (n=3).

3.2.3 Preparation of bare liposomes

The preparation method for bare liposomes was optimized to the desirable particle size and stability. In this study, different sonication types (water-bath sonicator and ultrasonic disintegrator) and modes (continuous mode and pulse mode) were compared. After sonication for 15 min, the liposomal solution prepared using the water-bath sonicator appeared milky, with the hydrodynamic particle size at 943.4 ± 67.9 nm. Whilst for the liposomes prepared using the ultrasonic disintegrator, the hydrodynamic particle size was 90.1 ± 1.4 nm. After storage at 4°C for three days, precipitation was observed in the liposomal sample prepared by the water-bath sonicator while the liposomes prepared by the ultrasonic disintegrator remained transparent. Therefore, in order to prepare small-sized liposomes with high stability, the ultrasonic disintegrator was chosen.

The ultrasonic disintegrator contains two modes: continuous and pulse (sonication for 1s, stop for 1s). Sample temperature would be increased by the heat generated by sonication, and might thus cause lipid oxidation and decrease the stability of liposomes. Further, some heat-sensitive drugs might be degraded during the sonication (Torchilin & Weissig, 2003). As shown in Figure 3-5, the pulse sonication model generated less heat than the continuous solution model. Therefore, the pulse mode was chosen to prepare all the liposome samples.

Figure 3-6 shows the effect of sonication time on the liposomal particle size. In the first 4 min, the particle size decreased dramatically from 1019.6 ± 100.3 nm to 264.8 ± 18.3 nm. The

size continued to decrease gradually within the extended sonication time. After sonication for 15 min, the particle size was 90.1 ± 1.4 nm. While after sonication for 30 min, the size further decreased to 77.8 ± 1.6 nm. Studies have shown that penetration of nanoparticles into the core of the 3D tumor environment was limited to particles smaller than 100 nm (Goodman et al., 2008, 2007). Other researchers reported that long-time sonication may cause drug degradation and lower efficiency of drug encapsulation in liposomes (Torchilin & Weissig, 2003). Thus, 15 min of sonication time was chosen for the liposomal preparation in this thesis.

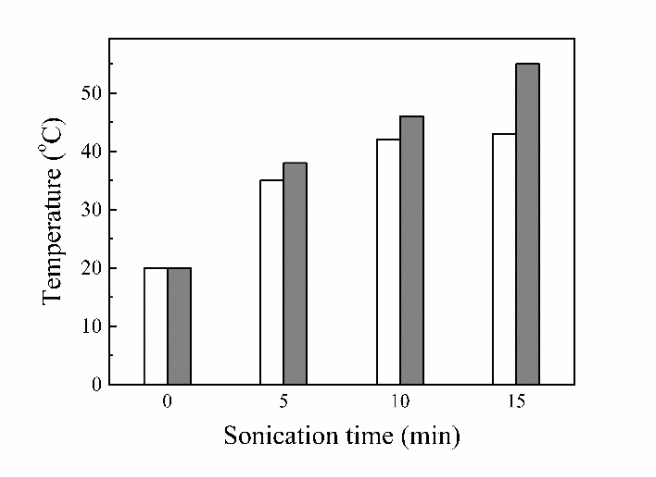

Figure 3-5. Effect of different sonication modes on sample temperature. Liposomes were prepared using the ultrasonic disintegrator with the pulse mode (open columns) and the continuous mode (close columns) for certain time.

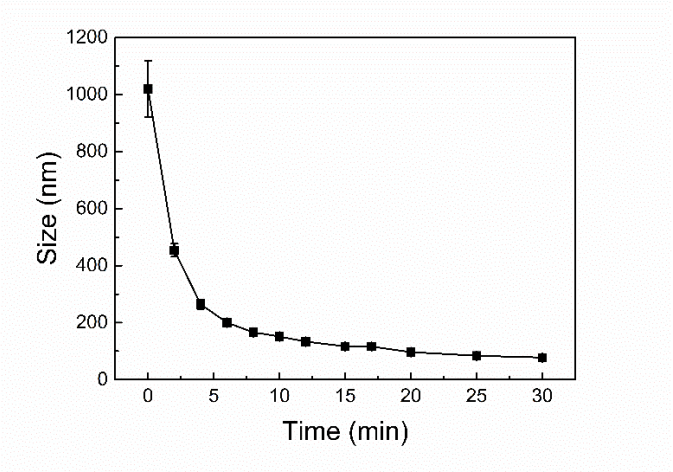

Figure 3-6. Effect of sonication time on liposomal size. Liposomes were prepared by the lipid film hydration method and sonicated by the untrasonic disintegrator using a pulse mode. Mean ± S.D. (n=3).

3.2.4 Development of virus-mimicking liposomes with Phe grafted PLP

After optimization of the liposomal preparation method, the virus-mimicking liposomes were developed by liposomal surface modification with the pseudopeptidic polymers bearing hydrophobic pendant L-phenylalanine. The pH-responsive drug release profiles of the virus-mimicking liposomes were investigated by a calcein-dequenching assay. The membrane-impermeable model drug, calcein, was encapsulated inside the liposomes at a self-quenching concentration (100 mM). Once released from the liposomes, the concentration of the calcein released in the medium would dramatically decrease and the fluorescence intensity would largely increase. By measuring the fluorescence change, the percentage of released payload can be calculated. Key parameters affecting the pH-responsiveness of the virus-mimicking liposomes, including the cholesterol percentage in the liposomal membrane, polymer hydrophobicity and concentration, modification time and dilution were studied.

3.2.4.1 Selection of cholesterol proportion in the liposomal membrane

The effect of cholesterol, an important component in maintaining the membrane integrity and fluidity, on the pH-dependent release profiles of the virus-mimicking liposomes was explored. Figure 3-7A shows the leakage of calcein from the virus-mimicking liposomes containing different cholesterol proportions during surface modification with PP75 for overnight at pH 7.4. For the liposome prepared without cholesterol, 98.9 ± 1.9% of the loaded calcein was leaked. However, with the increase in cholesterol proportion in the liposomal formulation, the calcein leakage percentage decreased dramatically. The liposome with 40 mol% cholesterol only displayed a 9.8 ± 0.3% calcein leakage while almost no clacein leakage was observed in the liposome containing 60 mol% cholesterol.

After removal of the unadsorbed pseudopeptide, it would be ideal that there is no payload leakage from the liposomes at physiological pH. Figure 3-7B shows the release profiles of the PP75-coated, virus-mimicking liposomes prepared with 40 and 60 mol% cholesterol at different pHs. Although no payload leakage was observed in the PP75-coated liposome containing 60 mol% cholesterol at neutral pH, it exhibited a much lower percentage of released calcein upon the pH decrease than the PP75-coated liposome containing 40 mol% cholesterol. This could be attributed to the enhanced membrane rigidity resulting from the increased amount of cholesterol in the liposomal membrane (Liu et al., 2000). As comparison, an efficient payload release within the endosomal pH range (5.0 – 6.8), induced by the coated PP75, was

observed for the virus-mimicking liposome containing 40% cholesterol, reaching up to 92.5 ± 3.0% at pH 5.0, while there was no leakage at pH 7.4. Therefore, 40 mol% cholesterol was chosen for the liposomal formulation in the following experiments to ensure desirable pH-dependent release behavior.

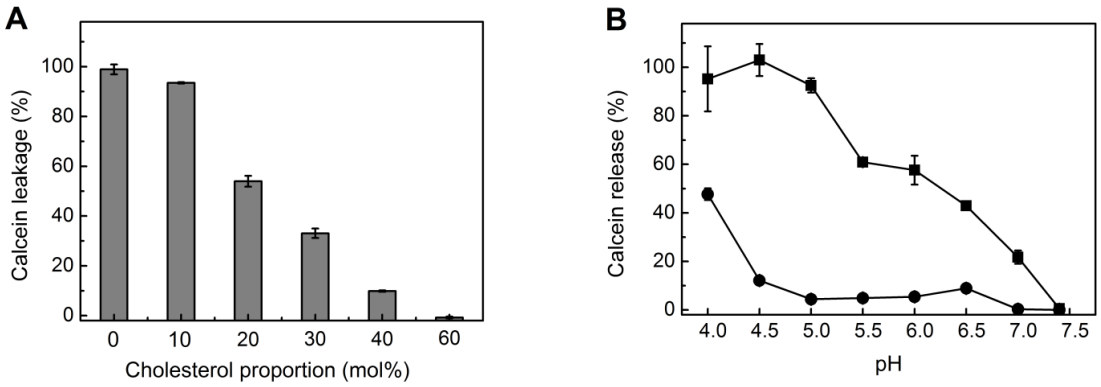

Figure 3-7. Effect of cholesterol proportion on the calcein release from the virus-mimicking liposomes. (A) Calcein leakage from the liposomes containing different amounts of cholesterol during modification with PP75 for overnight at pH 7.4. (B) pH-Dependent calcein release from the PP75-coated virus-mimicking liposomes (58.2 μM PP75, 5 mg mL^{-1} lipids) containing 40 (■) and 60 mol% (●) cholesterol. Mean ± S.D. (n=3).

The effect of cholesterol on the liposomal membrane permeability and the consequent pH-responsive drug release behavior of the virus-mimicking liposomal system could be due to the altered interaction between the coated polymer and the liposomal membrane (Figure 3-8). Without cholesterol addition in the lipid membrane, the hydrophobic parts of the polymer tend to insert into the apolar region of the membrane (Tribet & Vial, 2008). But the presence of cholesterol could affect the membrane fluidity to make it more rigid (Liu et al., 2000), condense the lipid packing (Gutiérrez de Rubalcava et al., 2000) and reduce the membrane permeability (Briuglia et al., 2015; Wu & Lee, 2009). Accordingly, cholesterol could prevent the hydrophobic parts from insertion into the lipid membrane. In addition, cholesterol could enhance the hydrophobicity of the liposomal surface, which as a result, would lead to the hydrophobic interaction between the polymer and lipid membrane mainly taken place at the liposomal surface, instead of translocation through the membrane (Gutiérrez de Rubalcava et al., 2000). This hypothesis was validated by the DLS results of the liposomal size. As shown in Table 3-1, after the surface modification, the hydrodynamic diameter of the PP75-coated

liposome without cholesterol was increased by 2.7 nm, which was lower than the size increase (6.4 nm) for the liposome containing 40% cholesterol. As a consequence, the increased membrane rigidity and elasticity as well as the polymer coating on the liposomal membrane surface could lead to a limited leakage at pH 7.4 when increasing the cholesterol ratio in the formulation. Upon reduction of pH, the coated PP75 could be transformed into a membrane-active state (Chen, *et al.*, 2009b) and induce the efficient drug release at mildly acidic pH for the virus-mimicking liposomes (Figure 3-7B), which is consistent with the report by other researchers that membrane destabilization does not always require a deep polymer insertion into the bilayer (Walrant et al., 2012).

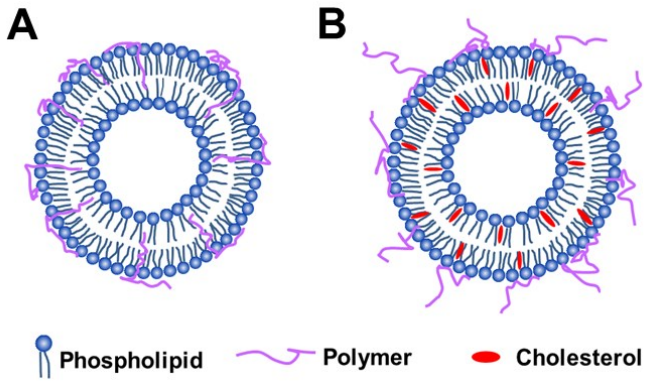

Figure 3-8. Schematic of the polymer-liposome interaction in the (A) absence and (B) presence of cholesterol.

Table 3-1. Mean hydrodynamic diameters of the liposomes before and after surface modification with PP75. Mean ± S.D. (n=3).

	Bare liposomes	PP75-coated liposomes
0 mol% cholesterol	85.5 ± 1.4 nm	88.2 ± 0.8 nm
40 mol% cholesterol	90.1 ± 1.4 nm	96.5 ± 2.5 nm

3.2.4.2 Effect of Polymer hydrophobicity

Generally, the polymer-lipid interactions include hydrogen bonding, hydrophobic interaction, electrostatic interaction and other possible effects (Marie et al., 2014). Side chain modification of the amphiphilic pseudopeptides with hydrophobic amino acid L-phenylalnine (PP25, PP50 and PP75) could be carried out to control their hydrophobic interaction with the neutral EPC/cholesterol liposomal membrane. As shown in Figure 3-9, at neutral pH, no

calcein release was observed for all the liposomes coated with PLP, PP25, PP50 and PP75 respectively. Once the pH dropped below 7.0, a considerable release was observed for the PP50- and PP75-coated liposomes, whilst there was almost no difference in release profiles between the liposomes coated with PP25 and PLP and the bare liposomes. The pH-responsive calcein release capacity of the virus-mimicking liposomes was ranked in the order of PP75-coated liposomes > PP50-coated liposomes > PP25-coated liposomes ≈ PLP-coated liposomes, which is in good correlation with the order of the increase in degree of grafting with Phe and in the degree of polymer hydrophobicity (Chen et al., 2009a).

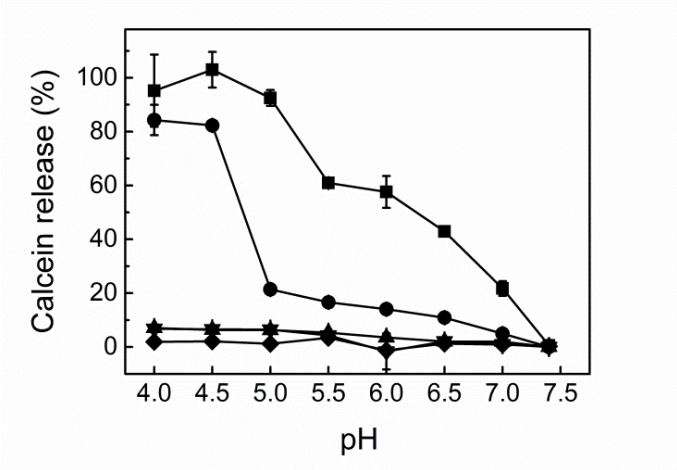

Figure 3-9. pH-Dependent calcein release from the bare liposomes (◆), and the virus-mimicking liposomes coated with PLP (▼), PP25 (▲), PP50 (●), and PP75 (■) respectively. Mean ± S.D. (n=3).

The hydrophobic interaction was crucial for controlling the polymer's adsorption onto the liposomal surface for the non-covalent polymer-liposome complexes (Schulz et al., 2012). The higher the polymer hydrophobicity, the stronger membrane association can be achieved. This result is in agreement with the recent report that the hydrophobic interaction was the main driving force for the binding of PP75 to the 1,2-dioleoyl-sn-glycero-3-phosphocholine (DOPC) monolayer model membrane (Zhang et al., 2011). Grafting Phe, the most hydrophobic natural amino acid with aromatic residues, to the PLP backbone could enhance the coating of the pseudopeptidic polymer on the liposomal membrane. This is consistent with the report that aromatic rings present in peptide structures could dramatically increase their interaction with the lipid membrane (Plank et al., 1994).

3.2.4.3 Effect of polymer concentration and dilution

Figure 3-10A shows the effect of the adsorbed PP75 on the pH-dependent release profiles of the virus-mimicking liposomes (lipid concentration fixed at 3.0 mM). Up to 92.5 ± 3.0% calcein was released upon acidification to pH 5.0 (late endosomal pH) for the liposomes coated with 58.2 μM PP75, significantly higher than the release efficiencies of the liposomes coated with 33.3 and 3.6 μM PP75 respectively. This proved that a higher concentration of the adsorbed polymer could destabilize the membrane more efficiently, which was probably due to the better interconnection of different vesicles (Chieng & Chen, 2011, 2010).

In order to study the dilution effect on the pH-responsive release profiles, the virus-mimicking liposomes coated with 58.2 μM PP75 were diluted with HBS buffer at pH 7.4 10- and 100-fold and then acidified to pH 4.5 before calcein release measurement. As a result of dilution, the concentration of adsorbed polymer was decreased from 58.2 to 5.82 and 0.582 μM respectively, but the polymer-to-lipid molar ratio was fixed at 1.9:100. As shown in Figure 3-10B, there was no significant difference in calcein release, indicating that the pH-sensitive drug release behavior of this virus mimicking liposome was dilution-independent. This characteristic is crucial for a drug carrier as the formulation concentration would be remarkably decreased due to the significant dilution during circulation in the bloodstream (Tribet & Vial, 2008).

It is worth noting that, upon 100-fold dilution, the PP75-coated liposome (the adsorbed PP75 at 0.582 μM, polymer-to-lipid molar ratio at 1.9:100) retained a high calcein release rate of 91.8 ± 28.7% at pH 4.5, as shown in Figure 3-10B. In contrast, the virus-mimicking liposome with over six times more adsorbed PP75 (3.6 μM) but with a lower polymer-to-lipid molar ratio (0.12:100) only released 25.6 ± 3.4% calcein at pH 4.5 (Figure 3-10A). This demonstrates that the polymer-to-lipid molar ratio is a more important parameter controlling destabilization of the liposomal membrane and controlled drug release than the concentration of adsorbed polymer.

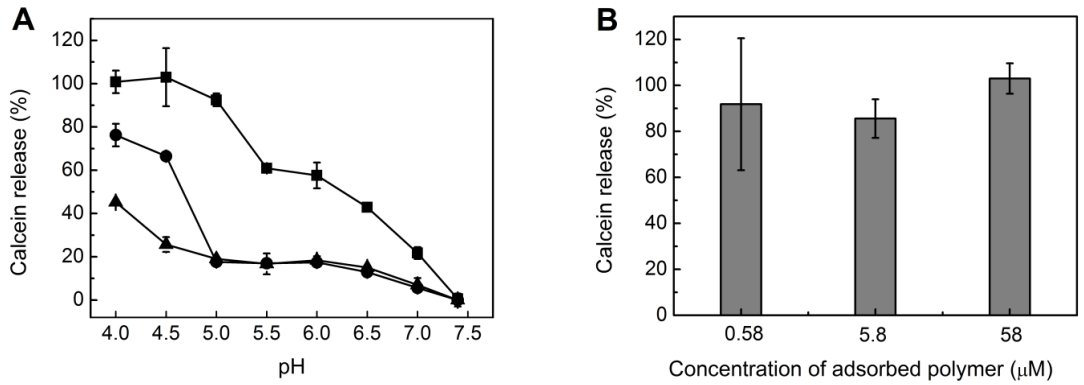

Figure 3-10. Effect of PP75 adsorbed on the liposomal membrane. (A) pH-Sensitive calcein release from the virus-mimicking liposomes, with a fixed lipid concentration at 3.0 mM, coated with 3.6 (▲), 33.3 (●) and 58.2 μM (■) PP75 respectively. (B) Calcein release from the PP75-coated virus-mimicking liposomes, with a fixed polymer-to-lipid molar ratio at 1.9:100, at pH 4.5 upon 0-, 10- and 100-fold dilution. Mean ± S.D. (n=3).

3.2.4.4 Effect of modification time

The effect of modification time on the pH-responsive behavior of the virus-mimicking liposomes was investigated. The bare liposomes were incubated with 202.0 μM PP75 for 5 min or overnight and then purified to remove free polymer before quantification of the amount of adsorbed polymer. As shown in Figure 3-11, 41.58 ± 0.20 μM PP75 was adsorbed on the liposomal surface after only 5 min of incubation, slightly lower than the concentration of the adsorbed polymer after an overnight incubation (58.2 ± 1.77 μM). This is indicative of a strong and efficient association of PP75 with the lipid bilayer. Furthermore, no significant difference in the pH-dependent calcein release was observed between the virus-mimicking liposomes surface-functionalized with PP75 for overnight and 5 min (Figure 3-12), thus ensuring a simple and rapid coating method to achieve a desirable pH-responsive drug release profile.

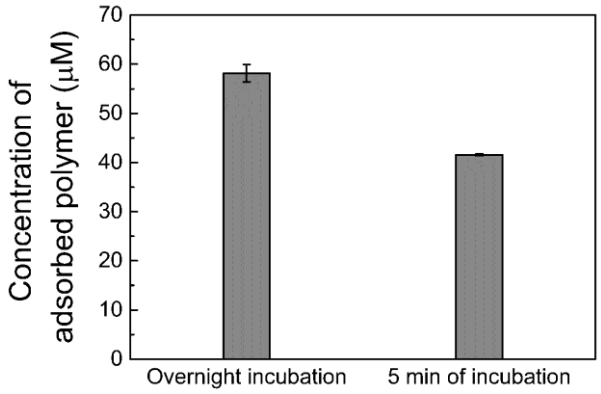

Figure 3-11. Effect of modification time on the concentration of PP75 adsorbed on the virus-mimicking liposomes. Mean ± S.D. (n=3).

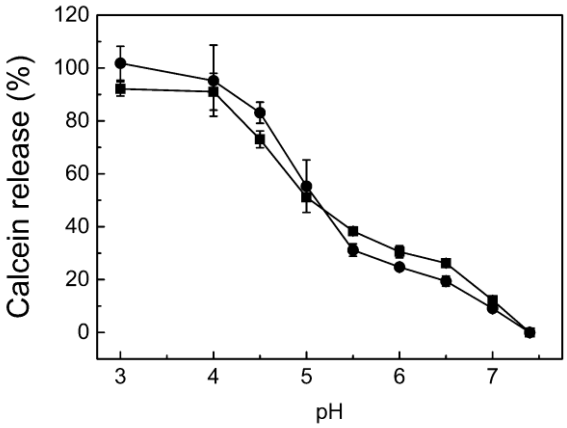

Figure 3-12. Effect of modification time on the pH-dependent calcein release from the virus-mimicking liposomes (containing a fixed lipid concentration at 3.0 mM) modified with PP75 for overnight (●) or 5 min (■). Mean ± S.D. (n=3).

3.2.4.5 Particle size

The mean hydrodynamic particle size of the bare liposomes was 90.1 ± 1.4 nm (Figure 3-13A). Surface modification with PP75 did not lead to a signification size change (Figure 3-13B). The diameter of about 100 nm is favorable for liposomes as drug delivery systems since the liposomes with this size were found to be large and stable enough to encapsulate payloads while small enough to circulate for adequate time to reach target sites (Torchilin et al., 2003).

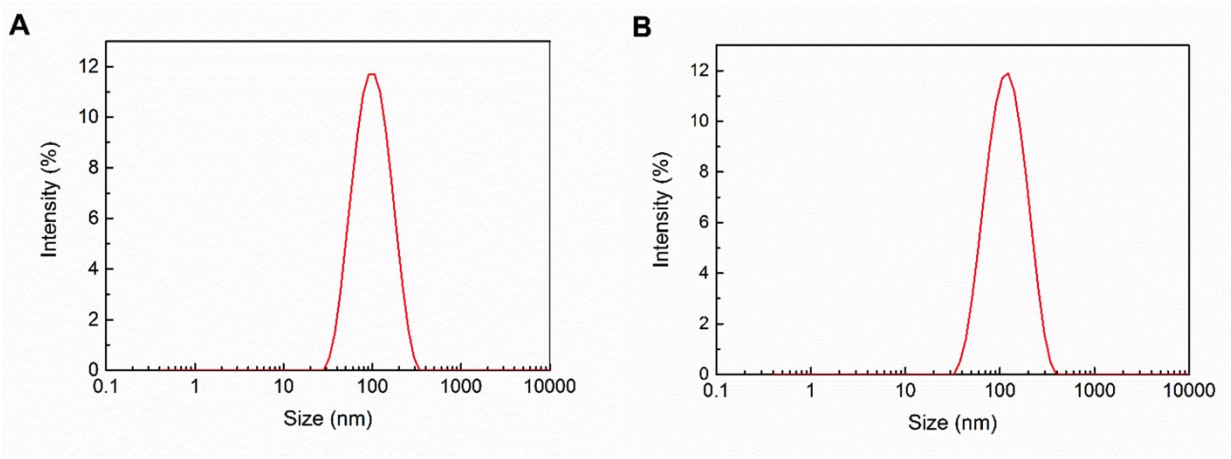

Figure 3-13. Size distributions of (A) the bare liposomes and (B) the PP75-coated, virus-mimicking liposomes.

3.2.4.6 pH-Triggered size change

The polymer-liposome interaction was further explored by investigating the pH-responsive size change of the bare liposomes and the virus-mimicking liposomes. As shown in Figure 3-14A, the hydrodynamic particle size of the bare liposomes without polymer coating remained unchanged within the pH range tested. Only a marginal size increase was observed at pH 4.0 for the PLP- and PP25-coated liposomes. However, for the PP50- and PP75-coated liposomes, a considerable size increase was detected at pH below 5.0. This trend was well consistent with the results described in the Section 3.2.4.2 that the PP75- and PP50-coated liposomes displayed a dramatically enhanced payload release at acidic pHs compared to the PP25- and PLP-coated liposomes. This could be due to the stronger anchoring of polymer on the liposomal membrane resulting from the increased polymer hydrophobicity, thus leading to the enhanced intervesicular interaction and consequent liposomal aggregation or fusion (Yuba et al., 2011).

The reversibility of the size change of the PP75-coated liposome was examined to investigate whether the increased particle size at acidic pHs was due to fusion or aggregation. As shown in Figure 3-14B, once the pH increased from 4.5 to 7.4, the PP-coated liposome rapidly reverted to its original size within 5 min. Immediately after titration from pH 7.4 to 4.5, the particle size increased noticeably again. The reversible size change was further consolidated by confocal microscopy using the liposome coated with 6-aminofluorescein-labelled PP75. At neutral pH, green fluorescence was evenly distributed in the sample solution. After the pH decrease to 4.5, liposomal aggregation was immediately observed. Upon titration back to pH

7.4, the aggregation vanished instantly and the homogenous fluorescence distribution was observed again. This suggests that the increase in liposomal size at acidic pH should not be due to liposomal fusion (Jahn & Südhof, 1999).

A fluorescence resonance energy transfer (FRET) assay was carried out to further confirm that the size increase was induced by liposomal aggregation instead of fusion. NBD-PE and Rh-PE were incorporated in the liposomal membrane, each at a concentration (1 mol%) where NBD-Rh fluorescence resonance energy transfer occurred. Once the labelled liposome was mixed with the unlabeled one at a molar ratio of 1:9, if membrane fusion took place, the separation of donor and acceptor probes would lead to an increase in the fluorescence intensity of NBD (Yuba et al., 2011). As shown in Figure 3-15, there was no significant fluorescence change when the PP75-coated liposomes was titrated from pH 7.4 to 4.5, which consolidates the argument that the size increase at acidic pH was not attributed to liposomal membrane fusion.

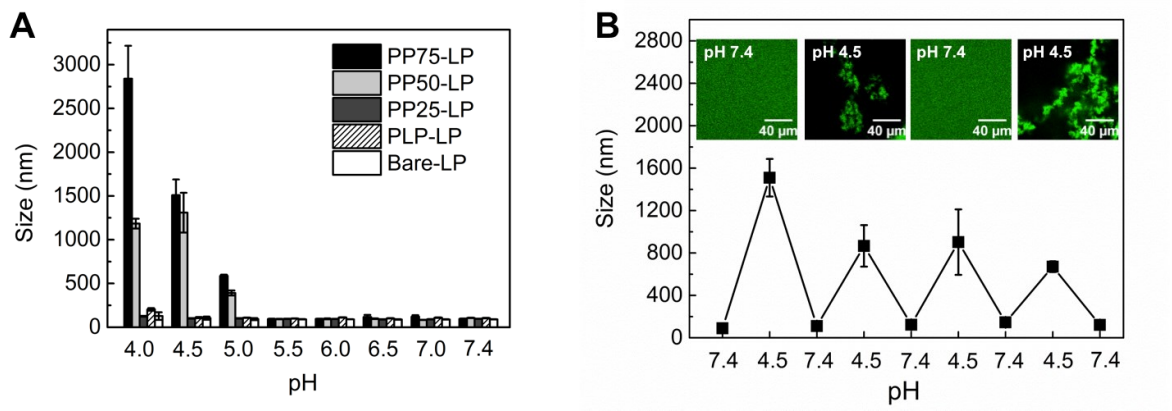

Figure 3-14. (A) pH-Dependent hydrodynamic size change of the bare liposomes (Bare-LP), PLP-coated liposomes (PLP-LP), PP25-coated liposomes (PP25-LP), PP50-coated liposomes (PP50-LP) and PP75-coated liposomes (PP75-LP). (B) Reversible size change of the PP75-coated liposomes between pH 7.4 and 4.5, imaged by confocal microscopy and measured by DLS. Mean ± S.D. (n=3).

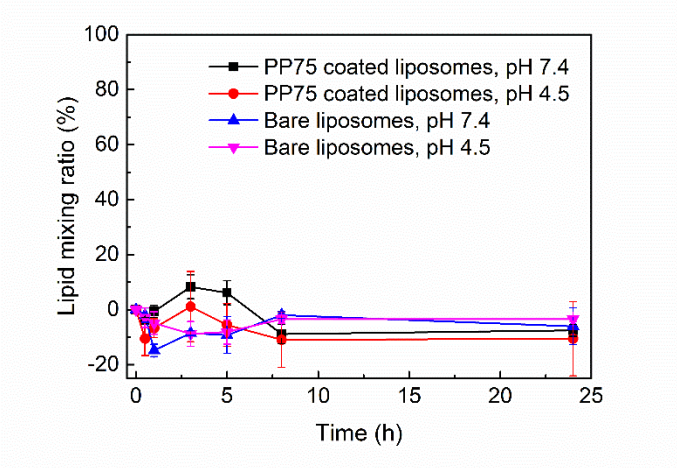

Figure 3-15. Lipid mixing assay of the bare liposomes and PP75-coated liposomes at pH 7.4 and 4.5 through the detection of NBD-Rh FRET. The liposomes were labelled with 1 mol% NBD-PE and 1 mol% Rh-PE. Time-dependent lipid mixing ratios were determined through measurement of the NBD fluorescence intensity upon incubation of the labelled liposomes with unlabeled one at the molar ratio of 1:9 at different pHs. Mean ± S.D. (n=3).

Figure 3-16 illustrates the bridging mechanism which could explain the pH-dependent reversible size change of the PP75-coated liposomes. Published work reported that the pseudopeptidic polymer undertook a reversible coil-to-globule conformational transition upon pH change (Chen et al., 2009a). PP75 bears a large amount of hydrophobic pendant groups. Once PP75 was coated on the liposomal surface, some hydrophobes of the polymer could be associated with the lipid membrane, while others could facilitate the intermolecular interaction, resulting in the PP75-bridged liposomal network. At physiological pH, PP75 displayed an expanded structure due to the predominant electrostatic repulsion (Chen et al., 2009a; Yessine & Leroux, 2004). Hence the PP75-coated liposomes would be homogeneously distributed in the loose polymer-bridged networks, exhibiting a similar particle size with the bare liposomes. Upon acidification, the carboxyl groups in PP75 were protonated and the predominant hydrophobic interaction would lead to the formation of the collapsed globular structure (Wang et al., 2015). As a result, the size of the virus-mimicking liposomes increased dramatically. When the pH was changed back to 7.4, the polymer exhibited an extended structure, leading to a significant reduction to the original liposomal size. The proposed mechanism is in well consistence with the report that grafting hydrophobic groups onto the biopolymers (e.g. hydroxyethylcellulose and chitosan) could increase the intermolecular interaction and the

consequent formation of bridged networks (Lee et al., 2005; Panmai et al., 1999). Similar aggregation and disaggregation of DOPC GUVs was also reported by other researchers (Quemeneur et al., 2010).

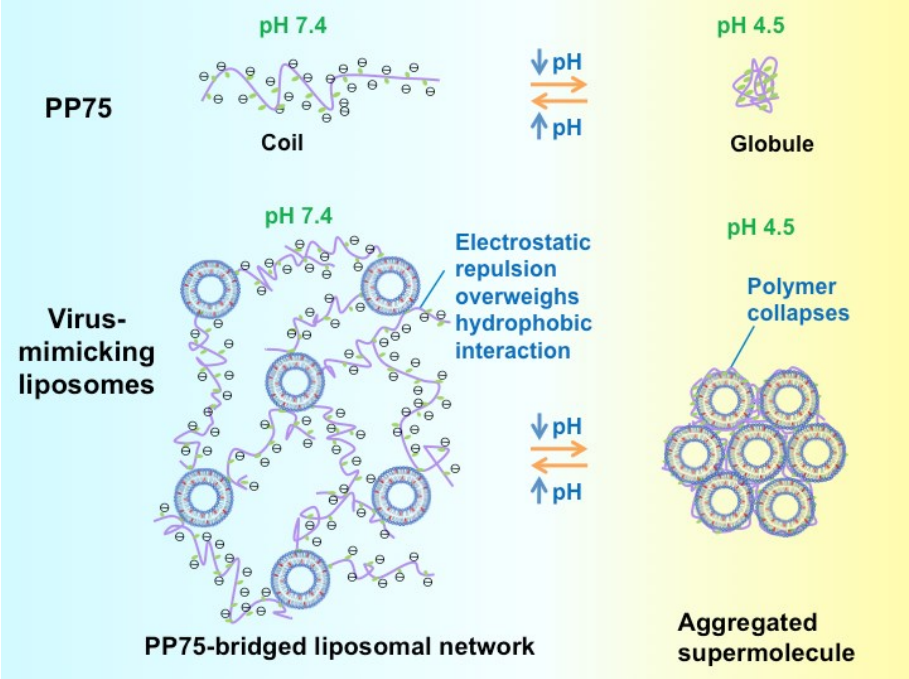

Figure 3-16. Schematic representation of the mechanism of the revisable size change between pH 7.4 and 4.5 for the PP75-coated, virus-mimicking liposomes.

It has been reported that the membrane fusion or formation of polymer-lipid micelles could result from the bridging effect involving liposomes and anionic (e.g. polyacrylic acid) or cationic polymers (e.g. polylysine) (Chieng & Chen, 2010; Yaroslavov et al., 2011). However, in this study, the liposomal size change was reversible for several cycles (Figure 3-14B), suggesting that the liposomal membrane was not lysed or fused during the formation of liposomal aggregates. Even kept at pH 4.5 for 7 days, the aggregates of the PP75-coated liposomes could still be easily disaggregated to the original liposomal size with increasing pH to 7.4. The lipid mixing assay (Figure 3-15) further confirmed the absence of liposomal membrane fusion at pH 4.5. When comparing the pH-dependent content release (Figure 3-9) and pH-triggered size change (Figure 3-14A), the release profile did not seem to be dependent on the size change. At pH 5.5, the PP75-coated liposomes displayed a significant content release (60.9 ± 0.5%), whilst no obvious size change was observed. The payload release could

result from the transformation of the surface-adsorbed PP75 to a membrane-destabilizing state (instead of the change of colloidal stability) upon pH reduction.

3.2.4.7 Hemolysis assay of the PP75-coated liposomes

The hemolysis assay was carried out using the RBC membrane as a model of the endosomal membrane to investigate whether the polymer adsorbed on the liposomal surface still retains its pH-responsive, endosomolytic activity. The relative hemolysis of the virus-mimicking liposomes, with a fixed polymer-to-lipid ratio at 1.9:100 but different concentrations of the adsorbed polymer, was compared between pH 7.4 and 6.5 (early endosomal pH). As shown in Figure 3-17A, the membrane disruption activity of the virus-mimicking liposomes was gradually decreased at both pHs with decreasing the PP75 concentration. The liposome coated with 0.5 μM PP75 showed the largest difference between the hemolysis at pH 6.5 (77.6 ± 1.8%) and 7.4 (27.7 ± 1.6%). This is favorable for cytoplasmic delivery, which requires limited hemolysis at physiological pH but efficient endosomal membrane disruption upon acidification in endosomes.

Figure 3-17B demonstrates the relative hemolysis of the PP75-coated liposomes and bare liposomes at pH range from 7.4 to 4.5, which mimics the endosomal and lysosomal pH range. Relative hemolysis of 77.6 ± 1.8% was achieved at a typical early endosomal pH 6.5 for the liposomes coated with 0.5 μM PP75, whilst the hemolysis at pH 7.4 was relatively low. In contrast, the bare liposomes exhibited almost no hemolysis within the pH range studied, suggesting that the hemolysis activity of the virus-mimicking liposomes resulted from the polymer coating layer instead of the liposomes. This is in agreement with the hemolysis result of PP75 shown in Figure 3-4, indicating that the polymer adsorbed on the liposomal surface well retained its membrane-destabilization activity. With increasing the concentration of the adsorbed PP75 to 5.8 μM, the virus-mimicking liposomes exhibited a high level of hemolysis at 71.9 ± 3.1% at physiological pH. This well correlated to the report of other researchers that increasing the concentration of PEAA to a sufficiently high level may lead to complete membrane lysis (Thomas et al., 1994). Once the pH decreased below 5.0, the virus-mimicking liposomes lost their hemolytic activity due to the formation of liposomal aggregates.

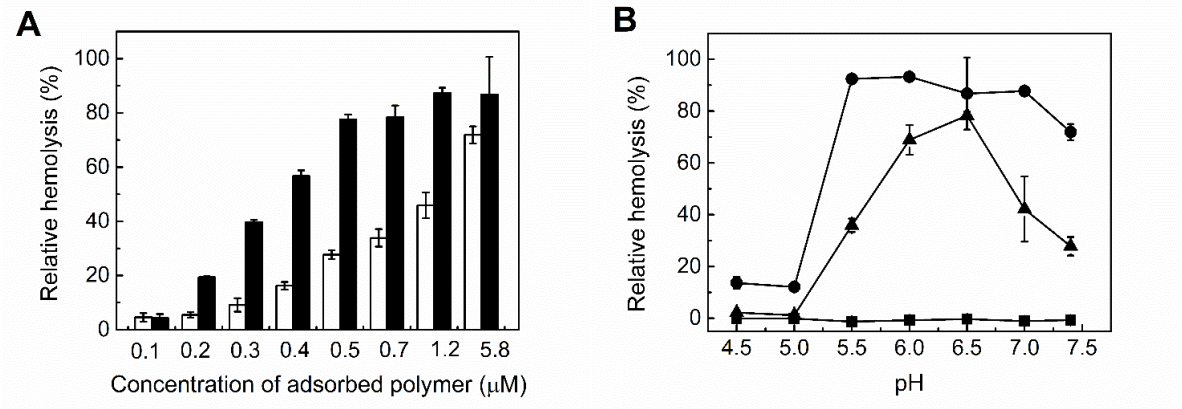

Figure 3-17. Relative hemolysis of the PP75-coated, virus-mimicking liposomes with a fixed polymer-to-lipid molar ratio at 1.9:100. (A) Relative hemolysis of the liposomes with different concentrations of the adsorbed PP75 at pH 6.5 (close columns) and pH 7.4 (open columns); (B) pH-dependent relative hemolysis of the bare liposomes (■) and the virus-mimicking liposomes with the concentration of the adsorbed PP75 at 0.5 (▲) and 5.8 μM (●). Mean ± S.D. (n=3).

3.2.4.8 Subcellular localization

The membrane-impermeable calcein was applied as a tracer molecule to further demonstrate the endosomal escape ability of the virus-mimicking liposomes. As shown in Figure 3-18A, calcein appeared as green punctate dots when HeLa cells were co-treated with the bare liposomes and free calcein. The co-localization of calcein and the red lysotracker suggests that calcein was entrapped inside the intracellular vesicles after endocytosis. Once HeLa cells were co-incubated with free calcein and the virus-mimicking liposomes, strong diffuse green fluorescence was observed throughout the cells (Figure 3-18B), suggesting that the polymer present in the liposomal coating layer still well retained its efficient membrane destabilizing activity and effectively released the endocytosed materials into the cytoplasm.

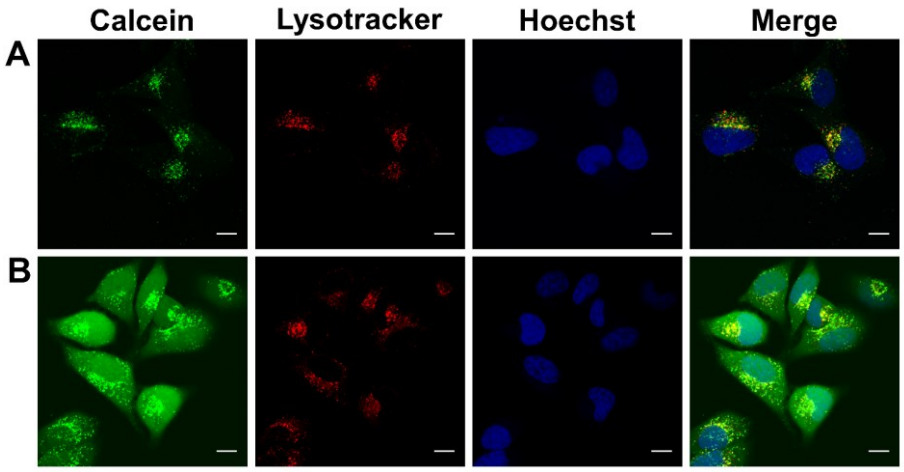

Figure 3-18. Laser scanning confocal microscopy images of HeLa cells demonstrating the escape of the endocytosed free calcein (3.2 mM) from intracellular vesicles into the cytoplasm facilitated by (A) the bare liposomes and (B) the PP75-coated, virus-mimicking liposomes (with a fixed polymer-to-lipid molar ratio at 1.9:100). Images were taken after 2 h of uptake and 2 h of further incubation (scale bar: 20 μm).

DOX, a widely used anticancer drug, was incorporated inside the liposomes for further evaluation of the efficient liposomal drug-release behavior and efficient endosomal escape ability of the novel virus-mimicking liposomal system. The mean hydrodynamic diameter of the DOX-loaded, PP75-coated liposomes was 94.2 ± 2.6 nm, the encapsulation efficiency of DOX was 53.1 ± 0.9 %, and the weigh percentage of DOX over the carrier was 15.2 ± 2.2%. Figure 3-19 demonstrates that the virus-mimicking liposomes were highly efficient for intracellular delivery of DOX into cancer cells as strong DOX fluorescence was seen inside the cells only after 1 h of treatment. Free DOX entered cells by direct diffusion (Cui et al., 2013). However, when it was encapsulated inside the liposomes, the cellular entry pathway was changed to endocytosis (Torchilin, 2005). After cellular uptake, the acidic pH inside endosomes/lysosomes could trigger efficient DOX release from the PP75-coated liposomes but also endosomal escape into the cytoplasm, consequently leading to nuclear accumulation to exert its toxicity. However, HeLa cells treated with the DOX-loaded bare liposomes without polymer coating exhibited much lower intracellular DOX fluorescence because of the absence of the endosomolytic pseudopeptide PP75.

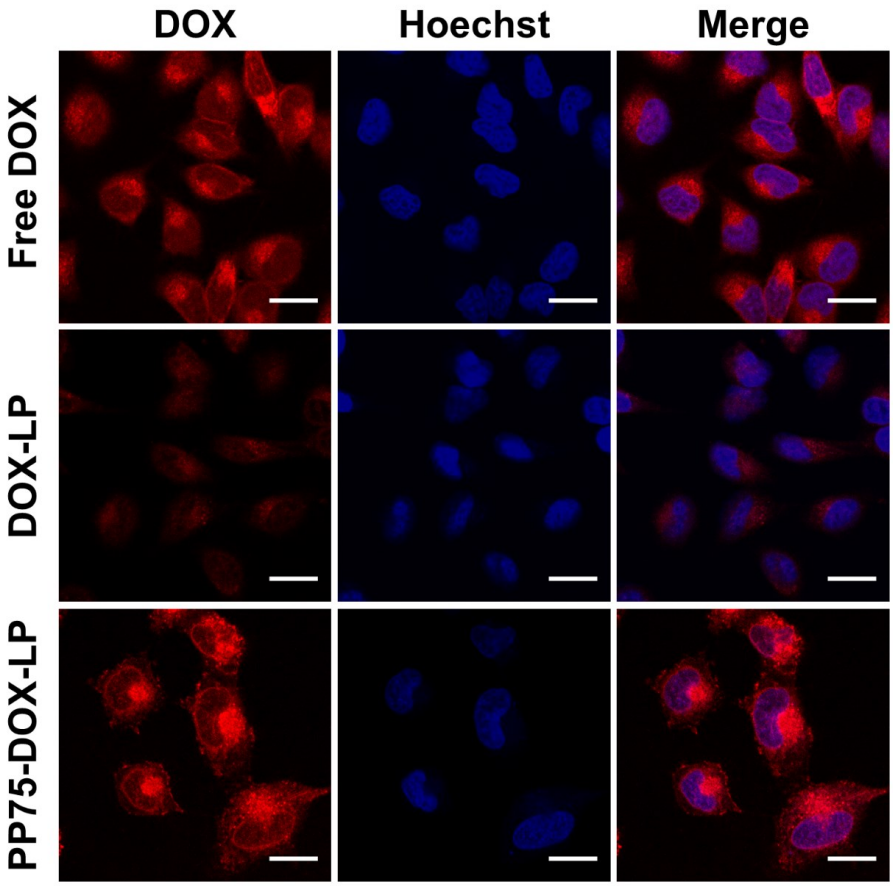

Figure 3-19. Laser scanning confocal microscopy images of HeLa cells showing the subcellular localization of the anticancer drug DOX. The cells were treated with free DOX, DOX-loaded bare liposomes (DOX-LP), and DOX-loaded, PP75-coated virus-mimicking liposomes with a polymer-to-lipid molar ratio at 1.9:100 (PP75-DOX-LP) for 1 h at the fixed equivalent DOX concentration of 2.5 μM (scale bar: 20 μm).

Quantitative flow cytometry analysis was further applied to verify the efficient intracellular delivery of DOX. As shown in Figure 3-20A and 3-20B, HeLa cells treated with DOX-loaded, virus-mimicking liposomes exhibited the similar mean fluorescence intensity (MFI) to those treated with free DOX, while significantly higher than those treated with DOX-loaded, conventional liposomes without polymer coating. This result was well correlated to the confocal microscopy images (Figure 3-19). The enhanced intracellular DOX fluorescence in the cells treated with the virus-mimicking liposomes was due to the pH-triggered efficient endosomal escape of DOX into the cytoplasm. Furthermore, surface modification of liposomes with the amphiphilic pseudopeptidic polymer could also lead to a higher cellular uptake due to the enhanced hydrophobic interaction between the hydrophobic components of the polymer

and the cell membrane, in addition to the help of scavenger receptors, a family of glycoproteins overexpressed on the surface of various cells including HeLa used herein (Yang et al., 2013).

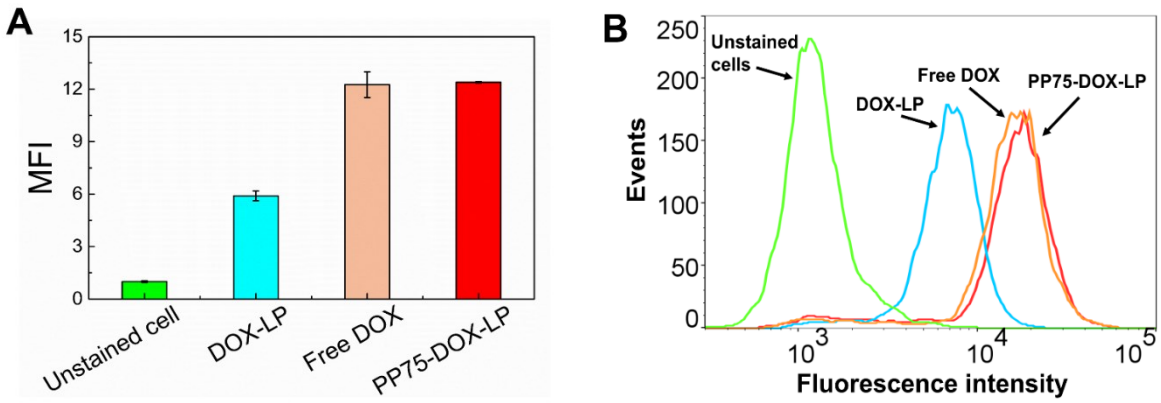

Figure 3-20. Cellular uptake of DOX was quantitatively analyzed by flow cytometry and presented as relative MFI (A) and representative histogram plots (B). All the samples were analyzed after 1 h of treatment of HeLa cells with a fixed DOX dosage of 2.5 μM. Mean ± S.D. (n=3).

To further confirm that the liposomal surface modification with the endosomolytic polymer can enhance cellular uptake, the liposomes were fluorescently labelled by incorporating 1 mol% Rh-PE in the lipid bilayer. As shown in Figure 3-21, the red dots represented the liposomes internalized inside cells. For cells treated with the bare liposomes without polymer coating, only a small number of red dots were observed, while for cells treated with the PP75-coated liposomes, the intensity of red fluorescence was remarkably stronger, indicating a considerably enhanced cellular uptake of the liposomes after polymer modification.

The cellular uptake was further quantified by flow cytometry. As shown in Figure 3-22, the MFI of cells treated with the PP75-coated, fluorophore-labelled liposomes was 11.2 ± 2.5 times higher than those treated with the bare liposomes. This result is well consistent with the intracellular delivery visualized by confocal microscopy. The significantly enhanced cellular uptake resulted from the improved interaction of the polymer with the cell membrane and its scavenger receptors. Scavenger receptors have been demonstrated to have a strong binding ability to negatively charged particles or macromolecules (Copolovici et al., 2014). Other researchers have reported that anionic polymers and anionic polymer-modified delivery vehicles could be recognized by scavenger receptors more efficiently than the non-charged ones. For example, 2-carboxycyclohexane-1-carboxylated poly(glycidol)-PE-containing

liposomes exhibited an approximately 9 times higher cellular uptake than the unmodified liposomes (Yuba et al., 2013). Also, the liposomes modified with the linear or hyperbranched anionic polymers increased the cell internalization efficiency (Fujiwara et al., 1996; Yuba et al., 2011).

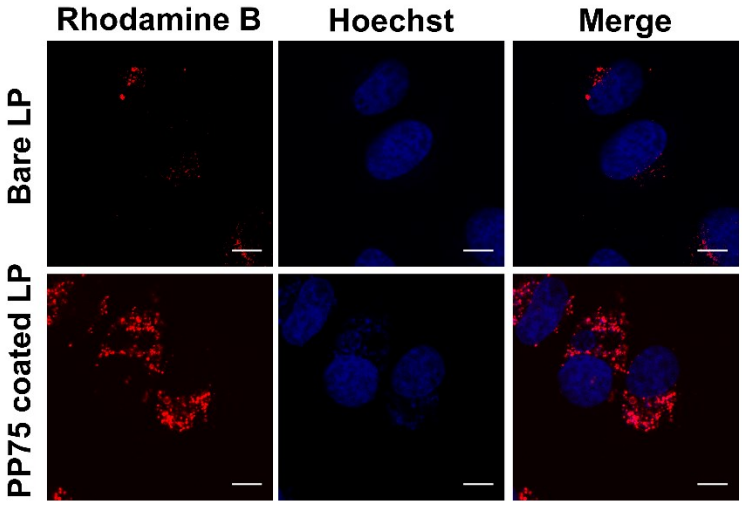

Figure 3-21. Confocal microscopy image shows subcellular localization of rhodamine B (red channel) labelled liposomes. Images were taken after 1h treatment followed by 3 times wash with PBS and further incubated for 3h. Scale bar: 10 µm.

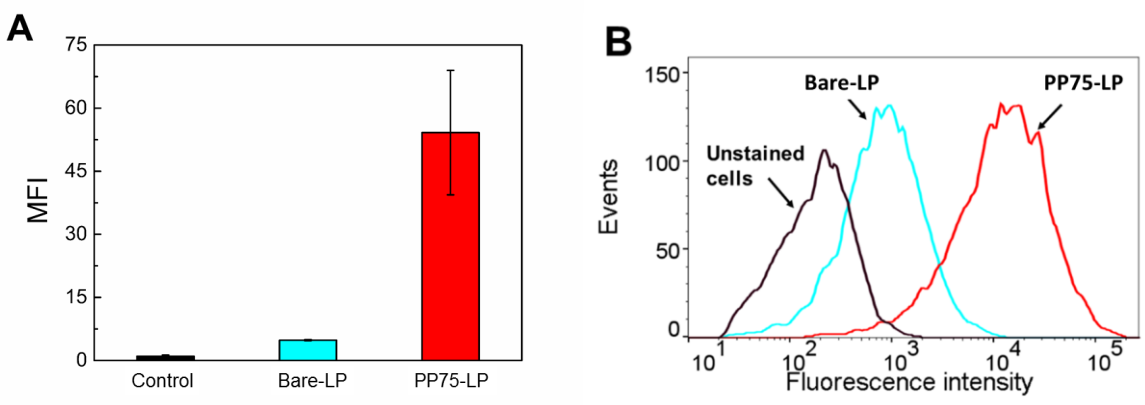

Figure 3-22. (A) MFI and (B) the representative histogram plots of the HeLa cell treated with the bare liposomes (Bare-LP) and the PP75-coated liposomes (PP75-LP), both labelled with 1 mol% Rh-PE. All samples were analyzed after 1 h of treatment followed by 3 h of further incubation. Mean ± S.D. (n=3).

3.2.4.9 In vitro cytotoxicity of virus-mimicking liposomes without drug loading

The cytotoxic effect of the virus-mimicking liposomes without drug loading against HeLa cells was evaluated by Alamar Blue assay which measures the metabolic activity. Alamar Blue, also called resazurin, is a blue and nonfluorescent compound that can permeate through the cell membrane. After entering cells, Alamar Blue is reduced to resorufin by metabolically active cells and produces bright red fluorescence. The conversion from resazurin to resorufin by live cells enables the calculation of the cytotoxicity by measuring the fluorescence change (Nociari et al., 1998). As shown in Figure 3-23A, no cytotoxic effect was observed for the bare liposomes with the lipid concentration ranging from 7.5 to 300.0 μM. The cytotoxicity of the virus-mimicking liposomes was also tested with various lipid concentrations but at a fixed polymer-to-lipid molar ratio (1.9:100). As shown in Figure 3-23A, the virus-mimicking liposomes were also well tolerated by the HeLa cells within the lipid concentration below 60 μM. When increasing the lipid concentration to 300.0 μM, the relative viability of HeLa cells was decreased to 75.9 ± 19.2%, indicating that increasing the polymer concentration to a sufficiently high level (5.7 μM) would lead to a reduction of cell metabolic activity.

LDH assay was applied to further investigate the effect of the PP75-coated liposomes on the plasma membrane integrity. LDH is a stable cytosolic enzyme. Once membrane damage occurs, LDH will be released into the cell culture media. The LDH released can be quantified by measuring the fluorescence of the formed product. LDH catalyzes lactate to pyruvate and reduce NAD^+ to NADH. The NADH then interacts with the tetrazolium salt (INT) to form formazan with red color which can be measured at 490 nm. Therefore, by measuring the level of formazan formation, the amount of LDH released into the medium can be quantified, which indicates the plasma membrane integrity (Decker & Lohmann-Matthes, 1988). As shown in Figure 3-23B, all the liposomal samples with or without polymer coating were well tolerated by HeLa cells below the lipid concentration of 300.0 μM, suggesting no significant cell membrane damage occurred once the cells were treated with PP75-coated liposomes within the lipid concentration tested.

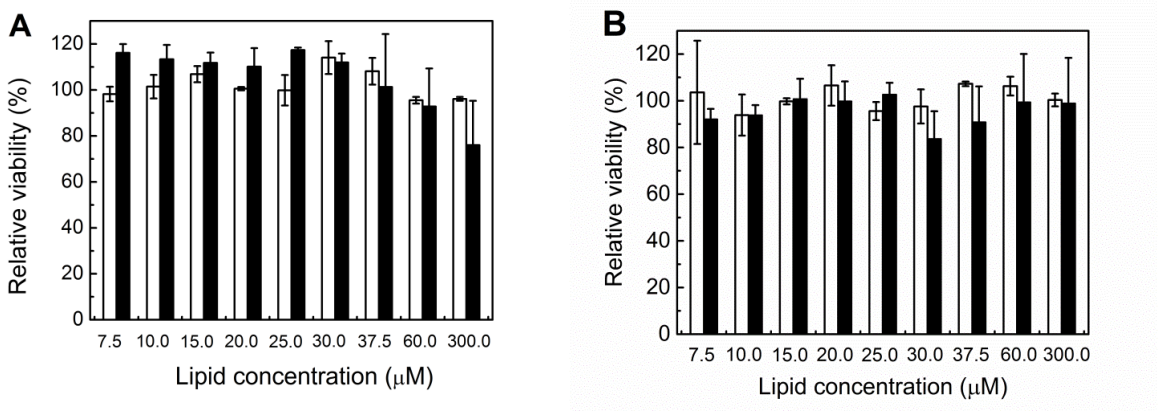

Figure 3-23. Relative viability of HeLa cells treated with the liposomes with (close columns) or without (open columns) PP75 coating at various lipid concentrations for 24 h, as determined by (A) Alamar Blue assay and (B) LDH assay. The polymer-to-lipid molar ratio of the virus-mimicking liposomes was fixed at 1.9:100. Mean ± S.D. (n=3).

3.2.4.10 In vitro cytotoxicity of the virus-mimicking liposomes loaded with doxorubicin

To assess the potency of the virus-mimicking liposomal delivery systems toward cancer cells, anticancer drug DOX was loaded into the liposomes. DOX can traverse across the cell membrane and enter the cytoplasm and nucleus by simple diffusion due to its small molecular weight. However, when DOX was loaded into nano-carriers such as liposomes to decrease its non-specific uptake and systemic side effects, the DOX-loaded delivery vesicles usually entered the cells via endocytosis. The change of cellular entry pathway from diffusion to endocytosis can lead to a remarkable reduction of the anticancer effect (Koren et al., 2012), which was consolidated by the substantially lower cytotoxicity of the DOX-loaded bare liposomes than free DOX at all concentrations tested (Figure 3-24). In contrast, the DOX-loaded, virus-mimicking liposomes exhibited a considerably enhanced potency against HeLa cells over the DOX-loaded bare liposomes ($P < 0.05$), showing a similar or even higher potency compared to free DOX within the concentration range tested. The half inhibition concentration (IC_{50}) of the DOX-loaded virus-mimicking liposomes was 0.86 μM, similar with the IC_{50} of free DOX (0.83 ± 0.18 μM) while substantively lower than the IC_{50} of the DOX-loaded bare liposomes (2.17 ± 0.10 μM). The enhanced anticancer effect of the DOX-loaded, virus-mimicking liposomes was due to the synergistic effect of the enhanced cellular uptake, efficient endosomal escape, and pH-triggered liposomal release of DOX. This implies that the

application of this virus-mimicking liposomal delivery platform for efficient intracellular drug delivery is promising.

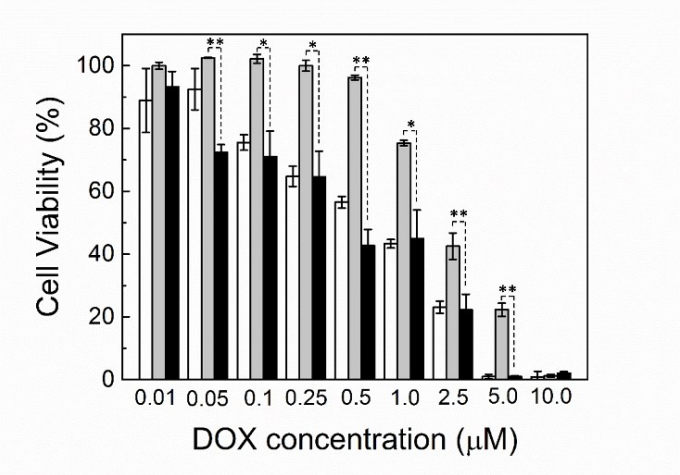

Figure 3-24. In vitro cytotoxicity of free DOX (open columns), DOX-loaded bare liposomes (gray columns), and DOX-loaded virus-mimicking liposomes (dark columns) toward HeLa cells after treatment for 24 h and further incubated for 24 h. The drug to lipid molar ratio was fixed at 20.2:100 and polymer-to-lipid molar ratio was kept at 1.9:100 for the virus-mimicking liposomes. Mean ± S.D. (n=3). *$P < 0.05$, **$P < 0.01$.

3.3 Conclusions

A novel, pH-responsive, virus-mimicking liposomal drug delivery platform was successfully developed by surface-modification of the conventional liposomes with the viral fusogenic peptide-mimicking, anionic pseudopeptides containing the pendant hydrophobic amino acid, L-phenylalanine. The pH-triggered release resulted from the liposomal membrane destabilization by the pseudopeptidic polymers. The release profile can be well controlled by varying key parameters, including the cholesterol proportion, the amphiphilicity and the amount of the adsorbed polymers. The optimal PP75-coated liposomes displayed a dramatic payload release triggered by acidification to the endosomal pH (5.0 – 6.8) while no leakage was observed at pH 7.4. The pH-responsive release behavior was dilution-independent, which is ideal for a drug delivery system, as the concentration would considerably decrease upon dilution once being administrated into the bloodstream. The size of the virus-mimicking liposomes was increased upon acidification, which was due to particle aggregation as a result of the bridging effect instead of membrane fusion. PP75 well retained its pH-responsive

membrane-destabilizing activity after being adsorbed on the liposomal surface. The PP75-coated liposomes effectively disrupted the erythrocyte membrane at early endosomal pH, while caused limited hemolysis at neutral pH. The PP75-coated, virus-mimicking liposomes exhibited enhanced cellular uptake, efficient endosomal escape and pH-triggered DOX release into the cytoplasm, leading to the significantly improved potency against HeLa cancer cell over the DOX-load conventional liposomes without polymer coating.

Chapter 4

pH-Responsive, membrane-anchoring pseudopeptides containing alkyl side chains

This chapter describes the development of a series of pH-responsive, comb-like pseudopeptides containing alkyl side chains as membrane anchors. The membrane-anchoring pseudopeptidic polymers with alkyl side chains at different lengths and different degrees of substitutions were synthesized. Their structures were characterized by FT-IR and ^{1}H-NMR. The effects of the hydrophobic alkyl side chains on the aqueous solution properties and cell membrane destabilization activity were systematically investigated. The mechanism of the polymer-membrane interaction was further explored.

4.1 Introduction

Viruses can effectively infect host cells by the endosomal release of their cargos induced by viral fusogenic peptides (Han et al., 2001; Skehel et al., 1982). However, the clinical application of viral vectors or viral peptides for cytoplasmic delivery is usually limited due to safety concerns and difficulties in large-scale production (Mhashilkar et al., 2001; Wang et al., 2012). In order to ensure efficient intracellular delivery, one strategy is to develop bio-inspired synthetic non-viral polymers that are capable of destabilizing the endosomal membrane and releasing the internalized payloads into the cytoplasm (Fleige et al., 2012; Mura et al., 2013; Stuart et al., 2010). Compared to polycations, the pH-responsive polyanions containing ionizable carboxyl groups exhibit lower cytotoxicity and more favorable biodistribution (Yessine & Leroux, 2004). Therefore, particular interest has been focused on designing and developing anionic pH-responsive endosomolytic polymers as drug carriers that mimic the membrane disruptive behavior of viral fusogenic peptides (Chen & Chen, 2016; El-Sayed et al., 2015).

The pH-responsive polyanions display a coil-to-globule conformational change due to the protonation of carboxylate ions once the pH is below the pKa, leading to the change of hydrophobic/hydrophilic balance and as a result inducing the membrane association and destabilization (Motornov et al., 2010). As the hydrophobic/hydrophilic balance plays an important role in affecting the polymer-membrane interaction, the membrane destabilization

activity can be optimized by manipulating the hydrophobicity of the polymer (Chen, 2013; Chen et al., 2005; Ho et al., 2011). Efforts on enhancing the hydrophobicity of the endosomolytic polymers have been mainly focused on conjugating hydrophobic short pendant groups on the polymer backbone, e.g. pseudopeptidic polymers bearing pendant hydrophobic natural amino acids (Chen et al., 2009a), vinyl polymers bearing short alkyl chains (Henry et al., 2006; Murthy et al., 1999), and lipopolymers bearing pendant cholesterol (Kim et al., 2007). In nature, one common strategy utilized by many membrane proteins to facilitate membrane binding is to exploit covalently attached long fatty alkyl chains as membrane anchors. These membrane proteins may have more than one attached hydrophobic fatty chains to ensure sufficiently strong hydrophobic interaction with the lipid bilayer (Cox, 2008). Thus, inspired by membrane-anchoring proteins, incorporating relatively long alkyl chains on the polymer backbone to form "comb-like" polymers can enhance the polymer-membrane interaction (Platé & Shibaev, 2012). The properties of the comb-like polymers can be tuned by varying the side chain length and grafting degree (Shi et al., 2013).

Extensive research has been carried out on vinyl poly(α-alkylacrylic acid) polymers with short (1-5 carbons) alkyl side chains (El-Sayed et al., 2015). PMAA, PEAA, PPAA and PBAA, which contain methyl, ethyl, propyl and butyl pendant groups respectively, exhibit an increasingly improved membrane disruption ability (Pack et al., 2005). Increasing the length of the short alkyl side chains has been reported to significantly enhance the polymer-membrane interaction due to the improved hydrophobicity of the polymer and deep insertion into the lipid bilayer (Resh, 2016, 1999). However, non-biodegradability remains a major drawback and limits the potential clinical application of these vinyl polymers. In order to overcome this hurdle, Eccleston *et al*. have developed an metabolite derived, pH-responsive anionic pseudopeptide PLP (Eccleston et al., 1999). PLP contains a hydrophobic backbone and pendant carboxyl groups, but without long aliphatic chains present in many membrane proteins. PLP only presents low cell membrane disruptive capacity at relatively low pHs (pH 4.5 – 5.0), which are falling outside of the endosomal pH range (Eccleston et al., 2000).

This chapter reveals the design and characterization of a series of membrane-anchoring, comb-like pseudopepdies containing hydrophobic relatively long alkyl side chains. By grafting hydrophobic relatively long alkyl chains at different chain lengths and various substitutions on the PLP backbone, the membrane binding and destabilization could be manipulated. The polymer structures were characterized by FT-IR and ^{1}H-NMR. The pH-mediated phase

separations and conformational transitions were investigated by UV-visible spectrophotometry and fluorescence spectroscopy respectively. The effect of chain length and grafting density of the relatively long alkyl chains on the polymer conformation, aggregation, hydrodynamic size and membrane destabilization were explored. The possible mechanism of the polymer-mediated cell membrane destabilization was further elucidated by hemolysis assay with the presence of osmoprotectants and the study of erythrocyte ghost formation using confocal microscopy.

4.2 Results and discussion

4.2.1 Structure characterization

HDA (C7), NDA (C10), TDA (C14) and ODA (C18) were conjugated onto the pendant carboxylic acid moieties along the PLP backbone at 18% grafting ratio (designated as PLP-HDA 18%, PLP-NDA 18%, PLP-TDA 18% and PLP-ODA 18%) via DCC/DMAP mediated amide coupling chemistry. NDA was further conjugated onto the PLP backbone at various grafting percentages (3%, 10% and 18%). The number n% denotes the actual molar percentage of hydrophobic relatively long side chains (HDA, NDA, TDA and ODA) relative to the pendant carboxylic acid groups of PLP. ^{1}H-NMR and FT-IR techniques were applied to identify the functional groups and bonds in the polymers.

In the FT-IR spectra (Figure 4-1), the peaks seen at 1629 and 1529 cm^{-1} indicate amide bond formation following polycondenzation. The peak at 1724 cm^{-1} shows the presence of carboxylic acid group. And the characteristic peaks located at 3292 cm^{-1} support the presence of N−H str and O−H str.

^{1}H-NMR was applied to further characterize the structure of the PLP and its derivatives (Figure 4-2). Compared to the ^{1}H-NMR of PLP, the comb-like polymers conjugated with alkyl chains have a unique peak at 0.77 − 0.91 ppm, which corresponds to proton in the CH_3 in the alkyl chain. Therefore, the ratio of the integral 0.77 − 0.91 ppm to the integral 7.45 − 7.64 ppm was used to calculate the degree of grafting.

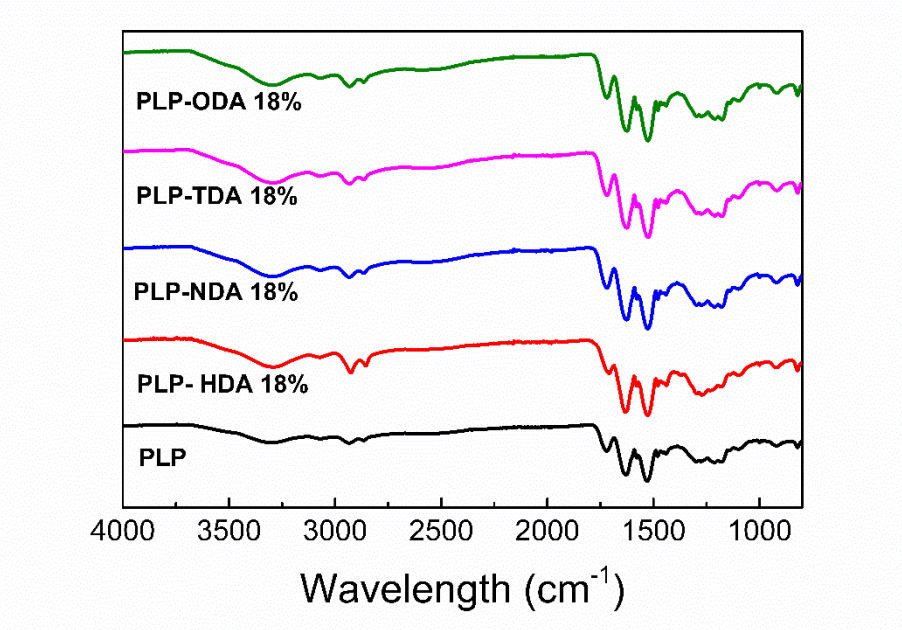

Figure 4-1. FT-IR spectra of PLP, PLP-HDA 18%, PLP-NDA 18%, PLP-TDA 18% and PLP-ODA 18% in their acid forms.

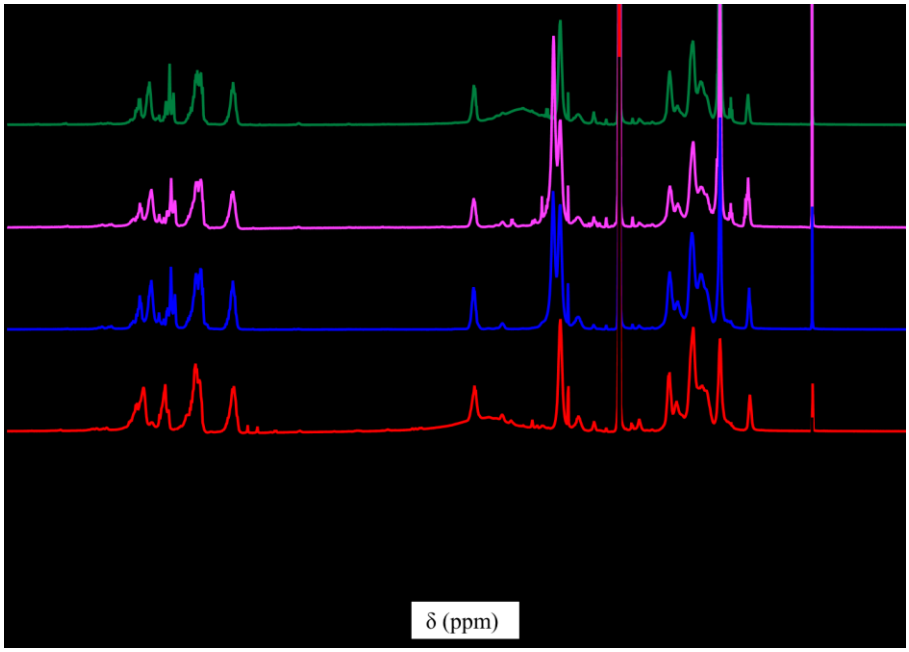

Figure 4-2. ^{1}H-NMR spectra of PLP, PLP-HDA 18%, PLP-NDA 18%, PLP-TDA 18% and PLP-ODA 18% in their acid forms in d_6-DMSO at room temperature.

4.2.2 pH-Mediated phase separation

The pH-mediated phase separation of the pH-responsive, comb-like PLP-NDA polymers with different grafting percentages of C10 alkyl chains was investigated at the polymer concentration of 1.0 mg mL^{-1}. The pH value at the onset of precipitation (pH_p), at which the transmittance started to decrease, can be tuned by varying the degree of grafting. As shown in Figure 4-3, compared to the linear counterpart PLP, the NDA-grafted, comb-like polymers with substitution ≤ 10% (PLP-NDA 3% and PLP-NDA 10%) showed a negligible change in pH_p. With a further increase in the side chain substitution, the pH_p value increased from 4.5 for PLP to 5.0 for PLP-NDA 18% (Table 4-1). This indicates that incorporating hydrophobic alkyl side chains can lead to the enhanced polymer hydrophobicity, which is consistent with the report that the increased degree grafting with hydrophobic amino acid pendant groups resulted in the improved polymer hydrophobicity (Chen et al., 2009a, 2009b).

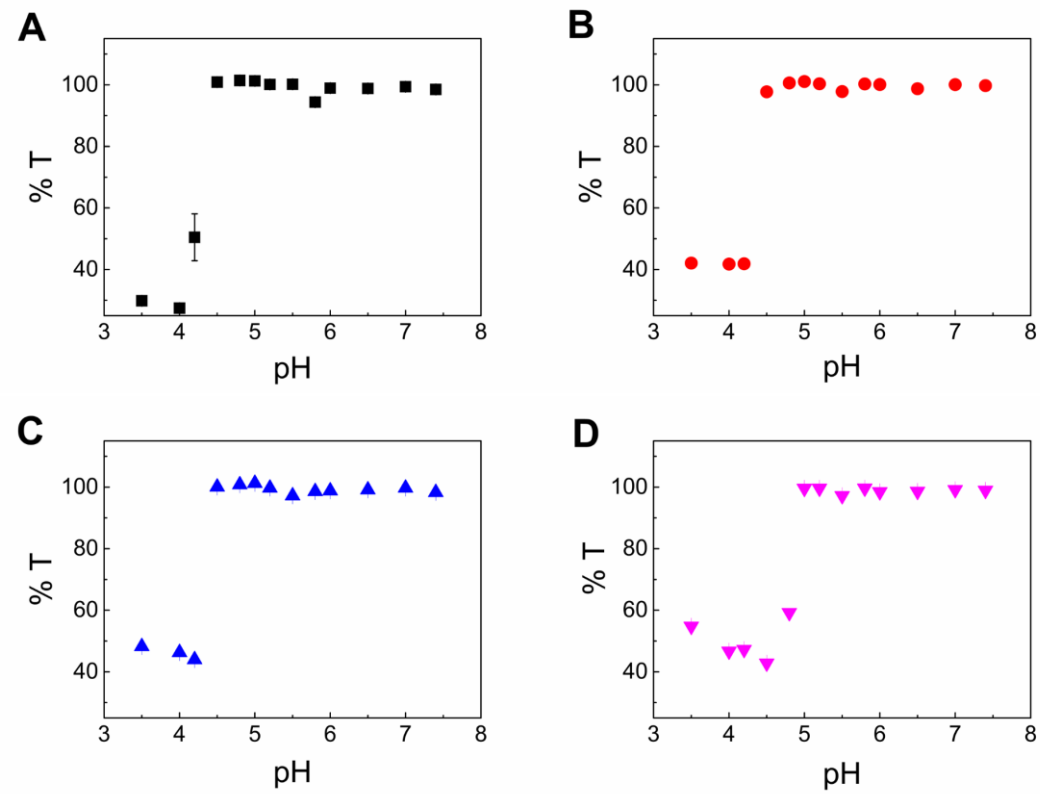

Figure 4-3. pH-Dependent transmittance of the aqueous solutions of (A) PLP, (B) PLP-NDA 3%, (C) PLP-NDA 10% and (D) PLP-NDA 18% at 1.0 mg mL^{-1} in 100 mM phosphate or citrate buffer. Mean ± S.D. (n=3).

4.2.3 Fluorescence characterization using pyrene as a probe

Pyrene, a commonly used microenvironmental polarity-sensitive probe, was employed to investigate the pH-mediated hydrophobic association of the pseudopeptidic polymers. The fluorescence intensity will increase dramatically once the pyrene transfers from a polar environment into a nonpolar environment, due to the improved solubility. There is a red shift of wavelength corresponding to the maximum intensity from 332.5 to 338 nm in the excitation spectrum of pyrene. Thus, the change of the intensity ratios (I_{338}/I_{333}) in the excitation spectra of pyrene can be applied to depict the polarities of the pyrene microenvironment (Chen et al., 2009b; Owen et al., 2012). Herein, the effect of grafting relatively long alkyl side chains on PLP and the polymer concentration on the hydrophobic association of the comb-like polymers were investigated by studying the changes in I_{338}/I_{333}. Figure 4-4 illustrates the changes of I_{338}/I_{333} as a function of pH in the aqueous solutions of PLP, PLP-NDA 3%, PLP-NDA 10% and PLP-NDA 18% at 0.5 mg mL^{-1}. The pH at the onset of hydrophobic association (pH_h), which is defined as the pH value where I_{338}/I_{333} started to increase, was 4.8 for PLP. At pH ≥ 4.8, the I_{338}/I_{333} value of PLP was almost constant around 0.6, suggesting that pyrene was in a polar environment with low solubility. Once the pH decreased below 4.8, a significant increase in I_{338}/I_{333} value was observed, indicating the transfer of pyrene to an increasingly hydrophobic environment. The rapid pH-mediated changes in I_{338}/I_{333} value can be ascribed to a pH-dependent coil-to-globule polymer conformational change (Schmaljohann, 2006). At pH 7.4, the polymer exhibited an expanded structure due to the electrostatic repulsion between the negatively charged carboxylate ions. Upon acidification, the carboxylate groups were protonated and hydrophobic association overweighed the electrostatic repulsion, resulting in a collapsed polymer structure with hydrophobic domains where pyrene was preferentially solubilized (Chen et al., 2009a).

The pH-mediated hydrophobic association was affected by incorporating different amounts of relative long alkyl side chains on the PLP backbone. Table 4-1 summarizes the variations in pH_h for PLP-NDA 3%, PLP-NDA 10% and PLP-NDA 18%. As shown in Table 4-1, increasing the degree of substitution led to a gradual increase in both I_{338}/I_{333} and pH_h. The enhanced hydrophobic association of the comb-like polymers compared to the linear counterpart PLP was due to the increased polymer hydrophobicity resulting from the hydrophobic pendant side chains. This is consistent with the report that grafting alkyl chains at a higher ratio led to enhanced hydrophobic association (Kang et al., 2001). However, the I_{338}/I_{333} value for PLP-

NDA 18% was almost constant at around 1.5 within the pH range studied. This indicates that the comb-like polymer with a high grafting percentage of hydrophobic NDA moieties self-aggregates at pH 7.4 at a certain polymer concentration, resulting in pyrene being localized in the hydrophobic core. As a result, only a negligible decrease in I_{338}/I_{333} was observed upon acidification.

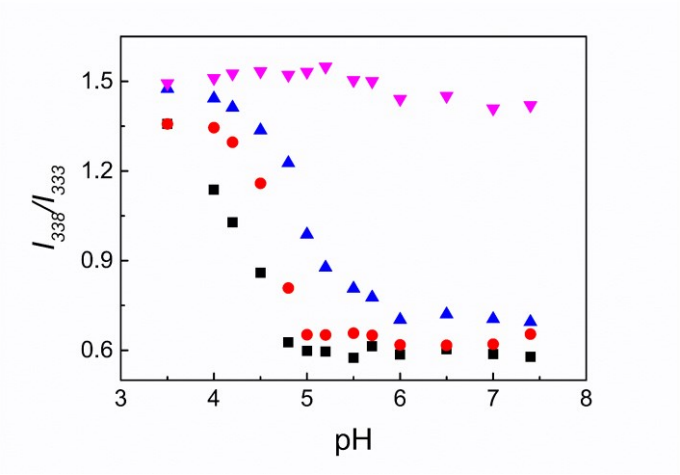

Figure 4-4. pH-Dependent I_{338}/I_{333} in the excitation spectra of pyrene dissolved in aqueous solutions of PLP (■), PLP-NDA 3% (●), PLP-NDA 10% (▲) and PLP-NDA 18% (▼) at 0.5 mg mL^{-1}. Mean ± S.D. (n=3).

The comb-like PLP-NDA polymers would self-assemble in the aqueous solution due to their amphiphilic nature. The CAC was determined by the variations in I_{338}/I_{333} as a function of polymer concentration at pH 7.4 (Figure 4-5). The CAC value was calculated from the intersection of the line through the points on the rapidly varying part and the line through the points at the low-concentration extreme of the plot (Mao et al., 2016). No micelle existed in the aqueous solution while the polymer concentration was below the CAC. At or above the CAC, the polymers started to associate and form micelles. Then pyrene was preferentially localized into the hydrophobic cores of the polymeric micelles. Table 4-1 shows that the CAC value decreased with the increasing the NDA grafting percentage, which was due to the enhanced hydrophobicity of the polymer.

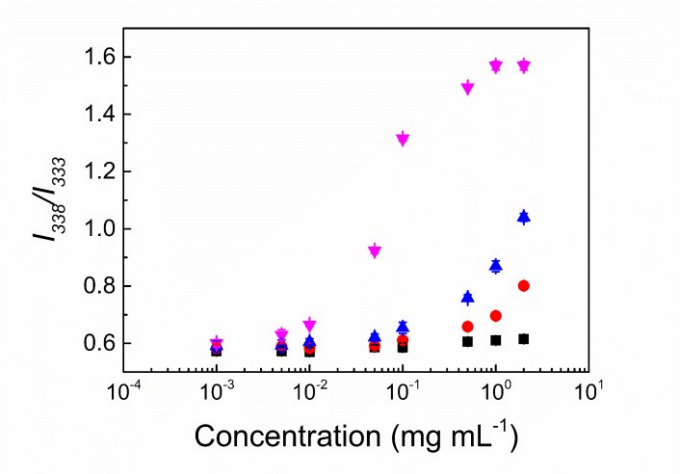

Figure 4-5. Concentration-dependent I_{338}/I_{333} in the excitation spectra of pyrene dissolved in aqueous solutions of PLP (■), PLP-NDA 3% (●), PLP-NDA 10% (▲) and PLP-NDA 18% (▼) at pH 7.4. Mean ± S.D. (n=3).

Table 4-1. pH Values at the onset of precipitation (pH_p), pH values at the onset of hydrophobic association (pH_h), and pH ranges for hydrophobic association of PLP and the comb-like polymers at 0.5 mg mL^{-1} and their CACs at pH 7.4. Mean ± S.D. (n=3).

	PLP	PLP-NDA 3%	PLP-NDA 10%	PLP-NDA 18%
pH_p	4.5	4.5	4.5	5.0
pH_h	4.8±0.2	5.0±0.2	6.0±0.2	N/A
pH range	3.5–4.8	4.0–5.0	3.5–6.0	N/A
CAC (mg mL^{-1})	N/A	0.342	0.282	0.031

4.2.4 Hydrodynamic size

4.2.4.1 Effect of side chain on particle size

The hydrodynamic size of the pseudopeptidic polymers was measured by DLS. As shown in Figure 4-6 and Table 4-2, both the comb-like polymers and their linear counterpart PLP displayed a bimodal size distribution at a concentration of 0.5 mg mL^{-1} at pH 7.4. PLP had a small particle population (mean size of 10.3 ± 2.3 nm) and a large population (mean size of 384.2 ± 34.5 nm). By increasing the grafting percentage of NDA side chains, the mean size of the small population remained similar, whilst the mean size of the large population was considerably decreased. The mean size of the large population of PLP-NDA 18% was 51.9 ±

1.6 nm. This was because the incorporation of hydrophobic side chains led to stronger intermolecular and intramolecular interactions (Kang et al., 2002, 2001). This result is consistent with Figure 4-4, which consolidates the conclusion that incorporating relatively long NDA as the side chains significantly enhanced the hydrophobicity of the polymer and subsequently resulted in the formation of more compact structures.

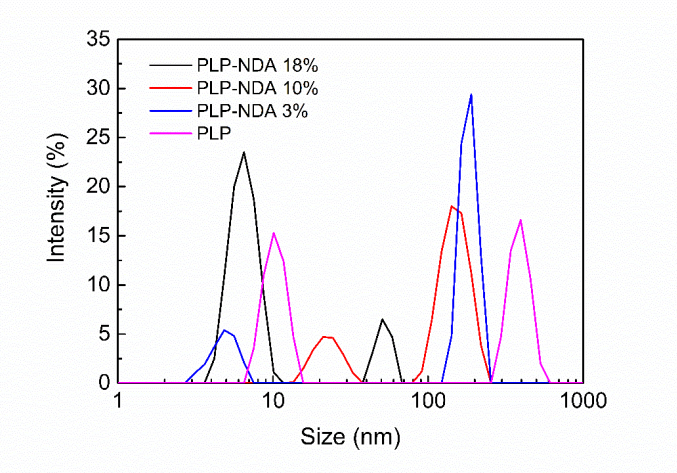

Figure 4-6. Particle size distributions of PLP, PLP-NDA 3%, PLP-NDA 10% and PLP-NDA 18% at the concentration of 0.5 mg mL^{-1} at pH 7.4.

Table 4-2. The mean hydrodynamic diameters of PLP and its derivatives at a concentration of 0.5 mg mL^{-1} at pH 7.4. Mean ± S.D. (n=3).

	PLP	PLP-NDA 3%	PLP-NDA 10%	PLP-NDA 18%
Population 1 mean size (nm)	10.3 ± 2.3	4.9 ± 1.2	22.7 ± 5.3	6.5 ± 2.0
Population 2 mean size (nm)	384.2 ± 34.5	183.4 ± 12.6	151.3 ± 11.7	51.9 ± 1.6

4.2.4.2 Effect of pH on particle size

The pH-dependent size change of the pseudopeptides was also investigated. As shown in Figure 4-7A, PLP exhibited two size populations at both pH 7.4 and 5.5. However, the mean particle size of its large population reduced remarkably from 384.2 ± 34.5 to 86.0 ± 10.5 nm upon acidification from pH 7.4 to 5.5. PLP-NDA 18% displayed two size populations at pH

7.4. In contrast, once the pH decreased to 5.5, only one particle population with a mean hydrodynamic size of 16.4 ± 5.6 nm was observed in Figure 4-7B. It was because of the pH-induced coil-to-globule conformational change. At neutral pH, the electrostatic repulsion between the negatively charged ionized carboxyl groups overweighed the hydrophobic interaction. Thus the polymer exhibited an extended coil conformation, leading to the formation of loose aggregates (Chen et al., 2008). Upon acidification, the protonation of carboxyl ions led to the predomination of the hydrophobic interaction, which resulted in a globular polymer confirmation. The polymeric amphiphiles consisting of relatively long alkyl side chains exhibited the comb-like architecture and therefore tended to form a more compact structure. As a result, a reduced particle size could be observed upon acidification. This is in agreement with the report by other researchers that the PLP bearing PEG side chains displayed a similar transition from a bimodal size distribution to a single-modal distribution upon acidification (Chen et al., 2008).

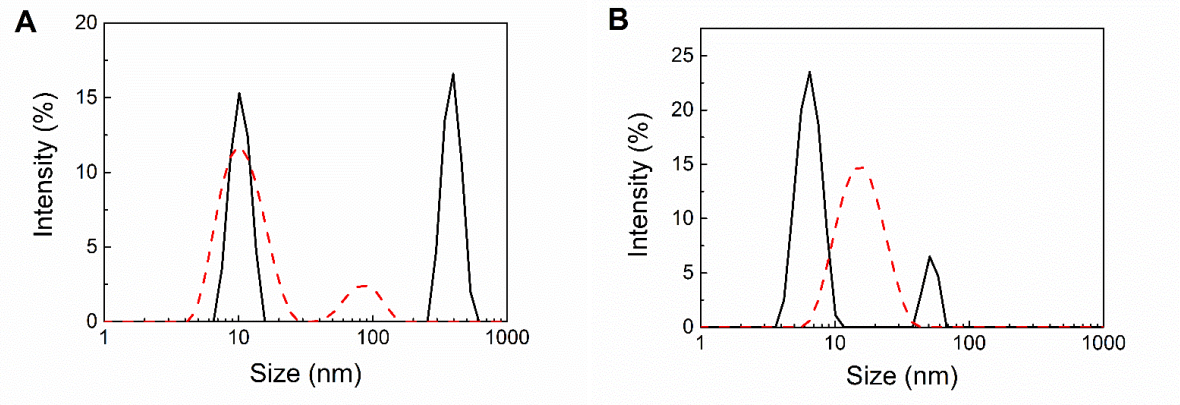

Figure 4-7. Particle size distributions of PLP (A) and PLP-NDA 18% (B) at a concentration of 0.5 mg mL^{-1} at pH 7.4 (solid) and pH 5.5 (dash).

4.2.4.3 Effect of polymer concentration on particle size

Figure 4-8 and Table 4-3 demonstrate variations of the hydrodynamic size of PLP-NDA 18% with the concentration ranging from 0.05 to 2 mg mL^{-1} at pH 7.4. At the concentration of 2 mg mL^{-1}, only one size population was detected with the mean size of 8.1 ± 1.6 nm, suggesting that the polymer formed a compact structure. With decreasing polymer concentration, the size distribution spilt into two populations. The mean particle size of the large population increased with decreasing the polymer concentration. At a concentration of 0.05 mg mL^{-1} at pH 7.4, the mean size of the large population increased to 122.7 ± 12.6 nm.

The consistency of DLS (Figure 4-8) and pyrene fluorescence (Figure 4-5) results reinforced the conclusion that an increase in the concentration of the comb-like polymer could enhance intermolecular interactions, and therefore facilitate the formation of a compact structure.

Table 4-3. The mean hydrodynamic diameters of PLP-NDA 18% with various concentrations at pH 7.4. Mean ± S.D. (n=3).

	2 mg mL^{-1}	1 mg mL^{-1}	0.5 mg mL^{-1}	0.1 mg mL^{-1}	0.05 mg mL^{-1}
Population 1 mean size (nm)	8.1 ± 1.6	6.3 ± 0.9	6.5 ± 2.0	6.3 ± 2.7	6.4 ± 3.6
Population 2 mean size (nm)	N/A	28.3 ± 2.4	51.9 ± 1.6	102.1 ± 3.2	122.7 ± 12.6

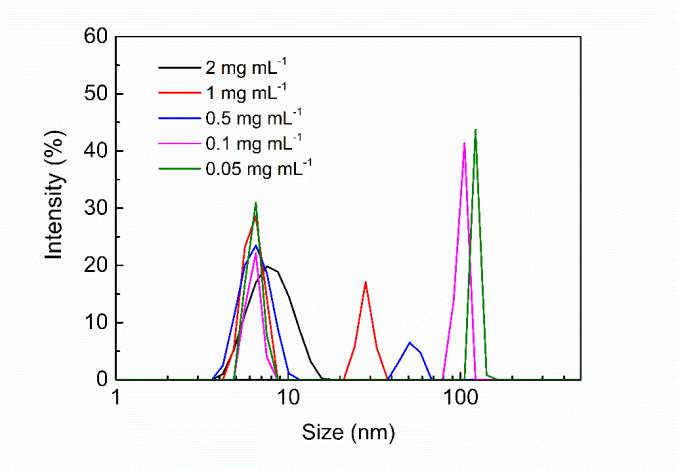

Figure 4-8. Particle size distributions of PLP-NDA 18% at different polymer concentrations at pH 7.4.

4.2.5 Membrane destabilization activity

4.2.5.1 pH-Dependent hemolytic activity of the comb-like polymers with various side chain of different lengths

The cell membrane destabilization activity of the pseudopeptidic polymers grafted with relatively long alkyl chains at different lengths was assessed by hemolysis assay using RBCs as a model for endosomal membranes (Chen et al., 2009c). The pH range of 7.4 – 4.5 mimics

the gradually acidifying environment during the endocytic pathway (Iversen et al., 2011). Figure 4-9 shows the pH-dependent hemolysis of PLP and the comb-like polymers grafted with 18% HDA (C7), NDA (C10), TDA (C14) or ODA (C18) at 0.5 mg mL^{-1}. PLP only displayed limited membrane disruption at pH 5.0. As comparison, the comb-like polymers containing relatively long alkyl side chains essentially showed limited hemolysis at pH 7.4, but displayed significantly enhanced hemolytic activity upon acidification compared to their linear counterpart PLP. Compared to PLP, the maximum degree of hemolysis was increased significantly to 55.3 ± 1.7% at pH 5.5 by grafting 18% HDA on PLP. The significantly enhanced membrane destabilization was due to the increased hydrophobicity of the polymer by grafting relatively long alkyl chains as membrane anchors. Vial *et al.* have reported that amphiphilic polymers lacking hydrophobic side chain cannot effectively bind or destabilize the vesicular membrane (Vial et al., 2005). With further extending the chain length to 10 carbons, the PLP-NDA 18% displayed 99.6 ± 0.2 % hemolysis at pH 5.5. Conjugation with longer alkyl chains could provide stronger membrane association and deeper insertion into the lipid membrane (Resh, 2016). By just increasing one methylene unit in the pendant alkyl group, PPAA displayed 15 times stronger membrane destabilization activity compared to PEAA (Murthy et al., 1999). Increasing the side chain length to 14 carbons resulted in a shift of pH for the onset of hemolytic activity to a higher value (pH 6.0). A similar finding has been reported that further increasing the pendant alkyl group of the vinyl-based polycarbonates by one methylene group from propyl (PPAA) to butyl group (PBAA), a significant increase in the pH at the onset of hemolytic activity was observed, while the PBAA polymer may cause the undesirable membrane destabilization at physiological pH (Murthy et al., 2001). However, the maximum degree of hemolysis for PLP-ODA 18% (76.7 ± 0.1%) was lower than PLP-TDA 18% (95.5 ± 0.7%). The hydrophobic/hydrophilic balance is of crucial importance for polymer-membrane interaction (Marie et al., 2014). Conjugation of a polymer backbone with alkyl chains above the critical chain length could lead to the reduced polymer-membrane interaction due to self-aggregation at physiological pH (Chen et al., 2004; Morille et al., 2008).

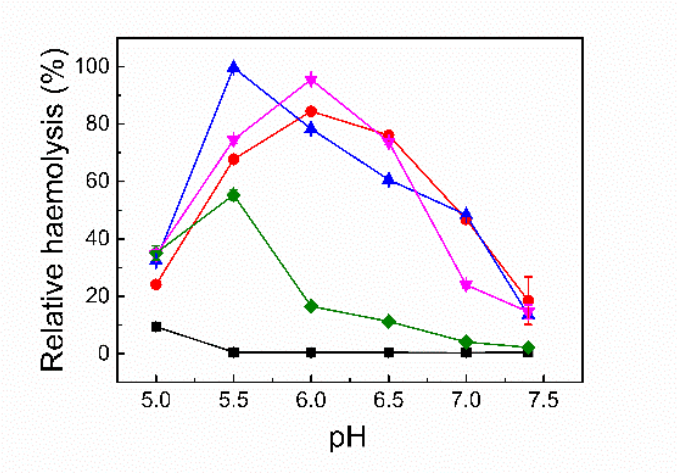

Figure 4-9. Relative hemolysis of RBCs incubated with PLP (■), PLP-HDA 18% (◆), PLP-NDA 18% (▲), PLP-TDA 18% (▼) and PLP-ODA 18% (●) at 0.5 mg mL^{-1} for 1 h. Mean ± S.D. (n=3).

4.2.5.2 pH-Dependent hemolytic activity of the comb-like polymers with different degrees of substitutions

The pH-dependent hemolytic activity of the polymers with different degrees of substitutions was further assessed to evaluate the effect of side chain grafting density on the membrane destabilization activity. The maximum degree of hemolysis was increased from 28.8 ± 0.9% for PLP to 42.3 ± 0.1%, 77.1 ± 3.7% and 99.6 ± 0.2% for PLP-NDA 3%, PLP-NDA 10% and PLP-NDA 18% respectively. The ranking of the hemolytic activity of the polymers within the endosomal pH range was PLP-NDA 18% > PLP-NDA 10% > PLP-NDA 3% > PLP, which was well correlated with the increasing amount of the hydrophobic NDA side chains and the increasing hydrophobicity of those polymers (Figure 4-4). In addition, the pH at the onset of hemolytic activity was also increased from a lysosomal pH 4.5 for PLP to an endosomal pH 5.5 for the polymers conjugated with NDA as side chain at varies degrees of substitutions. Increasing the degree of grafting resulted in a shift of pH at the onset of hemolytic activity to a higher value (Chen et al., 2009c), leading to the enhanced hemolytic activity of the comb-like polymers within the pH range of 6.0 – 6.8 that is typical of early endosomes (up to a hemolysis of 78.3 ± 0.2% for the PLP-NDA 18% polymer).

The improved cell membrane destabilizing activity of the comb-like polymers could be ascribed to the enhanced hydrophobicity of the polymer by incorporation of hydrophobic side chains. This result is consistent with the previous report that conjugating hydrophobic side

chains onto the polymer backbone resulted in stronger membrane disruptive activity (Chen et al., 2009b, 2009c). PEAA, which is poly(α-ethylacrylic acid) containing short ethyl pendant chains showed significantly improved membrane binding and disruption at acidic pHs compared to its parent polymer polyacrylic acid (Thomas et al., 1996). Other researchers have reported that even incorporating a small number of long alkyl side chains on the polymer backbone can promote deeper insertion of the hydrophobically modified poly(N-isopropylacrylamides) into the liposomal bilayer (Polozova & Winnik, 1997). Therefore, the comb-like PLP-NDA polymers containing a relatively large quantity of hydrophobic alkyl side chains as membrane anchors displayed the enhanced interaction with cell membranes, which is in agreement with the reports that the polymer-membrane interaction can be affected by polymer architecture (Frey et al., 2007; Qiu & Bae, 2006).

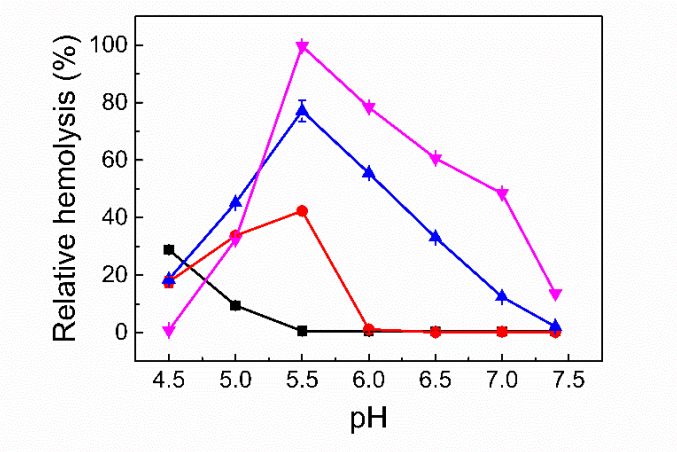

Figure 4-10. pH-Dependent hemolysis of RBCs incubated with PLP (■), PLP-NDA 3% (●), PLP-NDA 10% (▲) and PLP-NDA 18% (▼) at 0.5 mg mL^{-1} for 1h. Mean ± S.D. (n=3).

4.2.6 Concentration-dependent hemolysis

The ability of PLP-NDA 18% and PLP to hemolyze RBCs at endosomal pH and physiological pH was further assessed as a function of polymer concentration (Figure 4-11). As shown in Figure 4-11A, PLP-NDA 18% exhibited negligible hemolysis at pH 7.4 within the concentration range tested (0.005 – 10 mg mL^{-1}), but displayed vastly superior membrane disruptive activity at pH 5.5 within a wide concentration range (0.025 – 10 mg mL^{-1}). The membrane destabilization activity was also dilution-independent over a wide range. Diluting the polymer concentration 400-folder to as low as 0.025 mg mL^{-1}, PLP-NDA 18% still showed a high level of hemolysis (72.9 ± 0.5%) at pH 5.5. This dilution-independent characteristic of the comb-like polymer could be ascribed to the stable membrane anchoring as a result of the

deep insertion of the hydrophobic side chains into the lipid membrane (Marie et al., 2014). The pendent alkyl chains served as membrane anchors on the polymer or peptide were found to be aligned with the phospholipid alkyl chains in the lipid membrane, and thus strong binding with the membrane could be achieved (Khandelia et al., 2008). As comparison, the linear polymer PLP displayed less than 1% hemolysis at both acidic and neutral pHs with concentration up to 10 mg mL^{-1} (Figure 4-11B), possibly due to the lack of membrane anchors. The pH-responsive, dilution-independent characteristics of PLP-NDA 18% is desirable for intracellular drug delivery application, as the concentration of drug delivery systems would significantly decreased after administration because of the dilution in the bloodstream (Tribet & Vial, 2008).

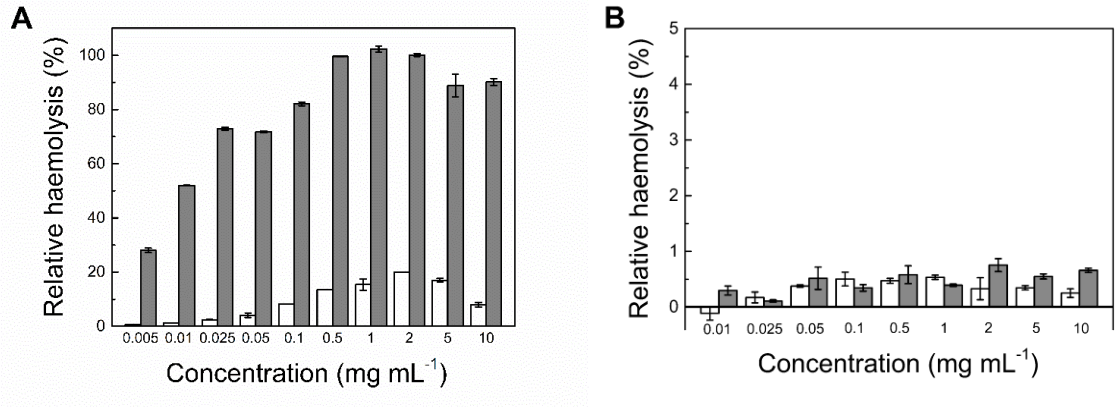

Figure 4-11. Concentration-dependent hemolysis of RBCs incubated with PLP-NDA 18% (A) and PLP (B) at pH 7.4 (open columns) and 5.5 (close columns). Mean ± S.D. (n=3).

4.2.7 Time-dependent hemolysis

The time-dependent hemolysis of the pseudopeptidic polymers was also investigated at a polymer concentration of 0.5 mg mL^{-1} at pH 5.5. As shown in Figure 4-12, after only 10 min of incubation, 72.8 ± 1.8% hemolysis was achieved by PLP-NDA 18%, followed by almost complete membrane destabilization after 20 min incubation. In contrast, the polymers with ≤ 3% NDA displayed not only limited membrane destabilization but also slower kinetics. A maximum degree of hemolysis of 47.1 ± 4.0% was caused by PLP-NDA 3% after 50 min of incubation, whilst almost no hemolysis was identified for the linear polymer PLP within the time period tested. This suggests that increasing the hydrophobicity of the polymer could lead to a stronger driving force, thus the electrostatic repulsion between the negatively charged polymer and cell membrane could be rapidly overweighed by hydrophobic interaction (Tribet

& Vial, 2008), resulting in faster membrane binding and superior membrane destabilization. The rapid membrane disruption activity of the comb-like polymers, in particular PLP-NDA 18%, would allow them to efficiently destabilize the endosomal membrane before the vesicular evolution from endosomes to lysosomes, which may take 30 min to several hours according to the reported work (Pack et al., 2005).

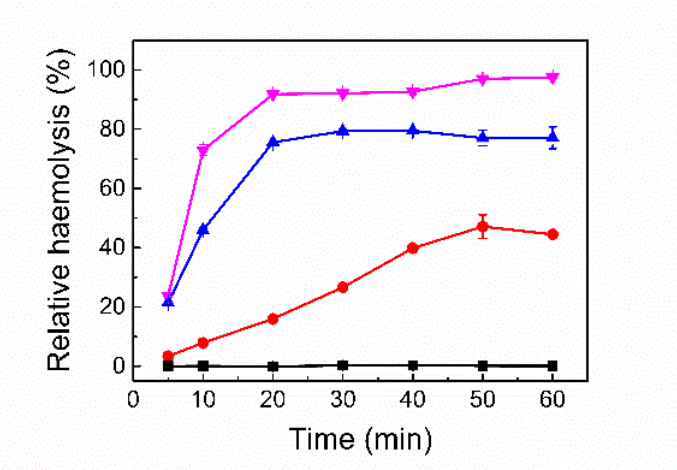

Figure 4-12. Time-dependent hemolysis of RBC incubated with PLP (■), PLP-NDA 3% (●), PLP-NDA 10% (▲), PLP-NDA 18% (▼) at 0.5 mg mL^{-1} at pH 5.5. Mean ± S.D. (n=3).

4.2.8 Mechanism of cell membrane destabilization

4.2.8.1 Hemolysis assay with the presence of osmoprotectants

The cause for the leakage of lipid membrane can be related to membrane fusion (Linhardt & Tirrell, 2000), pore formation (Matsuzaki et al., 1997) or membrane solubilization (Thomas et al., 1994). Further insights into the mechanism of cell membrane disruption were obtained by investigating the hemolysis of PLP-NDA 18% with the presence of sucrose (M_w = 342 Da) and PEGs with different molecular weights (M_w = 4 k, 6 k, 10 k, 12 k and 20 kDa). It has been demonstrated that the membrane disruptive polymers or peptides could cause osmotic imbalance of RBCs by forming defects such as pores or channels on the cell membrane. As only low molecular weight solutes can diffuse through the pores or channels while hemoglobin cannot, the osmotic pressure could result in swelling and/or rupture of cell membranes, leading to the release of cytoplasmic contents or complete lysis of RBCs (Sovadinova et al., 2011). PEGs have been reported to provide osmoprotection of RBCs against polymer-induced pore-formation (Chen et al., 2009c). As shown in Figure 4-13, the presence of sucrose did not inhibit

hemolysis whilst PEG 4 kDa displayed limited osmoprotection. However, the inhibition of hemolysis was significantly enhanced with increasing the PEG molecule weight. With the presence of 10 mM PEG 10 kDa, the hemolysis decreased to 38.5 ± 0.9%, whilst PEG 20 kDa almost completely inhibited the hemolysis. This result suggests that with the increase in the hydrodynamic size of PEGs, these solutes could reduce the osmolality difference between the cytoplasm and the buffer solution, and therefore protect the RBCs against hemolysis. This validates the hypothesis that the hemolysis occurred due to polymer-induced pore formation on the cell membrane.

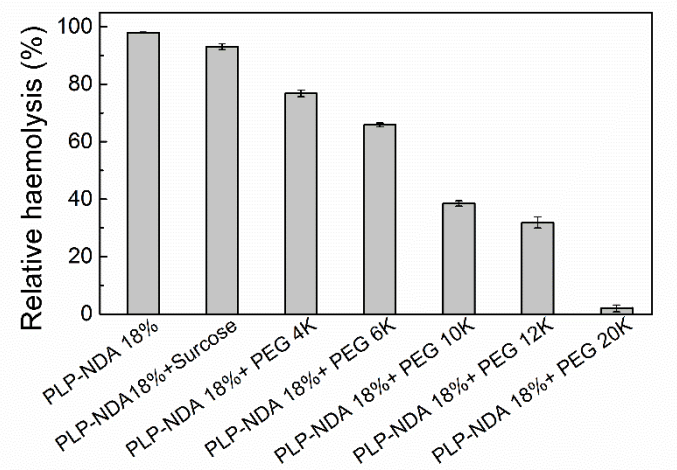

Figure 4-13. Relative hemolysis of RBCs incubated with 0.5 mg mL^{-1} PLP-NDA 18% with or without the presence of 10 mM sucrose or 10 mM PEG with different molecular weights at pH 5.5 for 1 h. Mean ± S.D. (n=3).

4.2.8.2 Investigation of erythrocyte ghost formation by confocal microscopy

In order to further confirm the pore formation mechanism of the hemolysis by the comb-like polymer, the membrane integration of RBCs was examined by laser scanning confocal microscopy. As shown in Figures 4-14 and 4-15, FITC-dextran (M_w = 4 kDa) and Texas Red® hydrazide could not pass though the RBC membrane treated with buffer only (at both pH 7.4 and 5.5), 0.5 mg mL^{-1} linear polymer PLP (at both pH 7.4 and 5.5), or 0.5 mg mL^{-1} comb-like polymer PLP-NDA 18% at pH 7.4. In contrast, when the RBCs were incubated with 0.5 mg mL^{-1} PLP-NDA 18% at pH 5.5 for 30 min, more than 90% of the RBCs were turned into erythrocyte ghosts (Figure 4-14). The membrane of erythrocyte ghosts showed bright red fluorescence due to the staining with Texas Red® hydrazide, which could react with the peroxidized lipids during the formation of erythrocyte ghosts (Matteo et al., 1998). No fluorescence intensity from the green channel (FITC-dextran 4 kDa) was observed between the

inside and the outside of the erythrocyte ghosts, suggesting that the FITC-dextran 4 kDa could efficiently permeate through the erythrocyte ghost membrane. No membrane fusion was seen, and the cell membrane remained integrated as shown in the confocal microscopy images, which further consolidates that the comb-like polymer destabilized the cell membrane at endosomal pH by pore formation without causing membrane fusion or rupture. It has been reported that the pseudopeptidic PLP bearing 1.3 mol% long methoxy PEG (M_n = 4.4 kDa) side chains could also release hemoglobin into the extracellular medium without lysing cell membranes (Chen et al., 2008).

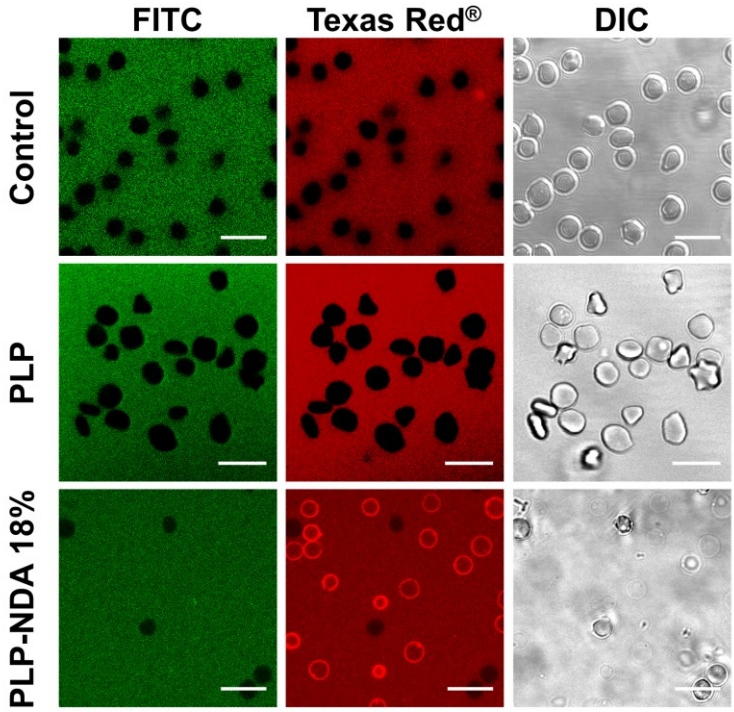

Figure 4-14. Confocal microscopy images of RBCs incubated with FITC-dextran (4 kDa) and Texas Red® with or without polymers (0.5 mg mL^{-1}) for 30 min at pH 5.5. Scale bar 10 µM.

Membrane binding and insertion are thought to be two important continuous steps for polymer introduced membrane destabilization (Marie et al., 2014). The electrostatic repulsion between the negatively charged cell membrane and the polyanions could hamper the effective membrane binding and insertion of the polymers. Thus, although the linear parent polymer PLP displayed a coil-to-globule conformational change (Eccleston et al., 2000), it displayed no or limited hemolysis at 0.5 mg mL^{-1} from pH 7.4 to 4.5 (Figure 4-10) due to the limited polymer-membrane interaction. However, conjugating relatively long hydrophobic side chains could largely enhance the hydrophobic interaction and overweigh the electrostatic repulsion. Besides,

the hydrophobic side chains could serve as membrane anchors (Resh, 2013), leading to pore formation in the lipid membrane with the presence of the comb-like polymer at acidic pHs.

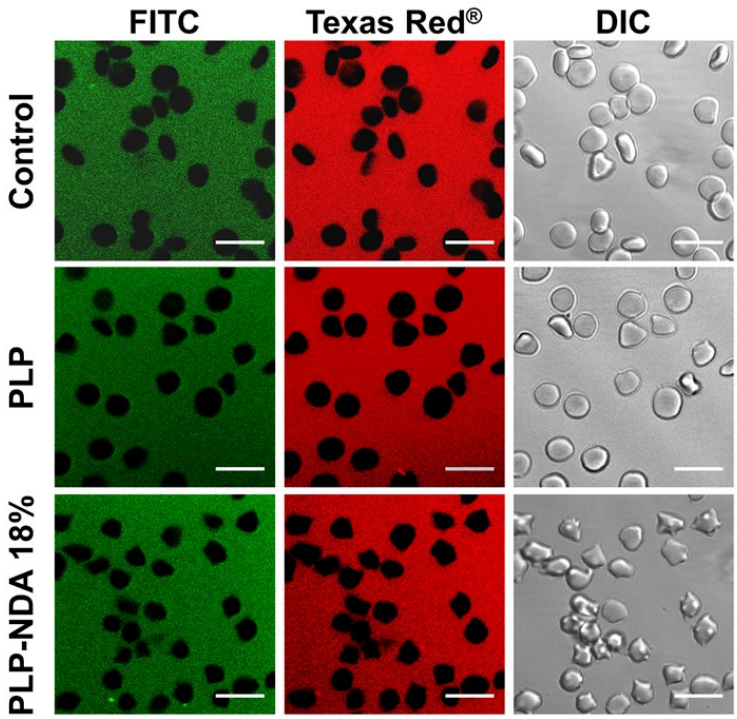

Figure 4-15. Confocal microscopy images of RBCs incubated with FITC-dextran (4 kDa) and Texas Red® with or without polymers (0.5 mg mL^{-1}) for 30 min at pH 7.4. Scale bar 10 μM.

Figure 4-16 depicts the confocal microscopy images of the RBCs incubated with FITC-dextran at different molecular weight (M_w = 10 – 2000 kDa) and 0.5 mg mL^{-1} PLP-NDA 18% at pH 5.5 for 30 min. FITC-dextran with a molecular weight up to 70 kDa efficiently entered the erythrocyte ghosts. The pore size formed by PLP-NDA 18% was estimated to be around 6 nm according to the Stoke's radius of FITC-dextran 70 kDa (information provided by supplier). It is interesting to compare the results shown in Figures 4-13 and 4-16. In Figure 4-13, hemolysis was almost totally inhibited with the presence of 10 mM 20 kDa PEG, while in Figure 4-16, FITC-dextran 70 kDa could still enter the erythrocyte ghosts. It might be due to the following reasons. First, the pore size might change during the hemolysis process. The membrane disruptive polymers might first create small pores, which would allow low molecular weight solutes to diffuse through the membrane. The second stage of hemolysis could be swelling and/or rupture of the membrane due to the gradually increased osmotic pressure, during which the pore size might increase (Sovadinova et al., 2011). The presence of 20 kDa PEG could effectively reduce the osmolality difference between the inside and the

outside of the cell, and therefore the hemolysis was inhibited without entering the second stage. However, in the confocal microscopy study using FITC-dextran, the lack of osmoprotectants would lead to membrane swelling, which might result in the increase in pore size. In addition, PEG and dextran might exhibit different viscosities and hydrodynamic sizes in aqueous solution, thus exerting different effects on the RBCs. The successful delivery of FITC-dextran with different molecular weights into the RBC model at endosomal pH suggests that the novel pH-responsive, comb-like polymer can destabilize the endosomal membrane to release endocytosed small molecules or macromolecules into the cell cytoplasm without totally lysing vesicular compartments.

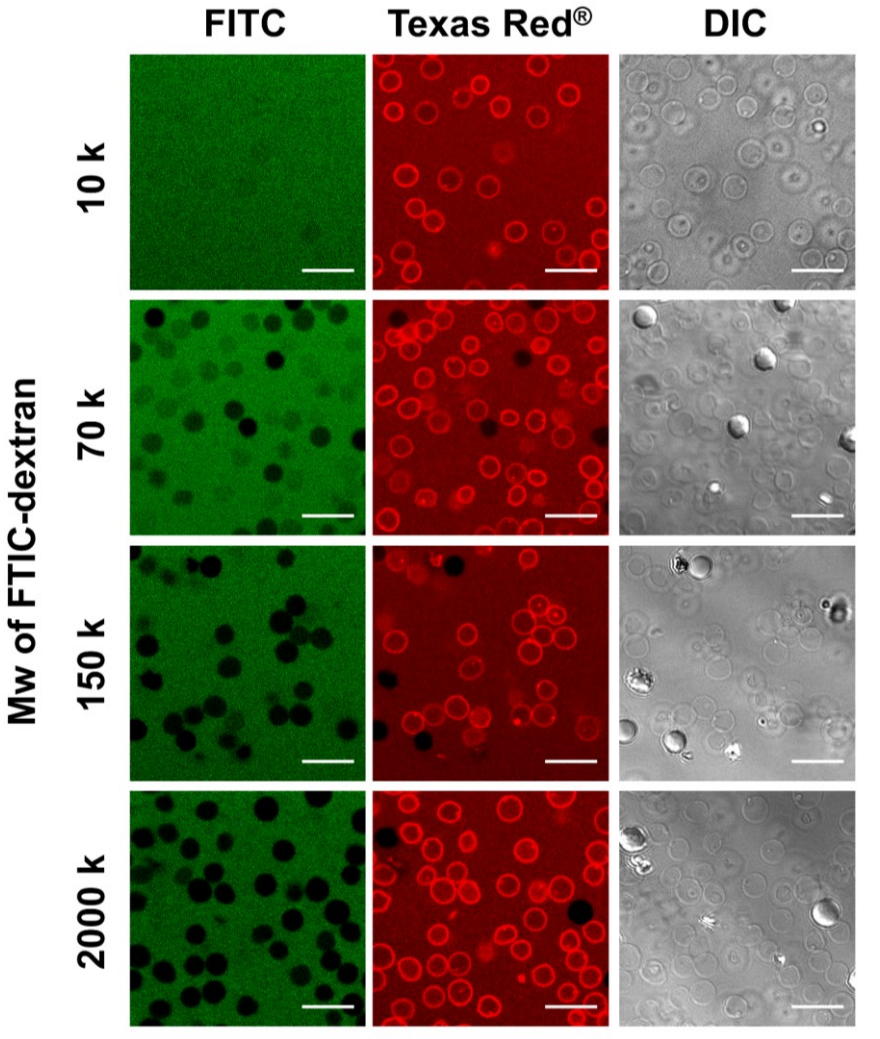

Figure 4-16. Confocal microscopy images of RBCs incubated with Texas Red® and different molecular weight of FITC-dextran with the presence of 0.5 mg mL^{-1} PLP-NDA 18% for 30 min at pH 5.5. Scale bar 10 μM.

4.3 Conclusions

A series of pH-responsive, comb-like polymers have been synthesized by grafting hydrophobic relatively long alkyl chains with different lengths onto the backbone of a linear pseudopeptide, PLP, at different substitution degrees. The pH-responsive changes in conformation, hydrodynamic size and membrane destabilization activity could be tuned by controlling the grafting degree of the side chain moieties. The side chain length affected the membrane disruptive activity of the polymer and shifted the pH at the onset of hemolytic activity. The optimal polymer displayed a superior membrane destabilization ability at endosomal pH compared to its linear counterpart PLP, because of the significantly enhanced hydrophobicity and the comb-like structure. At polymer concentration of 0.5 mg mL^{-1}, PLP-NDA 18% caused almost complete hemolysis of RBCs at pH 5.5, whilst only 0.5% hemolysis was achieved by its linear counterpart PLP at the same condition. The excellent pH-responsive membrane destabilization activity of the comb-like polymer was dilution-independent, which is of crucial importance to drug delivery application. The mechanism of the membrane disruption was found to be pore formation, as confirmed by the hemolysis study using osmoprotectants and the formation of erythrocyte ghosts.

Chapter 5

Application of the membrane-anchoring, comb-like pseudopeptides for intracellular delivery

This chapter describes the intracellular delivery using the optimal membrane-anchoring, comb-like pseudopeptide, PLP-NDA 18%, which contains hydrophobic relatively long alkyl side chains. At physiological pH, the PLP-NDA 18%-mediated intracellular delivery was tested in three different cell lines, and compared with its linear counterpart PLP. The in vitro cytotoxicity and IC_{50} were determined using different cell lines and incubation times. As the microenvironment of tumors is slightly acidic compare to the normal tissues, the polymer-mediated intracellular delivery was further assessed at acidic conditions. Key parameters, e.g. polymer concentration, side chain length, pH, incubation time, the presence of serum that may affect the delivery were explored. Intracellular delivery of payloads with different sizes and the delivery kinetics were investigated to demonstrate that PLP-NDA 18% can mediate efficient intracellular delivery of a wide size range of payloads into a variety of cell lines.

5.1 Introduction

Efficient delivery of pharmaceutical agents, especially macromolecules, into cells remains a major challenge for drug delivery (Canton & Battaglia, 2012; Varkouhi et al., 2011). The plasma membrane represents a barrier to the entry of pharmaceutical macromolecules and nanoparticulate drug carriers to the cell interior readily without the presence of active transport mechanisms (Belting et al., 2005; Hou et al., 2015; Sahay et al., 2010). Macromolecules and drug carriers are usually internalized via an endocytic pathway, which often leads to enzymatic degradation of the bioactive compounds in lysosomes due to insufficient endosomal escape (Iversen et al., 2011; Jeong & Gutowska, 2002; Mitragotri et al., 2014). In order to achieve cytoplasmic delivery, a number of methods have been developed, including the use of cell-penetrating peptides (CPPs), endosomolytic polymers, stimuli-responsive nanoparticles, etc. (Copolovici et al., 2014; Hou et al., 2015; Motornov et al., 2010; Nakase et al., 2010).

CPPs are one of the most popular and efficient vectors for intracellular delivery (Wang et al., 2014). They typically contain 5-30 amino acids and can cross the cell membrane (Vivès et al., 2008). Since the introduction of the first CPP (TAT) for protein transduction into the cell in 1988 (Frankel & Pabo, 1988), a variety of CPPs have been developed and applied as

molecular transporters for delivery of siRNA, nucleic acids, proteins, small molecular drugs, imaging agents and so on (Bolhassani, 2011; Copolovici et al., 2014; Milletti, 2012). The exact cellular uptake mechanism of CPPs is still not fully understood. The CPPs could be internalized through two major pathways: energy-independent direct translocation and/or energy-dependent endocytic pathway. The cellular entry pathway depends on the cargo type, properties and concentration of CPPs, cell type and membrane lipid composition (Farkhani et al., 2014). Besides delivery of the conjugated cargos, CPPs could also mediate non-covalent delivery. Chariot™ Protein Delivery Reagent (Active Motif, USA) is the first commercial peptide-based product for the non-covalent delivery of proteins into cells (Lagunavicius, 2015). Compared to the conjugation method, non-covalent delivery is easier to handle and does not suffer the risk of altering the compound's biological properties during the chemical conjugation (Fu et al., 2015).

Although CPPs could facilitate efficient intracellular delivery, they also have a few critical drawbacks, which limit their clinical application. Most known CPPs are positively charged, leading to high cytotoxicity toward normal tissues (Koren & Torchilin, 2012). Besides, using CPPs for intracellular delivery may induce humoral immune response against the therapy because majority of the CPPs are sequence from viral proteins (Farkhani et al., 2014). Difficulty in large-scale manufacturing is another hurdle that limits the wide application of CPPs. Therefore, anionic, synthetic endosomolytic polymers, which are easy to synthesis, can efficiently destabilize the phospholipid membrane and deliver payloads with limited cytotoxicity, has caught much attraction for intracellular delivery (Hoffman, 2013; Jeong & Gutowska, 2002; Stuart et al., 2010).

In Chapter 4, a series of membrane anchoring, comb-like, pH-responsive pseudopeptidic polymers containing hydrophobic relatively long alkyl chains have been developed and their membrane-destabilization activity has been demonstrated. Further investigation is needed to assess their cytotoxicity and their ability to deliver cargos into nucleated cells at neutral and acidic pHs, aiming to develop a simple, efficient and safe method for non-covalent delivery. The ability of the optimal membrane-anchoring polymer to release endocytosed materials from intracellular vesicles into the cell cytoplasm was assessed in HeLa adherent epithelial cells (human cervical cancer cells), A549 adherent epithelial cells (human lung cancer cells) and CHO adherent epithelial cells (Chinese hamster ovary cells) at physiological pH and compared with its linear counterpart PLP. The time-dependent and polymer concentration-dependent in vitro cytotoxicity toward different cell lines was evaluated. Furthermore, the polymer-mediated

non-covalent delivery at acidic conditions was examined at various polymer concentrations, incubation times, pHs, and with the presence/absence of serum by confocal microscopy and flow cytometry. A wide size range of payloads and 7 different cell types, including human bone marrow derived mesenchymal stem cells (hMSC) and multidrug resistant cells MES-SA/DX5, were applied to test the delivery capacity of PLP-NDA 18%. The polymer-mediated intracellular delivery efficacy at acidic pH was compared to that at neutral pH to demonstrate its advantages over CPPs. The cytotoxicity of polymer-mediated delivery toward different cell types at acidic pH was determined by Alamar Blue assay at various polymer concentrations and treatment times.

5.2 Results and discussion

5.2.1 Intracellular delivery at pH 7.4

The polymer-mediated delivery at pH 7.4 was assessed using membrane-impermeable calcein as a model drug and tested on three different cell lines, including human cervical carcinoma HeLa cells, human lung carcinoma A549 cells and non-cancerous CHO cells. Bright green punctate spots were observed in all the three cell lines treated with 2.0 mg mL^{-1} calcein alone (control, Figure 5-1), which was due to the entrapment of the membrane impermeable calcein within endosomes after endocytosis (Chen et al., 2009c). As shown in Figure 5-1, no considerable change was observed when the cells were treated with 0.5 mg mL^{-1} PLP and 2.0 mg mL^{-1} calcein. In contrast, with the presence of 0.5 mg mL^{-1} PLP-NDA 18%, strong diffuse green fluorescence was spread throughout the HeLa (Figure 5-2A), A549 (Figure 5-2B) and CHO (Figure 5-2C) cells. This suggests that the membrane-anchoring, comb-like, membrane-destabilizing polymer could release endocytosed calcein into the cytoplasm of various cancerous and non-cancerous cells at neutral external pH.

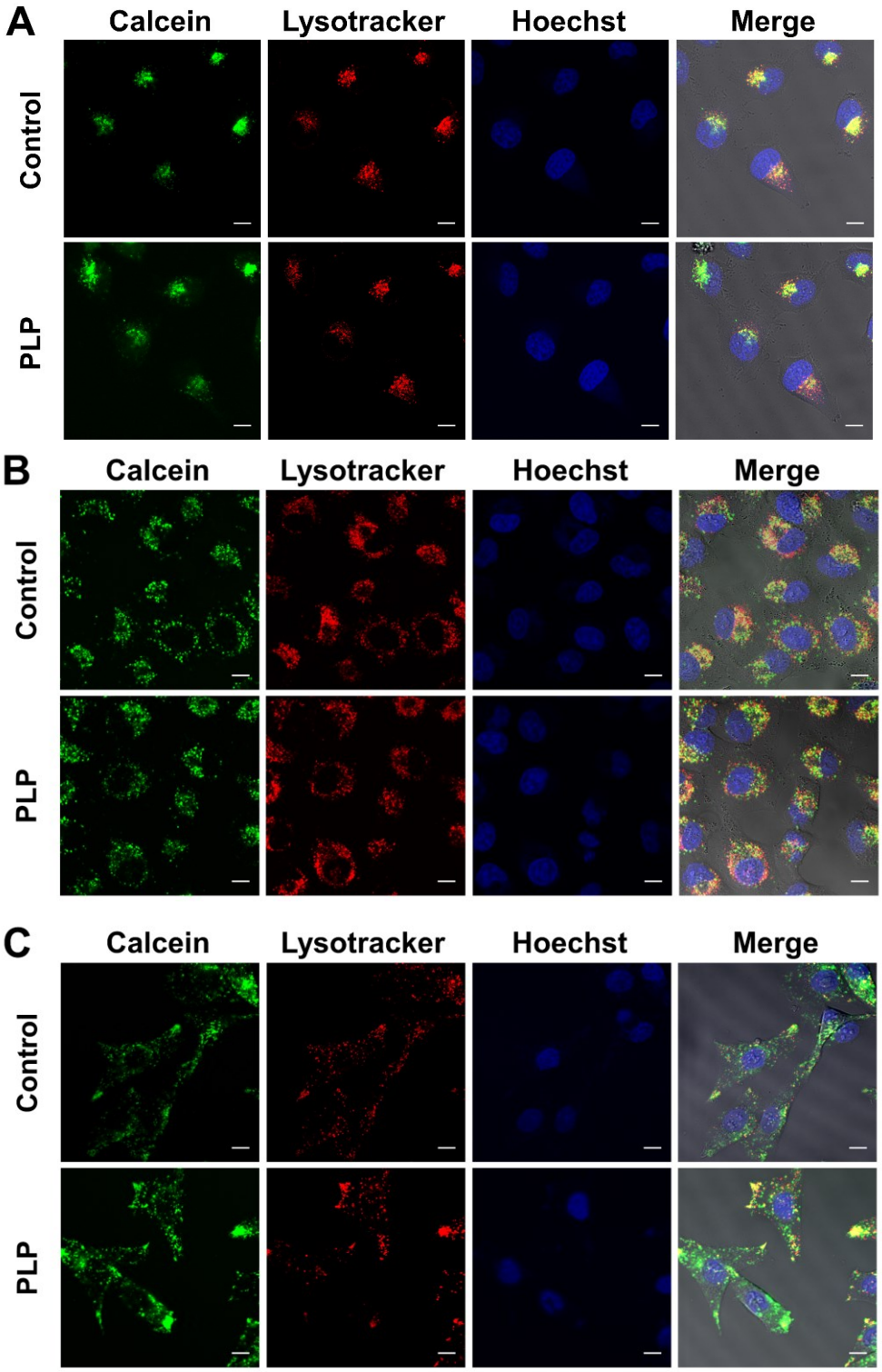

Figure 5-1. Confocal microscopy images of Hela (A), A549 (B) and CHO (C) cells showing the subcellular distribution of calcein fluorescence. The cells were treated with 2.0 mg mL^{-1} calcein alone (control) or both 2.0 mg mL^{-1} calcein and 0.5 mg mL^{-1} PLP. Images were acquired after 1 h of uptake and 3 h of further incubation in fresh DMEM for HeLa and CHO cells (2 h of uptake and 2 h of further incubation for A549 cells). Scale bar: 10 µm.

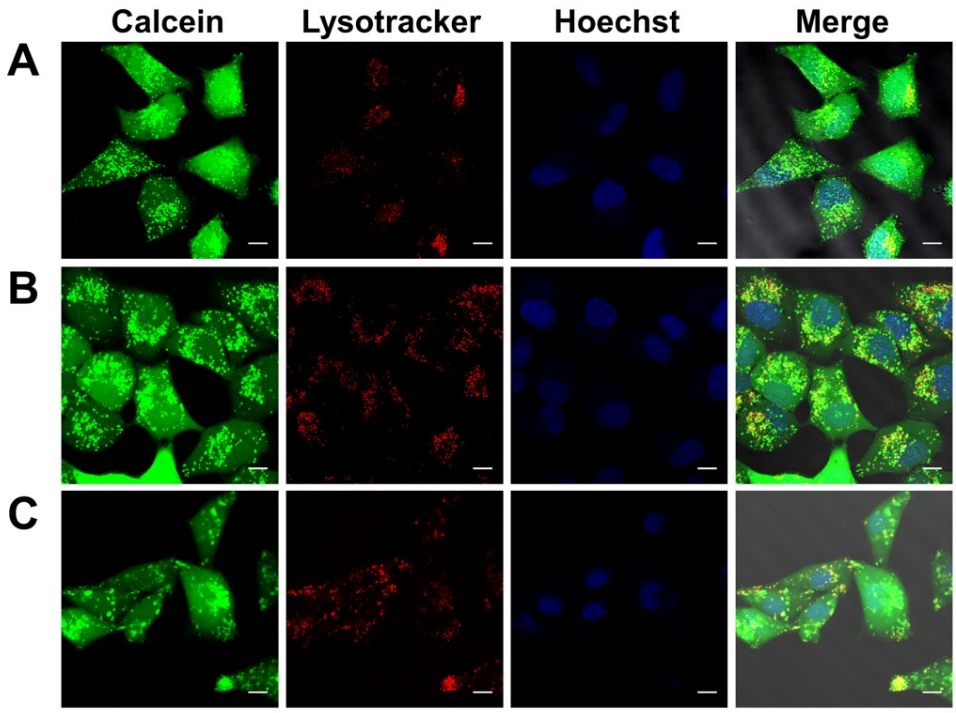

Figure 5-2. Confocal microscopy images of Hela (A), A549 (B) and CHO (C) cells showing the subcellular distribution of calcein fluorescence. The cells were treated with both 2.0 mg mL^{-1} calcein and 0.5 mg mL^{-1} PLP-NDA 18%. Images were acquired after 1 h of uptake and 3 h of further incubation in fresh DMEM for HeLa and CHO cells (2 h of uptake and 2 h of further incubation for A549 cells). Scale bar: 10 µm.

5.2.2 In vitro cytotoxicity at pH 7.4

The concentration- and time-dependent cytotoxic effects of PLP and the comb-like PLP-NDA 18% toward HeLa (Figure 5-3), CHO (Figure 5-4) and A549 cells (Figure 5-5) were evaluated by Alamar Blue assay. PLP and PLP-NDA 18% displayed no or negligible cytotoxicity against all the three cell lines within the polymer concentration range of 0.005 – 0.5 mg mL^{-1} after up to 48 h of treatment. With further increasing the polymer concentration from 1.0 to 10.0 mg mL^{-1}, different cell lines displayed different levels of tolerance to PLP and PLP-NDA 18%. The IC_{50} of PLP against HeLa after 24 and 48 h of treatment was 2.95 ± 1.39 and 0.77 ± 0.27 mg mL^{-1} respectively. After 24 and 48 h of treatment, the IC_{50} of PLP-NDA 18% against HeLa was 1.59 ± 0.22 and 1.05 ± 0.14 mg mL^{-1} respectively. CHO and A549 cells exhibited better tolerance than HeLa cells. The IC_{50} of PLP-NDA 18% against CHO and A549 after 48 h of treatment was 2.81 ± 0.95 and 4.51 ± 0.06 mg mL^{-1} respectively. It was not possible to calculate the IC_{50} value for PLP against CHO and A549 as the lowest cell viability

within the concentration range tested was above 50%. Compared to the linear counterpart PLP, the comb-like polymer PLP-NDA 18% did not show remarkable changes in the cytotoxicity against HeLa, CHO and A549 cells within the polymer concentration range of 0.005 – 1.0 mg mL^{-1} with treatment up to 48 h. This demonstrates that conjugating relatively long alkyl chain onto the PLP backbone at 18% degree of substitution did not significantly increase the cytotoxicity. However, when the polymer concentration was sufficiently high (5.0 – 10.0 mg mL^{-1}), PLP-NDA 18% showed a higher cytotoxicity than PLP.

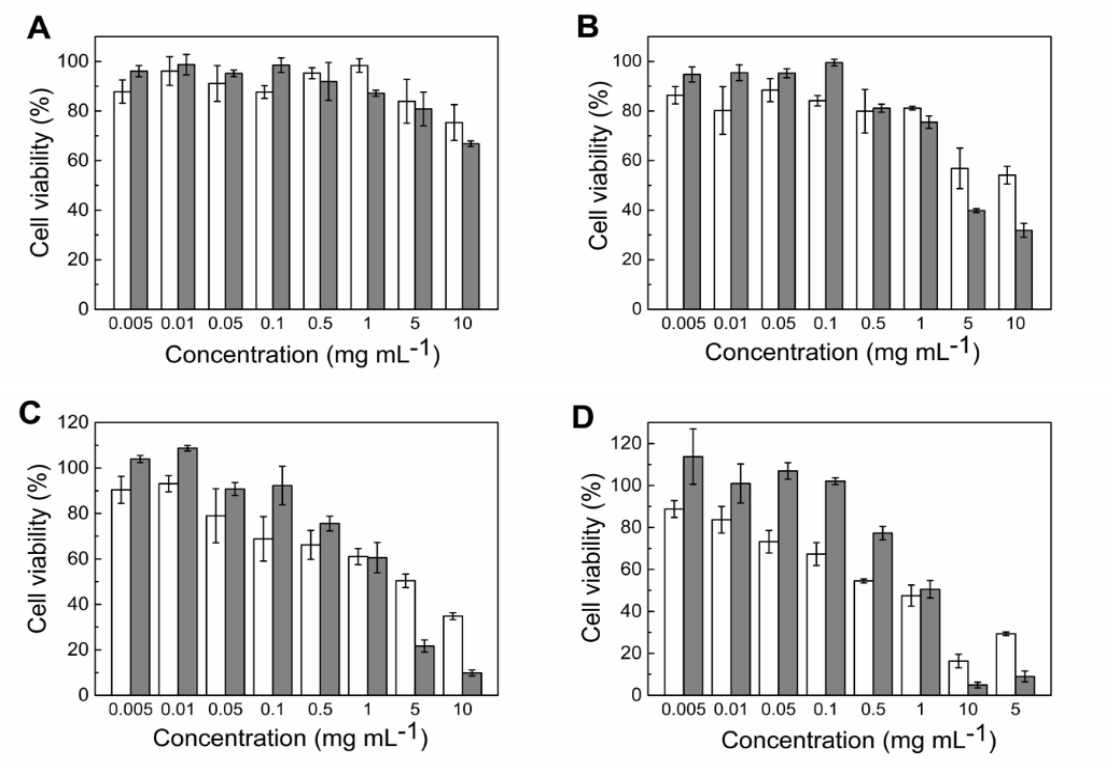

Figure 5-3. Viabilities of HeLa cells incubated with PLP (open columns) and PLP-NDA 18% (close columns) at various concentrations for 4 h (A), 12 h (B), 24 h (C) and 48 h (D), as determined by Alamar Blue assay. Mean ± S.D. (n=3).

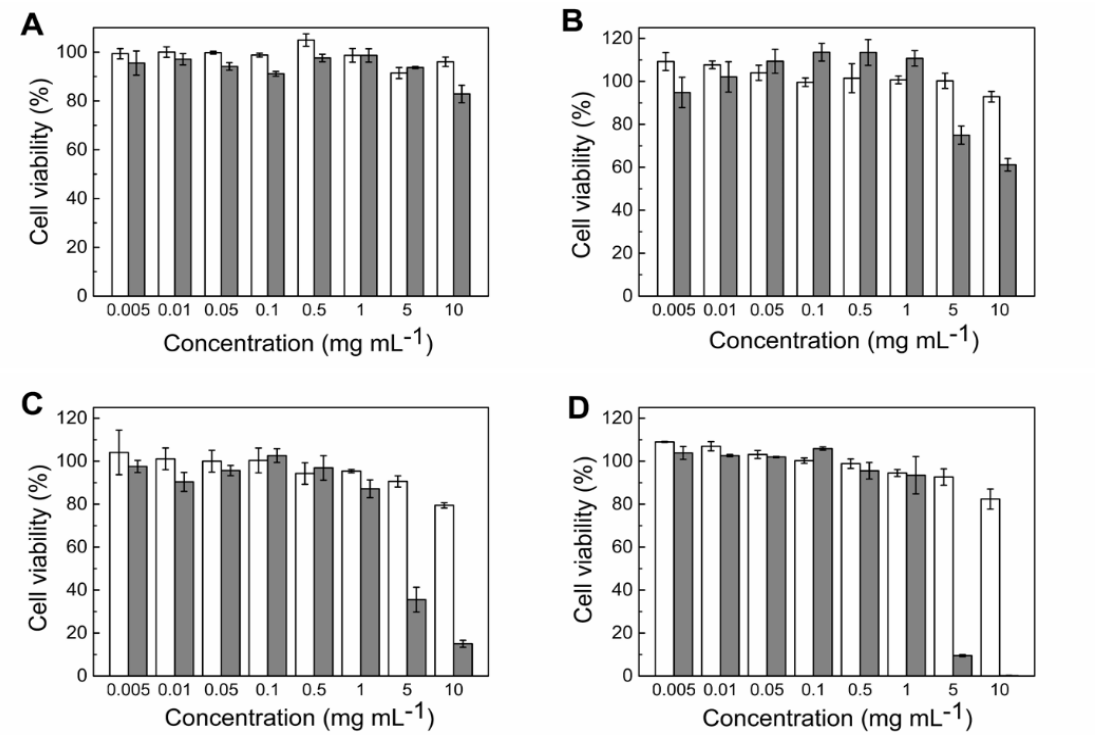

Figure 5-4. Viabilities of CHO cells incubated with PLP (open columns) and PLP-NDA 18% (close columns) at various concentrations for 4 h (A), 12 h (B), 24 h (C) and 48 h (D), as measured by Alamar Blue assay. Mean ± S.D. (n=3).

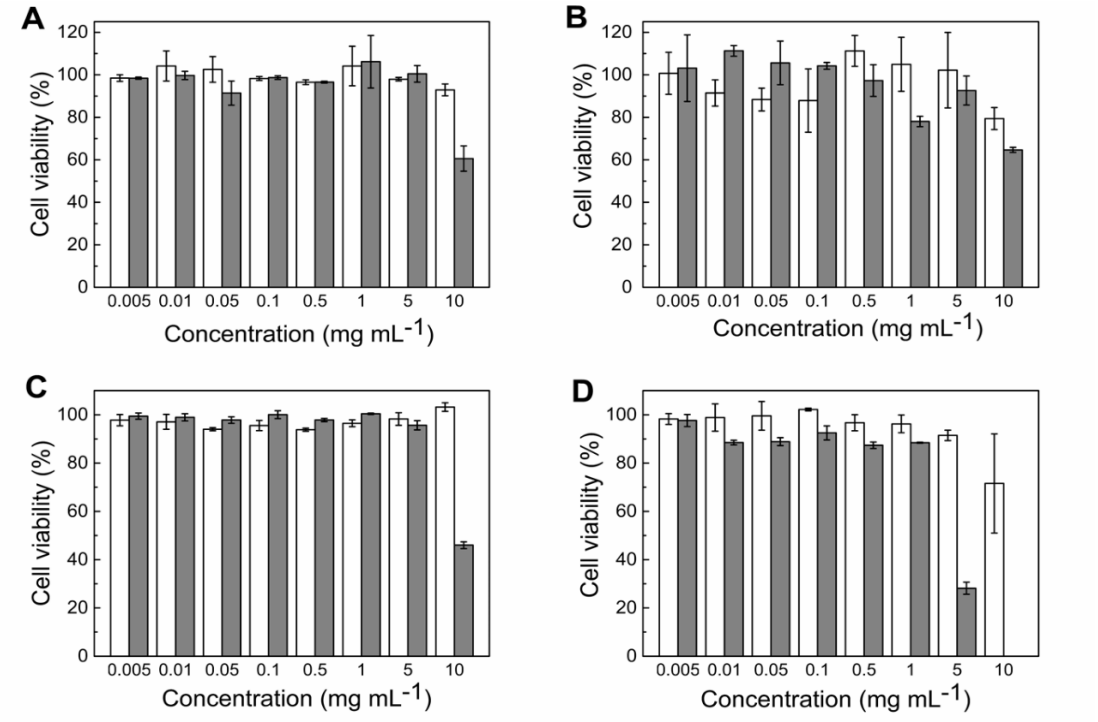

Figure 5-5. Viabilities of A549 cells incubated with PLP (open columns) and PLP-NDA 18% (close columns) at various concentrations for 4 h (A), 12 h (B), 24 h (C) and 48 h (D), as measured by Alamar Blue assay. Mean ± S.D. (n=3).

5.2.3 Intracellular delivery at acidic conditions

The tumor microenvironment is slightly acidic compared to normal tissues, which is due to the hypoxia-induced production of excess lactic acid in the tumor microenvironments (Warburg et al., 1927). As the membrane disruptive activity of the pseudopeptidic polymer is pH-dependent, it would be interesting to investigate the polymer-mediated intracellular delivery at acidic extracellular conditions and compare it with the delivery efficiency at neutral pH. The delivery capacity of the membrane-anchoring, comb-like pseudopeptidic polymer was studied by varying key parameters such as side chain length, polymer concentration, treatment time, pH, payload size, cell type and so on. In addition, the cytotoxicity assay was carried out to further characterize this delivery method.

5.2.3.1 Effect of polymer side chain length

Four membrane-anchoring, comb-like polymers were synthesized by conjugating hydrophobic anchors with different chain lengths on the PLP backbone. The intracellular delivery abilities of these polymers were tested in HeLa cells by confocal microscopy and flow cytometry. As shown in Figure 5-6A, when HeLa cells were treated with FITC-dextran 4 kDa alone at pH 6.5 (control), there was no intracellular green fluorescence. As comparison, homogenous green fluorescence was seen in all the cells treated with both FITC-dextran 4 kDa and the comb-like polymer (PLP-HDA 18%, PLP-NDA 18%, or PLP-TDA 18%, PLP-ODA 18%) at pH 6.5, which does not just prove successful cytoplasmic delivery, but also suggest nuclear localization. According to the flow cytometry data in Figure 5-6B, the cells treated with both payload and PLP-NDA 18% displayed the highest MFI, which was 6.5 ± 0.6 times higher than the cells treated with the payload without polymer. The MFI value was in the order of PLP-NDA 18% > PLP-TDA 18% > PLP-HDA 18% > PLP-ODA 18%. Conjugation with long alkyl side chains could significantly enhance the hydrophobicity of the polymer and provide stronger membrane association (Resh, 2016). However, the polymer-membrane interaction is affected by the hydrophobic/hydrophilic balance instead of simply by hydrophobicity (Marie et al., 2014). Conjugation with alkyl side chains longer than the critical chain length may lead to reduced polymer-membrane interaction due to self-aggregation of the polymer at physiological pH or undesired membrane lysis (Chen et al., 2004; El-Sayed et al., 2015; Morille et al., 2008). Therefore, the optimal side chain length could be dictated by the polymer backbone, side chain and degree of substitution. According to the intracellular

delivery results, PLP-NDA 18% displayed the most efficient cytoplasmic delivery. Therefore, PLP-NDA 18% was applied in the following experiment to further assess its delivery capacity.

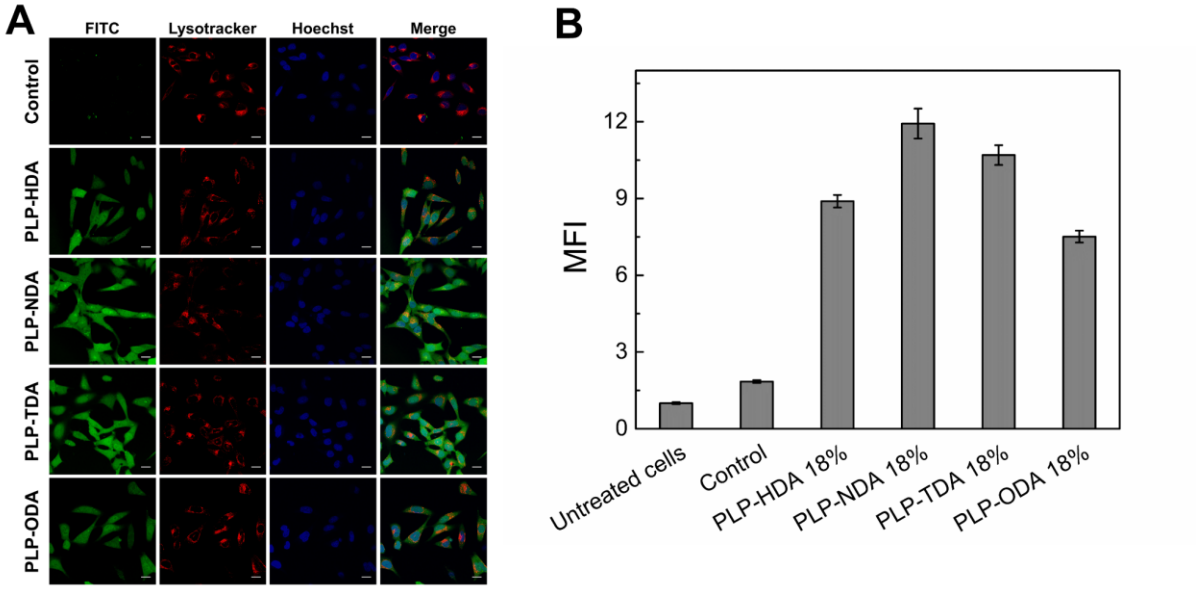

Figure 5-6. (A) Confocal microscopy images and (B) MFI of the polymer-mediated delivery analyzed by flow cytometry. HeLa cells were incubated with 200 μM FITC-dextran (4 kDa) and the comb-like polymer containing alkyl chains with different lengths at pH 6.5 for 30 min. Scale bar: 20 μm. Mean ± S.D. (n=3).

5.2.3.2 Effect of polymer concentration

The polymer concentration plays a vital role in affecting its membrane destabilization activity (Chen et al., 2009b, 2009c). Herein, the intracellular delivery capacity of the optimal comb-like polymer at different concentrations under acidic conditions was evaluated by confocal microscopy and flow cytometry. As shown in Figure 5-7, when HeLa cells were treated with FITC-dextran (4 kDa) and 0.01 mg mL^{-1} PLP-NDA 18% at pH 6.5 for 30 min, almost no green fluorescence was detected inside the cells, indicating that no or limited intracellular delivery of FITC-dextran. When the polymer concentration was increased to 0.05 mg mL^{-1}, diffuse green fluorescence was observed throughout the cells instead of being co-localized with the endosomes/lysosomes labelled with lysotracker (red channel), suggesting that FITC-dextran was successfully delivered into the cytoplasm and even into nucleus. With further increasing the polymer concentration from 0.05 to 2 mg mL^{-1}, the intracellular fluorescence intensity was significantly enhanced (Figure 5-7).

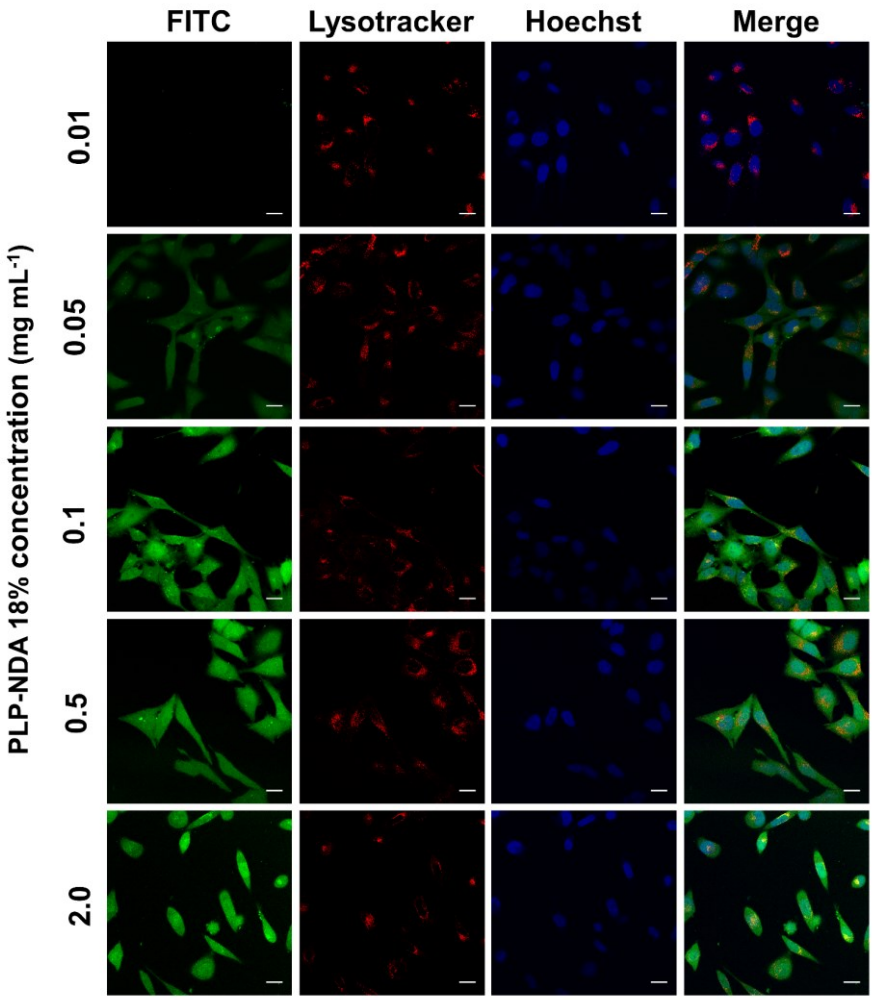

Figure 5-7. Confocal microscopy images of HeLa cells treated with PLP-NDA 18% at various concentrations and 200 μM FITC-dextran (4 kDa) at pH 6.5 for 30 min. Scale bar: 20 μm.

The intracellular delivery in response to the polymer concentration was quantitatively determined by flow cytometry. As shown in Figure 5-8, no significant difference in MFI was observed in the cells co-treated with PLP-NDA 18% at 0.01 mg mL^{-1} and FITC-dextran at pH 6.5 compared with those treated with FITC-dextran alone. This result suggests that the PLP-NDA 18% concentration of 0.01 mg mL^{-1} was not sufficiently high to facilitate intracellular delivery at pH 6.5. With increasing the polymer concentration to 0.1 mg mL^{-1}, the MFI of the FITC-dextran inside the cells was increased by 2.53 ± 0.36 times. The significantly enhanced intracellular delivery at a higher polymer concentration could be due to the its improved membrane destabilization activity resulting from the enhanced driving force for migration of polymer molecules to the lipid membrane (Chen et al., 2009c). Other researchers have reported

the similar concentration-dependent membrane destabilization and intracellular delivery by cell-penetrating poly(disulfide)s (Fu et al., 2015), TAT (Lee et al., 2010) and derivatives of poly(acrylic acid)s (Murthy et al., 1999). However, when the polymer concentration was further increased above 0.1 mg mL^{-1}, a slight decrease in MFI was seen (Figure 5-8), which could be due to the increased aggregation of the polymer at concentrations ≥ 0.5 mg mL^{-1} at pH 6.5. This is consistent with the hemolysis result of PLP-NDA 18% (Figure 4-11A) that the membrane destabilization activity at acidic pH was enhanced with increasing the polymer concentration until the maximum hemolysis was reached.

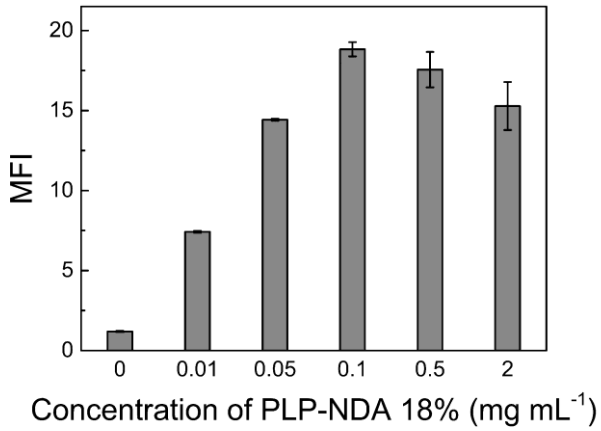

Figure 5-8. Relative MFI of HeLa cells treated with 200 μM FITC-dextran (4 kDa) in the absence (control) or presence of PLP-NDA 18% at various concentration at pH 6.5 for 30 min. The MFI was measured by flow cytometry. Mean ± S.D. (n=3).

5.2.3.3 Effect of extracellular pH

PLP-NDA 18% displayed pH-dependent membrane destabilization activity, which prompted the research into the effect of extracellular pH on the polymer-mediated intracellular delivery to demonstrate the potential of PLP-NDA 18% to exploit the acidic tumor microenvironment. Figure 5-9 shows the confocal images of the HeLa cells co-treated with PLP-NDA 18% (0.5 mg mL^{-1}) and FITC-dextran (4 kDa) for 30 min at various pHs. At pH 7.4, little green fluorescence was detected, suggesting a limited intracellular dextran delivery at physiological pH. When slightly decreasing the pH to 7.0, the intracellular green fluorescence started to increase and much of it was displayed in the form of punctate spots, indicative of enhanced intracellular delivery with a slight decrease in pH and endosomal/lysosomal entrapment. With decreasing pH ≤ 6.5, diffuse green fluorescence was observed throughout

the cell interior including the nuclei, and the fluorescence intensity increased considerably. It suggests that the acidic tumor microenvironment could be utilized to enhance the intracellular delivery of biomacromolecules.

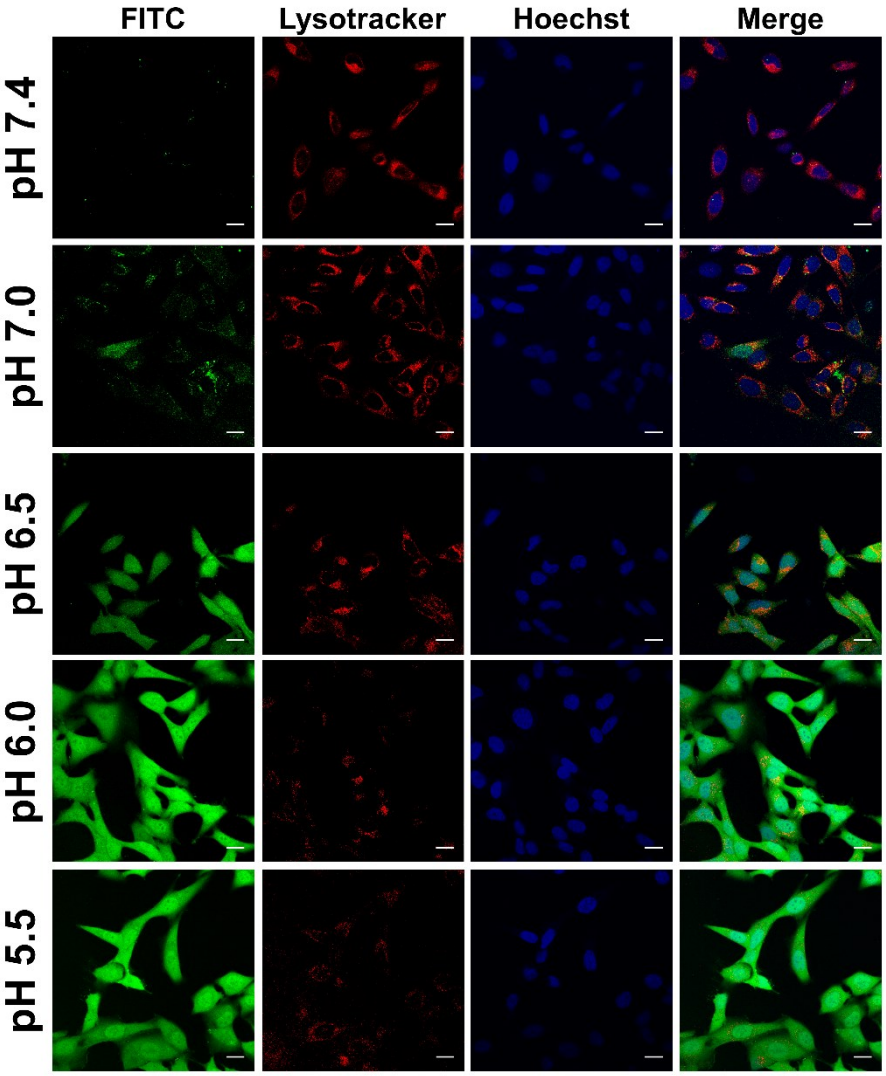

Figure 5-9. Confocal microscopy images of pH-dependent polymer-mediated intracellular delivery. HeLa cells were co-incubated with 0.5 mg mL^{-1} PLP-NDA 18% and 200 μM FITC-dextran (4 kDa) at various extracellular pHs for 30 min. Scale bar: 20 μm.

According to the quantitative data measured by flow cytometry (Figure 5-10), the MFI of the cells co-treated with PLP-NDA 18% (0.5 mg mL^{-1}) and FITC-dextran increased with decreasing pH from 7.4 to 6.0. At pH 6.0, the MFI of the cells co-treated with PLP-NDA 18% and FITC dextran was 26.3 ± 2.3 times higher than the cells treated with FITC-dextran alone at the same pH, while 5.5 ± 0.1 times higher than the cells co-treated with the polymer and the

payload at pH 7.4. There was limited change in MFI when the extracellular pH was decreased from 6.0 to 5.5. The pH-dependent intracellular delivery capacity of the membrane-anchoring pseudopeptidic polymer is in good correlation to its pH-responsive membrane destabilization activity as measured by hemolysis assay using RBCs as the model cell membrane (Figure 4-10). Compared to most CPPs, which can facilitate cytoplasmic delivery into cells without pH responsiveness (Farkhani et al., 2014; Koren & Torchilin, 2012), one major advantage of the PLP-NDA 18% is that it can mediate pH-triggered delivery. The pH-dependent delivery capacity is ideal for drug delivery, as the polymer will only mediate limited delivery of cargos into the cytoplasm at neutral pH during the circulation in the bloodstream. However, once it reaches to the tumor microenvironment, the slight decrease of pH would transform the polymer to be membrane active and facilitate payload delivery into tumor cells. Thus, the therapeutic value of the cargoes can be enhanced while unwanted side effects can be avoided or minimized.

It is interesting to compare the result in Figure 5-2 with those in Figures 5-9 & 5-10. As shown in Figure 5-2, 0.5 mg mL^{-1} PLP-NDA 18% could release the endocytosed materials into the cytoplasm after 1 h of treatment at pH 7.4 and 3 h of further incubation. However, in Figures 5-9 & 5-10, limited intracellular delivery was observed for the cells treated with the same polymer at the same concentration and pH for 30 min. This implies that although the polymer could also facilitate cytoplasmic delivery of endocytosed materials after treatment at physiological pH, it would need a longer time compared to the cell treatment at acidic extracellular conditions. This might be due to different delivery mechanisms or/and pre-activation of the membrane destabilization activity of the polymer. It is well documented that CPPs could rapidly deliver cargos into cells by direct translocation or/and endocytosis, while the direct translocation is less time consuming than endocytosis (Copolovici et al., 2014; Wang et al., 2014). CPPs could directly penetrate through the plasma membrane barrier and deliver cargos into the cytoplasm to avoid organelle confinement (Koren & Torchilin, 2012; Lee et al., 2013). As the PLP-NDA 18% exhibits membrane destabilization activity at acidic pHs, it is possible that the polymer enters cells like CPPs via direct translocation instead of endocytosis when the extracellular environment is acidic. As comparison, at physiological pH, the polymer displays limited membrane-lytic activity and might be internalized mainly by the endocytic pathway instead of direct translocation. The membrane disruptive activity will be activated during the mature of endosomes and release of the cargos into the cytoplasm. Therefore, at physiological pH it needs a longer time to enable the endosomal escape of the cargos into the cytoplasm. Another possible reason is that the polymer is internalized by cells via the endocytic pathway at acidic pHs. Due to the acidic external environment, its membrane destabilization

activity is already triggered before the endocytic uptake of the polymer. As a result, instead of waiting for the pH to decrease during the maturation of the endosomes, the already activated membrane disruptive polymer will promote the endosomal escape of the cargos more quickly compared to the delivery under the physiological external condition.

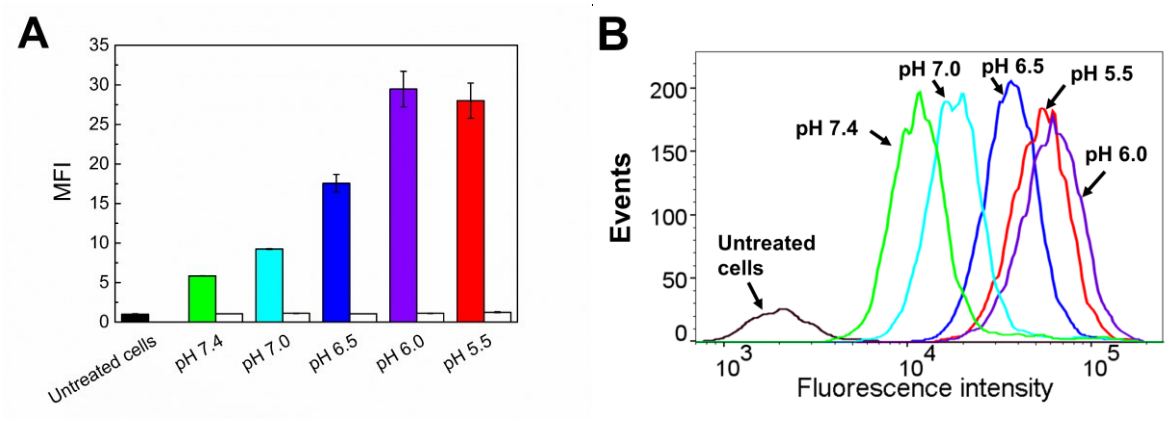

Figure 5-10. (A) Relative MFI and (B) representative histogram plots of the polymer-mediated delivery of 200 μM FITC-dextran (4 kDa) at different extracellular pHs analyzed by flow cytometry. HeLa cells were incubated without (open columns) or with PLP-NDA 18% at 0.5 mg mL^{-1} (close columns) at different extracellular pHs for 30 min. Mean ± S.D. (n=3).

5.2.3.4 Delivery kinetics

As seen in Figure 5-11, almost no intracellular green fluorescence was detected when HeLa cells were co-treated with 0.5 mg mL^{-1} PLP-NDA 18% and 200 μM FITC-dextran (4 kDa) at pH 6.5 for only 5 min. Only one cell with diffuse green fluorescence was seen once the treatment was extended to 10 min. When further increasing the treatment time to 20 min, green fluorescence was evenly distributed throughout the interior of all the cells. Stronger fluorescence was achieved by increasing the treatment time. For the cells treated with 0.5 mg mL^{-1} PLP-NDA 18% at pH 6.5 for 60 min, bright diffuse green fluorescence was detected, indicative of no entrapment in endosomal/lysosomal compartments. No detectable change of cell morphology was observed, indicating the good tolerance of HeLa cells toward treatment with 0.5 mg mL^{-1} polymer and 200 μM FITC-dextran at pH 6.5 for 1 h.

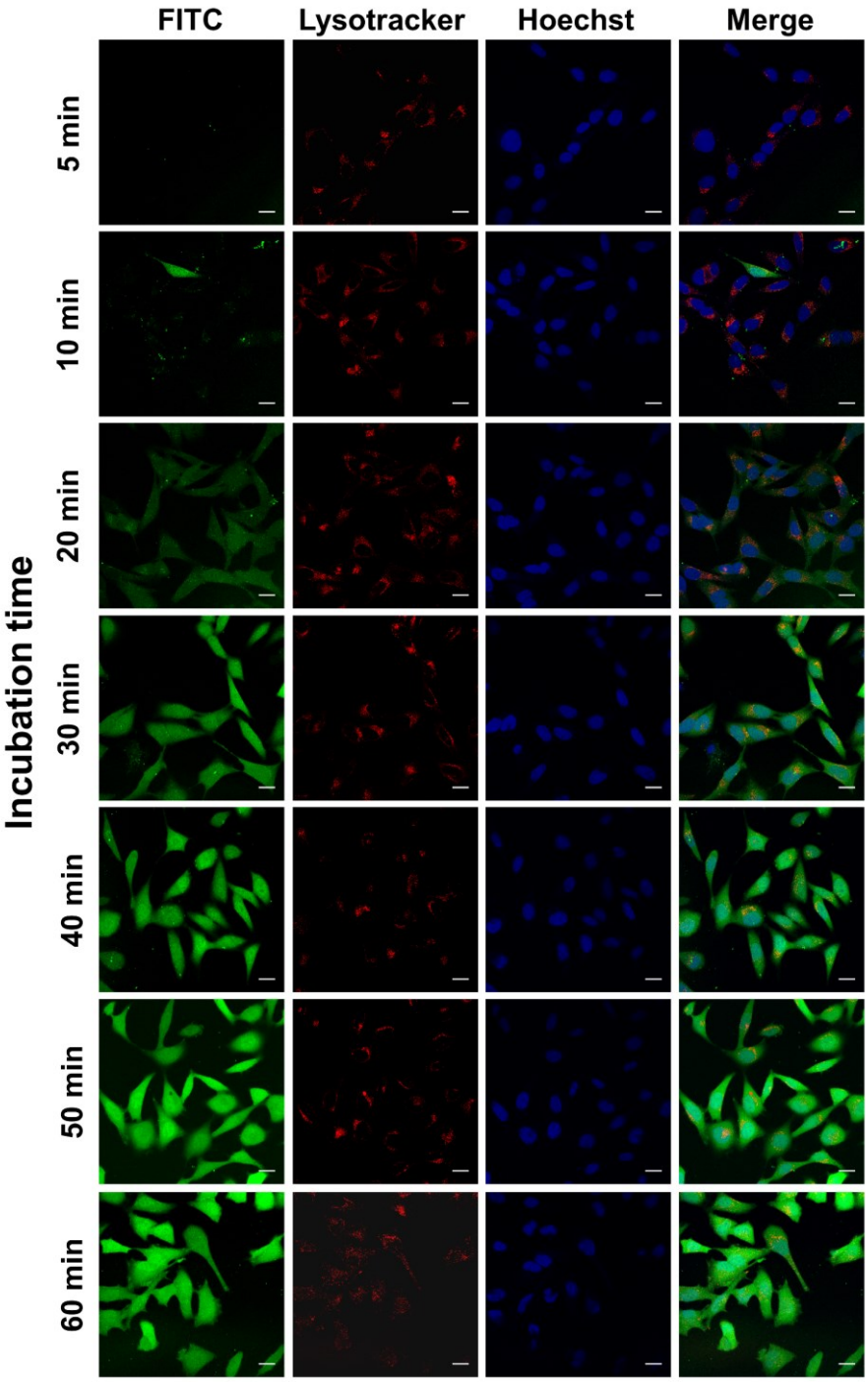

Figure 5-11. Confocal microscopy images of polymer-mediated delivery kinetics. HeLa cells were co-incubated with 0.5 mg mL^{-1} PLP-NDA 18% and 200 μM FITC-dextran (4 kDa) at pH 6.5 for various time periods. Scale bar: 20 μm.

The delivery kinetics of the comb-like polymer was further investigated by flow cytometry. As shown in Figure 5-12, the MFI of the HeLa cells treated with FITC-dextran and 0.5 mg mL^{-1} PLP-NDA 18% at pH 6.5 for 5 min was similar with the MFI of the cells treated with FITC-

dextran alone. When increasing the incubation time to 10 min, the polymer-mediated intracellular delivery started to be detected. The rapid intracellular delivery might be due to the above-mentioned argument that the polymer could probably deliver cargos into cells via direct translocation at acidic external pH or/and that the pre-activated polymer under acidic conditions might lead to more efficient endosomal escape. With the presence of PLP-NDA 18%, the MFI of the cells increased tremendously with the extension of treatment time. The MFI of the cells treated with the polymer for 180 min at pH 6.5 was 17.3 ± 0.7 times higher than the cells treated with FITC in the absence of the polymer at the same condition.

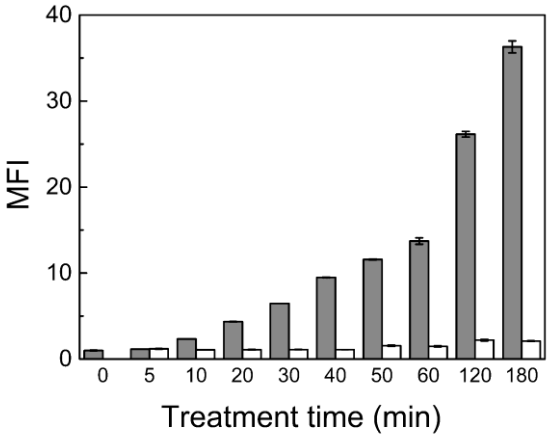

Figure 5-12. Relative MFI of polymer-mediated delivery kinetics analyzed by flow cytometry. HeLa cells were incubated with 200 μM FITC-dextran (4 kDa) in the absence (open columns) or presence of 0.5 mg mL^{-1} PLP-NDA 18% (close columns) at pH 6.5 for various treatment times. Mean ± S.D. (n=3).

5.2.3.5 Different sized payloads

Efficient intracellular delivery of macromolecules remains a major challenge for most delivery systems (Canton & Battaglia, 2012; Sahay et al., 2010). Usually macromolecules enter cells via the endocytic pathway, which remains a rate-limiting process. Endosomal escape is needed to avoid degradation in lysosomes (Iversen et al., 2011; Varkouhi et al., 2011; Yessine & Leroux, 2004). FITC-dextran with a wide size range from 4 k to 2,000 kDa were selected as model payloads to investigate the ability of the optimal comb-like polymer to deliver different sized cargos into the cell interior. As shown in Figure 5-13, diffuse green fluorescence was observed for all the HeLa cells treated with FITC-dextran at different molecular weights (4 k, 10 k, 70 k, 150 k and 2,000 kDa) with the presence of 0.5 mg mL^{-1} PLP-NDA 18% at pH 6.5

after only 30 min of treatment. The molecular weight range of 4 – 2,000 kDa covers the wide size range of siRNAs, peptides, proteins, antibodies, and even some types of nanoparticles and plasmids (Watkins & Chen, 2015). The successful delivery of a wide size range of payloads indicates the potential of the pH-responsive, membrane-anchoring comb-like polymer to facilitate intracellular delivery of a wide size range of therapeutic agents, from small molecular drugs to macromolecules. In contrast, no or limited green fluorescence was seen for the cells treated with different sized FITC-dextrans in the absence of the polymer (Figure 5-14), suggesting that the efficient intracellular delivery of payload was induced by PLP-NDA 18%. As comparison, only limited green fluorescence was observed for HeLa cells co-treated with 0.5 mg mL^{-1} PLP-NDA 18% and 200 μM FITC-dextran at pH 7.4 (Figure 5-15), implying that the polymer did not prompt intracellular delivery of various sized macromolecular payloads at physiological pH after 30 min of treatment at the polymer concentration of 0.5 mg mL^{-1}.

It was interesting to compare Figure 4-16 and Figure 5-13. As shown in Figure 5-13, all different sized FITC-dextran payloads (4 – 2,000 kDa) were delivered into HeLa cells with the presence of 0.5 mg mL^{-1} PLP-NDA 18% at pH 6.5 for 30 min of treatment. As shown in Figure 4-16, FITC-dextran with a molecular weight up to 70 kDa could efficiently enter RBCs with the presence of the polymer at same concentration at pH 5.5. However, 150 kDa and 2,000 kDa FITC-dextran could not enter RBCs. The might be attributed to the difference in the cell structure and membrane composition between RBCs and nucleated cells. Mature RBCs lack cell nucleus and most organelles, thus it is commonly believed that the cell entry does not rely on endocytosis (Marchesi et al., 1976). The FITC-dextran with a size smaller than the diameter of the pores created by PLP-NDA 18% could enter erythrocytes while the FITC-dextran with a larger size (150 k and 2,000 kDa) could not. However, FITC-dextran with a molecular weight larger than 150 kDa could be internalized by nucleated cells via the endocytic pathway (Li et al., 2015). The presence of PLP-NDA 18% could facilitate endosomal release of the endocytosed FITC-dextran into the cell cytoplasm. Another possible reason is that the lipid membrane composition varies between different cell types (Binder et al., 2003) and could thus affect the polymer-lipid interaction (Hao et al., 2015; Henry et al., 2006; Kono et al., 1999). As a result, the size of transient pores formed on the RBC membrane by the comb-like polymer could be different from the size of those formed on the nucleated cell membrane.

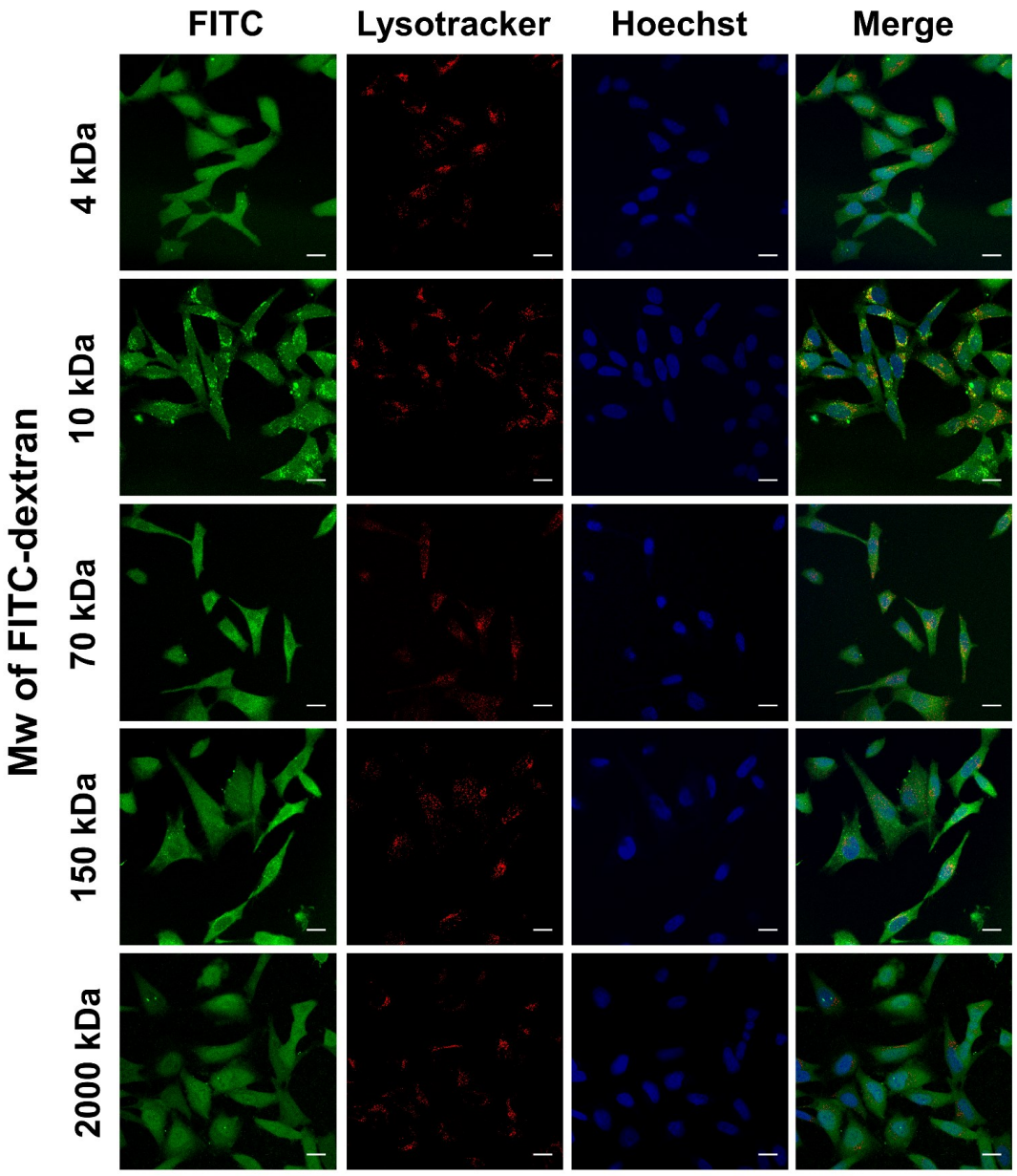

Figure 5-13. Confocal microscopy images of polymer-mediated intracellular delivery of different sized FITC-dextran at acidic external pH. HeLa cells were co-incubated with 0.5 mg mL^{-1} PLP-NDA 18% and different sized FITC-dextran at pH 6.5 for 30 min. Scale bar: 20 μm.

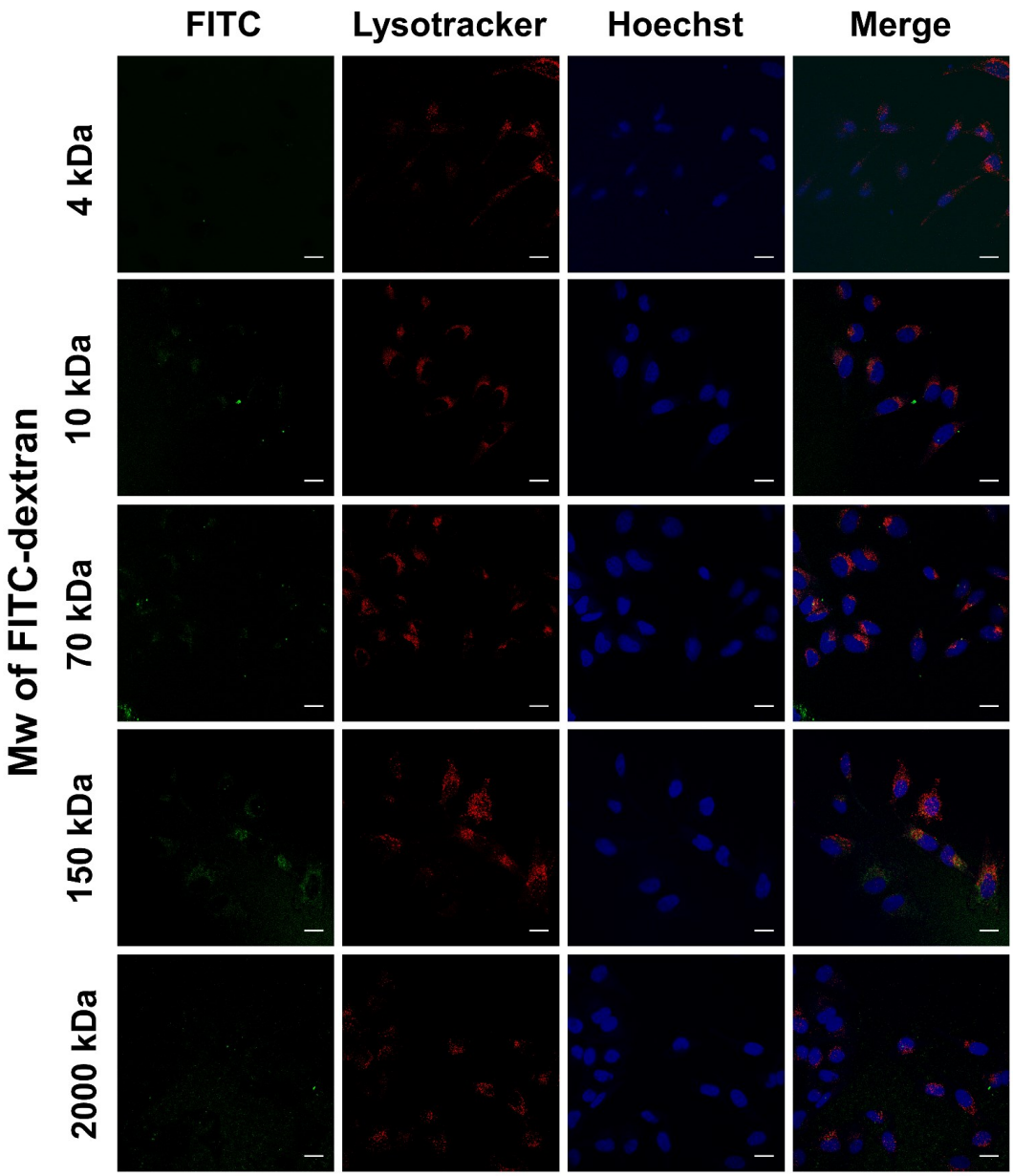

Figure 5-14. Confocal microscopy images of HeLa cells co-incubated with different sized FITC-dextran alone at pH 6.5 for 30 min. Scale bar: 20 μm.

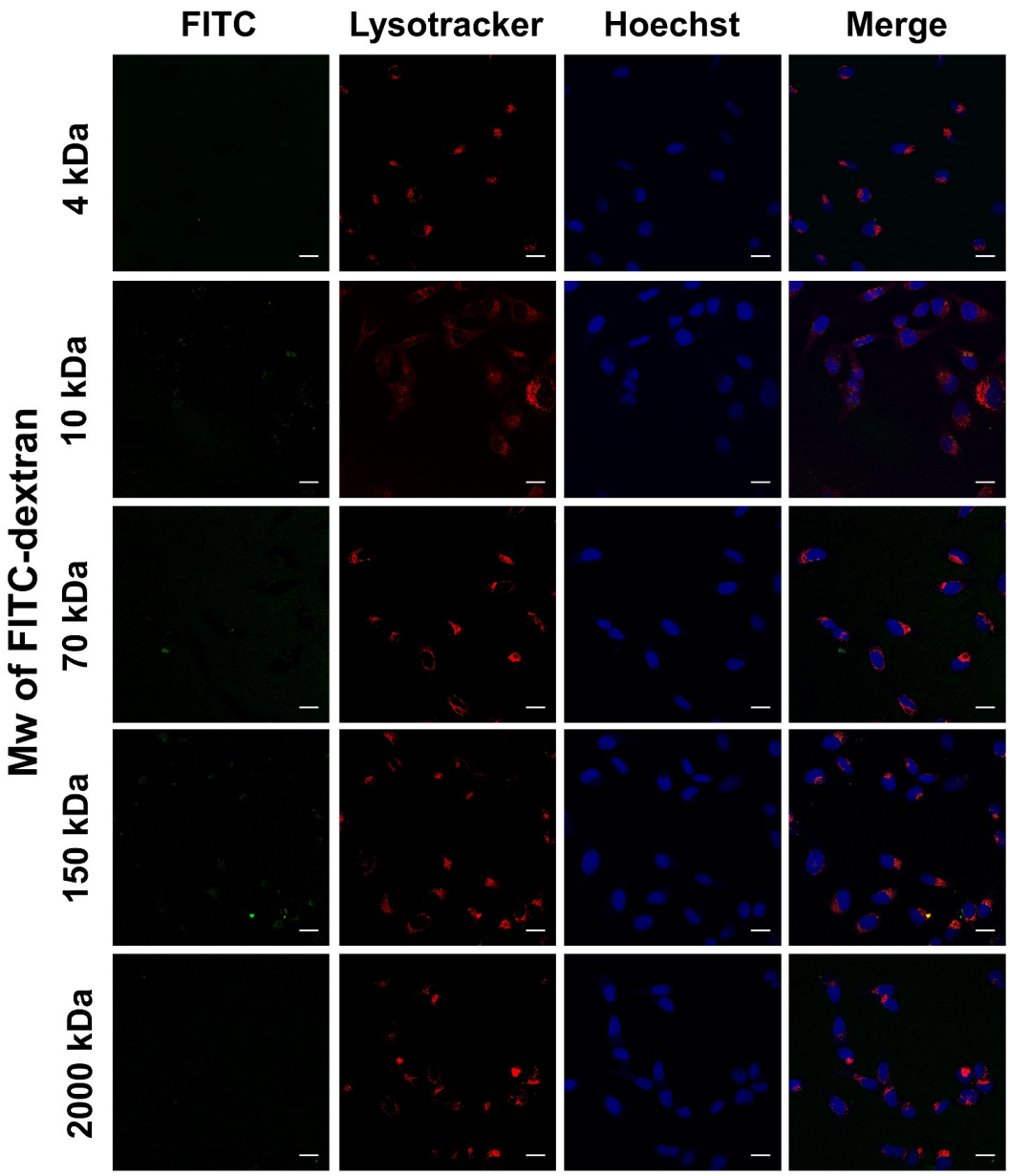

Figure 5-15. Confocal microscopy images of polymer-mediated intracellular delivery of different sized FITC-dextran at physiological pH. HeLa cells were incubated with 0.5 mg mL^{-1} PLP-NDA 18% and different sized FITC-dextran at pH 7.4 for 30 min. Scale bar: 20 μm.

5.2.3.6 Effect of serum

A key limitation for in vivo application of pH-responsive polymers is the loss of acid-induced fusogenicity in the presence of serum, possibly due to the interaction between the polymers and the serum proteins (Guo et al., 2002; Khalil et al., 2011; Shi et al., 2002). Therefore, the study of the effect of serum on the comb-like polymer-mediated intracellular

delivery was necessary. As shown in Figure 5-16A, after 1 h of incubation, significantly reduced fluorescence intensity was seen in the HeLa cells co-treated with PLP-NDA 18% (0.5 mg mL^{-1}) and FITC-dextran in the presence of 10% FBS compared to the cells treated with the same amounts of polymer and payload in the absence of serum. Once the treatment time was extended to 3 h (Figure 5-16B), the green fluorescence inside the cells with the presence of serum was increased significantly, although still weaker than that in the cells in the absence of serum. This demonstrates that the comb-like polymer could still mediate cytoplasmic delivery under acidic condition with the presence of serum although with a decreased delivery efficiency. The polymer-mediated intracellular delivery under the serum-containing condition could be improved by increasing the treatment time. This implies the possible application of this membrane-anchoring, comb-like pseudopeptidic polymer in vivo.

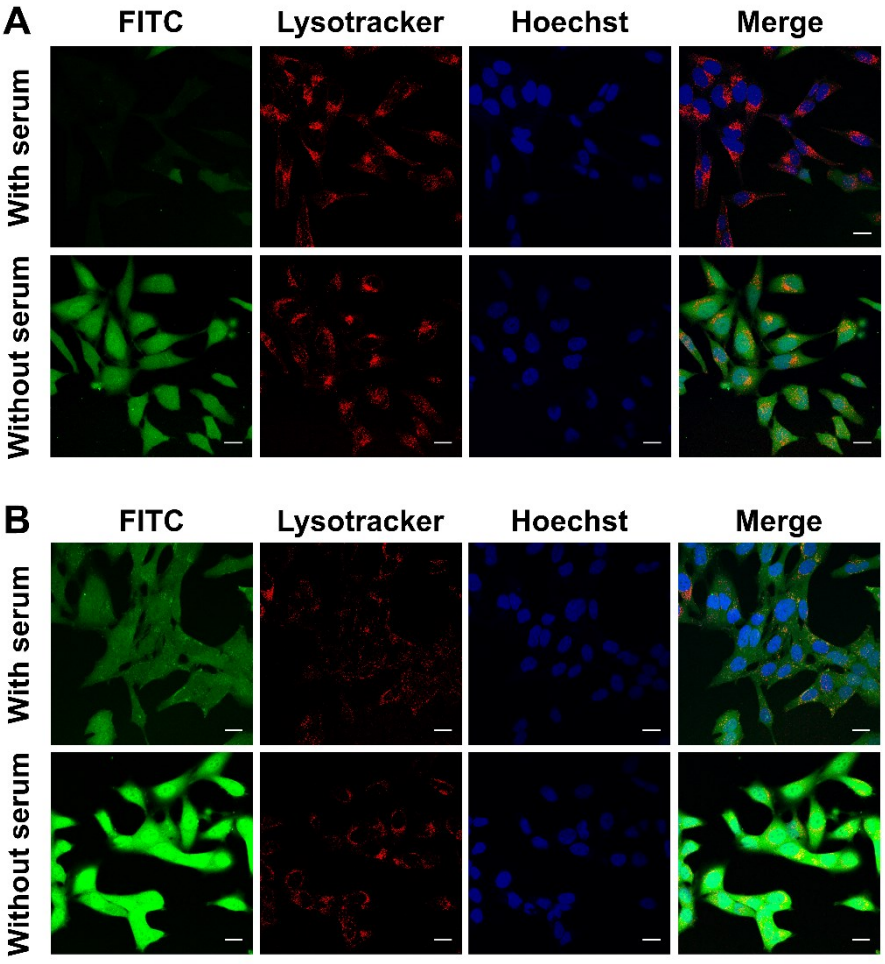

Figure 5-16. Confocal microscopy images of polymer-mediated intracellular delivery with or without the presence of serum. HeLa cells were co-incubated with 0.5 mg mL^{-1} PLP-NDA 18% and 200 μM FITC-dextran (4 kDa) with or without 10% serum at pH 6.5 for 1 h (A) and 3 h (B). Scale bar: 20 μm.

5.2.3.7 Delivery into different cell types

The general applicability of the comb-like polymer-mediated intracellular delivery was assessed by testing the delivery of FITC-dextran 4 kDa to seven different cell types, including stem cells and multidrug resistant cells that are traditionally difficult to transfect (Sharei et al., 2013). As shown in Figure 5-17, strong green diffuse fluorescence was observed in all different cell types tested, including HeLa adherent epithelial cells (human cervical cells), CHO adherent epithelial cells (Chinese hamster ovary cells), A549 adherent epithelial cells (human lung cells), SU-DHL-8 suspension B lymphocyte cell line (human lymph node cells), MES-SA adherent epithelial cell line (human uterus cells), MES-SA/DX5 adherent multi-drug resistant cell line and human mesenchymal stem cells (hMSCs, human bone marrow derived), which were co-treated with PLP-NDA 18% (0.5 mg mL^{-1}) and FITC-dextran at pH 6.5. This confirms that the comb-like polymer can efficiently deliver macromolecules into a variety of cell types, e.g. adherent and suspension cells, cancerous and non-cancerous cells, multidrug resistant cells and even stem cells.

The delivery efficiency was further quantitatively evaluated by flow cytometry. As seen in Figures 5-18A and 5-18B, the cellular uptake of FITC-dextran (4 kDa) mediated by the comb-like polymer at pH 6.5 was significantly higher than the polymer-mediated delivery at physiological pH and the cellular uptake in the absence of polymer at pH 6.5 across all the cell types tested. The MFI of the multidrug resistant cells (MES-SA/DX5) co-treated with PLP-NDA 18% (0.5 mg mL^{-1}) and FITC-dextran at pH 6.5 was 2.15 ± 0.03 times higher than that of the cells co-treated with the polymer and FITC-dextran at pH 7.4, whilst 2.32 ± 0.03 times higher than that of the cells treated with FITC-dextran alone at pH 6.5. Similarly, the MFI of the human bone marrow derived hMSCs co-treated with PLP-NDA 18% (0.5 mg mL^{-1}) and FITC-dextran at pH 6.5 was 5.72 ± 0.04 times higher than that of the cells treated with the polymer and FITC-dextran at pH 7.4, while 2.15 ± 0.03 times higher than that of the cells treated with FITC-dextran alone at pH 6.5. The flow cytometry data combined with confocal microscopy data consolidated that the comb-like polymer-mediated, intracellular delivery technology could be generalizable to different types of cells, which indicates its great potential in drug delivery application.

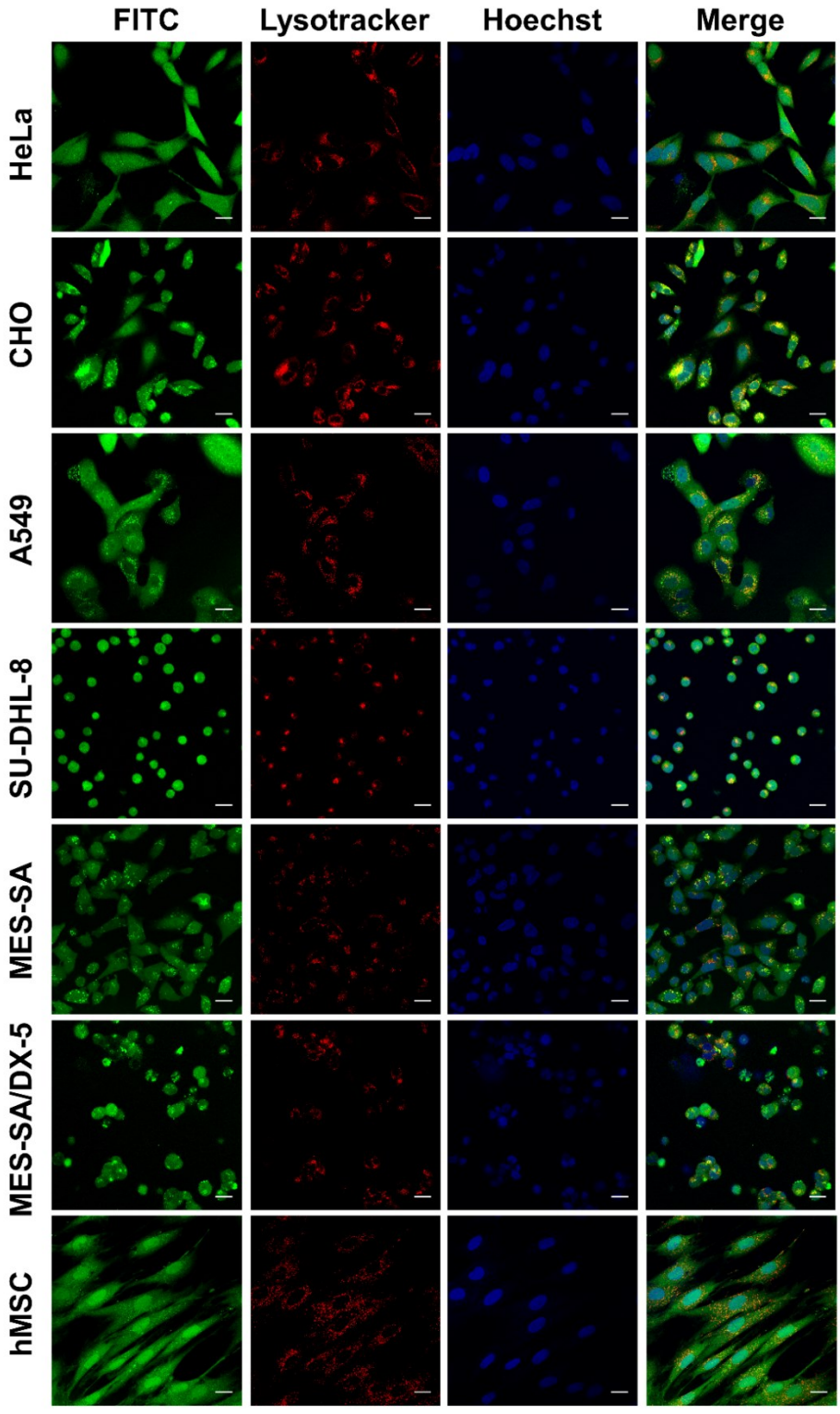

Figure 5-17. Confocal microscopy images of polymer-mediated delivery of FITC-dextran (4 kDa) into difference cell types. All the cells were co-treated with 0.5 mg mL^{-1} PLP-NDA 18% and 200 μM FITC-dextran at pH 6.5. The treatment time was 30 min for HeLa, CHO and SU-DHL-8, 180 min for A549, and 60 min for MES-SA, MES-SA/DX5 and hMSCs. Scale bar: 20 μm.

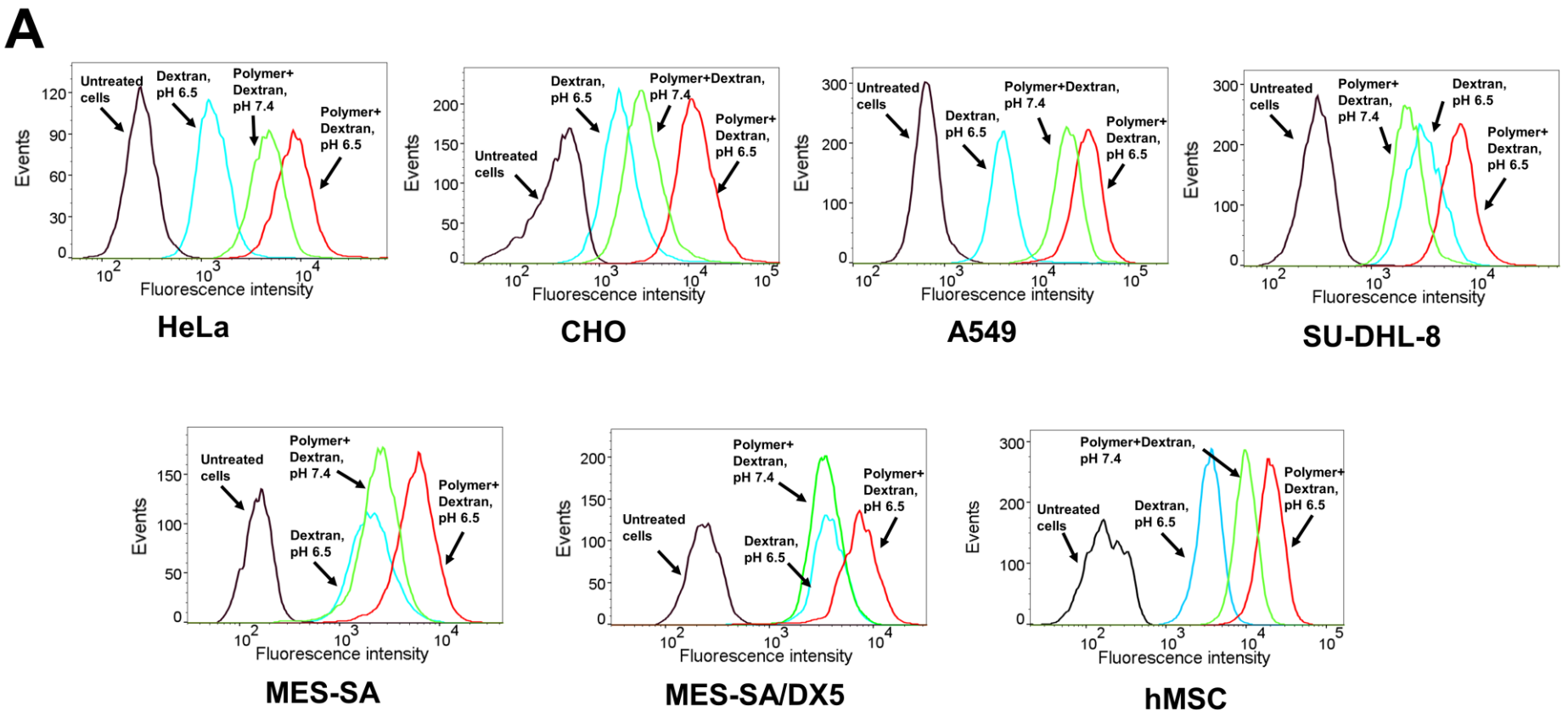
A
Untreated cells
Dextran, pH 6.5
Polymer+ Dextran, pH 7.4
Polymer+ Dextran, pH 6.5
Polymer+Dextran, pH 7.4
Events
Fluorescence intensity
HeLa
CHO
A549
SU-DHL-8
MES-SA
MES-SA/DX5
hMSC

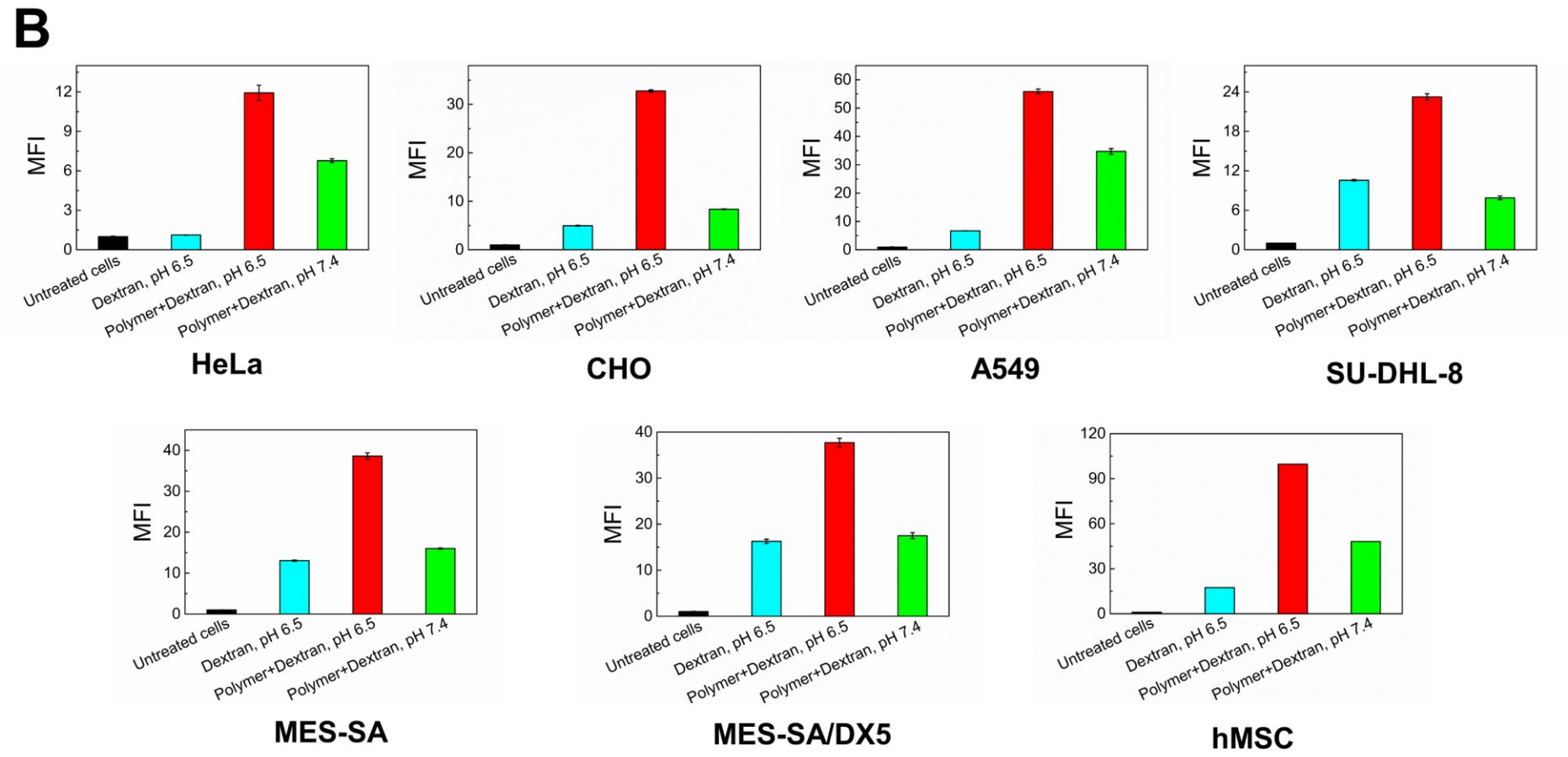

Figure 5-18. (A) Relative MFI and (B) representative histogram plots showing the polymer-mediated delivery of FITC-dextran into difference cell types. All the cells were treated with 0.5 mg mL^{-1} PLP-NDA 18% and 200 μM FITC-dextran (4 kDa) at pH 6.5. The treatment time was 30 min for HeLa, CHO and SU-DHL-8, 180 min for A549, and 50 min for MES-SA, MES-SA/DX5 and hMSCs. Mean ± S.D. (n=3).

5.2.4 In vitro cytotoxicity

In vitro cytotoxicity of the membrane-anchoring, comb-like pseudopeptidic polymer was measured by Alamar Blue assay to evaluate their effects on the metabolic activity of a variety of cell types treated at various polymer concentrations and treatment times. As shown in Figure 5-19A, no cytotoxicity was detected for the HeLa cells treated with PLP-NDA 18% at the concentration up to 2 mg mL^{-1} at pH 6.5 and 7.4 for 1 h, suggesting the cells were well tolerated within the comb-like polymer. Figure 5-19B shows the time-dependent viability of HeLa cells treated with 0.5 mg mL^{-1} PLP-NDA 18% at pH 6.5 and 7.4. The cell viability remained similar (all around 100%) with the extension of treatment time to 360 min at pH 6.5 and 7.4, indicating that almost no cytotoxicity was observed when HeLa cells were treated with 0.5 mg mL^{-1} PLP-NDA 18% at pH 6.5 for up to 6 h of treatment. Finally, the cytotoxicity of the comb-like polymer was evaluated across a variety of cell types. As shown in Figure 5-19C, PLP-NDA 18% (0.5 mg mL^{-1}) had no or limited cytotoxic effect toward all the cell types tested (e.g. HeLa, A549, SU-DHL-8, MES-SA, MES-SA/DX5 and hMSCs) at pH 6.5 and 7.4 after 4 h of treatment. All these prove that this novel, pH-responsive, membrane-anchoring, comb-like polymer is well tolerated by a variety of cell types within a wide polymer concentration range and various treatment times.

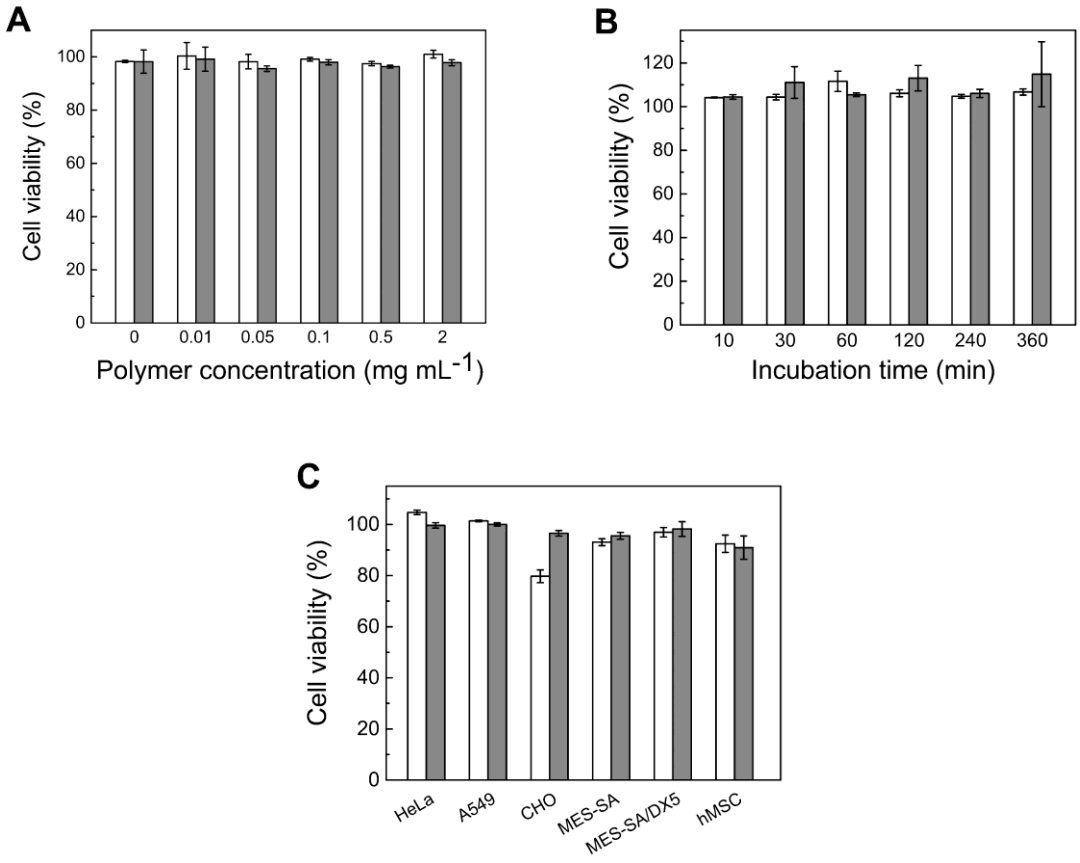

Figure 5-19. In vitro cytotoxicity of PLP-NDA 18%. (A) Polymer concentration-dependent in vitro cytotoxicity. HeLa cells were treated with PLP-NDA 18% at various concentrations at pH 6.5 (close columns) and pH 7.4 (open columns) for 1 h. (B) Time-dependent in vitro cytotoxicity. HeLa cells were treated with PLP-NDA 18% at 0.5 mg mL^{-1} at pH 6.5 (close columns) and pH 7.4 (open columns) for various incubation times. (C) In vitro cytotoxicity of PLP-NDA 18% against a variety of cell lines. HeLa, A549, CHO, MES-SA, MES-SA/DX5, hMSCs were treated with PLP-NDA 18% at 0.5 mg mL^{-1} at pH 6.5 (close columns) and pH 7.4 (open columns) for 3 h. Mean ± S.D. (n=3).

5.3 Conclusions

The pH-responsive, membrane-anchoring, comb-like polymer was demonstrated to deliver a variety of macromolecules into cells treated at neutral and acidic pHs. The delivery efficacy was higher when the extracellular environment was mildly acidic. The effects of the side chain length, polymer concentration, treatment time, serum and pH on the intracellular delivery efficacy of the polymer was investigated. The PLP-NDA 18% was shown to efficiently deliver a wide size range of FITC-dextran (the molecular weight range covering siRNA, peptides, proteins, antibodies, and even some types of nanoparticles and plasmids) at pH 6.5 into a

variety of cell types, including cancer and noncancerous cells, adherent and suspension cells, multidrug resistant cells and stem cells. The comb-like polymers displayed negligible cytotoxicity toward all the seven different cell types tested. The advantages of the comb-like polymer-mediated intracellular delivery, listed below, suggest that great potential of the comb-like polymer for intracellular drug delivery:

(1) Simple method. Payloads could be efficiently delivered into the cell cytoplasm by simple co-incubation with the comb-like polymer.

(2) Fast delivery. The cytoplasmic delivery of a wide size range of payloads could be detected within 20 min of treatment.

(3) Versatile delivery. A wide size range of payloads could be delivered into a variety of cell types.

(4) Non-cytotoxic.

(5) pH-Responsive delivery. Unlike most CPPs, the comb-like polymer-mediated, efficient, cytoplasmic delivery of a wide size range of payload could be triggered under a mildly acidic condition typical of acidic tumor microenvironments.

Chapter 6

Multifunctional liposomes coated with the membrane-anchoring, comb-like polymers

This chapter describes the development of another type of multifunctional liposomes coated with the bio-inspired membrane-anchoring, comb-like pseudopeptides for pH-triggered payload release and enhanced intracellular delivery. The effects of cholesterol, hydrophobicity of the polymer, polymer coating density and dilution on the pH-responsive release behavior were systematically investigated. pH-Dependent size change was explored and the mechanism of polymer-membrane interaction was proposed. Furthermore, the anticancer drug DOX was loaded into this multifunctional delivery system. The intracellular delivery and in vitro cytotoxicity of the DOX-loaded, multifunctional liposomes were tested using four different cancer cell lines including a multidrug resistant cell line, and compared with free DOX and conventional DOX-loaded liposomes.

6.1 Introduction

pH-Responsive liposomes that can respond to the pH decrease in the tumor microenvironment or during the endocytic pathway to release the cargos at the target site have caught great research interest (Felber et al., 2012; Ferreira et al., 2013; Ganta et al., 2008; Schmaljohann, 2006). Surface modification of conventional liposomes with pH-sensitive synthetic polymers could be applied to most liposomal formulations, thus resulting in relatively lower costs while diminishing safety concerns associated with the viral fusogentic peptide-modified liposomes (Karanth & Murthy, 2007; McTaggart & Al-Rubeai, 2002; Plank et al., 1998). By post-modification of already formulated liposomes, the polymers would only need to be localized on the surface of liposomes and thus provide more inner core space for loading of hydrophilic drugs (Nag & Awasthi, 2013). In order to anchor the polymer chain on the liposomal surface, the polymers need to be conjugated onto the liposomal membrane, or via electrostatic interaction, or have hydrophobic groups which can insert into the lipid bilayer to secure the membrane binding (Torchilin, 2005). The challenges for the chemical conjugation-mediated polymer coating include the difficulty of free reactant removal, as well as the aggregation and destabilization of liposomes (Nag & Awasthi, 2013). Therefore, it is more

favorable to modify the liposomal surface with pH-responsive polymers bearing hydrophobic pendant chains as membrane anchors (Chen & Chen, 2016; Yessine & Leroux, 2004).

Membrane proteins attach to or span across the biological membranes (Cho & Stahelin, 2005; Lesieur et al., 1997). They are usually immobilized on the cell surface through the utilization of long hydrophobic lipid-like chains, hydrophobic loops, amphipathic α-helices and/or electrostatic interactions (Cox, 2008; Resh, 2016). Many membrane proteins contain prenyl or/and alkyl chains as membrane anchors (Resh, 1999). Saturated alkyl chains may provide stronger binding to phospholipid membranes than the unsaturated prenyl chains (Khandelia et al., 2008). Inspired by membrane proteins, alkyl chains have been conjugated onto synthetic polymers for the development of polymer-modified multifunctional liposomes (Chen et al., 2004; Kono, 2001; Leroux et al., 2001; Lu et al., 2012; Yessine & Leroux, 2004; Zignani et al., 2000). A variety of alkyl anchor-bearing polymers have been developed, such as PEG-lipid (Nakamura et al., 2012; Yamada et al., 2008), poly(vinyl alcohol)-alkyl (Inui et al., 2010; Teramura et al., 2008), P(NIPAM-co-MAA-co-ODA) (Kono, 2001; Leroux et al., 2001) and alkylated derivatives of PEAA (Chen et al., 2004), which displayed stronger interaction with the lipid membrane compared to their unmodified counterparts. However, the non-biodegradability of those polymer backbones remains a problem for potential clinical application (Duncan, 2006).

Multidrug resistance (MDR) is another major hurdle that limits the therapeutic efficacy of many chemotherapeutic drugs. The resistance enables tumor cells to resist the cytostatic or cytotoxic action of multiple, structurally dissimilar and functionally divergent drugs (Abbasi et al., 2013). The utilization of a broad spectrum of anticancer drugs, such as DOX, vincristine, etoposide and paclitaxel is affected by the MDR (Baguley, 2010; Krishna & Mayer, 2000). A variety of drug resistance mechanisms have been reported, including over-expression of efflux pumps such as P-glycoprotein (Pgp), antiapototic bcl-2 protein and multidrug resistance protein (MRP), altered expression of topisomerase II (Topo II), and modifications of glutathione S-transferase (Amin, 2013; Baguley, 2010; Krishna & Mayer, 2000). High dose of cytotoxic drugs is needed to overcome MDR, which may result in unfavorable side effects. Combination therapy that combines two different drugs could act on multiple signaling pathways, block the drug pump and therefore enhance anticancer activity at a lower dose with equal or increased efficacy (Creixell & Peppas, 2012; Hu & Zhang, 2012; Liboiron & Mayer, 2014; Parhi et al., 2012). Another attractive strategy to overcome MDR is to use an intelligent drug delivery

system to change the mode of cell uptake from diffusion to endocytosis (Goren et al., 2000; Kim et al., 2008; Liu et al., 2014). A number of stimuli-responsive delivery systems that can achieve a sufficiently high level of intracellular chemotherapeutic drugs have demonstrated their ability to overcome MDR, such as pH-responsive micelles composed of poly(L-lactic acid)-b-poly(ethylene glycol)-b-poly(L-histidine)-TAT and poly(L-histidine)-b-poly(ethylene glycol) (Lee et al., 2008), and redox-responsive nanoparticles assembled from poly(ε-caprolactone) and poly(ethyl ethylene phosphate) (Wang et al., 2011).

Therefore, it would be interesting to develop multifunctional liposomes modified with biodegradable, synthetic, membrane-anchoring polymers with alkyl side chains for efficient intracellular drug delivery and evaluate their ability to overcome MDR. The pH-responsive, comb-like, membrane-anchoring, anionic polymers, PLP-NDAs, have been developed by grafting the metabolite-derived linear polyamide, PLP, with relatively long hydrophobic NDA side chains as membrane anchors at various degrees of substitution. The NDA grafting changed the hydrophobicity/hydrophilicity balance of the polymer and the optimal comb-like polymer, PLP-NDA 18%, was non-lytic at neutral pH but displayed superior membrane destabilization activity at endosomal pHs. It has been shown that 0.5 mg mL^{-1} PLP-NDA 18% could cause almost complete hemolysis of RBCs at pH 5.5 within only 20 min, while only 0.5% hemolysis was observed for its linear counterpart PLP under the same condition (Chapter 4). Besides, PLP-NDA 18% has been successfully applied for intracellular delivery of a wide size range of payloads (up to 2,000 kDa) into a variety of cell types, including stem cells and multidrug resistant cells, with relatively short treatment (Chapter 5). All of these characteristics suggest the membrane-anchoring, comb-like PLP-NDA 18% polymer an ideal candidate for the liposomal surface coating. Chapter 3 presents a novel virus-mimicking liposomal system, which was surface-modified with the PLP bearing hydrophobic pendant amino acid Phe. It would be interesting to compare these two different novel liposomal delivery systems modified with different polymers and further investigate the key parameters affecting polymer-membrane interaction.

This chapter describes development of another type of virus-mimicking, multifunctional liposomes with the membrane protein-mimicking PLP-NDA 18% for the higher polymer coating efficiency and consequently enhanced and controllable intracellular delivery. The pH-triggered release profile, polymer adsorption efficiency and liposomal size change were investigated and compared with the PP75-modified virus-mimicking liposomes. The

endosomal escape ability of the novel PLP-NAD 18%-modified multifunctional liposomes was examined via hemolysis assay using RBCs as the model endosomal membrane. The cellular uptake of the fluorescently labeled liposomes was visualized by confocal microscopy and quantitatively analyzed by flow cytometry. The cellular uptake and potency of the DOX-loaded multifunctional liposomes against four different cancer cell lines including multidrug resistant cell line were assessed and compared with free DOX and conventional liposomes.

6.2 Results and discussion

6.2.1. Effect of cholesterol proportion in the liposomal membrane

During surface modification of liposomes with polymer, content leakage could occur due to the insertion of the polymer into the liposomal bilayer. Cholesterol plays an important role in altering the permeability of the lipid membrane, and therefore the proportion of cholesterol in the membrane should be optimized to minimize the content leakage during polymer coating. Figure 6-1 shows the leakage of the model drug calcein from the liposomes containing different percentages of cholesterol incubated with various PLP-DNA polymers for overnight modification at pH 7.4. Limited content leakage was observed when the liposomes containing various amounts of cholesterol were modified with the linear counterpart PLP or the comb-like polymer with a sufficiently low degree of NDA grafting (e.g. PLP-NDA 3%). However, once the degree of substitution of the hydrophobic NDA anchors was increased (e.g. PLP-NDA 10% and PLP-NDA 18%), the calcein leakage could be increased dependent on the cholesterol percentage. For the liposomes prepared without cholesterol, the percentages of calcein leakage during the liposomal surface modification with PLP-NDA 3% and PLP-NDA 10% were 3.8 ± 0.1% and 64.9 ± 1.2% respectively, whilst almost all the loaded content was lost during surface modification with PLP grafted with 18 mol% NDA. The leakage can be reduced by increasing the cholesterol ratio in the liposomal formulation. By rising the cholesterol proportion to 40 mol%, the content leakage of liposomes modified with PLP-NDA 18% can be decreased to 27.3 ± 2.9 %. For the liposomes containing 60 mol% cholesterol, almost no leakage was detected from liposomes modified with any polymers.

The possible explanation is the present of cholesterol in the membrane may hamper the polymer and lipid interaction (Chen & Chen, 2016). Polyelectrolyte-induced membrane destabilization is sensitive to cholesterol ratio in the liposomal composition (Yessine & Leroux, 2004). A well-known ability of cholesterol is lipid condensing. Cholesterol can tighten alkyl

chains of phospholipids in the lipid bilayer, and induce a high order degree in the membrane resulting in a pronounced thickening of the lipid bilayer, thus increase the membrane rigidity and decrease the membrane permeability (Aloia, Roland C., 1985; de Meyer & Smit, 2009; Hung et al., 2007). Therefore, in the absence of cholesterol in the lipid membrane, the hydrophobic anchors of the polymer tend to insert into the lipid membrane, which may introduce content leakage. While with the presence of cholesterol, the lipid membrane would become more rigid, fluid and more difficult to permeabilize (Briuglia et al., 2015). As a result, content leakage from liposomes could be avoided or minimized. Researches about liposomes surface-bounded with PEAA have shown that a higher cholesterol content results in greater membrane rigidity and lower permeability (Needham et al., 1999). Incorporating cholesterol in the formulation could maintain the integration of lipid membrane during polymer modification step and improve the stability of the liposomes, but still able to release their contents under acidic conditions (Lu et al., 2012; Mills et al., 1999). Besides, the polymer-liposomes interaction would mainly take place at the liposomal surface instead of translocation through the membrane due to the enhanced hydrophobicity of membrane surface with the addition of cholesterol, as discussed in Section 3.2.4.1.

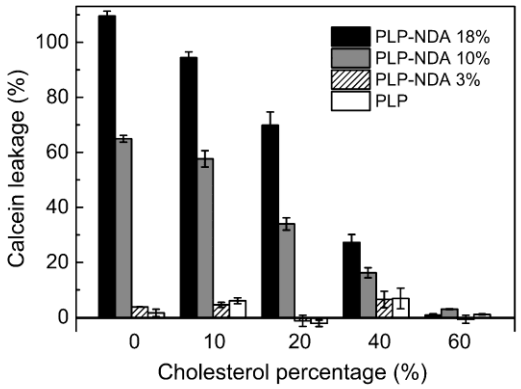

Figure 6-1. Calcein leakage from the liposomes containing different proportions of cholesterol during surface functionalization with 10 mg mL^{-1} various PLP-NDA polymers for overnight at pH 7.4. Mean ± S.D. (n=3).

6.3.2 Effect of NDA grafting degree

The main interactions between the polymer and the lipid membrane include hydrophobic interaction, electrostatic interaction, hydrogen bonding and so on (Schulz et al., 2012). For the

amphiphilic pseudopeptides and the neutral liposome membrane, hydrophobic interaction is a major driving force for adsorption (Yessine & Leroux, 2004). By grafting different percentages (0-18%) of relatively long hydrophobic alkyl anchors on the PLP backbone, the hydrophobicity of the pseudopeptidic polymer was changed accordingly. The effect of hydrophobicity/hydrophilicity balance on the polymer-membrane interaction was investigated.

As shown in Figure 6-2, after removal of unadsorbed polymers and leaked content, almost no calcein release was observed for the liposomes coated with PLP within the pH range (4.0 – 7.4) tested, indicating that the PLP-coated liposomes could not display a pH-triggered release. As comparison, pH-dependent release was observed for all the liposomes surface-modified with the comb-like polymers containing different amounts of relatively long hydrophobic NDA anchors. With increasing the degree of NDA grafting, the pH-responsive payload release of the multifunctional liposomes were increased in the order of PLP-coated liposomes < PLP-NDA 3%-coated liposomes < PLP-NDA 10%-coated liposomes < PLP-NDA 18%-coated liposomes. For the liposomes coated with PLP-NDA 18%, 91.6 ± 18.8% of the payload was released at pH 4.5 while no calcein release was detected at pH 7.4. This release profile is ideal for the development of a smart drug delivery system that is stable during the blood circulation but could quickly respond to the environmental pH change and release the payloads. The order of pH-responsiveness of the multifunctional liposomes is in agreement with the hemolysis result of the comb-like pseudopeptidic polymers (Figure 4-10). Hydrophobic interaction is of crucial importance for the anionic polymer to interact with neutral or negatively charged lipid membranes (Marie et al., 2014; Schulz et al., 2012; Yessine & Leroux, 2004). The hydrophobicity of the polymer will be enhanced by increasing the degree of substitution with relatively long hydrophobic alkyl side chain, leading to stronger membrane association (El-Sayed et al., 2015; Murthy et al., 1999).

Increasing the NDA grafting degree would increase the pH-responsiveness of the comb-like polymer-coated liposomes, which was similar with coating liposomes with the PLP grafted with hydrophobic amino acid Phe (Figure 3-9). However, almost no difference in the release profile was observed for the liposomes coated with PP25 compared to the PLP-coated liposomes. Instead, the pH-responsiveness of the PLP-NDA 3%-coated liposomes was considerably increased compared to the PLP-coated liposomes. Only 6.4 ± 0.6 % of calcein was released from the liposomes coated with PP25 at pH 4.5, while 35.5 ± 5.6 % of calcein was released for the PLP-NDA 3% modified liposomes at the same pH. Increasing the grafting

percentage of NDA to 18%, almost all the content was released for the PLP-NDA 18% modified liposomes at pH 4.5. This finding indicates that a lower degree of grafting is required for the comb-like polymers to achieve a desirable release profile, as compared with the polymers containing pendant Phe groups. Fatty-alkyl side chains are important contributors for a variety of membrane proteins and antimicrobial peptides/polymers to bind with the lipid membrane (Economou et al., 2013; Resh, 1999; Sato & Feix, 2006). Even relatively short alkyl groups, such as ethyl, can promote the membrane binding against the charge repulsion between polymers and the membrane (Thomas et al., 1996). Long alkyl side chains could provide more stable membrane anchoring due to the deeper insertion (Resh, 2016). Although the hydrophobic amino acid Phe with an aromatic group is able to interact with the lipid bilayer (Hong et al., 2007; Lee et al., 2015; MacCallum et al., 2007), Großauer et al. have found that, compared with the Phe residue in a peptide hormone ghrelin, its hydrophobic octanoyl (C8) chain can facilitate a deeper insertion of the peptide into the lipid membrane due to the relatively long chain length (Großauer et al., 2010). With the absence of octanoyl, no membrane binding was observed for the des-octanoyl ghrelin (Großauer et al., 2010).

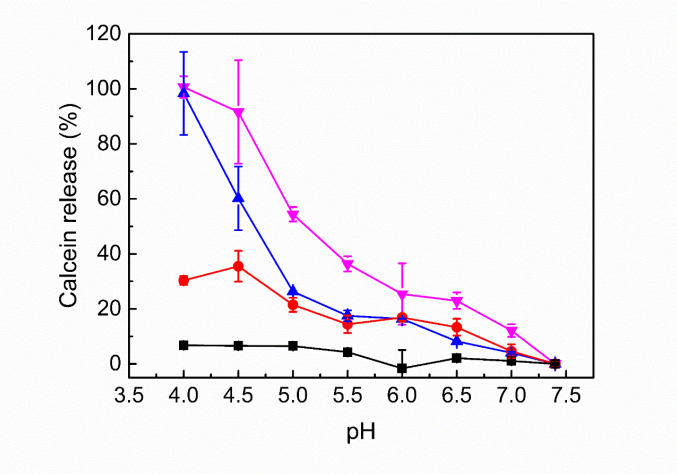

Figure 6-2. pH-Dependent calcein release from the virus-mimicking liposomes coated with PLP (■), PLP-NDA 3% (●), PLP-NDA 10% (▲), and PLP-NDA 18% (▼) respectively. Mean ± S.D. (n=3).

6.2.3 Effect of polymer concentration

The effect of coating density with the comb-like polymer on the pH-responsive payload release profile of virus-mimicking liposomes was also investigated. Liposomes with a fixed lipid concentration at 3.0 mM were coated with different amounts of PLP-NDA 18%, and then

dialysis was carried out to remove the unadsorbed polymers. Figure 6-3 illustrates the pH-triggered release profiles of the virus-mimicking liposomes coated with different amounts of PLP-NDA 18%. The liposomes treated with 0.1 – 10 mg mL^{-1} PLP-NDA 18% all displayed pH-responsive payload release profiles, indicative of successful polymer coating. The liposomes treated with 10 and 1 mg mL^{-1} PLP-NDA 18% showed similar release rates at acidic pHs, while considerably higher than those of the liposomes treated with 0.1 mg mL^{-1} PLP-NDA 18%.

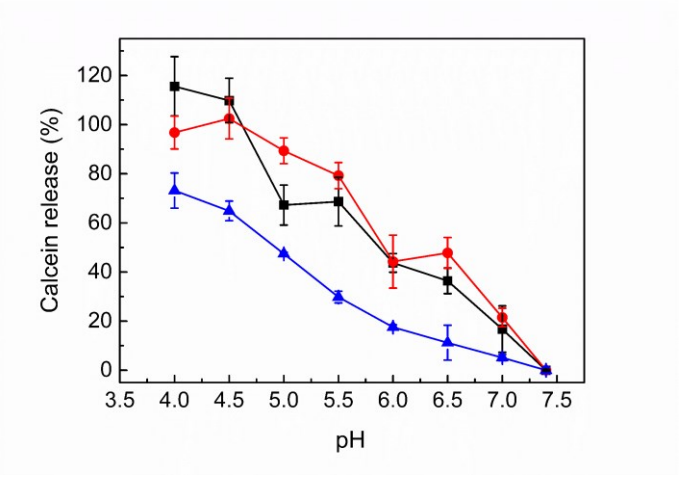

Figure 6-3. pH-Dependent calcein release from the cholesterol (40 mol%)-containing liposomes treated with PLP-NDA 18% at 10 mg mL^{-1} (■), 1 mg mL^{-1} (●) and 0.1 mg mL^{-1} (▲) followed by the removal of unadsorbed polymer. Mean ± S.D. (n=3).

Further study was then carried out to quantify the membrane adsorption of the comb-like polymer. 6-aminofluorescein was conjugated on PLP-NDA 18% and the amount of adsorbed polymer was quantified after liposomal modification and removal of unadsorbed polymers. 3.45 ± 0.01 mg mL^{-1} PLP-NDA 18% was adsorbed on the liposomal surface after treatment of the liposomes with 10 mg mL^{-1} PLP-NDA 18%. The polymer adsorption efficiency was relatively higher compared to the coating of the liposomes with PP75 under the same condition (2.88 ± 1.03 mg mL^{-1} PP75 adsorbed on the liposomal membrane). The higher coating efficiency of the PLP-NDA 18% modified liposomes might due to the more efficient membrane binding of PLP-NDA 18% with relatively long hydrophobic alkyl side chains compared with PP75 with pendant Phe groups (Großauer et al., 2010). 0.24 ± 0.01 mg mL^{-1} PLP-NDA 18% was adsorbed on the liposomal surface after treatment of the liposomes with 1 mg mL^{-1} PLP-NDA 18%, indicating that a small amount of adsorbed PLP-NDA 18% on the liposomal

membrane could be sufficient for pH-triggered membrane destabilization and content release. Thus, lower amount of PLP-NDA 18% was needed for the liposomal modification in order to achieve the same pH-responsiveness compared to the surface coating with PP75. In other words, PLP-NDA 18% was more efficient in liposomal surface modification for developing pH-sensitive, virus-mimicking liposomes.

6.2.4 Dilution effect

Dilution-independent release behavior is of crucial importance due to the remarkable dilution of drug delivery formulations during circulation in the bloodstream (Tribet & Vial, 2008). The pH-dependent release profile of the PLP-NDA 18%-coated multifunctional liposomes upon dilution was further evaluated. The polymer-to-lipid ratio was fixed at 2.85:100. After the polymer-coated liposomes were diluted for various folds at pH 7.4, the content release at pH 4.5 was then measured. As shown in Figure 6-4, the PLP-NDA 18%-coated liposomes displayed dilution-independent, pH-responsive release behavior. Upon acidification almost all the content was released from the PLP-NDA 18%-coated, virus-mimicking liposomes diluted for 5-, 10- and 50-folds. Even after 100-fold dilution, 81.5 ± 5.0% of payload was released from the PLP-NDA 18% modified liposomes at pH 4.5. This result suggests that the strongly membrane-bound, comb-like polymer retained on the liposomal surface after tremendous dilution and still retained its pH-dependent membrane destabilization activity.

Dilution-independent release behavior is of key importance for a drug delivery system. The major limitation to the drug delivery application of polymeric micelles is the instability after dilution which may lead to the disassembly of the delivery system and unwanted drug release during blood circulation (Discher & Eisenberg, 2002; Owen et al., 2012). In order to maintain the colloidal stability and membrane destabilization activity of polymer-based delivery systems, the polymer concentration need to be kept above its CAC (Kataoka et al., 2001; Yokoyama, 2010). By grafting hydrophobic segments on the side chain, the CAC value of the modified polymer would be reduced (Kim et al., 2009), leading to the improved dilution-independent release behavior that is favorable for drug delivery application.

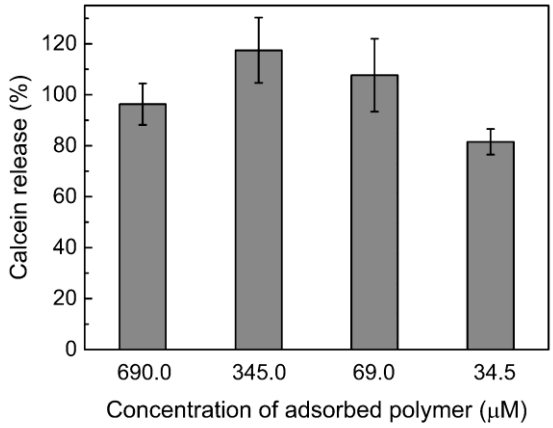

Figure 6-4. Calcein release from the PLP-NDA 18%-coated liposomes (with a fixed polymer-to-lipid molar ratio at 2.85:100 upon 5-, 10-, 50- and 100-fold dilution) at pH 4.5. Mean ± S.D. (n=3).

6.2.5. pH-Triggered liposomal size change

The liposomal size before and after surface modification was investigated. As shown in Figure 6-5, the mean hydrodynamic particle size of the liposomes was 77.1 ± 0.7 nm, after modification with PLP-NDA 18%, the particle size increased to 89.2 ± 0.5 nm. The size increase due to the modification with PLP-NDA 18% (12.1 ± 0.6 nm) was higher than that due to the modification with PP75 (6.4 ± 2.2 nm), indicative of a thicker polymer coating layer of the PLP-NDA 18%-coated liposomes compared to the PP75-coated liposomes.

The pH-triggered liposomal size change was also investigated. As shown in Figure 6-6, the particle size of the unmodified liposomes remained the same within the pH range (4.0 – 7.4) tested. Negligible pH-dependent size change was observed for the liposomes modified with PLP and PLP-NDA 3%. However, for the liposomes coated with PLP-NDA 10%, a noticeable size increase was detected at pH 4.0. While for the liposomes coated with PLP-NDA 18%, a remarkable size change was displayed at pH below 5.5. This could be attributed to the enhanced hydrophobicity of the comb-like polymer with increasing the degree of substitution of relatively long hydrophobic NDA side chains, which led to the increased inter-vesicular interaction and the consequent liposomal aggregation or fusion (Yuba et al., 2011; Yessine & Leroux, 2004).

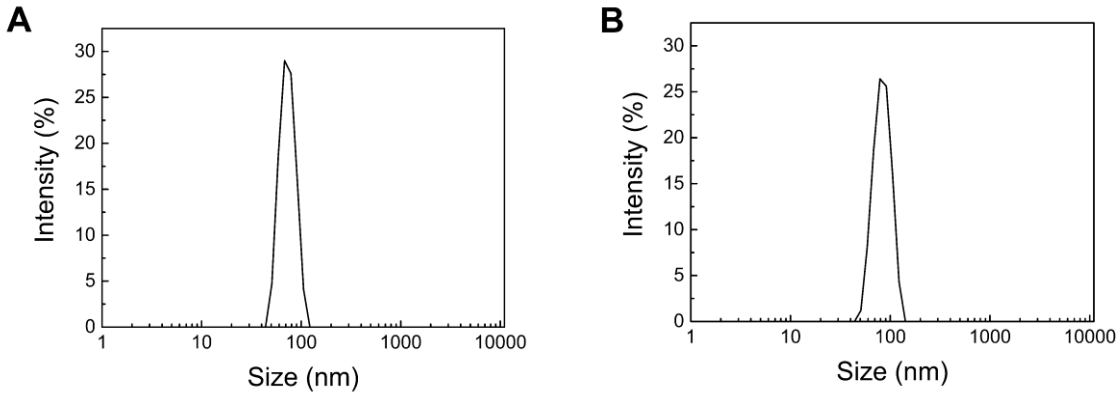

Figure 6-5. Size distributions of (A) the bare liposomes and (B) the PLP-NDA 18%-coated liposomes.

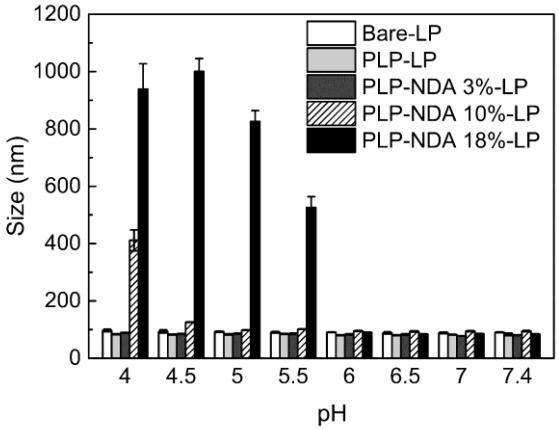

Figure 6-6. The mean hydrodynamic size of the bare liposomes (Bare-LP), PLP-coated liposomes (PLP-LP), PLP-NDA 3%-coated liposomes (PLP-NDA 3%-LP), PLP-NDA 10%-coated liposomes (PLP-NDA 10%-LP) and PLP-NDA 18%-coated liposomes (PLP-NDA 18%-LP) at different pHs. Mean ± S.D. (n=3).

6.2.6 Mechanism of inter-vesicular interaction

The mechanism of inter-vesicular interaction was investigated to elucidate if the pH-triggered increase in the size of the comb-like polymer-modified liposomes was due to membrane fusion or particle aggregation. Fusion of lipid bilayers is usually assessed by dye dilution assay, during which fluorescent markers are incorporated into the lipid membrane and the fluorescence intensity change is monitored (Martens et al., 2014). Dye dilution can be detected by dimer quenching, FRET or dye dequenching. FRET is a more frequently used

technique which measures the distance-dependent fluorescence intensity of a pair of donor and acceptor fluorophores (Hyvönen et al., 2012). In this study, lipid-mixing assay was applied to confirm whether fusion took place by measuring the FRET between NBD-PE and Rh-PE incorporated in the probe liposomes (1 mol%). As shown in Figure 6-7, almost no lipid mixing was detected within 24 h at both pH 7.4 and 4.5 for the liposomes with or without PLP-NDA 18% coating, indicative of no occurrence of membrane fusion.

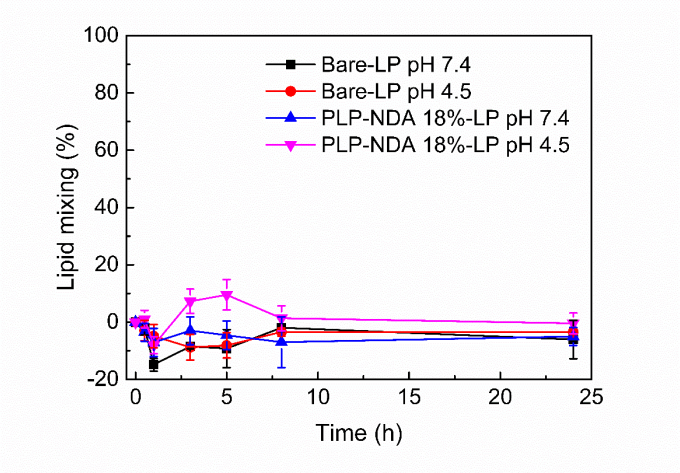

Figure 6-7. Lipid mixing assay of the bare and PLP-NDA 18%-coated liposomes at pH 7.4 and 4.5. Membrane fusion was assessed by FRET. The probe liposomes were prepared by incorporating 1 mol% NBD-PE and 1 mol% Rh-PE in the liposomal formulation. The lipid-mixing ratio was determined by measuring the fluorescence intensity of NBD after incubation of the probe liposomes with the nonprobe liposomes (1:9 molar) at different pHs for different periods of time. Mean ± S.D. (n=3).

The reversibility of the size change was examined to further investigate the mechanism of inter-vesicular interaction. As shown in Figure 6-8, once pH decreased from 7.4 to 4.5, a dramatic size increase was observed for the liposomes coated with PLP-NDA 18%. Upon titration of the pH from 4.5 to 7.4, the particle changed back to its original size within 5 min. This reversible size change was detected for several pH circles. This consolidates that the liposomal size increase at acidic pHs was not induced by the membrane fusion, otherwise it would not be possible for the virus-mimicking liposomes to display a reversible size change within such a short time (Chen & Chen, 2016; Jahn & Südhof, 1999). Therefore, the pH-triggered size increase was probably due to vesicle aggregation instead of membrane fusion. This result was in good agreement with the pH-dependent, reversible size change of the PP75-coated liposomes. The polymer-bridged liposomal network model proposed in Figure 3-16

could be applied here to interpret the pH-triggered size change of the liposomes coated with the comb-like polymer. Specifically, the hydrophobic relatively long alkyl side chains on PLP-NDA 18% could facilitate its binding with more than one liposome, which resulted in a polymer-bridged liposomal network (Chen & Chen, 2016). At neutral pH no significant liposomal size change was observed due to the expanded polymer structure. However, with the decrease of the pH, the polymer displayed a coil-to-globule conformational change (Chen et al., 2017). Thus the compact polymer structure led to the aggregation of the polymer-bridged liposomal network, which resulted in a dramatic size increase (Chieng & Chen, 2010). The size was reduced because of the polymer expansion once the pH was changed back to neutral.

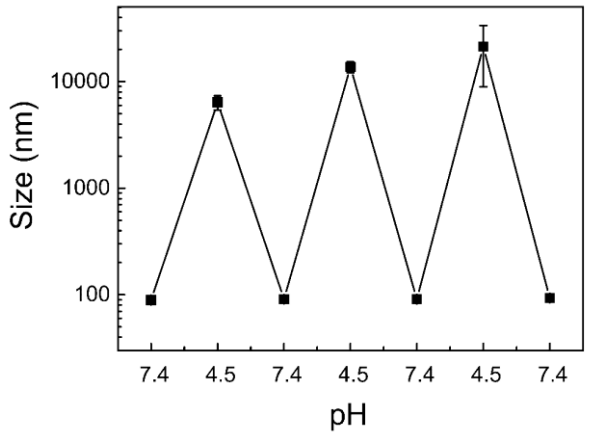

Figure 6-8. Reversible size change of the PLP-NDA 18%-coated liposomes, as measured by DLS. Mean ± S.D. (n=3).

6.2.7 Hemolysis assay

It has been demonstrated that the PLP-NDA 18% could adsorb on the liposomal surface and destabilize the liposomal membrane at acidic conditions, leading to pH-responsive release of the liposomal content. On the other hand, it is important to investigate whether the comb-like polymer could retain its endosomolytic activity after being coated on the liposomal surface, thus enabling the endosomal escape. The endosomolytic activity of the polymer-coated liposomes was quantified by hemolysis assay using sheep RBCs as a model of the endosomal membrane (Chen et al., 2009c). As shown in Figure 6-9, no hemolysis was detected when the RBCs were treated with the bare liposomes or PLP-modified liposomes within the pH range (5.0 – 7.4) tested. At pH 7.4, 10.4 ± 0.3% hemolysis was detected for the RBCs treated with

the PLP-NDA 18%-coated liposomes (concentration of the adsorbed PLP-NDA 18% at 8.8 μM), considerably lower than the hemolysis value (71.9 ± 3.1%) of the PP75-coated liposomes (concentration of the adsorbed PP75 at 5.8 μM) at the same pH (Figure 3-17B). This indicates that the PLP-NDA 18%-coated liposomes was more biocompatible at neutral pH compared to the PP75-coated liposomes. At pH 6.0 typical of early endosomal pH, the RBCs treated with the PLP-NDA 18%-coated liposomes showed the hemolysis of 92.1 ± 1.5%. The hemolytic activity of PLP-NDA 18% adsorbed on the liposomal surface was similar with the free comb-like polymer (Figure 4-10), suggesting that the polymer well retained its pH-triggered membrane destabilization functionality. The pH-dependent membrane disruption activity of the multifunctional liposomes is ideal for cytoplasmic drug delivery. The liposomal drug delivery systems would display minimal cytotoxicity during blood circulation. However, once they reach the tumor with an acidic microenvironment and enter a cell via the endocytic pathway, the acidity in the tumor microenvironment and endosomal/lysosomal compartments could activate their membrane disruptive activity and thus efficiently deliver payloads into the cell cytoplasm (de Las Heras Alarcon et al., 2005; Jeong & Gutowska, 2002; Joglekar & Trewyn, 2013).

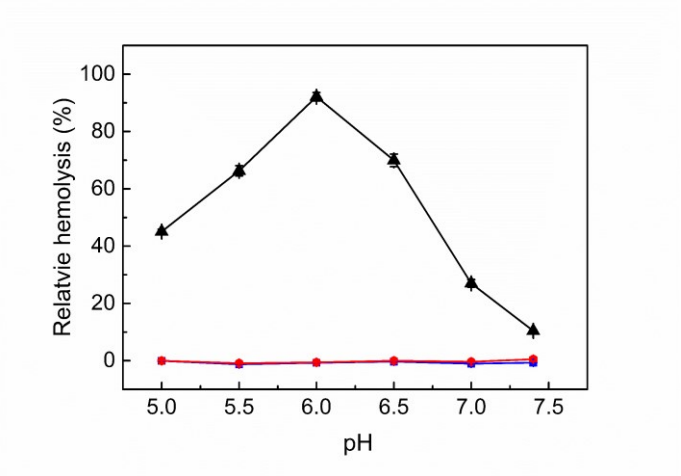

Figure 6-9. pH-Dependent relative hemolysis of the bare liposomes (■), PLP-coated liposomes (●) and PLP-NDA 18%-coated liposomes (▲). Mean ± S.D. (n=3).

6.2.8 Cellular uptake

The comb-like polymer coated, virus-mimicking liposomes were labelled with 1 mol% Rh-PE and the cellular uptake and subcellular localization of the fluorescent liposomes was

determined by confocal microscopy and flow cytometry. The distribution of red fluorescence, shown in Figure 6-10A, exhibited the intracellular localization of the liposomes. Compared to the bare liposomes, PLP-NDA 18%-coated liposomes displayed a significantly enhanced uptake by HeLa cells. According to the quantitative flow cytometry data shown in Figures 6-10B and 6-10C, the MFI of the cells treated with the PLP-NDA 18%-coated liposomes was 4.7 ± 0.2 times higher than those treated with the bare liposomes. The improved cellular uptake of the virus-mimicking liposomes could be due to the presence of the comb-like pseudopeptides containing hydrophobic relatively long NDA side chains. Alkyl chains have been utilized as membrane anchors by a variety of membrane proteins to bind with the lipid membrane (Rapoport, 2007; Resh, 1999). Therefore, the comb-like polymer PLP-NDA 18% containing NDA side chains exhibited the enhanced hydrophobicity and membrane binding. After being coated on the liposomal membrane, the accessible free NDA chains on the PLP-NDA 18% would facilitate the hydrophobic interaction of the multifunctional liposomes with the cell membrane, thus improving the cellular uptake. Besides, the scavenger receptors expressed in a wide range of cells including HeLa have been reported to play an important role in the enhanced cellular uptake of negatively charged systems (Yang et al., 2013b; Copolovici et al., 2014; Chen & Chen, 2016). This is probably due to the recognition of anionic delivery systems by the scavenger receptors (Fujiwara et al., 1996; Yuba et al., 2013, 2011).

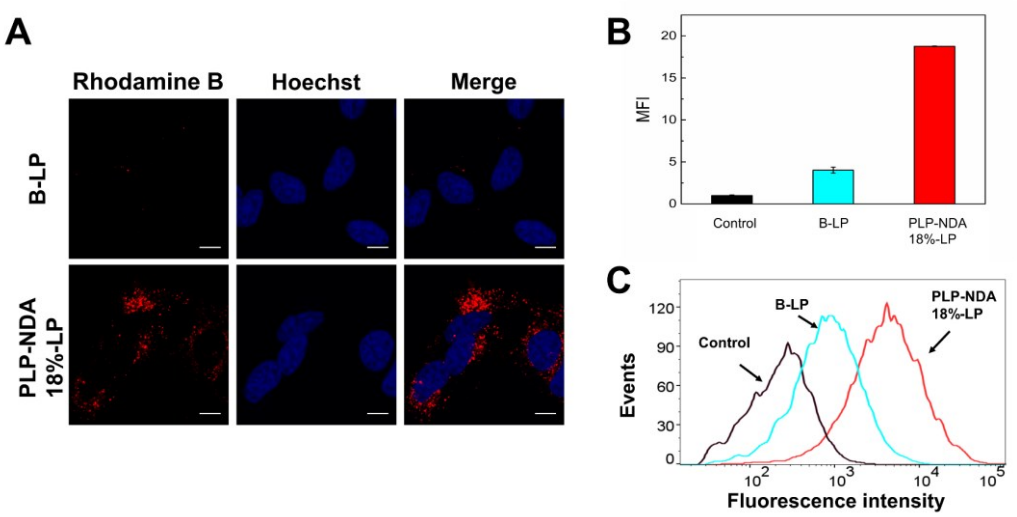

Figure 6-10. (A) Confocal microscopy images of HeLa cells showing the subcellular localization of the bare liposomes (B-LP) and the PLP-NDA 18%-coated liposomes (PLP-NDA 18%-LP) labeled with 1 mol% Rh-PE. Cellular uptake of the fluorescent liposomes was further analyzed by flow cytometry and presented as (B) relative MFI and (C) representative histogram plots. All the samples were analyzed after 1 h of uptake and 3 h of further incubation. Scale bar: 20 μm. Mean ± S.D. (n=3).

6.2.9 Intracellular delivery

A widely used anticancer drug DOX was used as a model payload in order to further evaluate the endosomal escape ability and intracellular drug delivery potential of the multifunctional liposomes. As shown in Figure 6-11A, the red fluorescence intensity in the HeLa cells treated with the DOX-loaded bare liposomes was significantly lower than the cells treated with free DOX at the same drug concentration. As a small molecular drug, free DOX usually enters cells by simple diffusion (Cui et al., 2013). As comparison, the DOX-loaded liposomes were internalized mainly through endocytosis (Canton & Battaglia, 2012; Iversen et al., 2011). It is interesting to note that the DOX fluorescence in the cells treated with the PLP-NDA 18%-coated liposomes was similar compared to the free DOX, while much higher compared to the bare liposomes. This was consolidated by the flow cytometry data (Figures 6-11B and 6-11C). The MFI of the HeLa cells treated with free DOX was similar with the cells treated with the DOX-loaded, PLP-NDA 18%-coated liposomes, while was 2.4 ± 0.3 times higher than the cells treated with the DOX-loaded bare liposomes. The significantly increased intracellular DOX fluorescence might be because of the significantly enhanced cellular uptake and efficient endosomal escape of the virus-mimicking liposomes coated with the comb-like

polymer compared to the bare liposomes (Figure 6-10). After cell internalization via endocytosis, the acidification process inside the endosomes/lysosomes could trigger the membrane disruptive activity of PLP-NDA 18%, followed by the liposomal membrane destabilization and endosomal escape (Chen & Chen, 2016).

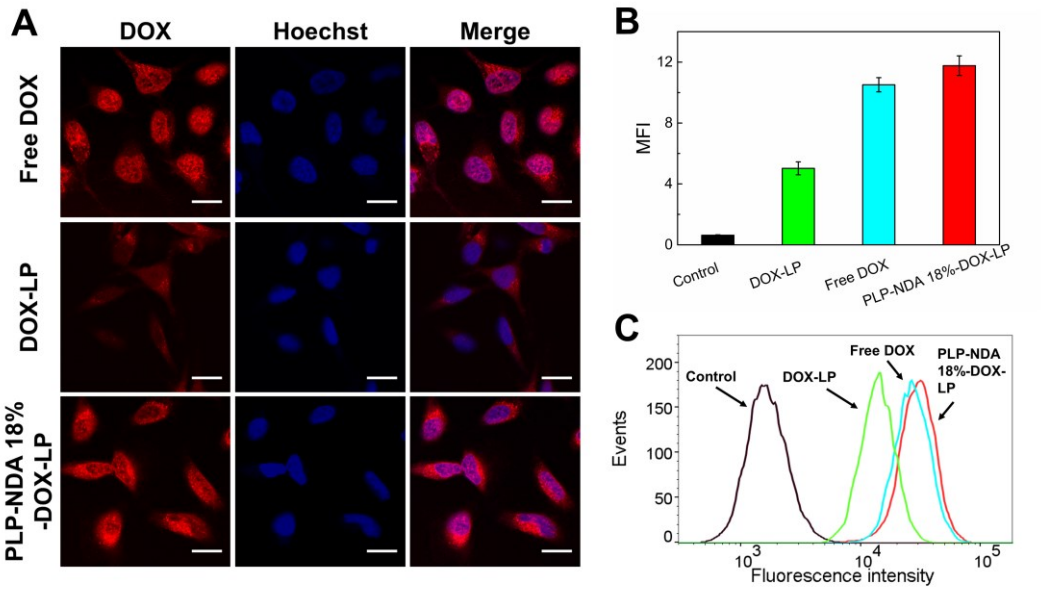

Figure 6-11. (A) Confocal microscopy images, (B) MFI and (C) representative histogram plots showing the subcellular distribution and cellular uptake of free DOX, DOX-loaded bare liposomes, and DOX-loaded, PLP-NDA 18%-coated liposomes in HeLa cells. The DOX concentration was fixed at 2.5 μM. Confocal Imaging and flow cytometry analysis were carried out after 1 h of incubation. Scale bar: 20 μm. Mean ± S.D. (n=3).

To further assess the generalizability of the virus-mimicking liposomes for intracellular delivery application, A549 lung cancer cell line, MES-SA uterus cancer cell line and MES-SA/DX5 drug resistant cancer cell line were employed. As shown in Figure 6-12, the A549 cells treated with the DOX-loaded, PLP-NDA 18%-coated liposomes displayed 2.3 ± 0.5 times higher intracellular DOX fluorescence compared to the cells treated with the bare liposomes. Interestingly, for the MES-SA (Figure 6-13) and MES-SA/DX5 (Figure 6-14) cell lines, the intracellular DOX fluorescence resulting from the DOX delivery by the PLP-NDA 18%-coated liposomes was even higher than the simple diffusion of free DOX. These suggest that the PLP-NDA 18%-coated liposomes could facilitate efficient intracellular drug delivery to a variety of cell lines, including multidrug resistant cells.

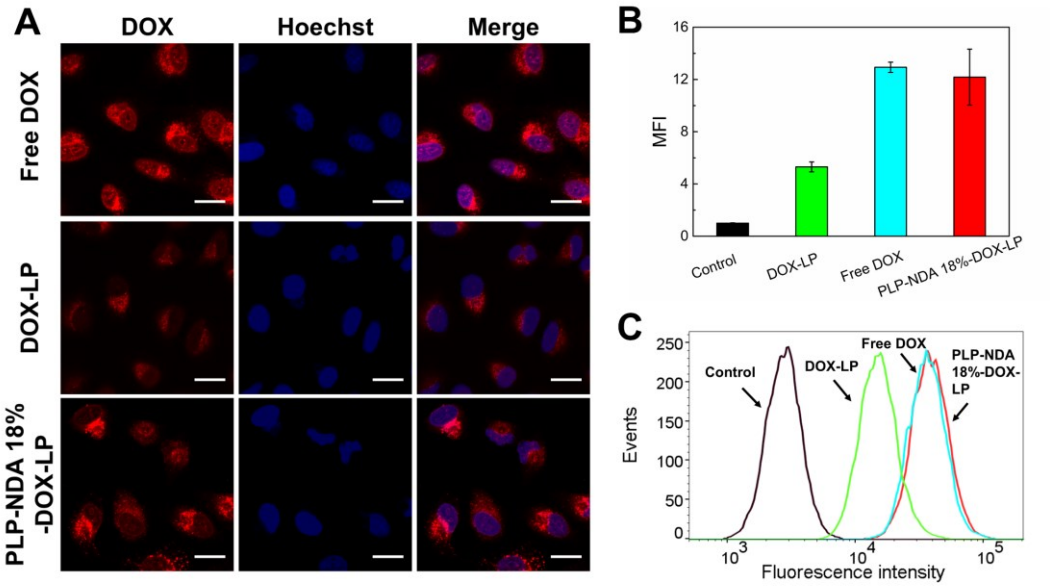

Figure 6-12. (A) Confocal microscopy images, (B) MFI and (C) representative histogram plots showing the subcellular distribution and cellular uptake of free DOX, DOX-loaded bare liposomes, and DOX-loaded, PLP-NDA 18%-coated liposomes in A549 cells. The DOX concentration was fixed at 2.5 μM. Confocal imaging and flow cytometry analysis were carried out after 1 h of incubation. Scale bar: 20 μm. Mean ± S.D. (n=3).

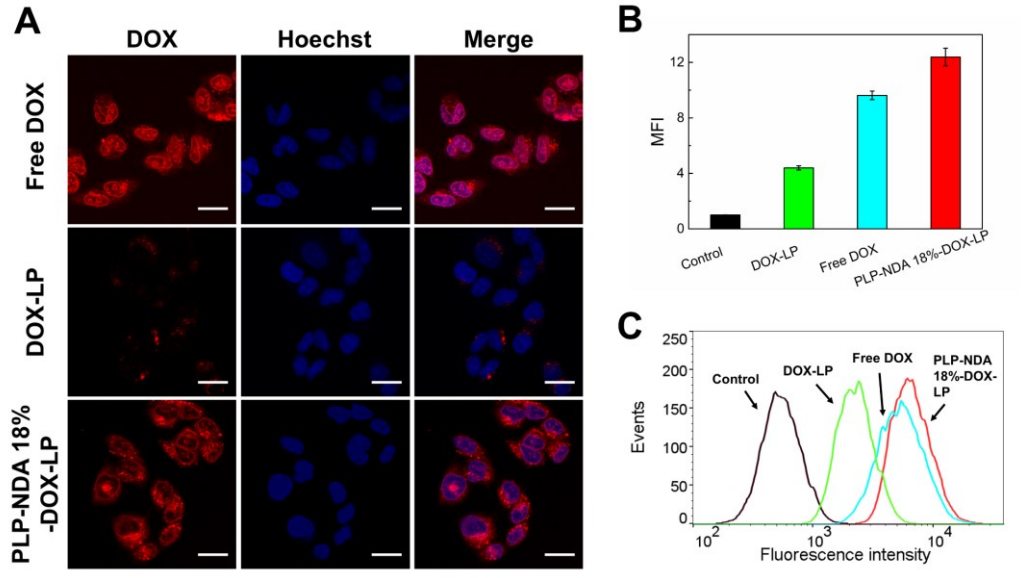

Figure 6-13. (A) Confocal microscopy images, (B) MFI and (C) representative histogram plots showing the subcellular distribution and cellular uptake of free DOX, DOX-loaded bare liposomes, and DOX-loaded, PLP-NDA 18%-coated liposomes in MES-SA cells. The DOX concentration was fixed at 2.5

μM. Confocal imaging and flow cytometry analysis were carried out after 1 h of incubation. Scale bar: 20 μm. Mean ± S.D. (n=3).

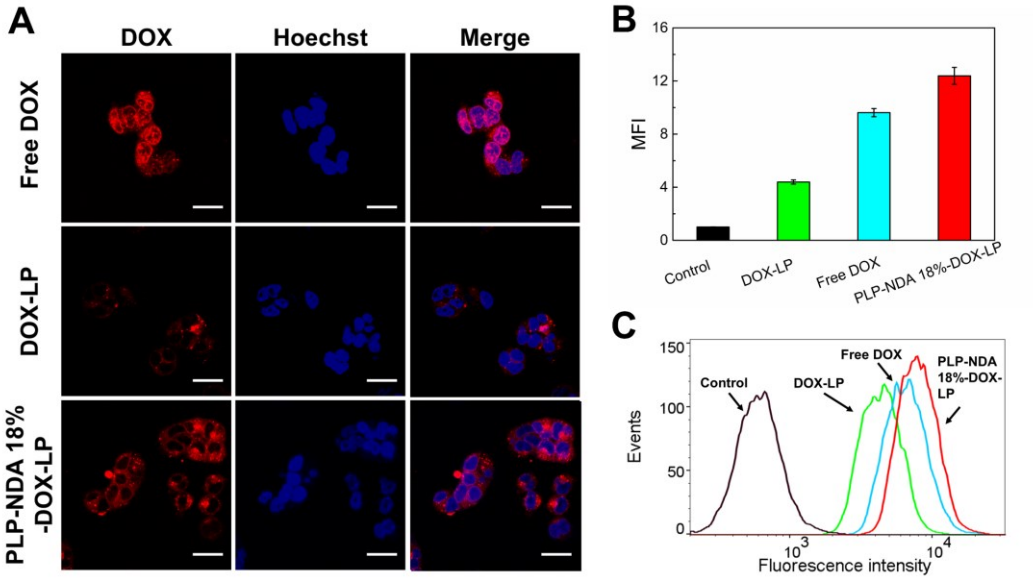

Figure 6-14. (A) Confocal microscopy images, (B) MFI and (C) representative histogram plots showing the subcellular distribution and cellular uptake of free DOX, DOX-loaded bare liposomes, and DOX-loaded, PLP-NDA 18%-coated liposomes in MES-SA/DX5 cells. The DOX concentration was fixed at 5 μM. Confocal imaging and flow cytometry analysis were carried out after 1 h of incubation. Scale bar: 20 μm. Mean ± S.D. (n=3).

6.2.10 In vitro cytotoxicity of the liposomal carrier

Alamar Blue assay was carried out to assess the in vitro cytotoxicity of the liposomes with or without polymer coating toward a variety of cell lines. Alamar Blue (resazurin) is applied as an indicator of the effect of a material on the metabolic activity of a cell (Nociari et al., 1998). As shown in Figure 6-15, the virus-mimicking liposomes coated with PLP-NDA 18% was well tolerated by HeLa cells for 24 h (Figure 6-15A) or 48 h (Figure 6-15B) of treatment with the lipid concentration up to 300 μM (fixed polymer-to-lipid ratio of 2.85:100). Similarly, no or limited cytotoxicity effect was observed for the polymer-coated liposomes against A549 (Figure 6-16) or MES-SA/DX5 cells (Figure 6-18) for up to 48 h of treatment within the lipid concentration range (5 – 300 μM) tested, comparable to the bare liposomes without polymer coating. However, with increasing the lipid concentration ≥ 75 μM, a significantly reduced cell

viability was observed for the MES-SA cells treated with the comb-like polymer coated liposomes for 24 h, indicating that an increase in the concentration of the adsorbed PLP-NDA 18% above 2.1 μM led to significant cytotoxicity against MES-SA cells, As comparison, the conventional liposomes were well tolerated by MES-SA cells for up to 24 h within the lipid concentration range (5 – 300 μM) tested (Figure 6-17A). Once the treatment time was extended to 48 h, considerably reduced viability of MES-SA cells was even noticed in the bare liposomes at the lipid concentration ≥ 200 μM. This was because that MES-SA cells were sensitive to a number of compounds (Harker et al., 1983).

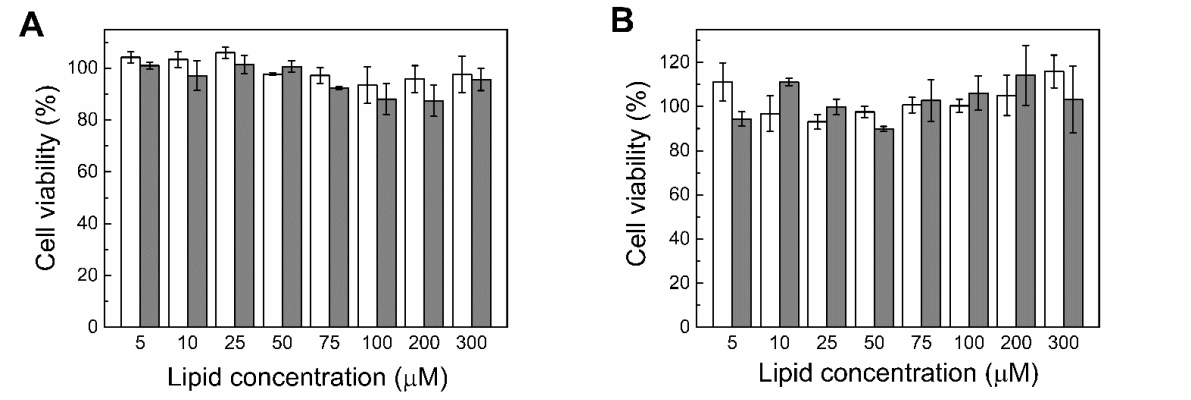

Figure 6-15. Concentration-dependent relative viabilities of HeLa cells treated with the liposomes with (close columns) or without (open columns) PLP-NDA 18% for (A) 24 h and (B) 48 h as determined by Alamar Blue assay. Mean ± S.D. (n=3).

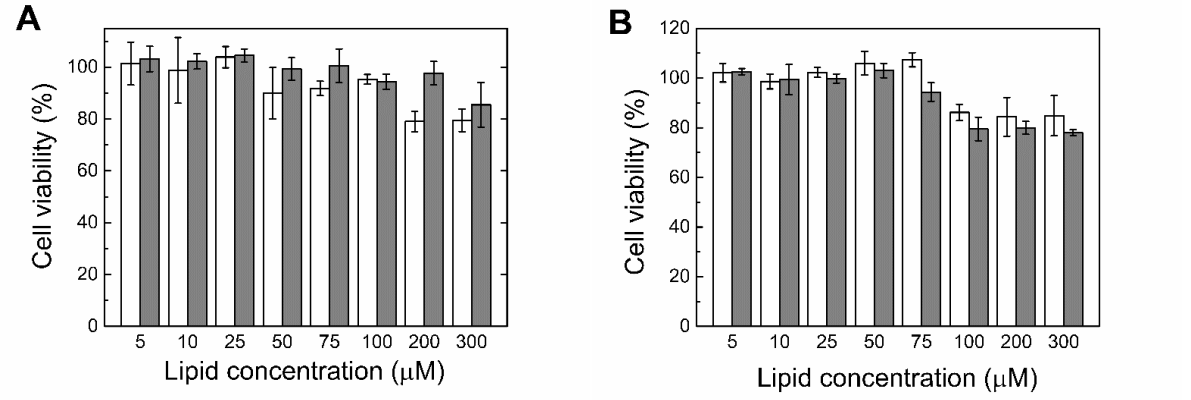

Figure 6-16. Concentration-dependent relative viabilities of A549 cells treated with the liposomes with (close columns) or without (open columns) PLP-NDA 18% for (A) 24 h and (B) 48 h as determined by Alamar Blue assay. Mean ± S.D. (n=3).

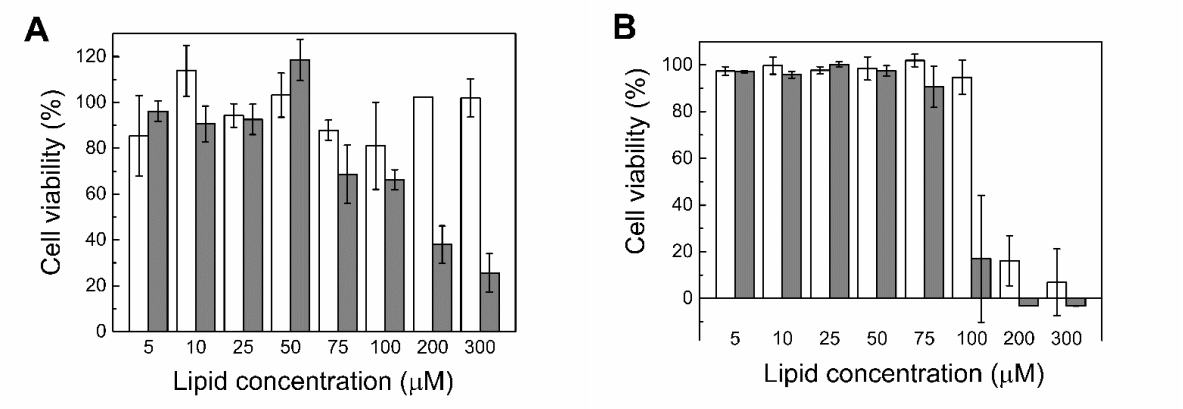

Figure 6-17. Concentration-dependent relative viabilities of MES-SA cells treated with the liposomes with (close columns) or without (open columns) PLP-NDA 18% for (A) 24 h and (B) 48 h as determined by Alamar Blue assay. Mean ± S.D. (n=3).

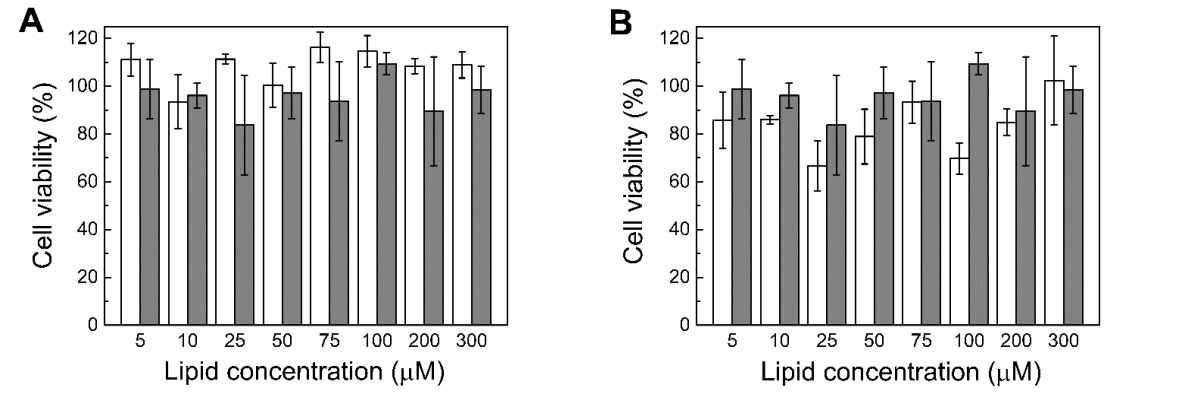

Figure 6-18. Concentration-dependent relative viabilities of MES-SA/DX5 cells treated with the liposomes with (close columns) or without (open columns) PLP-NDA 18% for (A) 24 h and (B) 48 h as determined by Alamar Blue assay. Mean ± S.D. (n=3).

6.2.11 In vitro cytotoxicity of the DOX-loaded liposomes

Potency against a variety of cancer cell lines was carried out to evaluate the therapeutic effectiveness of the anticancer drug loaded liposomes with or without polymer coating. Free DOX enters cells by simple diffusion, while the DOX-loaded delivery systems are usually internalized by cells via endocytosis (Cui et al., 2013). The endocytic mode of cellular uptake could result in not only the decreased internalization, but also the entrapment within the intracellular vesicles, the latter leading to the possible lysosomal degradation of DOX and as a result the reduced anticancer effect (Koren et al., 2012). Thus, it is important to develop a new

drug delivery system, which can enhance the cellular uptake and cytoplasmic localization. In Figure 6-19A, the DOX-loaded bare liposomes showed higher cell viability compared to free DOX at the DOX concentration above 0.25 μM. However, the DOX-loaded, PLP-NDA 18%-coated liposomes displayed a bit higher potency than free DOX, while significantly enhanced potency ($P < 0.01$) than the DOX-loaded bare liposomes, against HeLa cells within the equivalent DOX concentration ranging from 1 to 10 μM. The IC_{50} of the DOX-loaded, PLP-DNA 18%-coated liposomes against HeLa cells was 0.80 ± 0.01 μM, which was lower than the IC_{50} of the free DOX (1.25 ± 0.07 μM) and the DOX-loaded bare liposomes (5.62 ± 0.87 μM). In addition, the DOX-loaded, PLP-NDA 18%-coated liposomes also displayed similar or even higher cytotoxicity against A549 cells (Figure 6-19B) compared to free DOX, while remarkably higher than the DOX-loaded bare liposomes.

MDR remains one of the major barriers to successful cancer therapy (Baguley, 2010). In this study, the human uterine sarcoma cell line MES-SA and the multidrug resistant cell line MES-SA/DX5 that derived from MES-SA, were employed to test the therapeutic efficacy of the liposomes coated with the comb-like polymer. As shown in Figures 6-19C and 6-19D, the IC_{50} of free DOX against the drug-resistant MES-SA/DX5 cells was 21.51 ± 1.02 μM, which was considerably higher than the IC_{50} value of free DOX against the non-resistant MES-SA cells (0.78 ± 0.04 μM). However, the IC_{50} value of DOX-loaded, PLP-NDA 18%-coated liposomes against the MES-SA/DX5 cells was 7.50 ± 0.62 μM (Figure 6-19D), which was significantly lower than free DOX and the DOX-loaded bare liposomes (44.87 ± 7.06 μM). In other words, a lower dose of DOX was needed to achieve the same anticancer effect once it was encapsulated inside the virus-mimicking liposomes coated with the comb-like polymer compared to free DOX or DOX-loaded bare liposomes. The remarkably enhanced cytotoxicity of the comb-like polymer-coated liposomes against multidrug resistant cells could be due to: i) the change of the mode of cellular entry mechanism from simple diffusion for free DOX to endocytosis for the DOX-loaded, PLP-NDA 18%-coated liposomes would enable the escape of DOX from the pump-out by the multidrug efflux pump; ii) the higher plasma membrane binding and the consequent higher cell internalization of the PLP-NDA 18%-coated liposomes; iii) pH-triggered drug release and efficient endosomal escape of the virus-mimicking liposomes. Similar observations have been reported by other researchers that pH-responsive endsomolytic drug delivery systems and CPP-drug conjugates or CPPs-modified delivery systems as were proved to be powerful tools for overcoming the MDR (Farkhani et al., 2014; Kim et al., 2008; Lee et al., 2008, 2005; Pan et al., 2013).

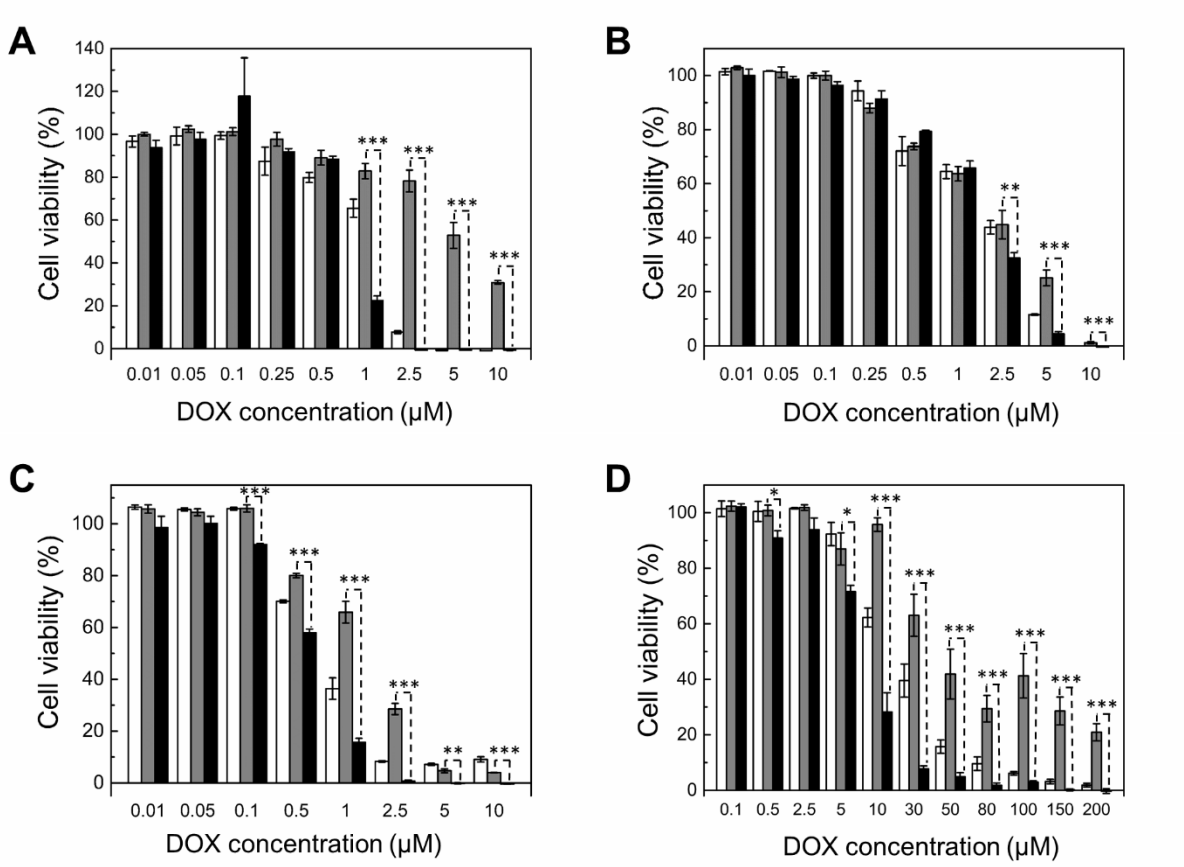

Figure 6-19. Potency of free DOX (open columns), DOX-loaded bare liposomes (gray columns), and DOX-loaded, PLP-NDA 18%-coated liposomes (dark columns) against (A) HeLa, (B) A549, (C) MES-SA and (D) MES-SA/DX5 cells after 24 h of treatment and 24 h of further incubation. The drug to lipid molar ratio was kept at 20.2:100. Mean ± S.D. (n=3). *P < 0.05, **P < 0.01, ***P < 0.001.

6.3 Conclusions

A novel virus-mimicking, multifunctional liposomal drug delivery system was successfully developed via surface modification with the comb-like pseudopeptidic polymers containing hydrophobic relatively long alkyl anchors. Compared to the pseudopeptidic polymers grafted with Phe, the comb-like pseudopeptidic polymers with relatively long fatty alkyl anchors displayed a high affinity to the liposomal membrane, resulting in a higher polymer coating density. Similar pH-triggered release could be achieved by the liposomes coated with much lower amount of comb-like PLP-NDA 18% compared to the liposomes coated with PP75, owing to the enhanced membrane binding activity of PLP-NDA 18%. The pH-responsive release profile of the liposomes coated with the comb-like polymer could be manipulated by

controlling key parameters, such as cholesterol proportion, polymer amphiphilicity and polymer coating density. The multifunctional liposomes displayed dilution-independent pH-triggered release and had no leakage at neutral pH. The mean hydrodynamic size of the multifunctional liposomes was increased upon acidification, which was due to aggregation of the network of liposomes bridged by the comb-like polymer that changed its conformation in response to pH. After liposomal surface coating, the pH-dependent endosomolytic activity of the comb-like polymer was well retained, as proved by hemolysis assay with the RBC membrane as a model of the endosomal membrane. The significantly enhanced cellular uptake of the virus-mimicking liposomes could be attributed to the improved membrane binding and the recognition by scavenger receptors. The improved intracellular delivery of DOX was further confirmed by confocal microcopy and flow cytometry using four different cancer cell lines including a multidrug resistant cell line. The significantly improved potency of the DOX-loaded, virus-mimicking liposomes coated with the comb-like polymer against these cancer cell lines compared to the DOX-loaded bare liposomes was observed as well. The potency of the DOX-loaded liposomes coated with the comb-like polymer against the multidrug resistant cell line was even higher than free DOX. All these characteristics of this novel multifunctional liposomes implies its promising application in the field of drug delivery.

Chapter 7

Conclusions and future work

7.1 Conclusions

Biomimetic nanoscale systems have been successfully developed in this project for efficient intracellular delivery. Throughout the research, a variety of novel pH-responsive, comb-like, pseudopeptidic polymers were synthesized by grafting PLP with hydrophobic relatively long alkyl side chains at different chain lengths and degrees of substitution. Their physicochemical properties, membrane disruptive activity, payload delivery capacity and cytotoxicity were systematically examined. Two types of novel virus-mimicking liposomal delivery systems were developed by surface modification with two different pseudopeptidic polymers, i.e. the comb-like polymers containing hydrophobic relatively long alkyl side chains or the polymers containing pendant hydrophobic amino acid, Phe. The key parameters affecting the content loading and pH-triggered release were extensively investigated, and their cellular uptake and subcellular localization were examined. The potency of the DOX-loaded, virus-mimicking delivery systems against a variety of cancer cell lines, including the multidrug resistant cell line, were evaluated and compared with the DOX-loaded, conventional liposomes and free DOX.

In brief, the major achievements of this project include three major aspects:

1) A novel, virus-mimicking liposomal drug delivery platform, which enables pH-triggered release, enhanced cellular uptake, efficient endosomal escape and improved cancer-killing activity, was successfully developed by surface modification of the conventional liposomes with pH-responsive, endosomolytic pseudopeptidic polymer such as PP75.

2) A library of novel, pH-responsive, comb-like pseudopeptidic polymers bearing hydrophobic relatively long alkyl chains as membrane anchors have been synthesized. The optimal membrane-anchoring polymer exhibited superior and rapid membrane destabilization activity at endosomal pH, but remained non-lytic at physiological pH. The mechanism of the comb-like polymer-mediated membrane destabilization was proved to be pore formation.

3) The promising application of the membrane-anchoring, comb-like pseudopeptidic polymers in drug delivery was successfully demonstrated. The optimal polymer PLP-NDA 18%

effectively delivered a wide size range of payloads (with M_w up to 2,000 kDa) into a variety of cell types (including stem cells and multidrug resistant cells) rapidly at mildly acidic pH. This non-covalent delivery method is simple, fast, effective, non-cytotoxic and pH-responsive. In addition, the optimal comb-like polymer PLP-NDA 18% was further employed to develop another novel, endosomolytic, virus-mimicking liposomal drug delivery platform through liposomal surface modification, which was employed to overcome the MDR via smart and efficient intracellular delivery of DOX.

7.1.1 Virus-mimicking liposomes coated with PP75 bearing hydrophobic amino acids

Novel virus-mimicking liposomes were developed by liposomal surface modification with pH-responsive endosomolytic pseudopeptidic polymer PP75 bearing pendant hydrophobic amino acid, Phe. In this biomimetic nanoscale system, the drug payload mimics the viral genome, the lipid bilayer mimics the viral envelope, and the novel pseudopeptide PP75 mimics the fusogenic peptide in the viral spikes. The key parameters affecting the pH-responsiveness of the multifunctional liposomes, including cholesterol proportion in the liposomal membrane, the amphiphilicity of the polymer, polymer coating density and coating time. By optimizing the liposomal preparation and surface modification protocols, the PP75-coated, virus-mimicking liposomes could efficiently release its payload at endosomal pH while exhibit no leakage at neutral pH. The pH-responsiveness of the smart liposomes was dilution-independent. The hydrodynamic size of the liposomes was controlled to be around 100 nm and no significant size increase was observed after surface modification with the pH-responsive, endosomolytic polymer. pH-Induced size increase was found to result from liposomal aggregation by the bridging effect. The surface-adsorbed polymer well retained its pH-responsive, membrane-disruption activity as confirmed by hemolysis assay. Enhanced cellular uptake was observed for the fluorescence-labelled liposomes, together with efficient endosomal escape and pH-sensitive content release into the cell cytoplasm. These properties enabled the significantly improved intracellular DOX delivery. The potency of the DOX-loaded, virus-mimicking liposomes against HeLa cells was similar to free DOX, while considerably higher than the DOX-loaded bare liposomes without polymer coating.

7.1.2 pH-Responsive pseudopeptidic polymers bearing hydrophobic relatively long alkyl side chains as membrane anchors

A series of pH-responsive, comb-like, membrane-anchoring pseudopeptidic polymers were synthesized by grafting hydrophobic relatively long alkyl side chains with different lengths

onto the PLP at different degrees of substitution. The physicochemical prosperities of these polymers, e.g. pH-dependent aggregation, conformational change, critical association concentration, and hydrodynamic size were systematically characterized. Conjugation of relatively long alkyl side chains could considerably increase the hydrophobicity of the polymer. The alkyl chains, which act as membrane anchors, could facilitate interaction of the comb-like polymers with the lipid membrane. PLP-NDA 18%, which is PLP conjugated with 18 mol% NDA side chains, displayed superior membrane-destabilization ability at endosomal pHs compared to its linear counterpart PLP and other derivatives. The optimal comb-like polymer PLP-NDA 18% can cause complete hemolysis at a concentration of 0.5 mg mL^{-1} at pH 5.5 with only 20 min of treatment while was almost non hemolytic at pH 7.4. The membrane destabilization acidity was dilution-independent over a wide concentration range (0.5 – 10 mg mL^{-1}). The mechanism of cell membrane disruption was pore formation rather than membrane lysis or fusion, as confirmed by hemolysis assay with osmoprotectants and the study of erythrocyte ghost formation.

7.1.3 Efficient intracellular delivery of a wide size range of payload into a wide range of cell types using the pH-responsive, comb-like pseudopeptidic polymer

The optimal, pH-responsive, comb-like polymer PLP-NDA 18% was demonstrated to efficiently release endocytosed materials into the cytoplasm followed by nuclear localization in various cancerous and non-cancerous cell lines treated at physiological pH. It displayed negligible cytotoxicity at physiological pH at the polymer concentration below 1 mg mL^{-1}. At acidic extracellular pH, the polymer-mediated, non-covalent delivery was significantly enhanced compared to the delivery at physiological pH. Varying the side chain length could control the intracellular delivery capacity. PLP-NDA 18% exhibited the highest delivery efficiency compare to other PLP derivatives bearing hydrophobic alkyl side chains. The delivery efficiency was also dependent on polymer concentration, treatment time and the presence of serum. The comb-like polymer was able to utilize the extracellular acidity to deliver a wide size range of payloads (up to 2000 kDa) into the cell interior. The efficient, pH-responsive delivery capacity was confirmed with a variety of cell types, including cancer and noncancerous cell lines, adherent or suspension cell lines, multidrug resistant cell line and stem cells. In contrast to the other commonly used delivery methods, this comb-like polymer-mediated, non-covalent delivery method is simple, non-toxic and widely applicable.

7.1.4 Virus-mimicking liposomes coated with pH-responsive, comb-like, membrane-anchoring pseudopeptides containing relatively long hydrophobic alkyl side chains

Another type of novel virus-mimicking liposomal drug delivery system was developed by coating conventional liposomes with the optimal comb-like, endosomolytic polymer PLP-NDA 18%. Compared to PP75, the comb-like pseudopeptidic polymers with hydrophobic relatively long fatty alkyl anchors displayed a high affinity to the liposomal membrane, leading to a higher polymer coating efficiency. The PLP-NDA 18%-coated liposomes showed higher pH-responsiveness than the PP75-coated liposomes. This multifunctional liposomal delivery system also showed the pH-responsive release profile and the release behavior could be manipulated by tuning key parameters, e.g. polymer side chain length, polymer concentration, pH, treatment time, the presence of serum. The pH-responsiveness of the PLP-NDA 18%-coated liposomes was dilution-independent. pH-Triggered, reversible particle size increase was also observed and it was found to be due to the liposomal aggregation by the bridging effect. The multifunctional liposomes were endosomolytic at endosomal pH, as confirmed by hemolysis assay. The surface coating with the comb-like polymer could significantly enhance the cellular uptake of the liposomes according to confocal microscopy and flow cytometry results. Significantly improved intracellular DOX delivery was observed in four different cancer cell lines including the multidrug resistant cell line. Potency of the DOX-loaded, PLP-NDA 18%-coated liposomes against these cell lines was considerably higher than the convectional liposomes without polymer coating.

7.2 Future work

To further optimize the pH-responsive biomimetic nanoscale systems and fully explore their potential for drug delivery applications, the following future work is recommended:

7.2.1 Investigation of the mechanism of polymer-mediated intracellular delivery at acidic extracellular pH

It has been demonstrated by confocal microscopy and flow cytometry that the PLP-NDA 18% could facilitate the enhanced intracellular delivery of a wide size range of payload at acidic extracellular pH compared to the physiological pH. However, the mechanism of the improved delivery mediated by the comb-like polymer was not well understood and is worth being further explored in the future. Polymer-mediated intracellular delivery has been reported to be due to direct membrane penetration (Wang et al., 2014) or endosomal escape (Varkouhi et al., 2011).

LDH assay could be applied to investigate whether the enhanced payload delivery mediated by the comb-like polymer was due to alteration of the integrity of the plasma membrane. Besides, endocytosis can be categorized into several types (Iversen et al., 2011). Different inhibitors could be used to block specific endocytosis pathway, e.g. sucrose for inhibition of clathrin-mediated endocytosis, cytochalasin D for inhibition of micropinocytosis and methyl-β-cyclodextrin (MβCD) for affecting the lipid raft and caveolae-mediated endocytosis (Sahay et al., 2010). Thus, future work could be done to block specific endocytosis pathways by using different types of inhibitors and explore which endocytic pathways would be involved.

7.2.2 Subcellular fate and biodegradability

According to the confocal microscopy results, both PP75 and PLP-NDA 18% could facilitate the release of endocytosed materials into the cytoplasm. However, the subcellular fate of these polymers needs to be further confirmed in the future. By fluorescently labelling the polymers, the membrane binding, internalization and endosomal escape could be visualized by confocal microscopy and quantified by flow cytometry. Bioarkers commonly used to identify intracellular organelles (e.g. EAA1 to identify early endosomes, ESCRTs to identify late endosomes and LAMP-1 to identify lysosomes) will be applied and the co-localization of the polymers with these biomarkers will provide the useful information about at which stage the polymer-mediated endosomal escape occurs (Martens et al., 2014). In addition, the biodegradability of the polymers could be evaluated by enzymatic degradation to ensure that the polymer could be excreted from the body after biodegradation instead of unfavorable accumulation (Mallakpour & Dinari, 2011). The information obtained from these studies will enable a better understanding of the polymer-membrane interaction and membrane disruption, which will be beneficial for further exploration of their potential application in drug delivery.

7.2.3 Further modification of polymer structure

7.2.3.1 Incorporation of targeting ligand

It has been recognized that through incorporation of targeting ligands, such as folic acid, transferrin, biotin, antibodies, the uptake of the polymer or polymer-coated liposomes by specific cells could be enhanced due to the improved binding to the corresponding receptors expressed on the specific cell surface (Etheridge et al., 2013; Hoffman, 2013; van der Meel et al., 2013). The selectivity of the cell internalization can be evaluated by flow cytometry analysis different types of cells treated with the fluorescently labelled polymers.

7.2.3.2 Conjugation with other membrane anchors

By conjugating relatively long alkyl side chains as membrane anchors on the PLP backbone, the membrane binding and disruption activity of the comb-like polymer increased significantly. Inspired by the natural existing membrane protein, future work can be done to conjugate other membrane anchors, e.g. cholesterol, phospholipid, glycosyl phosphatidyl inositol (GPI) (Khandelia et al., 2008) on the PLP backbone for development of new membrane-anchoring polymers. The effect of the degree of grafting, hydrophobic-hydrophilic balance and types of side chains on the polymer properties in aqueous solution, membrane disruption and cytotoxicity will be studied to lay the foundation to design of more efficient smart membrane-disruptive polymers.

7.2.4 Intracellular delivery of genetic therapeutic agents

Gene therapy may provide inhibitory activity in specific cells, which makes it attractive for cancer treatment. However, delivery of genetic therapeutic agents remains a major challenge due to their poor in vivo stability, low cellular uptake and susceptible lysosomal degradation. Therefore, the biomimetic nanoscale delivery systems arising from this project will be further optimized to efficiently deliver and release genes into the cell cytoplasm and also increase the stability and blood circulation time.

7.2.4.1 Genetic payload delivery mediated by the pH-responsive, endosomolytic polymer

PP75 has been reported to successfully deliver siRNA that was conjugated to the polymer through disulfide linkage, into the cell cytoplasm and inhibit tumor growth for malignant glioma treatment in vitro and in vivo (Khormaee et al., 2013). Further work can be carried out on cytoplasmic delivery of various genetic materials using the comb-like polymer PLP-NDA 18%. The conjugation chemistry, the endosomal escape ability, payload release profile and targeting effect can be investigated to optimize the polymeric drug delivery platform.

7.2.4.2 Genetic payload delivery mediated by the virus-mimicking liposomes

Liposomes are one of the most widely applied non-viral vectors for gene delivery (Wirth et al., 2013). Liposomes prepared with cationic lipids, such as 1,2-di-o-octadecenyl-3-trimethylammonium propane (DOTMA), DOTAP, or 3β-[*N*-(*N*',*N*'-dimethylaminoethane)-carbamoyl] cholesterol (DC-Chol), displayed higher transfection efficiency compared to the liposomes prepared with anionic or neutral lipids (Zhang et al., 2004). However, the overall

positive charge will lead to non-specific binding with serum proteins followed by fast elimination, unfavorable biodistribution and high cytotoxicity. Through surface modification with the anionic polymer arising from this project, the charge of the cationic liposomes could be changed to neutral or even negative. In addition, the membrane disruptive activity of the polymer could provide pH-triggered release and enable endosomal escape, thus further improving the intracellular gene delivery efficiency.

7.2.5 Co-delivery mediated by the virus-mimicking liposomes

Combination therapy is an attractive strategy for anticancer treatment, in particular treatment of drug-resistant cancer, owing to the synergistic effect of multiple drug payloads (Hu & Zhang, 2012). In a formulation for co-delivery of two chemotherapeutic drugs, Pgp inhibitor can block the efflux pump and thus increase the intracellular concentration of the co-delivered drugs (Patel et al., 2011). In addition, single-drug therapy usually acts through a particular pathway. When combining two different drug payloads, the treatment could act on multiple signaling pathways, thus enhancing anticancer activity at a lower dose (Parhi et al., 2012). By loading different chemotherapeutic agents inside the endosomolytic, virus-mimicking liposomes, the therapeutic efficacy of the nano delivery systems could be further improved. This delivery platform can be further extended to co-delivery of chemotherapeutic drugs and genetic materials for chemo-gene combination therapy of cancer or other diseases.

7.3 Closing remarks

Several types of novel biomimetic nanoscale systems were successfully developed in this project for pH-triggered, cytoplasmic drug delivery. The novel, pH-responsive, PP75-coated virus-mimicking liposomes arising from this project will open a door to more promising application of PP75 for drug delivery. The novel, bio-inspired, comb-like, membrane-anchoring pseudopeptidic polymers containing hydrophobic relatively long fatty alkyl side chains as membrane anchors represent a new class of promising candidates for intracellular delivery. The optimal comb-like polymer could facilitate significantly enhanced intracellular delivery of a wide size range of payloads into a wide variety of cell lines by simple co-incubation at acidic extracellular pHs. The new method is simple, fast, non-cytotoxic and pH-responsive. It can further be applied to develop another type of novel virus-mimicking liposomal delivery systems for treatment of various diseases including the drug-resistant cancer. The major achievements arising from this project and the recommended future work are summarized in Figure 7-1.

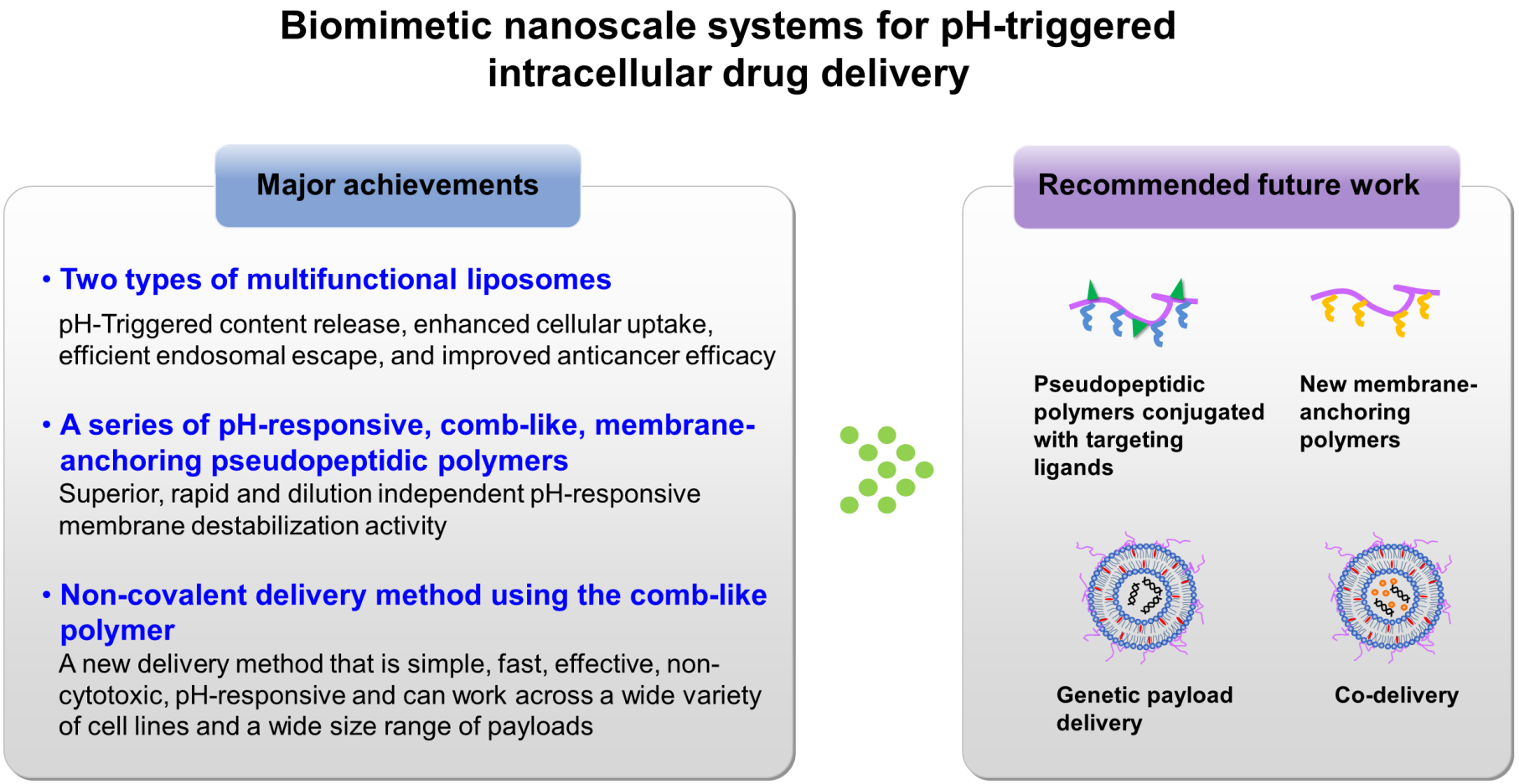

Figure 7-1. Summary of the major achievements arising from this project and recommended future work.

References

Abbasi, M., Lavasanifar, A. & Uludag, H. (2013) Recent attempts at RNAi-mediated P-glycoprotein downregulation for reversal of multidrug resistance in cancer. *Medicinal Research Reviews*. 33 (1), 33–53.

Abraham, S.A., Waterhouse, D.N., Mayer, L.D., Cullis, P.R., et al. (2005) The liposomal formulation of doxorubicin. *Methods in enzymology*. 391, 71-97.

Aguiar, J., Carpena, P., Molina-Bolívar, J.A. & Carnero Ruiz, C. (2003) On the determination of the critical micelle concentration by the pyrene 1:3 ratio method. *Journal of Colloid and Interface Science*. 258 (1), 116–122.

Akhtar, S. (2010) Cationic nanosystems for the delivery of small interfering ribonucleic acid therapeutics: a focus on toxicogenomics. *Expert Opinion on Drug Metabolism & Toxicology*. 6 (11), 1347–1362.

Al-Jamal, W. & Kostarelos, K. (2011) Liposomes: from a clinically established drug delivery system to a nanoparticle platform for theranostic nanomedicine. *Accounts of Chemical Research*. 44 (10), 1094–1104.

Allen, T.M. & Cullis, P.R. (2004) Drug delivery systems: entering the mainstream. *Science*. 303 (5665), 1818–1822.

Allen, T.M. & Cullis, P.R. (2013) Liposomal drug delivery systems: from concept to clinical applications. *Advanced Drug Delivery Reviews*. 65 (1), 36–48.

Aloia, Roland C., J.M.B. (1985) The relationship of membrane fluidity to degenerative mscular diseases. In: *Membrane fluidity in biology: disease processes.* London, Academic Press. 162–244.

Amin, M.L. (2013) P-glycoprotein inhibition for optimal drug delivery. *Drug Target Insights*. 7, 27–34.

Andrade, B., Song, Z., Li, J., Zimmerman, S.C., et al. (2015) New frontiers for encapsulation in the chemical industry. *ACS Applied Materials & Interfaces*. 7 (12), 6359–6368.

Lagunavicius, A. and Zaliauskiene, L., Fermentas Uab, 2015. Delivery agent. *U.S. Patent* 8,951,957.

Bader, H., Ringsdorf, H. & Schmidt, B. (1984) Watersoluble polymers in medicine. *Angewandte Makromolekulare Chemie*. 123 (1), 457–485.

Bae, Y., Fukushima, S., Harada, A. & Kataoka, K. (2003) Design of environment-sensitive supramolecular assemblies for intracellular drug delivery: polymeric micelles that are responsive to intracellular pH change. *Angewandte Chemie*. 115 (38), 4788–4791.

Bae, Y., Nishiyama, N., Fukushima, S., Koyama, H., et al. (2005) Preparation and biological characterization of polymeric micelle drug carriers with intracellular pH-triggered drug release property: tumor permeability, controlled subcellular drug distribution, and enhanced in vivo antitumor efficacy. *Bioconjugate Chemistry.* 16 (1), 122–130.

Baguley, B.C. (2010) Multiple drug resistance mechanisms in cancer. *Molecular Biotechnology*. 46 (3), 308–316.

Bangham, A.D., Standish, M.M. & Watkins, J.C. (1965) Diffusion of univalent ions across the lamellae of swollen phospholipids. *Journal of Molecular Biology*. 13 (1), 238–252.

Barenholz, Y. (2012) Doxil® – the first FDA approved nano-drug: lessons learned. *Journal of Controlled Release*. 160 (2), 117–134.

Barenholz, Y. (2001) Liposome application: problems and prospects. *Current Opinion in Colloid & Interface Science*. 6 (1), 66–77.

Barreto, J.A., O'Malley, W., Kubeil, M., Graham, B., et al. (2011) Nanomaterials: applications in cancer imaging and therapy. *Advanced Materials*. 23 (12), 18-40.

Belting, M., Sandgren, S. & Wittrup, A. (2005) Nuclear delivery of macromolecules: barriers and carriers. *Advanced Drug Delivery Reviews*. 57 (4), 505–527.

Bertrand, N., Fleischer, J.G., Wasan, K.M. & Leroux, J.C. (2009) Pharmacokinetics and biodistribution of *N*-isopropylacrylamide copolymers for the design of pH-sensitive liposomes. *Biomaterials*. 30 (13), 2598–2605.

Binder, W.H. (2008) Polymer-induced transient pores in lipid membranes. *Angewandte Chemie International Edition*. 47 (17), 3092–3095.

Binder, W.H., Barragan, V. & Menger, F.M. (2003) Domains and rafts in lipid membranes. *Angewandte Chemie International Edition*. 42 (47), 5802–5827.

Bolhassani, A. (2011) Potential efficacy of cell-penetrating peptides for nucleic acid and drug delivery in cancer. *Biochimica et Biophysica Acta*. 1816 (2), 232–246.

Brandl, M. (2001) Liposomes as drug carriers: a technological approach. *Biotechnology Annual Review*. 7, 59–85.

Briuglia, M.L., Rotella, C., McFarlane, A. & Lamprou, D. A. (2015) Influence of cholesterol on liposome stability and on in vitro drug release. *Drug Delivery and Translational Research*. 5 (3), 231–242.

Bulmus, V., Ding, Z., Long, C.J., Stayton, P.S., et al. Site-specific polymer-streptavidin bioconjugate for pH-controlled binding and triggered release of biotin. *Bioconjugate Chemistry*. 11 (1), 78–83.

C˘eh, B., Winterhalter, M., Frederik, P.M., Vallner, J.J., et al. (1997) Stealth® liposomes: from theory to product. *Advanced Drug Delivery Reviews*. 24 (2), 165–177.

Cabral, H. & Kataoka, K. (2014) Progress of drug-loaded polymeric micelles into clinical studies. *Journal of Controlled Release*. 190, 465–476.

Canton, I. & Battaglia, G. (2012) Endocytosis at the nanoscale. *Chemical Society Reviews*. 41 (7), 2718–2739.

Castile, J.D. & Taylor, K.M.. (1999) Factors affecting the size distribution of liposomes produced by freeze–thaw extrusion. *International Journal of Pharmaceutics*. 188 (1), 87–95.

Cheung, C.Y., Murthy, N., Stayton, P.S. and Hoffman, A.S. (2001). A pH-sensitive polymer that enhances cationic lipid-mediated gene transfer. *Bioconjugate chemistry*. 12 (6), 906-910.

Chen, R. (2013) Polymers in drug delivery: concepts, developments and potential. In: *Drug Delivery Systems: Advanced Technologies Potentially Applicable in Personalised Treatment*. Dordrecht, Springer Netherlands. 1–34.

Chen, R., Eccleston, M.E., Yue, Z. & Slater, N.K.H. (2009) Synthesis and pH-responsive properties of pseudopeptides containing hydrophobic amino acid grafts. *Journal of Materials Chemistry*. 19 (24), 4217–4224.

Chen, R., Folarin, N., Ho, V.H.B., McNally, D., et al. (2010) Affinity recovery of lentivirus by diaminopelargonic acid mediated desthiobiotin labelling. *Journal of Chromatography. B,*

Analytical Technologies In the Biomedical and Life Sciences. 878 (22), 1939–1945.

Chen, R., Khormaee, S., Eccleston, M.E. & Slater, N.K.H. (2009a) Effect of L-leucine graft content on aqueous solution behavior and membrane-lytic activity of a pH-responsive pseudopeptide. *Biomacromolecules*. 10 (9), 2601–2608.

Chen, R., Khormaee, S., Eccleston, M.E. & Slater, N.K.H. (2009b) The role of hydrophobic amino acid grafts in the enhancement of membrane disruptive activity of pH-responsive pseudopeptides. *Biomaterials*. 30 (10), 1954–1961.

Chen, R., Yue, Z., Eccleston, M.E. & Slater, N.K.H. (2008) Aqueous solution behaviour and membrane disruptive activity of pH-responsive PEGylated pseudopeptides and their intracellular distribution. *Biomaterials*. 29 (32), 4333–4340.

Chen, R., Yue, Z., Eccleston, M.E., Williams, S., et al. (2005) Modulation of cell membrane disruption by pH-responsive pseudopeptides through grafting with hydrophilic side chains. *Journal of Controlled Release*. 108 (1), 63–72.

Chen, S. & Chen, R. (2016) A virus-mimicking, endosomolytic liposomal system for efficient, pH-triggered intracellular drug delivery. *ACS Applied Materials & Interfaces*. 8 (34), 22457–22467.

Chen, S., Wang, S., Kopytynski, M., Bachelet, M. and Chen, R., 2017. Membrane-Anchoring, Comb-Like Pseudopeptides for Efficient, pH-Mediated Membrane Destabilization and Intracellular Delivery. ACS Applied Materials & Interfaces. 9 (9), 8021–8029.

Chen, T., Mcintosh, D., He, Y., Kim, J., et al. (2004) Alkylated derivatives of poly (ethylacrylic acid) can be inserted into preformed liposomes and trigger pH-dependent intracellular delivery of liposomal contents. *Molecular Membrane Biology*. 21 (6), 385–393.

Cheng, Y., Yumul, R.C. & Pun, S.H. (2016) Virus-inspired polymer for efficient in vitro and in vivo gene delivery. *Angewandte Chemie*. 128 (39), 12192–12196.

Chiang, Y. T. & Lo, C. L. (2014) pH-responsive polymer-liposomes for intracellular drug delivery and tumor extracellular matrix switched-on targeted cancer therapy. *Biomaterials*. 35 (20), 5414–5424.

Chieng, Y.Y. & Chen, S.B. (2011) Complexation of cationic polyelectrolyte with anionic phospholipid vesicles: concentration, molecular weight and salt effects. *Journal of Colloid and*

Interface Science. 354 (1), 226–233.

Chieng, Y.Y. & Chen, S.B. (2010) Interaction between poly (acrylic acid) and phospholipid vesicles: effect of pH, concentration, and molecular weight. *The Journal of Physical Chemistry B*. 114 (14), 4828–4835.

Cho, W. & Stahelin, R. V. (2005) Membrane-protein interactions in cell signaling and membrane trafficking. *Annual Review of Biophysics and Biomolecular Structure*. 34 (1), 119–151.

Chou, L.Y.T., Ming, K. & Chan, W.C.W. (2011) Strategies for the intracellular delivery of nanoparticles. *Chemical Society Reviews*. 40 (1), 233–245.

Coelho, J.F., Ferreira, P.C., Alves, P., Cordeiro, R., et al. (2010) Drug delivery systems: advanced technologies potentially applicable in personalized treatments. *The EPMA journal*. 1 (1), 164–209.

Conner, S.D. & Schmid, S.L. (2003) Regulated portals of entry into the cell. *Nature*. 422 (6927), 37–44.

Copolovici, D.M., Langel, K., Eriste, E. & Langel, Ü. (2014) Cell-penetrating peptides: design, synthesis, and applications. *ACS nano*. 8 (3), 1972–1994.

Cox, D.L.N. and M.M. (2008) Biological Membranes and Transport. In: *Lehninger Principles of Biochemistry*. 5th editio. W.H.Freeman and Company, New York. 379–380

Creixell, M. & Peppas, N.A. (2012) Co-delivery of siRNA and therapeutic agents using nanocarriers to overcome cancer resistance. *Nano Today*. 7 (4), 367–379.

Cui, C., Xue, Y. N., Wu, M., Zhang, Y., et al. (2013) Cellular uptake, intracellular trafficking, and antitumor efficacy of doxorubicin-loaded reduction-sensitive micelles. *Biomaterials*. 34 (15), 3858–3869.

Dai, J., Nagai, T., Wang, X., Zhang, T., et al. (2004) pH-sensitive nanoparticles for improving the oral bioavailability of cyclosporine A. *International Journal of Pharmaceutics*. 280 (1), 229–240.

Das, S. & Chaudhury, A. (2011) Recent advances in lipid nanoparticle formulations with solid matrix for oral drug delivery. *AAPS PharmSciTech*. 12 (1), 62–76.

David, S., Pitard, B., Benoît, J. P. & Passirani, C. (2010) Non-viral nanosystems for systemic siRNA delivery. *Pharmacological Research*. 62 (2), 100–114.

Deamer, D.W. (1978) Preparation and properties of ether-injection liposomes. *Annals of the New York Academy of Sciences*. 308 (1), 250–258.

Decker, T. & Lohmann-Matthes, M. L. (1988) A quick and simple method for the quantitation of lactate dehydrogenase release in measurements of cellular cytotoxicity and tumor necrosis factor (TNF) activity. *Journal of Immunological Methods*. 115 (1), 61–69.

Discher, D.E. & Eisenberg, A. (2002) Polymer vesicles. *Science*. 297 (5583), 967–973.

Drummond, D.C., Zignani, M. & Leroux, J.C. (2000) Current status of pH-sensitive liposomes in drug delivery. *Progress in Lipid Research*. 39 (5), 409–460.

Duncan, R. (2006) Polymer conjugates as anticancer nanomedicines. *Nature Reviews Cancer*. 6 (9), 688–701.

Düzgüneş, N., Wilschut, J., Hong, K., Fraley, R., et al. (1983) Physicochemical characterization of large unilamellar phospholipid vesicles prepared by reverse-phase evaporation. *Biochimica et Biophysica Acta (BBA) - Biomembranes*. 732 (1), 289–299.

Eccleston, M.E., Kuiper, M., Gilchrist, F.M. & Slater, N.K.H. (2000) pH-responsive pseudopeptides for cell membrane disruption. *Journal of Controlled Release*. 69 (2), 297–307.

Eccleston, M.E., Slater, N.K.H. & Tighe, B.J. (1999) Synthetic routes to responsive polymers: co-polycondensation of tri-functional amino acids with diacylchlorides. *Reactive and Functional Polymers*. 42 (2), 147–161.

Eccleston, M.E., Williams, S.L., Yue, Z., Chen, R., et al. (2005) Design and in-vitro testing of effective poly(L-lysine iso-phthalamide) based drug targeting systems for solid tumours. *Food and Bioproducts Processing*. 83 (2), 141–146.

Economou, N.J., Zentner, I.J., Lazo, E., Jakoncic, J., et al. (2013) Structure of the complex between teicoplanin and a bacterial cell-wall peptide: use of a carrier-protein approach. Acta Crystallographica Section D: Biological Crystallography. 69, 520–533.

El-Sayed, M.E., Hoffman, A.S. & Stayton, P.S. (2015) Smart polymeric carriers for enhanced intracellular delivery of therapeutic macromolecules. *Expert Opinion on Biological Therapy*.

5 (1), 23–32.

Eldar-Boock, A., Polyak, D., Scomparin, A. & Satchi-Fainaro, R. (2013) Nano-sized polymers and liposomes designed to deliver combination therapy for cancer. *Current Opinion in Biotechnology*. 24 (4), 682–689.

Epand, R.M. (2003) Fusion peptides and the mechanism of viral fusion. *Biochimica et Biophysica Acta (BBA) - Biomembranes*. 1614 (1), 116–121.

Etheridge, M.L., Campbell, S.A., Erdman, A.G., Haynes, C.L., et al. (2013) The big picture on nanomedicine: the state of investigational and approved nanomedicine products. *Nanomedicine: Nanotechnology, Biology and Medicine*. 9 (1), 1–14.

Fang, J., Nakamura, H. & Maeda, H. (2011) The EPR effect: unique features of tumor blood vessels for drug delivery, factors involved, and limitations and augmentation of the effect. *Advanced Drug Delivery Reviews*. 63 (3), 136–151.

Farkhani, S.M., Valizadeh, A., Karami, H., Mohammadi, S., et al. (2014) Cell penetrating peptides: efficient vectors for delivery of nanoparticles, nanocarriers, therapeutic and diagnostic molecules. *Peptides*. 57, 78–94.

Farokhzad, O.C. & Langer, R. (2009) Impact of nanotechnology on drug delivery. *ACS nano*. 3 (1), 16–20.

Fattal, E., Couvreur, P. & Dubernet, C. (2004) 'Smart' delivery of antisense oligonucleotides by anionic pH-sensitive liposomes. *Advanced Drug Delivery Reviews*. 56 (7), 931–946.

Felber, A.E., Dufresne, M. H. & Leroux, J. C. (2012) pH-sensitive vesicles, polymeric micelles, and nanospheres prepared with polycarboxylates. *Advanced Drug Delivery Reviews*. 64 (11), 979–992.

Fenske, D.B. & Cullis, P.R. (2008) Liposomal nanomedicines. *Expert Opinion on Drug Delivery*. 5 (1), 25–44.

Ferreira, D.D.S., Lopes, S.C. de A., Franco, M.S. & Oliveira, M.C. (2013) pH-sensitive liposomes for drug delivery in cancer treatment. *Therapeutic Delivery*. 4 (9), 1099–1123.

Fleige, E., Quadir, M.A. & Haag, R. (2012) Stimuli-responsive polymeric nanocarriers for the controlled transport of active compounds: concepts and applications. *Advanced Drug Delivery*

Reviews. 64 (9), 866–884.

Foster, S., Duvall, C.L., Crownover, E.F., Hoffman, A.S., et al. (2010) Intracellular delivery of a protein antigen with an endosomal-releasing polymer enhances CD8 T-cell production and prophylactic vaccine efficacy. *Bioconjugate Chemistry*. 21 (12), 2205–2212.

Frankel, A.D. & Pabo, C.O. (1988) Cellular uptake of the tat protein from human immunodeficiency virus. *Cell*. 55 (6), 1189–1193.

Frey, S.L., Zhang, D., Carignano, M.A., Szleifer, I., et al. (2007) Effects of block copolymer's architecture on its association with lipid membranes: experiments and simulations. *The Journal of Chemical Physics*. 127, 114904.

Fritze, A., Hens, F., Kimpfler, A., Schubert, R., et al. (2006) Remote loading of doxorubicin into liposomes driven by a transmembrane phosphate gradient. *Biochimica et Biophysica Acta (BBA) - Biomembranes*. 1758 (10), 1633–1640.

Fu, J., Yu, C., Li, L. & Yao, S.Q. (2015) Intracellular delivery of functional proteins and native drugs by cell-penetrating poly(disulfide)s. *Journal of the American Chemical Society*. 137 (37), 12153–12160.

Fujiwara, M., Baldeschwieler, J.D. & Grubbs, R.H. (1996) Receptor-mediated endocytosis of poly(acrylic acid)-conjugated liposomes by macrophages. *Biochimica et Biophysica Acta - Biomembranes*. 1278 (1), 59–67.

Gaitanis, A. & Staal, S. (2010) Liposomal doxorubicin and nab-paclitaxel: nanoparticle cancer chemotherapy in current clinical use. In: *Cancer Nanotechnology: Methods and Protocols*. New York, Humana Press. 385–392.

Ganta, S., Devalapally, H., Shahiwala, A. & Amiji, M. (2008) A review of stimuli-responsive nanocarriers for drug and gene delivery. *Journal of Controlled Release*. 126 (3), 187–204.

Gerweck, L.E. & Seetharaman, K. (1996) Cellular pH gradient in tumor versus normal tissue: potential exploitation for the treatment of cancer. *Cancer Research*. 56 (6), 1194–1198.

Goodman, T.T., Ng, C.P. & Pun, S.H. (2008) 3-D Tissue Culture Systems for the Evaluation and Optimization of Nanoparticle-Based Drug Carriers. Bioconjugate Chemistry. 19 (10), 1951–1959.

Goodman, T.T., Olive, P.L. & Pun, S.H. (2007) Increased nanoparticle penetration in collagenase-treated multicellular spheroids. International journal of nanomedicine. 2 (2), 265–274.

Goren, D., Horowitz, A.T., Tzemach, D., Tarshish, M., et al. (2000) Nuclear delivery of doxorubicin via folate-targeted liposomes with bypass of multidrug-resistance efflux pump. *Clinical Cancer Research*. 6 (5), 1949–1957.

Großauer, J., Kosol, S., Schrank, E. & Zangger, K. (2010) The peptide hormone ghrelin binds to membrane-mimetics via its octanoyl chain and an adjacent phenylalanine. *Bioorganic & Medicinal Chemistry*. 18 (15), 5483–5488.

Guan, H., McGuire, M.J., Li, S. & Brown, K.C. (2008) Peptide-targeted polyglutamic acid doxorubicin conjugates for the treatment of α_v β_6 -positive cancers. *Bioconjugate Chemistry*. 19 (9), 1813–1821.

Guo, F., Yu, M., Wang, J., Tan, F., et al. (2015) Smart IR780 theranostic nanocarrier for tumor-specific therapy: hyperthermia-mediated bubble-generating and folate-targeted liposomes. *ACS Applied Materials & Interfaces*. 7 (37), 20556–20567.

Guo, W., Gosselin, M.A. & Lee, R.J. (2002) Characterization of a novel diolein-based LPDII vector for gene delivery. *Journal of Controlled Release*. 83 (1), 121–132.

Gutiérrez de Rubalcava, C., Rodriguez, J.L., Duro, R., Alvarez-Lorenzo, C., et al. (2000) Interactions between liposomes and hydroxypropylmethylcellulose. *International Journal of Pharmaceutics*. 203 (1–2), 99–108.

Hamilton, R.L., Goerke, J., Guo, L.S., Williams, M.C., et al. (1980) Unilamellar liposomes made with the French pressure cell: a simple preparative and semiquantitative technique. *Journal of lipid research*. 21 (8), 981–992.

Han, X., Bushweller, J.H., Cafiso, D.S. & Tamm, L.K. (2001) Membrane structure and fusion-triggering conformational change of the fusion domain from influenza hemagglutinin. *Nature Structural Biology*. 8 (8), 715–720.

Hao, W., Han, X., Shang, Y., Xu, S., et al. (2015) Insertion of pH-sensitive bola-type copolymer into liposome as a 'stability anchor' for control of drug release. *Colloids and Surfaces B: Biointerfaces*. 136, 809–816.

Harde, H., Das, M. & Jain, S. (2011) Solid lipid nanoparticles: an oral bioavailability enhancer vehicle. *Expert Opinion on Drug Delivery*. 8 (11), 1407–1424.

Harker, W.G., MacKintosh, F.R. & Sikic, B.I. (1983) Development and characterization of a human sarcoma cell line, MES-SA, sensitive to multiple drugs. *Cancer Research*. 43 (10), 4943–4950.

Heedeok H., Sangho P., Ricardo H. F. J., Dennis R., and, et al. (2007) Role of aromatic side chains in the folding and thermodynamic stability of integral membrane proteins. *Journal of the American Chemical Society.*129 (26), 8320–8327.

Henry, S.M., El-Sayed, M.E.H., Pirie, C.M., Hoffman, A.S., et al. (2006) pH-responsive poly(styrene-alt-maleic anhydride) alkylamide copolymers for intracellular drug delivery. *Biomacromolecules*. 7 (8), 2407–2414.

Ho, V.H.B., Slater, N.K.H. & Chen, R. (2011) pH-responsive endosomolytic pseudopeptides for drug delivery to multicellular spheroids tumour models. *Biomaterials*. 32 (11), 2953–2958.

Hoffman, A.S. (2013) Stimuli-responsive polymers: biomedical applications and challenges for clinical translation. *Advanced Drug Delivery Reviews*. 65 (1), 10–16.

Hornung, V., Bauernfeind, F., Halle, A., Samstad, E.O., et al. (2008) Silica crystals and aluminum salts activate the NALP3 inflammasome through phagosomal destabilization. *Nature Immunology*. 9 (8), 847–856.

Hou, K.K., Pan, H., Schlesinger, P.H. & Wickline, S.A. (2015) A role for peptides in overcoming endosomal entrapment in siRNA delivery: a focus on melittin. *Biotechnology Advances*. 33 (6), 931–940.

Hu, C. M.J. & Zhang, L. (2012) Nanoparticle-based combination therapy toward overcoming drug resistance in cancer. *Biochemical Pharmacology*. 83 (8), 1104–1111.

Hubbell, J.A. & Chilkoti, A. (2012) Nanomaterials for drug delivery. *Science*. 337 (6092), 303–305.

Hung, W. C., Lee, M. T., Chen, F. Y. & Huang, H.W. (2007) The condensing effect of cholesterol in lipid bilayers. *Biophysical Journal*. 92 (11), 3960–3967.

Hyvönen, Z., Hämäläinen, V., Ruponen, M., Lucas, B., et al. (2012) Elucidating the pre- and

post-nuclear intracellular processing of 1,4-dihydropyridine based gene delivery carriers. *Journal of Controlled Release*. 162 (1), 167–175.

Immordino, M.L., Dosio, F. & Cattel, L. (2006) Stealth liposomes: review of the basic science, rationale, and clinical applications, existing and potential. *International Journal of Nanomedicine*. 1 (3), 297–315.

Inui, O., Teramura, Y. & Iwata, H. (2010) Retention dynamics of amphiphilic polymers PEG-lipids and PVA-alkyl on the cell surface. *ACS Applied Materials & Interfaces*. 2 (5), 1514–1520.

Iqbal, M.A., Md, S., Sahni, J.K., Baboota, S., et al. (2012) Nanostructured lipid carriers system: recent advances in drug delivery. *Journal of Drug Targeting*. 20 (10), 813–830.

Ito, Y., Ochiai, Y., Park, Y. S., and Imanishi, Y. (1997) pH-sensitive gating by conformational change of a polypeptide brush grafted onto a porous polymer membrane. *Journal of the American Chemical Society*. 119 (7), 1619–1623.

Iversen, T. G., Skotland, T. & Sandvig, K. (2011) Endocytosis and intracellular transport of nanoparticles: present knowledge and need for future studies. *Nano Today*. 6 (2), 176–185.

Jahn, R. & Südhof, T.C. (2003) Membrane fusion and exocytosis. *Annual Review of Biochemistry*. 68, 863–911.

Jeong, B. & Gutowska, A. (2002) Lessons from nature: stimuli-responsive polymers and their biomedical applications. *Trends in Biotechnology*. 20 (7), 305–311.

Jesorka, A. & Orwar, O. (2008) Liposomes: technologies and analytical applications. *Annual Review of Analytical Chemistry*. 1, 801–832.

Jiskoot, W., Teerlink, T., Beuvery, E.C. & Crommelin, D.J.A. (1986) Preparation of liposomes via detergent removal from mixed micelles by dilution. *Pharmaceutisch Weekblad Scientific Edition*. 8 (5), 259–265.

Joglekar, M. & Trewyn, B.G. (2013) Polymer-based stimuli-responsive nanosystems for biomedical applications. *Biotechnology Journal*. 8 (8), 931–945.

Jølck, R.I., Feldborg, L.N., Andersen, S., Moghimi, S.M., et al. (2011) Engineering liposomes and nanoparticles for biological targeting. *Advances in Biochemical*

Engineering/Biotechnology. 125, 251–280.

Jones, R., Cheung, C., Black, F., ZIA, J., et al. (2003) Poly (2-alkylacrylic acid) polymers deliver molecules to the cytosol by pH-sensitive disruption of endosomal vesicles. *Biochemical Journal.* 372, 65–75.

Joseph. R. Robinson (1978) *Sustained and controlled release drug delivery systems*. In *Modern Pharmaceutics*, Fourth Edition. CRC Press. 747–755.

Kaiden, T., Yuba, E., Harada, A., Sakanishi, Y., et al. (2011) Dual signal-responsive liposomes for temperature-controlled cytoplasmic delivery. *Bioconjugate Chemistry*. 22 (10), 1909–1915.

Kale, A.A. & Torchilin, V.P. (2010) Environment-responsive multifunctional liposomes. In: *Liposomes: Methods and Protocols, Volume 1: Pharmaceutical Nanocarriers.* New York, Humana Press. 213–242.

Kaliberov, S.A. & Buchsbaum, D.J. (2012) Cancer treatment with gene therapy and radiation therapy. *Advances in Cancer Research*. 115, 221–263.

Kamaly, N., Xiao, Z., Valencia, P.M., Radovic-Moreno, A.F., et al. (2012) Targeted polymeric therapeutic nanoparticles: design, development and clinical translation. *Chemical Society Reviews*. 41 (7), 2971–3010.

Kang, H., Kim, J. D., Han, S. H. & Chang, I. S. (2002) Self-aggregates of poly(2-hydroxyethyl aspartamide) copolymers loaded with methotrexate by physical and chemical entrapments. *Journal of Controlled Release*. 81 (1–2), 135–144.

Kang, H.S., Yang, S.R., Kim, J. D., Han, S. H., et al. (2001) Effects of grafted alkyl groups on aggregation behavior of amphiphilic poly(aspartic acid). *Langmuir*. 17 (24), 7501–7506.

Karanth, H. & Murthy, R.S.R. (2007) pH-sensitive liposomes – principle and application in cancer therapy. *Journal of Pharmacy and Pharmacology*. 59 (4), 469–483.

Kataoka, K., Harada, A. & Nagasaki, Y. (2001) Block copolymer micelles for drug delivery: design, characterization and biological significance. *Advanced Drug Delivery Reviews*. 47 (1), 113–131.

Kaufmann, S.H.E. (2008) Immunology's foundation: the 100-year anniversary of the Nobel Prize to Paul Ehrlich and Elie Metchnikoff. *Nature Immunology*. 9 (7), 705–712.

Kazunori, K., Glenn S., K., Masayuki, Y., Teruo, O., et al. (1993) Block copolymer micelles as vehicles for drug delivery. *Journal of Controlled Release*. 24 (1), 119–132.

Kedar, U., Phutane, P., Shidhaye, S. & Kadam, V. (2010) Advances in polymeric micelles for drug delivery and tumor targeting. *Nanomedicine: Nanotechnology, Biology and Medicine*. 6 (6), 714–729.

Khalil, I.A., Hayashi, Y., Mizuno, R. & Harashima, H. (2011) Octaarginine- and pH sensitive fusogenic peptide-modified nanoparticles for liver gene delivery. *Journal of Controlled Release*. 156 (3), 374–380.

Khandare, J. & Minko, T. (2006) Polymer–drug conjugates: Progress in polymeric prodrugs. *Progress in Polymer Science*. 31 (4), 359–397.

Khandelia, H., Ipsen, J.H. & Mouritsen, O.G. (2008) The impact of peptides on lipid membranes. *Biochimica et Biophysica Acta (BBA) - Biomembranes*. 1778 (7), 1528–1536.

Khormaee, S., Choi, Y., Shen, M.J., Xu, B., et al. (2013) Endosomolytic anionic polymer for the cytoplasmic delivery of siRNAs in localized in vivo applications. *Advanced Functional Materials*. 23 (5), 565–574.

Kim, D., Lee, E.S., Oh, K.T., Gao, Z.G., et al. (2008) Doxorubicin-loaded polymeric micelle overcomes multidrug resistance of cancer by double-targeting folate receptor and early endosomal pH. *Small*. 4 (11), 2043–2050.

Kim, S., Kim, J. H., Jeon, O., Kwon, I.C., et al. (2009) Engineered polymers for advanced drug delivery. *European Journal of Pharmaceutics and Biopharmaceutics*. 71 (3), 420–430.

Kim, W.J., Chang, C. W., Lee, M. & Kim, S.W. (2007) Efficient siRNA delivery using water soluble lipopolymer for anti-angiogenic gene therapy. *Journal of Controlled Release*. 118 (3), 357–363.

Kirby, C. & Gregoriadis, G. (1984) Dehydration-Rehydration Vesicles: A Simple Method for High Yield Drug Entrapment in Liposomes. *Bio/Technology*. 2 (11), 979–984.

Kono, K. (2001) Thermosensitive polymer-modified liposomes. *Advanced Drug Delivery Reviews*. 53 (3), 307–319.

Kono, K., Henmi, A., Yamashita, H., Hayashi, H., et al. (1999) Improvement of temperature-

sensitivity of poly(*N*-isopropylacrylamide)-modified liposomes. *Journal of Controlled Release*. 59 (1), 63–75.

Kono, K., Igawa, T. & Takagishi, T. (1997) Cytoplasmic delivery of calcein mediated by liposomes modified with a pH-sensitive poly(ethylene glycol) derivative. *Biochimica et Biophysica Acta (BBA) - Biomembranes*. 1325 (2), 143–154.

Koren, E., Apte, A., Jani, A. & Torchilin, V.P. (2012) Multifunctional PEGylated 2C5-immunoliposomes containing pH-sensitive bonds and TAT peptide for enhanced tumor cell internalization and cytotoxicity. *Journal of controlled release*. 160 (2), 264–273.

Koren, E. & Torchilin, V.P. (2012) Cell-penetrating peptides: breaking through to the other side. *Trends in Molecular Medicine*. 18 (7), 385–393.

Krishna, R. & Mayer, L.D. (2000) Multidrug resistance (MDR) in cancer: Mechanisms, reversal using modulators of MDR and the role of MDR modulators in influencing the pharmacokinetics of anticancer drugs. *European Journal of Pharmaceutical Sciences*. 11 (4), 265–283.

Kurosaki, T., Kitahara, T., Fumoto, S., Nishida, K., et al. (2009) Ternary complexes of pDNA, polyethylenimine, and γ-polyglutamic acid for gene delivery systems. *Biomaterials*. 30 (14), 2846–2853.

Kurosaki, T., Kitahara, T., Nakamura, T., Nishida, K., et al. (2012) Development of effective cancer vaccine using targeting system of antigen protein to APCs. *Pharmaceutical Research*. 29 (2), 483–489.

Kyriakides, T.R., Cheung, C.Y., Murthy, N., Bornstein, P., et al. (2002) pH-Sensitive polymers that enhance intracellular drug delivery in vivo. *Journal of Controlled Release*. 78 (1), 295–303.

De Las Heras Alarcon, C., Pennadam, S. & Alexander, C. (2005) Stimuli responsive polymers for biomedical applications. *Chemical Society reviews*. 34 (3), 276–285.

Lackey, C.A., Press, O.W., Hoffman, A.S. and Stayton, P.S.. (2002) A biomimetic pH-responsive polymer directs endosomal release and intracellular delivery of an endocytosed antibody complex. *Bioconjugate chemistry*, 13 (5), 996-1001.

Lasic, D.D., Čeh, B., Stuart, M.C.A., Guo, L., et al. (1995) Transmembrane gradient driven

phase transitions within vesicles: lessons for drug delivery. *Biochimica et Biophysica Acta (BBA)-Biomembranes*. 1239 (2), 145–156.

Lee, E., Kim, J. K., Jeon, D., Jeong, K. W., et al. (2015) Functional roles of aromatic residues and helices of papiliocin in its antimicrobial and anti-inflammatory activities. *Scientific Reports*. 5, 12048, 1–17.

Lee, E.S., Gao, Z., Kim, D., Park, K., et al. (2008) Super pH-sensitive multifunctional polymeric micelle for tumor pHe specific TAT exposure and multidrug resistance. *Journal of Controlled Release*. 129 (3), 228–236.

Lee, E.S., Na, K. & Bae, Y.H. (2005) Doxorubicin loaded pH-sensitive polymeric micelles for reversal of resistant MCF-7 tumor. *Journal of Controlled Release*. 103 (2), 405–418.

Lee, J.H., Gustin, J.P., Chen, T., Payne, G.F., et al. (2005) Vesicle-biopolymer gels: networks of surfactant vesicles connected by associating biopolymers. *Langmuir*. 21 (1), 26–33.

Lee, S.H., Castagner, B. & Leroux, J. C. (2013) Is there a future for cell-penetrating peptides in oligonucleotide delivery? *European Journal of Pharmaceutics and Biopharmaceutics*. 85 (1), 5–11.

Lee, Y. J., Erazo-Oliveras, A. & Pellois, J. P. (2010) Delivery of macromolecules into live cells by simple co-incubation with a peptide. *ChemBioChem*. 11 (3), 325–330.

Leroux, J. C. (2004) pH-responsive carriers for enhancing the cytoplasmic delivery of macromolecular drugs. *Advanced Drug Delivery Reviews*. 56 (7), 925–926.

Leroux, J.C., Roux, E., Le Garrec, D., Hong, K., et al. (2001) *N*-isopropylacrylamide copolymers for the preparation of pH-sensitive liposomes and polymeric micelles. *Journal of Controlled Release*. 72 (1–3), 71–84.

Lesieur, C., Vécsey-Semjén, B., Abrami, L., Fivaz, M., et al. (1997) Membrane insertion: the strategies of toxins. *Molecular Membrane Biology*. 14 (2), 45–64.

Li, C. & Wallace, S. (2008) Polymer-drug conjugates: recent development in clinical oncology. *Advanced Drug Delivery Reviews*. 60 (8), 886–898.

Li, L., Wan, T., Wan, M., Liu, B., et al. (2015) The effect of the size of fluorescent dextran on its endocytic pathway. *Cell Biology International*. 39 (5), 531–539.

Liboiron, B.D. & Mayer, L.D. (2014) Nanoscale particulate systems for multidrug delivery: towards improved combination chemotherapy. *Therapeutic Delivery*. 5 (2), 149–171.

Liechty, W.B., Chen, R., Farzaneh, F., Tavassoli, M., et al. (2009) Synthetic pH-responsive polymers for protein transduction. *Advanced Materials*. 21 (38–39), 3910–3914.

Linhardt, J.G. & Tirrell, D.A. (2000) pH-induced fusion and lysis of phosphatidylcholine vesicles by the hydrophobic polyelectrolyte poly (2-ethylacrylic acid). *Langmuir*. 16 (1), 122–127.

Liu, D.Z., Chen, W.Y., Tasi, L.M. & Yang, S.P. (2000) Microcalorimetric and shear studies on the effects of cholesterol on the physical stability of lipid vesicles. *Colloids and Surfaces A: Physicochemical and Engineering Aspects*. 172 (1–3), 57–67.

Liu, Y., Li, L. L., Qi, G. B., Chen, X. G., et al. (2014) Dynamic disordering of liposomal cocktails and the spatio-temporal favorable release of cargoes to circumvent drug resistance. *Biomaterials*. 35 (10), 3406–3415.

Lu, H. L., Syu, W. J., Nishiyama, N., Kataoka, K., et al. (2011) Dendrimer phthalocyanine-encapsulated polymeric micelle-mediated photochemical internalization extends the efficacy of photodynamic therapy and overcomes drug-resistance in vivo. *Journal of Controlled Release*. 155 (3), 458–464.

Lu, T., Zhao Wang, Y.M., Zhang, Y. & Chen, T. (2012) Influence of polymer size, liposomal composition, surface charge, and temperature on the permeability of pH-sensitive liposomes containing lipid-anchored poly (2-ethylacrylic acid). *International Journal of Nanomedicine*. 7, 4917–4926.

Lundstrom, K. (2003) Latest development in viral vectors for gene therapy. *Trends in Biotechnology*. 21 (3), 117–122.

Lynch, A.L., Chen, R., Dominowski, P.J., Shalaev, E.Y., et al. (2010) Biopolymer mediated trehalose uptake for enhanced erythrocyte cryosurvival. *Biomaterials*. 31 (23), 6096–6103.

Lynch, A.L., Chen, R. & Slater, N.K.H. (2011) pH-responsive polymers for trehalose loading and desiccation protection of human red blood cells. *Biomaterials*. 32 (19), 4443–4449.

MacCallum, J.L., Bennett, W.F.D. & Tieleman, D.P. (2007) Partitioning of amino acid side chains into lipid bilayers: results from computer simulations and comparison to experiment.

The Journal of General Physiology. 129 (5), 371–377.

Malam, Y., Loizidou, M. & Seifalian, A.M. (2009) Liposomes and nanoparticles: nanosized vehicles for drug delivery in cancer. *Trends in Pharmacological Sciences*. 30 (11), 592–599.

Mallakpour, S. & Dinari, M. (2011) Progress in synthetic polymers based on natural amino acids. *Journal of Macromolecular Science, Part A*. 48 (8), 644–679.

Mallick, S. & Choi, J.S. (2014) Liposomes: versatile and biocompatible nanovesicles for efficient biomolecules delivery. *Journal of Nanoscience and Nanotechnology*. 14 (1), 755–765.

Mao, J., Li, Y., Wu, T., Yuan, C., et al. (2016) A simple dual-pH responsive prodrug-based polymeric micelles for drug delivery. *ACS Applied Materials & Interfaces*. 8 (27), 17109–17117.

Marchesi, V.T., Furthmayr, H. & Tomita, M. (1976) The red cell membrane. *Annual review of biochemistry*. 45, 667–698.

Marie, E., Sagan, S., Cribier, S. & Tribet, C. (2014) Amphiphilic macromolecules on cell membranes: from protective layers to controlled permeabilization. *The Journal of Membrane Biology*. 247 (9–10), 861–881.

Marqués-Gallego, P. & de Kroon, A.I.P.M. (2014) Ligation strategies for targeting liposomal nanocarriers. *BioMed Research International*. 2014, 1-12.

Martens, T.F., Remaut, K., Demeester, J., De Smedt, S.C., et al. (2014) Intracellular delivery of nanomaterials: how to catch endosomal escape in the act. *Nano Today*. 9 (3), 344–364.

Martin, F. & MacDonald, R. (1974) Liposomes can mimic virus membranes. *Nature*. 252, 161–163.

Martins, S., Sarmento, B., Ferreira, D.C. & Souto, E.B. (2007) Lipid-based colloidal carriers for peptide and protein delivery–liposomes versus lipid nanoparticles. *International Journal of Nanomedicine*. 2 (4), 595–607.

Mastrobattista, E., Koning, G.A., van Bloois, L., Filipe, A.C.S., et al. (2002) Functional characterization of an endosome-disruptive peptide and its application in cytosolic delivery of immunoliposome-entrapped proteins. *Journal of Biological Chemistry*. 277 (30), 27135–27143.

Matsuzaki, K., Yoneyama, S. & Miyajima, K. (1997) Pore formation and translocation of

melittin. *Biophysical Journal*. 73 (2), 831–838.

Matteo, R., Proverbio, T., Córdova, K., Proverbio, F., et al. (1998) Preeclampsia, lipid peroxidation, and calcium adenosine triphosphatase activity of red blood cell ghosts. *American Journal of Obstetrics and Gynecology*. 178 (2), 402–408.

McNeeley, K.M., Karathanasis, E., Annapragada, A.V. and Bellamkonda, R.V., 2009. Masking and triggered unmasking of targeting ligands on nanocarriers to improve drug delivery to brain tumors. Biomaterials, 30(23), 3986-3995.

McTaggart, S. & Al-Rubeai, M. (2002) Retroviral vectors for human gene delivery. *Biotechnology Advances*. 20 (1), 1–31.

Van der Meel, R., Fens, M.H.A.M., Vader, P., Van Solinge, W.W., et al. (2014) Extracellular vesicles as drug delivery systems: lessons from the liposome field. *Journal of Controlled Release*. 195, 72–85.

Van der Meel, R., Vehmeijer, L.J.C., Kok, R.J., Storm, G., et al. (2013) Ligand-targeted particulate nanomedicines undergoing clinical evaluation: current status. *Advanced Drug Delivery Reviews*. 65 (10), 1284–1298.

Mellman, I. (1996) Endocytosis and molecular sorting. *Annual Review of Cell and Developmental Biology*. 12 (1), 575–625.

Mellman, I. & Warren, G. (2000) The road taken: past and future foundations of membrane traffic. *Cell*. 100 (1), 99–112.

De Meyer, F. & Smit, B. (2009) Effect of cholesterol on the structure of a phospholipid bilayer. *Proceedings of the National Academy of Sciences of the United States of America*. 106 (10), 3654–3658.

Meyer, O., Papahadjopoulos, D. & Leroux, J.C. (1998) Copolymers of *N*-isopropylacrylamide can trigger pH sensitivity to stable liposomes. *FEBS Letters*. 421 (1), 61–64.

Mhashilkar, A., Chada, S., Roth, J.A. & Ramesh, R. (2001) Gene therapy: therapeutic approaches and implications. *Biotechnology Advances*. 19 (4), 279–297.

Miele, E., Spinelli, G.P., Miele, E., Di Fabrizio, E., et al. (2012) Nanoparticle-based delivery of small interfering RNA: challenges for cancer therapy. *International Journal of*

Nanomedicine. 7, 3637–3657.

Milletti, F. (2012) Cell-penetrating peptides: classes, origin, and current landscape. *Drug Discovery Today*. 17 (15–16), 850–860.

Mills, J.K., Eichenbaum, G. & Needham, D. (1999) Effect of bilayer cholesterol and surface grafted poly (ethylene glycol) on pH-induced release of contents from liposomes by poly (2-ethylacrylic acid). *Journal of Liposome Research*. 9 (2), 275–290.

Mitragotri, S., Burke, P.A. & Langer, R. (2014) Overcoming the challenges in administering biopharmaceuticals: formulation and delivery strategies. *Nature Reviews Drug Discovery*. 13 (9), 655–672.

Morille, M., Passirani, C., Vonarbourg, A., Clavreul, A., et al. (2008) Progress in developing cationic vectors for non-viral systemic gene therapy against cancer. *Biomaterials*. 29 (24), 3477–3496.

Motornov, M., Roiter, Y., Tokarev, I. & Minko, S. (2010) Stimuli-responsive nanoparticles, nanogels and capsules for integrated multifunctional intelligent systems. *Progress in Polymer Science*. 35 (1–2), 174–211.

Mudhakir, D. & Harashima, H. (2009) Learning from the viral journey: how to enter cells and how to overcome intracellular barriers to reach the nucleus. *The AAPS Journal*. 11 (1), 65–77.

Mukherjee, S., Ghosh, R.N. & Maxfield, F.R. (1997) Endocytosis. *Physiological Reviews*. 77 (3), 759–803.

Müller, R.H., Mäder, K. & Gohla, S. (2000) Solid lipid nanoparticles (SLN) for controlled drug delivery – a review of the state of the art. *European Journal of Pharmaceutics and Biopharmaceutics*. 50 (1), 161–177.

Müller, R.H., Petersen, R.D., Hommoss, A. & Pardeike, J. (2007) Nanostructured lipid carriers (NLC) in cosmetic dermal products. *Advanced Drug Delivery Reviews*. 59 (6), 522–530.

Mura, S., Nicolas, J. & Couvreur, P. (2013) Stimuli-responsive nanocarriers for drug delivery. *Nature Materials*. 12 (11), 991–1003.

Murthy, N., Chang, I., Stayton, P. & Hoffman, A. (2001) pH-sensitive hemolysis by random copolymers of alkyl acrylates and acrylic acid. *Macromolecular Symposia*. 172 (1), 49–56.

Murthy, N., Robichaud, J.R., Tirrell, D.A., Stayton, P.S., et al. (1999) The design and synthesis of polymers for eukaryotic membrane disruption. *Journal of Controlled Release*. 61 (1–2), 137–143.

Nag, O.K. & Awasthi, V. (2013) Surface engineering of liposomes for stealth behavior. *Pharmaceutics*. 5 (4), 542–569.

Nakamura, K., Yamashita, K., Itoh, Y., Yoshino, K., et al. (2012) Comparative studies of polyethylene glycol-modified liposomes prepared using different PEG-modification methods. *Biochimica et Biophysica Acta (BBA) - Biomembranes*. 1818 (11), 2801–2807.

Nakamura, Y., Mochida, A., Choyke, P.L. & Kobayashi, H. (2016) Nanodrug delivery: is the enhanced permeability and retention effect sufficient for curing cancer? *Bioconjugate Chemistry*. 27 (10), 2225–2238.

Nakase, I., Kobayashi, S. & Futaki, S. (2010) Endosome-disruptive peptides for improving cytosolic delivery of bioactive macromolecules. *Biopolymers*. 94 (6), 763–770.

Needham, D., Mills, J. & Eichenbaum, G. (1999) Interactions between poly (2-ethylacrylic acid) and lipid bilayer membranes: effects of cholesterol and grafted poly (ethylene glycol). *Faraday Discuss.* 111, 103–110.

Ng, L. T., Yuba, E. & Kono, K. (2009) Modification of liposome surface with pH-responsive polyampholytes for the controlled-release of drugs. *Research on Chemical Intermediates*. 35 (8–9), 1015–1025.

Nishiyama, N. & Kataoka, K. (2006) Current state, achievements, and future prospects of polymeric micelles as nanocarriers for drug and gene delivery. *Pharmacology & Therapeutics*. 112 (3), 630–648.

Noble, C.O., Kirpotin, D.B., Hayes, M.E., Mamot, C., et al. (2004) Development of ligand-targeted liposomes for cancer therapy. *Expert Opinion on Therapeutic Targets*. 8 (4), 335–353.

Noble, G.T., Stefanick, J.F., Ashley, J.D., Kiziltepe, T., et al. (2014) Ligand-targeted liposome design: challenges and fundamental considerations. *Trends in Biotechnology*. 32 (1), 32–45.

Nociari, M.M., Shalev, A., Benias, P. & Russo, C. (1998) A novel one-step, highly sensitive fluorometric assay to evaluate cell-mediated cytotoxicity. *Journal of Immunological Methods*. 213 (2), 157–167.

Owen, S.C., Chan, D.P.Y. & Shoichet, M.S. (2012) Polymeric micelle stability. *Nano Today*. 7 (1), 53–65.

Pack, D.W., Hoffman, A.S., Pun, S. & Stayton, P.S. (2005) Design and development of polymers for gene delivery. *Nature Reviews Drug discovery*. 4 (7), 581–593.

Pan, L., Liu, J., He, Q., Wang, L., et al. (2013) Overcoming multidrug resistance of cancer cells by direct intranuclear drug delivery using TAT-conjugated mesoporous silica nanoparticles. *Biomaterials*. 34 (11), 2719–2730.

Panmai, S., Prud'homme, R.K. & Peiffer, D.G. (1999) Rheology of hydrophobically modified polymers with spherical and rod-like surfactant micelles. *Colloids and surfaces A: physicochemical and engineering aspects*. 147 (1–2), 3–15.

Parhi, P., Mohanty, C. & Sahoo, S.K. (2012) Nanotechnology-based combinational drug delivery: an emerging approach for cancer therapy. *Drug Discovery Today*. 17 (17), 1044–1052.

Park, K. (2014) Controlled drug delivery systems: past forward and future back. *Journal of Controlled Release*. 190, 3–8.

Park, K. (2007) Nanotechnology: what it can do for drug delivery. *Journal of Controlled Release*. 120 (1–2), 1–3.

Patel, N.R., Rathi, A., Mongayt, D. & Torchilin, V.P. (2011) Reversal of multidrug resistance by co-delivery of tariquidar and paclitaxel using long-circulating liposomes. *International Journal of Pharmaceutics*. 416 (1), 296–299.

Peppas, N.A., Huang, Y., Torres-Lugo, M., Ward, J.H., et al. (2000) Physicochemical foundations and structural design of hydrogels in medicine and biology. *Annual Review of Biomedical Engineering*. 2 (1), 9–29.

Pick, U. (1981) Liposomes with a large trapping capacity prepared by freezing and thawing of sonicated phospholipid mixtures. *Archives of Biochemistry and Biophysics*. 212 (1), 186–194.

Plank, C., Oberhauser, B., Mechtler, K., Koch, C., et al. (1994) The influence of endosome-disruptive peptides on gene transfer using synthetic virus-like gene transfer systems. *The Journal of Biological Chemistry.* 269 (17), 12918–12924.

Plank, C., Zauner, W. & Wagner, E. (1998) Application of membrane-active peptides for drug and gene delivery across cellular membranes. *Advanced Drug Delivery Reviews*. 34 (1), 21–35.

Platé, N.A. & Shibaev, V.P. (2012) Structure of Comb-shaped polymers. In: *Comb-shaped polymers and liquid crystals*. New York, Plenum Press. 9–93.

Platta, H.W. & Stenmark, H. (2011) Endocytosis and signaling. *Current Opinion in Cell Biology*. 23 (4), 393–403.

Polozova, A. & Winnik, F.M. (1997) Mechanism of the interaction of hydrophobically-modified poly-(*N*-isopropylacrylamides) with liposomes. *Biochimica et Biophysica Acta (BBA) - Biomembranes*. 1326 (2), 213–224.

Polozova, A., Yamazaki, A., Brash, J.L. & Winnik, F.M. (1999) Effect of polymer architecture on the interactions of hydrophobically-modified poly-(*N*-isopropylamides) and liposomes. *Colloids and Surfaces A: Physicochemical and Engineering Aspects*. 147 (1–2), 17–25.

Pons, M., Foradada, M. & Estelrich, J. (1993) Liposomes obtained by the ethanol injection method. *International Journal of Pharmaceutics*. 95 (1–3), 51–56.

Pradhan, P., Giri, J., Rieken, F., Koch, C., et al. (2010) Targeted temperature sensitive magnetic liposomes for thermo-chemotherapy. *Journal of Controlled Release*. 142 (1), 108–121.

Priya Prakash Karmali, A.C. (2006) Cationic liposomes as non-viral carriers of gene medicines: resolved issues, open questions, and future promises. *Medicinal Research Reviews.* 27 (5), 696-722.

Qiu, L.Y. & Bae, Y.H. (2006) Polymer architecture and drug delivery. *Pharmaceutical Research*. 23 (1), 1–30.

Quemeneur, F., Rinaudo, M., Maret, G. & Pépin Donat, B. (2010) Decoration of lipid vesicles by polyelectrolytes: mechanism and structure. *Soft Matter*. 6 (18), 4471–4481.

Rapoport, T.A. (2007) Protein translocation across the eukaryotic endoplasmic reticulum and bacterial plasma membranes. *Nature*. 450 (7170), 663–669.

Resh, M.D. (2013) Covalent lipid modifications of proteins. *Current Biology*. 23 (10), 431–435.

Resh, M.D. (1999) Fatty acylation of proteins: new insights into membrane targeting of myristoylated and palmitoylated proteins. *Biochimica et Biophysica Acta (BBA) - Molecular Cell Research*. 1451 (1), 1–16.

Resh, M.D. (2016) Fatty acylation of proteins: the long and the short of it. *Progress in Lipid Research*. 63, 120–131.

Ringsdorf, H. (1975) Structure and properties of pharmacologically active polymers. *Journal of Polymer Science: Polymer Symposia*. 51 (1), 135–153.

Rosenberg, S.A., Aebersold, P., Cornetta, K., Kasid, A., et al. (1990) Gene transfer into humans — immunotherapy of patients with advanced melanoma, using tumor-infiltrating lymphocytes modified by retroviral gene transduction. *New England Journal of Medicine*. 323 (9), 570–578.

Roux, E., Francis, M., Winnik, F.M. & Leroux, J. C. (2002) Polymer based pH-sensitive carriers as a means to improve the cytoplasmic delivery of drugs. *International Journal of Pharmaceutics*. 242 (1–2), 25–36.

Roux, E., Lafleur, M., Lataste, É., Moreau, P., et al. (2003) On the characterization of pH-sensitive liposome/polymer complexes. *Biomacromolecules*. 4 (2), 240–248.

Safari, J. & Zarnegar, Z. (2014) Advanced drug delivery systems: nanotechnology of health design A review. *Journal of Saudi Chemical Society*. 18 (2), 85–99.

Sahay, G., Alakhova, D.Y. & Kabanov, A. V (2010) Endocytosis of nanomedicines. *Journal of Controlled Release*. 145 (3), 182–195.

Sahoo, S.K., Labhasetwar, V., Davaran, S., Joo, S.W., et al. (2003) Nanotech approaches to drug delivery and imaging. *Drug Discovery Today*. 8 (24), 1112–1120.

Sakaguchi, N., Kojima, C., Harada, A. & Kono, K. (2008) Preparation of pH-sensitive poly(glycidol) derivatives with varying hydrophobicities: their ability to sensitize stable liposomes to pH. *Bioconjugate Chemistry*. 19 (5), 1040–1048.

Samad, A., Sultana, Y. & Aqil, M. (2007) Liposomal Drug Delivery Systems: An Update Review. *Current Drug Delivery*. 4 (4), 297–305.

Sant, V.P., Smith, D. & Leroux, J. C. (2004) Novel pH-sensitive supramolecular assemblies for oral delivery of poorly water soluble drugs: preparation and characterization. *Journal of*

Controlled Release. 97 (2), 301–312.

Sapra, P. & Allen, T.M. (2003) Ligand-targeted liposomal anticancer drugs. *Progress in Lipid Research*. 42 (5), 439–462.

Sato, H. & Feix, J.B. (2006) Peptide–membrane interactions and mechanisms of membrane destruction by amphipathic α-helical antimicrobial peptides. *Biochimica et Biophysica Acta (BBA) - Biomembranes*. 1758 (9), 1245–1256.

Sawant, R.R. & Torchilin, V.P. (2012) Challenges in development of targeted liposomal therapeutics. *The AAPS Journal*. 14 (2), 303–315.

Schmaljohann, D. (2006) Thermo- and pH-responsive polymers in drug delivery. *Advanced Drug Delivery Reviews*. 58 (15), 1655–1670.

Schubert, M.A. & Müller-Goymann, C.C. (2005) Characterisation of surface-modified solid lipid nanoparticles (SLN): Influence of lecithin and nonionic emulsifier. *European Journal of Pharmaceutics and Biopharmaceutics*. 61 (1–2), 77–86.

Schulz, M., Olubummo, A. & Binder, W.H. (2012) Beyond the lipid-bilayer: interaction of polymers and nanoparticles with membranes. *Soft Matter*. 8 (18), 48-49.

Seki, K. & Tirrell, D.A. (1984) pH-Dependent complexation of poly (acrylic acid) derivatives with phospholipid vesicle membranes. *Macromolecules*. 17 (9), 1692–1698.

Severino, P., Andreani, T., Macedo, A.S., Fangueiro, J.F., et al. (2011) Current state-of-art and new trends on lipid nanoparticles (SLN and NLC) for oral drug delivery. *Journal of drug delivery*. 2012, 1-10.

Sharei, A., Zoldan, J., Adamo, A., Sim, W.Y., et al. A vector-free microfluidic platform for intracellular delivery. *Proceedings of the National Academy of Sciences.* 110 (6), 2082-2087.

Sharma, A. & Sharma, U.S. (1997) Liposomes in drug delivery: progress and limitations. *International Journal of Pharmaceutics*. 154 (2), 123–140.

Shi, G., Guo, W., Stephenson, S.M. & Lee, R.J. (2002) Efficient intracellular drug and gene delivery using folate receptor-targeted pH-sensitive liposomes composed of cationic/anionic lipid combinations. *Journal of Controlled Release*. 80 (1–3), 309–319.

Shi, H., Zhao, Y., Dong, X., Zhou, Y., et al. (2013) Frustrated crystallisation and hierarchical

self-assembly behaviour of comb-like polymers. *Chemical Society Reviews*. 42 (5), 2075–2099.

Shi, J., Kantoff, P.W., Wooster, R. & Farokhzad, O.C. (2017) Cancer nanomedicine: progress, challenges and opportunities. *Nature Reviews Cancer*. 17, 20-37.

Shim, G., Kim, M. G., Park, J.Y. & Oh, Y. K. (2013) Application of cationic liposomes for delivery of nucleic acids. *Asian Journal of Pharmaceutical Sciences*. 8 (2), 72-80.

Shim, M.S. & Kwon, Y.J. (2012) Stimuli-responsive polymers and nanomaterials for gene delivery and imaging applications. *Advanced Drug Delivery Reviews*. 64 (11), 1046–1059.

Simões, S., Moreira, J.N., Fonseca, C., Düzgüneş, N., et al. (2004) On the formulation of pH-sensitive liposomes with long circulation times. *Advanced Drug Delivery Reviews*. 56 (7), 947–965.

Skehel, J.J., Bayley, P.M., Brown, E.B., Martin, S.R., et al. (1982) Changes in the conformation of influenza virus hemagglutinin at the pH optimum of virus-mediated membrane fusion. *Proceedings of the National Academy of Sciences*. 79 (4), 968–972.

Skehel, J.J. & Wiley, D.C. (2000) Receptor binding and membrane fusion in virus entry: the influenza hemagglutinin. *Annual Review of Biochemistry*. 69, 531–569.

Sovadinova, I., Palermo, E.F., Huang, R., Thoma, L.M., et al. (2011) Mechanism of polymer-induced hemolysis: nanosized pore formation and osmotic lysis. *Biomacromolecules*. 12 (1), 260–268.

Stuart, M.A.C., Huck, W.T.S., Genzer, J., Müller, M., et al. (2010) Emerging applications of stimuli-responsive polymer materials. *Nature Materials*. 9 (2), 101–113.

Suk, J.S., Xu, Q., Kim, N., Hanes, J., et al. (2016) PEGylation as a strategy for improving nanoparticle-based drug and gene delivery. *Advanced Drug Delivery Reviews*. 99, 28–51.

Szoka, F. & Papahadjopoulos, D. (1978) Procedure for preparation of liposomes with large internal aqueous space and high capture by reverse-phase evaporation. *Proceedings of the National Academy of Sciences of the United States of America*. 75 (9), 4194–4198.

Teramura, Y., Kaneda, Y., Totani, T. & Iwata, H. (2008) Behavior of synthetic polymers immobilized on a cell membrane. *Biomaterials*. 29 (10), 1345–1355.

Thomas, J.L., Barton, S.W. & Tirrell, D.A. (1994) Membrane solubilization by a hydrophobic

polyelectrolyte: surface activity and membrane binding. *Biophysical journal*. 67 (3), 1101–1106.

Thomas, J.L., Borden, K.A. & Tirrell, D.A. (1996) Modulation of mobilities of fluorescent membrane probes by adsorption of a hydrophobic polyelectrolyte. *Macromolecules*. 29 (7), 2570–2576.

Thomas, J.L., Devlin, B.P. & Tirrell, D.A. (1996) Kinetics of membrane micellization by the hydrophobic polyelectrolyte poly(2-ethylacrylic acid). *Biochimica et Biophysica Acta (BBA) - Biomembranes*. 1278 (1), 73–78.

Thomas, J.L. & Tirrell, D.A. (1992) Polyelectrolyte-sensitized phospholipid vesicles. *Accounts of Chemical Research*. 25 (8), 336–342.

Tirrell, D.A., Takigawa, D.Y. & Seki, K. (1985) pH sensitization of phospholipid vesicles via complexation with synthetic poly(carboxylic acid)s. *Annals of the New York Academy of Sciences*. 446 (1), 237–248.

Torchilin, V. (2009) Multifunctional and stimuli-sensitive pharmaceutical nanocarriers. *European Journal of Pharmaceutics and Biopharmaceutics*. 71 (3), 431–444.

Torchilin, V.P. (2014) Multifunctional, stimuli-sensitive nanoparticulate systems for drug delivery. *Nature reviews Drug discovery*. 13 (11), 813–827.

Torchilin, V.P. (2006) Multifunctional nanocarriers. *Advanced Drug Delivery Reviews*. 58 (14), 1532–1555.

Torchilin, V.P. (2005) Recent advances with liposomes as pharmaceutical carriers. *Nature Reviews Drug Discovery*. 4 (2), 145–160.

Torchilin, V.P. & Weissig, V. (2003) Preparation of liposomes. In: *Liposomes: a practical approach*. Oxford, Oxford University Press. 3–27.

Torchilin, V.P., Zhou, F. & Huang, L. (1993) pH-sensitive liposomes. *Journal of Liposome Research*. 3 (2), 201–255.

Tribet, C. & Vial, F. (2008) Flexible macromolecules attached to lipid bilayers: impact on fluidity, curvature, permeability and stability of the membranes. *Soft Matter*. 4 (1), 68-81.

Varkouhi, A.K., Scholte, M., Storm, G. & Haisma, H.J. (2011a) Endosomal escape pathways

for delivery of biologicals. *Journal of Controlled Release*. 151 (3), 220–228.

Varkouhi, A.K., Scholte, M., Storm, G. & Haisma, H.J. (2011b) Endosomal escape pathways for delivery of biologicals. *Journal of Controlled Release*. 151 (3), 220–228.

Venditto, V.J. & Szoka Jr, F.C. (2013) Cancer nanomedicines: so many papers and so few drugs! *Advanced drug delivery reviews*. 65 (1), 80–88.

Vial, F., Rabhi, S. & Tribet, C. (2005) Association of octyl-modified poly(acrylic acid) onto unilamellar vesicles of lipids and kinetics of vesicle disruption. *Langmuir*. 21 (3), 853–862.

Vivès, E., Schmidt, J. & Pèlegrin, A. (2008) Cell-penetrating and cell-targeting peptides in drug delivery. *Biochimica et Biophysica Acta*. 1786 (2), 126–138.

Walrant, A., Vogel, A., Correia, I., Lequin, O., et al. (2012) Membrane interactions of two arginine-rich peptides with different cell internalization capacities. *Biochimica et Biophysica Acta*. 1818 (7), 1755–1763.

Wang, F., Wang, Y., Zhang, X., Zhang, W., et al. (2014) Recent progress of cell-penetrating peptides as new carriers for intracellular cargo delivery. *Journal of Controlled Release*. 174, 126–136.

Wang, H. C., Zhang, Y., Possanza, C.M., Zimmerman, S.C., et al. (2015) Trigger chemistries for better industrial formulations. *ACS Applied Materials & Interfaces*. 7 (12), 6369–6382.

Wang, M. & Thanou, M. (2010) Targeting nanoparticles to cancer. *Pharmacological Research*. 62 (2), 90–99.

Wang, T., Upponi, J.R. & Torchilin, V.P. (2012) Design of multifunctional non-viral gene vectors to overcome physiological barriers: dilemmas and strategies. *International Journal of Pharmaceutics*. 427 (1), 3–20.

Wang, Y. C., Wang, F., Sun, T. M. & Wang, J. (2011) Redox-responsive nanoparticles from the single disulfide bond-bridged block copolymer as drug carriers for overcoming multidrug resistance in cancer cells. *Bioconjugate Chemistry*. 22 (10), 1939–1945.

Warburg, O., Wind, F. & Negelein, E. (1927) The metabolism of tumours within the body. *The Journal of General Physiology*. 8 (6), 519–530.

Watkins, K.A. & Chen, R. (2015) pH-responsive, lysine-based hydrogels for the oral delivery

of a wide size range of molecules. *International Journal of Pharmaceutics*. 478 (2), 496–503.

White, J.M. (1990) Viral and cellular membrane fusion proteins. *Annual Review of Physiology*. 52 (1), 675–697.

Wirth, T., Parker, N. & Ylä-Herttuala, S. (2013) History of gene therapy. *Gene*. 525 (2), 162–169.

Wissing, S.A., Kayser, O. & Müller, R.H. (2004) Solid lipid nanoparticles for parenteral drug delivery. *Advanced Drug Delivery Reviews*. 56 (9), 1257–1272.

Wong, H.L., Bendayan, R., Rauth, A.M., Li, Y., et al. (2007) Chemotherapy with anticancer drugs encapsulated in solid lipid nanoparticles. *Advanced Drug Delivery Reviews*. 59 (6), 491–504.

Woodle, M.C. & Papahadjopoulos, D. (1989) Liposome preparation and size characterization. *Methods in enzymology*. 171193.

Wu, G. & Lee, K.Y.C. (2009) Effects of poloxamer 188 on phospholipid monolayer morphology: an atomic force microscopy study. *Langmuir*. 25 (4), 2133–2139.

Wysocki, P.J., Mackiewicz-Wysocka, M. & Mackiewicz, A. (2002) Cancer gene therapy – state-of-the-art. *Reports of Practical Oncology & Radiotherapy*. 7 (4), 149–155.

Xu, H., Deng, Y., Chen, D., Hong, W., Lu, Y. and Dong, X., 2008. Esterase-catalyzed dePEGylation of pH-sensitive vesicles modified with cleavable PEG-lipid derivatives. Journal of Controlled Release, 130 (3), 238–245.

Yamada, A., Taniguchi, Y., Kawano, K., Honda, T., et al. (2008) Design of folate-linked liposomal doxorubicin to its antitumor effect in mice. *Clinical Cancer Research*. 14 (24), 8161–8168.

Yang, X. P., Amar, M.J., Vaisman, B., Bocharov, A. V, et al. (2013) Scavenger receptor-BI is a receptor for lipoprotein. *Journal of Lipid Research*. 54 (9), 2450–2457.

Yaroslavov, A.A., Sybachin, A. V, Kesselman, E., Schmidt, J., et al. (2011) Liposome fusion rates depend upon the conformation of polycation catalysts. *Journal of the American Chemical Society*. 133 (9), 2881–2883.

Yessine, M.A. & Leroux, J.C. (2004) Membrane-destabilizing polyanions: interaction with

lipid bilayers and endosomal escape of biomacromolecules. *Advanced Drug Delivery Reviews*. 56 (7), 999–1021.

Yin, H., Kanasty, R.L., Eltoukhy, A.A., Vegas, A.J., et al. (2014) Non-viral vectors for gene-based therapy. *Nature Reviews Genetics*. 15 (8), 541–555.

Yokoyama, M. (2010) Polymeric micelles as a new drug carrier system and their required considerations for clinical trials. *Expert Opinion on Drug Delivery*. 7 (2), 145–158.

Yoo, J. W., Irvine, D.J., Discher, D.E. & Mitragotri, S. (2011) Bio-inspired, bioengineered and biomimetic drug delivery carriers. *Nature Reviews Drug Discovery*. 10 (7), 521–535.

Yu, W., Pirollo, K.F., Yu, B., Rait, A., et al. (2004) Enhanced transfection efficiency of a systemically delivered tumor-targeting immunolipoplex by inclusion of a pH-sensitive histidylated oligolysine peptide. *Nucleic acids research*. 32 (5), e48.

Yuba, E., Harada, A., Sakanishi, Y. & Kono, K. (2011) Carboxylated hyperbranched poly(glycidol)s for preparation of pH-sensitive liposomes. *Journal of Controlled Release*. 149 (1), 72–80.

Yuba, E., Kojima, C., Sakaguchi, N., Harada, A., et al. (2008) Gene delivery to dendritic cells mediated by complexes of lipoplexes and pH-sensitive fusogenic polymer-modified liposomes. *Journal of Controlled Release*. 130 (1), 77–83.

Yuba, E., Kono, Y., Harada, A., Yokoyama, S., et al. (2013) The application of pH-sensitive polymer-lipids to antigen delivery for cancer immunotherapy. *Biomaterials*. 34 (22), 5711–5721.

Zhang, L., Wang, Y., Yang, Y., Liu, Y., Ruan, S., Zhang, Q., Tai, X., Chen, J., Xia, T., Qiu, Y., Gao, H., He, Q., 2015. High Tumor Penetration of Paclitaxel Loaded pH Sensitive Cleavable Liposomes by Depletion of Tumor Collagen I in Breast Cancer. ACS Appl. Mater. Interfaces 7, 9691–9701.

Zhang, S., Nelson, A., Coldrick, Z. & Chen, R. (2011) The effects of substituent grafting on the interaction of pH-responsive polymers with phospholipid monolayers. *Langmuir*. 27 (13), 8530–8539.

Zhang, S., Xu, Y., Wang, B., Qiao, W., et al. (2004) Cationic compounds used in lipoplexes and polyplexes for gene delivery. *Journal of Controlled Release*. 100 (2), 165–180.

Zhang, S., Zhao, B., Jiang, H., Wang, B., et al. (2007) Cationic lipids and polymers mediated vectors for delivery of siRNA. *Journal of Controlled Release*. 123 (1), 1–10.

Zhao, Y., Zhang, S., Cui, S., Wang, B., et al. (2012) Peptide-based cationic liposome-mediated gene delivery. *Expert Opinion on Drug Delivery*. 9 (1), 127–139.

Zignani, M., Drummond, D.C., Meyer, O., Hong, K., et al. (2000) In vitro characterization of a novel polymeric-based pH-sensitive liposome system. *Biochimica et Biophysica Acta - Biomembranes*. 1463 (2), 383–394.

Appendix A

Linear relationship between the absorbance of DOX and concentration in different solutions

Before measurement of drug loading and encapsulation efficiency of DOX loaded liposomes, the relationship between the DOX absorbance and the DOX concentration in different solutions was investigated. As seen in Figure A-1, within DOX concentration range of 10 – 50 μg mL^{-1}, the absorbance of DOX was in linear relationship with the concentration of DOX in aqueous solution or in ethanol. The standard curve obtained in HBS buffer and ethanol gave R^2 values of 0.9993 and 0.9994 respectively.

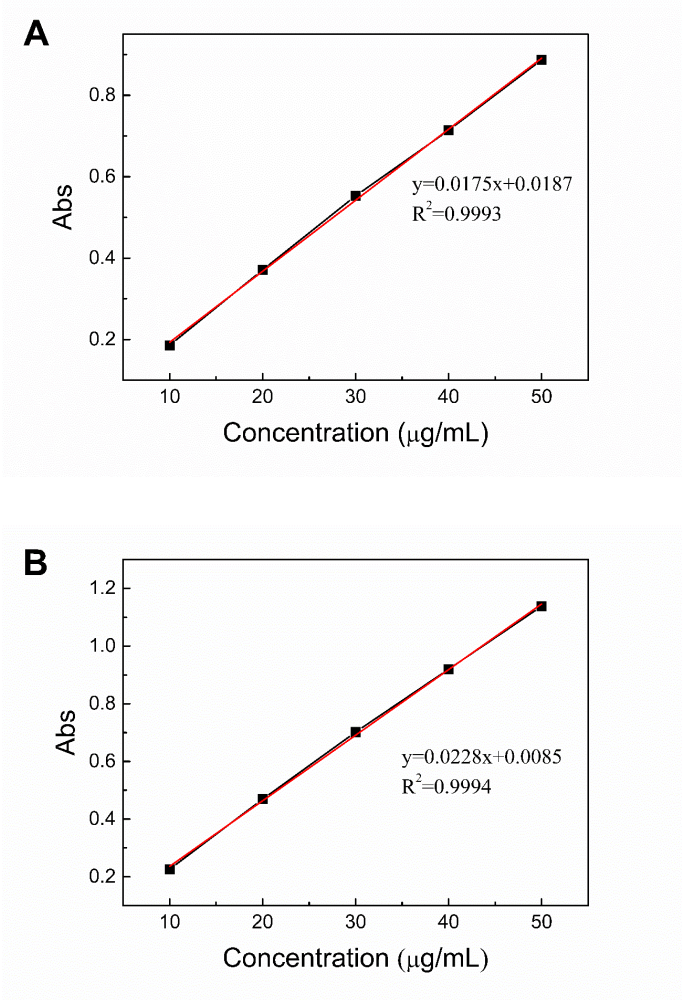

Figure A-1. The linear relationship between the absorbance of DOX and the concentration of DOX in HBS buffer (A) and ethanol (B).

Appendix B

Linear relationship between the fluorescence intensity and the concentration of fluorophore labelled polymers

In order to quantify the amount of adsorbed polymer on liposomal membrane, the relationship between the fluorescence intensity and the concentration of the polymers labelled with 6-aminofluorescein was explored. As shown in Figure A-2, the fluorescence intensity was in linear relationship with the concentration of 6-aminofluoresce modified PP75 (Figure A-2A) and PLP-NDA 18% (Figure A-2B) within the polymer concentration tested. The calibration curve obtained for PP75 and PLP-NDA 18% gave R^2 values of 0.9975 and 0.9993 respectively.

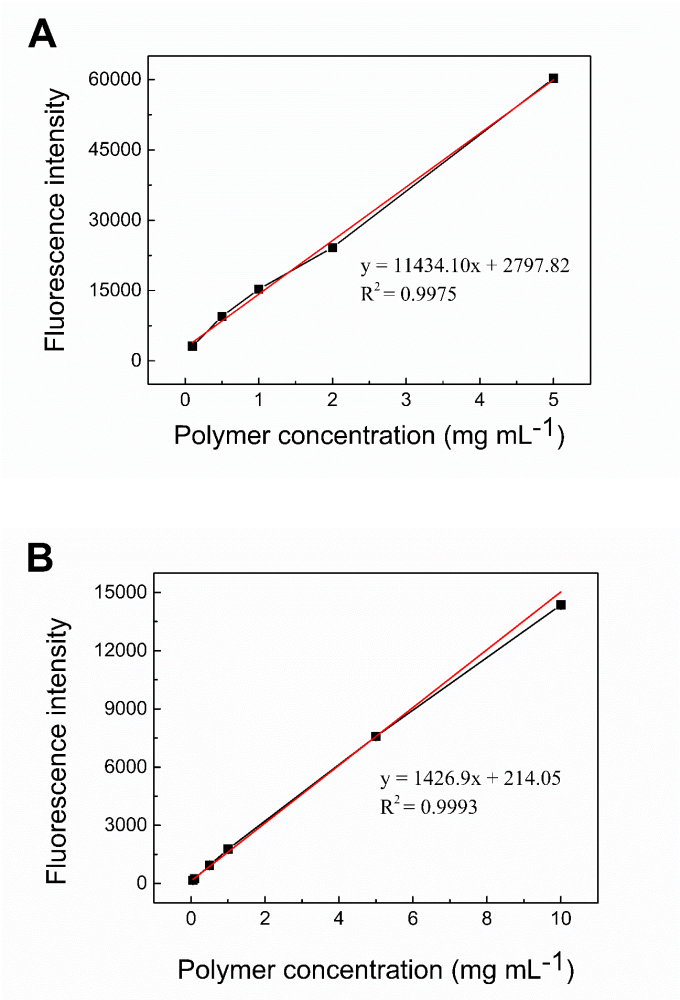

Figure A-2. The linear relationship between the fluorescence intensity and the concentration of 6-aminofluoresce labelled PP75 (A) and PLP-NDA 18% (B).

Appendix C

Linear relationship between the absorbance of hemoglobin and the RBCs concentration

Before hemolysis assay, the relationship between the absorbance of hemoglobin and the RBCs concentration was investigated to ensure the RBCs concentration used in hemolysis assay was performed within the linear relationship range. According to Figure A-3, after totally lyse the RBCs with deionized water, the absorbance of hemoglobin was shown to be in linear relationship with the concentration of RBCs up to a concentration of 4.12×10^8 RBCs mL^{-1} with a R^2 value of 0.9993. Once the RBCs concentration was higher than 4.12×10^8 RBCs $mL^{-1,}$ the absorbance of hemoglobin was no longer corresponding to the change of RBCs concentration. Therefore, the RBCs concentration for hemolysis need to be controlled between $0.41\times 10^8 – 4.12 \times 10^8$ RBCs mL^{-1}.

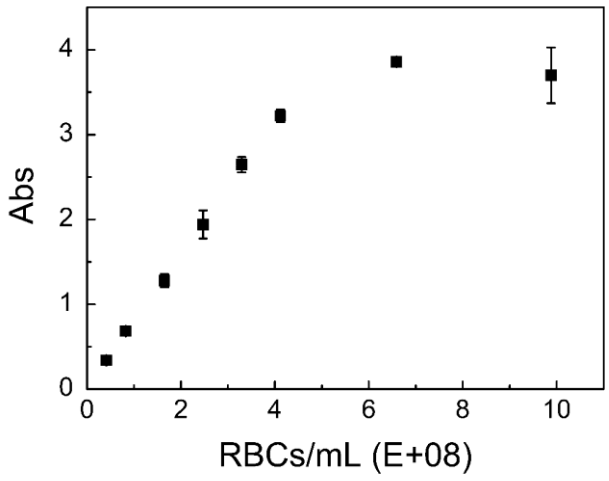

Figure A-3. Graph representing the relationship between absorbance of the release hemoglobin from the lysed RBCs in deionized water and the concentration of RBCs.

Appendix D

Calcein dequenching assay

Calcein will self-quench at high concentration. The linear relationship range of florescence intensity and calcein concentration was investigated. As shown in Figure A-4, the fluorescence intensity was in linear relationship with calcein concentration up to 15 μM. The standard curve obtained gave a R^2 values of 0.9933. Therefore, the calcein concentration was kept lower than 15 μM for calcein dequenching assay to ensure the linear relationship.

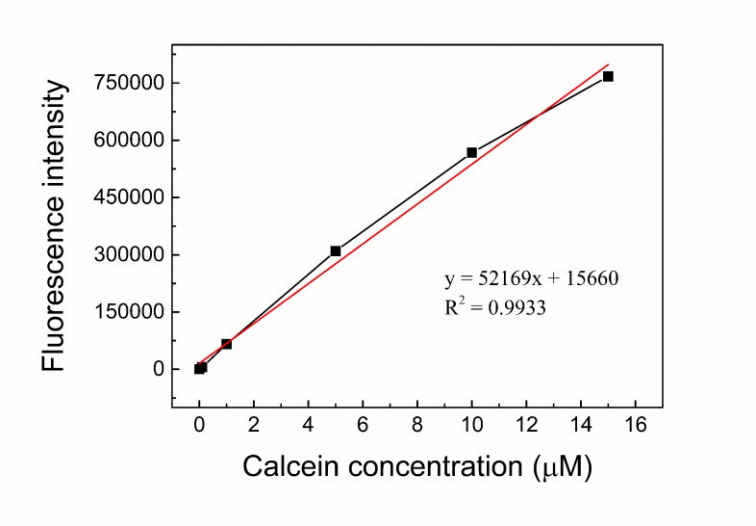

Figure A-4. The linear relationship between the fluorescence intensity and calcein concentration.

In order to ensure completely lyse of liposomes membrane, the volume of 10% triton X®-100 was studied. As shown in Figure A-5, with addition of 1 μL 10% triton X®-100, the fluorescence intensity of the liposomes sample increased significantly compared to the liposomes without the presence of triton, indicating the rupture of liposomal membrane and release of the encapsulated calcein into buffer. However, with the increase of triton volume added into liposomes, the fluorescence intensity remained consistent, suggesting 1 μL 10% triton X®-100 was sufficient to totally disrupt liposomal membrane. Thus, 1 μL 10% triton X-100 was applied to lyse liposomes for calcein dequenching assay.

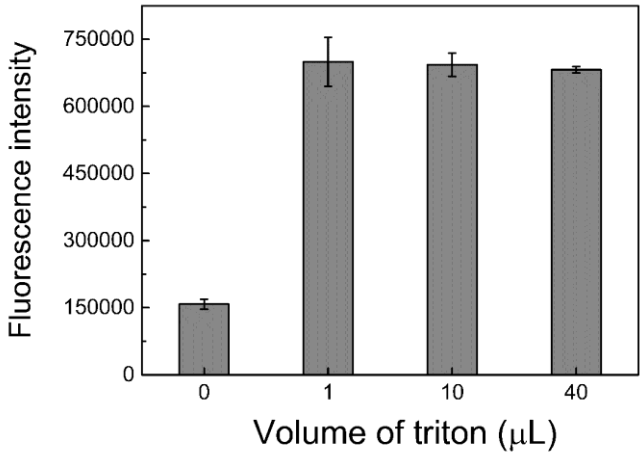

Figure A-5. The relationship between the fluorescence intensity and the volume of trition. Different volumes of 10% triton® X-100 was added to 100 μL liposomes loaded with 100 mM calcein to lyse liposomal membrane. Fluorescence reading was performed after 10 min incubation at room temperature and shaking for 2 min.

Appendix E

Thin-layer chromatography (TLC)

TLC was utilized to exam the PLP and NDA conjugation via DCC/DMAP coupling. As shown in Figure A-6A, amine group in NDA could be detected by ninhydrin staining. PLP was run on the same plate as a control to ensure no amine group presented in the polymer (Figure A-6B). After reaction, no amine group was detected from PLP-NDA 18% by TLC (Figure A-6C), indicating the successful conjugation of NDA on the PLP backbone.

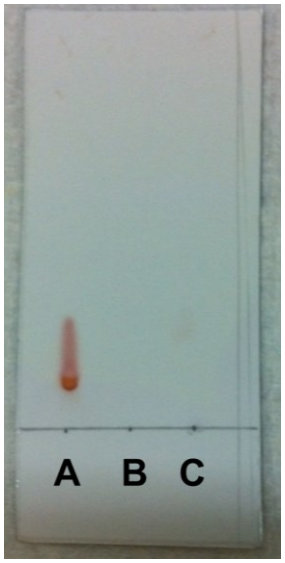

Figure A-6. TLC of NDA (A), PLP (B) and PLP-NDA 18% (C). Mobile phase: Chloroform: methanol: triethylamine = 8: 2: 0.2. Amine was visualized by ninhydrin.

Appendix F

Permissions summary table for third party copyright works

Page No.	Type of work:	Name of work	Source of work	Copyright holder and contact	Permission requested on	I have permission yes /no	Permission note
4	Figure	Figure 1-1. Ringsdorf model of a polymer-drug conjugate, contains a soluble polymer backbone, a biodegradable linker and a covalently linked drug.	Polymer–drug conjugates: Progress in polymeric prodrugs. Progress in Polymer Science. 31 (4), 359–397.	© 2006 Elsevier Ltd.	2017.01.06	Yes	Rightslink® by Copyright Clearance Centre License Number 4023150540093
5	Figure	Figure 1-2. Polymeric micelles are formed by amphiphilic block copolymers. They have a hydrophobic core as a drug reservoir and hydrophilic shell which improve the biocompatibility of the polymeric micelles.	Current state, achievements, and future prospects of polymeric micelles as nanocarriers for drug and gene delivery. Pharmacology & Therapeutics. 112 (3), 630–648.	© 2006 Elsevier Ltd.	2017.01.06	Yes	Rightslink® by Copyright Clearance Centre License Number 4023161431537

7	Figure	**Figure 1-3.** (A) Solid lipid nanoparticles (SLNs) and (B) Nanostructured lipid carriers (NLCs)	Recent advances in lipid nanoparticle formulations with solid matrix for oral drug delivery. AAPS PharmSciTech. 12 (1), 62–76.	© American Association of Pharmaceutical Scientists 2010	2017.01.06	Yes	Rightslink® by Copyright Clearance Centre License Number 4023170547876
8	Figure	Figure 1-4. Schematic of a liposome which presents a bilayer structure. Hydrophilic drugs or genes will be encapsulated in the aqueous core, while hydrophobic drugs will be incorporated into the bilayer.	Liposomes and nanoparticles: nanosized vehicles for drug delivery in cancer. Trends in Pharmacological Sciences. 30 (11), 592–599.	© 2009 Elsevier Ltd.	2017.01.06	Yes	Rightslink® by Copyright Clearance Centre License Number 4023170893233
10	Figure	Figure 1-5. Liposome-cell interaction. Liposomes can specifically (a) or non-specifically (b) adsorb on the cell surface.	Recent advances with liposomes as pharmaceutical carriers. Nature Reviews Drug Discovery. 4 (2), 145–160.	© 2005 Nature Publishing Group	2017.01.06	Yes	Rightslink® by Copyright Clearance Centre License Number 4023180443913
12-13	Table	Table 1-2. Marketed liposomal and lipid–based anticancer products, plus a	Liposomal drug delivery systems: from concept to clinical applications.	© 2012 Elsevier B.V.	2017.01.06	Yes	Rightslink® by Copyright Clearance Centre

		selection of products in clinical development	Advanced Drug Delivery Reviews. 65 (1), 36–48.				License Number 4023180728009
14	Figure	Figure 1-6. Extracellular uptake by endocytosis in a typical eukaryotic cell.	Endocytosis at the nanoscale. Chemical Society Reviews. 41 (7), 2718–2739.	© 2012 Royal Society of Chemistry	2017.01.06	Yes	Rightslink® by Copyright Clearance Centre License Number 4023181135519
16	Figure	Figure 1-7. Different types of endosomal escape.	Intracellular delivery of nanomaterials: how to catch endosomal escape in the act. Nano Today. 9 (3), 344–364.	© 2014 Elsevier Ltd.	2017.01.06	Yes	Rightslink® by Copyright Clearance Centre License Number 4023181360899
18	Figure	Figure 1-8. Schematic illustration of the "proton-sponge" effect hypothesis	Design and development of polymers for gene delivery. *Nature Reviews Drug discovery*. 4 (7), 581–593.	© 2005 Nature Publishing Group	2017.01.06	Yes	Rightslink® by Copyright Clearance Centre License Number 4023190114671
20	Figure	Figure 1-9. Schematic illustration of coil-to-globule conformational change of	A virus-mimicking, endosomolytic liposomal system for efficient, pH-	© 2016 American	2017.01.06	Yes	Rightslink® by Copyright Clearance Centre

		polyanions using poly(acrylic acid) as an example.	triggered intracellular drug delivery. *ACS Applied Materials & Interfaces*. 8 (34), 22457–22467.	Chemical Society			License is granted to use the full article as the author's original work
27	Figure	Figure 1-12. Destabilization of the endosomal membrane.	Recent advances with liposomes as pharmaceutical carriers. Nature Reviews Drug Discovery. 4 (2), 145–160.	© 2005 Nature Publishing Group	2017.01.06	Yes	Rightslink® by Copyright Clearance Centre License Number 4023190689799
54	Figure	**Figure 3-1.** Schematic of the virus-mimicking multifunctional liposome and its endonsomal escape pathway.	A virus-mimicking, endosomolytic liposomal system for efficient, pH-triggered intracellular drug delivery. *ACS Applied Materials & Interfaces*. 8 (34), 22457–22467.	© 2016 American Chemical Society	2017.01.06	Yes	Rightslink® by Copyright Clearance Centre License is granted to use the full article as the author's original work
55	Figure	**Figure 3-2.** FT-IR spectra of PLP, PP25, PP50 and PP75 in their acid forms.	A virus-mimicking, endosomolytic liposomal system for efficient, pH-triggered intracellular drug delivery. *ACS Applied*	© 2016 American Chemical Society	2017.01.06	Yes	Rightslink® by Copyright Clearance Centre

			Materials & Interfaces. 8 (34), 22457–22467.				License is granted to use the full article as the author's original work
56	Figure	**Figure 3-3.** ^{1}H-NMR spectra of PLP, PP25, PP50 and PP75 in their acid forms in d_6-DMSO at room temperature.	A virus-mimicking, endosomolytic liposomal system for efficient, pH-triggered intracellular drug delivery. *ACS Applied Materials & Interfaces*. 8 (34), 22457–22467.	© 2016 American Chemical Society	2017.01.06	Yes	Rightslink® by Copyright Clearance Centre License is granted to use the full article as the author's original work
60	Figure	**Figure 3-7.** The effect of cholesterol proportion of the virus-mimicking liposomes.	A virus-mimicking, endosomolytic liposomal system for efficient, pH-triggered intracellular drug delivery. *ACS Applied Materials & Interfaces*. 8 (34), 22457–22467.	© 2016 American Chemical Society	2017.01.06	Yes	Rightslink® by Copyright Clearance Centre License is granted to use the full article as the author's original work
60	Figure	**Figure 3-8.** Schematic of the polymer-liposome interaction in the absence (left) and presence of cholesterol (right).	A virus-mimicking, endosomolytic liposomal system for efficient, pH-triggered intracellular drug delivery. *ACS Applied*	© 2016 American Chemical Society	2017.01.06	Yes	Rightslink® by Copyright Clearance Centre

			Materials & Interfaces. 8 (34), 22457–22467.				License is granted to use the full article as the author's original work
61	Table	**Table 3-1.** Mean hydrodynamic diameter of liposomes with or without 40% cholesterol before and after surface modification.	A virus-mimicking, endosomolytic liposomal system for efficient, pH-triggered intracellular drug delivery. *ACS Applied Materials & Interfaces*. 8 (34), 22457–22467.	© 2016 American Chemical Society	2017.01.06	Yes	Rightslink® by Copyright Clearance Centre License is granted to use the full article as the author's original work
63	Figure	**Figure 3-9.** pH-dependent calcein release from the bare liposomes (◆), and the virus-mimicking liposomes coated with PLP (▼), PP25 (▲), PP50 (●), and PP75 (■) respectively.	A virus-mimicking, endosomolytic liposomal system for efficient, pH-triggered intracellular drug delivery. *ACS Applied Materials & Interfaces*. 8 (34), 22457–22467.	© 2016 American Chemical Society	2017.01.06	Yes	Rightslink® by Copyright Clearance Centre License is granted to use the full article as the author's original work
64	Figure	**Figure 3-10.** The effect of PP75 adsorption amount on the liposomal membrane.	A virus-mimicking, endosomolytic liposomal system for efficient, pH-triggered intracellular drug delivery. *ACS Applied*	© 2016 American Chemical Society	2017.01.06	Yes	Rightslink® by Copyright Clearance Centre

			Materials & Interfaces. 8 (34), 22457–22467.				License is granted to use the full article as the author's original work
66	Figure	**Figure 3-13.** Size distributions of (A) the unmodified liposomes and (B) the PP75-coated liposomes.	A virus-mimicking, endosomolytic liposomal system for efficient, pH-triggered intracellular drug delivery. *ACS Applied Materials & Interfaces*. 8 (34), 22457–22467.	© 2016 American Chemical Society	2017.01.06	Yes	Rightslink® by Copyright Clearance Centre License is granted to use the full article as the author's original work
67	Figure	**Figure 3-14.** pH-dependent liposomal size change.	A virus-mimicking, endosomolytic liposomal system for efficient, pH-triggered intracellular drug delivery. *ACS Applied Materials & Interfaces*. 8 (34), 22457–22467.	© 2016 American Chemical Society	2017.01.06	Yes	Rightslink® by Copyright Clearance Centre License is granted to use the full article as the author's original work
68	Figure	**Figure 3-15.** Lipid mixing assay of bare liposomes and PP75-coated liposomes at pH 7.4 and pH 4.5.	A virus-mimicking, endosomolytic liposomal system for efficient, pH-triggered intracellular drug delivery. *ACS Applied*	© 2016 American Chemical Society	2017.01.06	Yes	Rightslink® by Copyright Clearance Centre

			Materials & Interfaces. 8 (34), 22457–22467.				License is granted to use the full article as the author's original work
69	Figure	**Figure 3-16.** Schematic representation of the possible mechanism of the revisable size change of the pseudopeptidic polymer-coated liposomes between pH 7.4 and 4.5.	A virus-mimicking, endosomolytic liposomal system for efficient, pH-triggered intracellular drug delivery. *ACS Applied Materials & Interfaces*. 8 (34), 22457–22467.	© 2016 American Chemical Society	2017.01.06	Yes	Rightslink® by Copyright Clearance Centre License is granted to use the full article as the author's original work
71	Figure	**Figure 3-17.** Relative hemolysis of the virus-mimicking liposomes with a fixed polymer-to-lipid ratio at 1.9:100 (mol/mol).	A virus-mimicking, endosomolytic liposomal system for efficient, pH-triggered intracellular drug delivery. *ACS Applied Materials & Interfaces*. 8 (34), 22457–22467.	© 2016 American Chemical Society	2017.01.06	Yes	Rightslink® by Copyright Clearance Centre License is granted to use the full article as the author's original work
72	Figure	**Figure 3-18.** Laser scanning confocal microscopy images of HeLa cells demonstrating the endosomal escape of free calcein (3.2 mM) from intracellular vesicles into the	A virus-mimicking, endosomolytic liposomal system for efficient, pH-triggered intracellular drug delivery. *ACS Applied*	© 2016 American Chemical Society	2017.01.06	Yes	Rightslink® by Copyright Clearance Centre

		cytoplasm facilitated by (A) the bare liposomes and (B) the virus-mimicking liposomes.	*Materials & Interfaces*. 8 (34), 22457–22467.				License is granted to use the full article as the author's original work
73	Figure	**Figure 3-19.** Laser scanning confocal microscopy images of HeLa cells showing the subcellular localization of the anticancer drug DOX.	A virus-mimicking, endosomolytic liposomal system for efficient, pH-triggered intracellular drug delivery. *ACS Applied Materials & Interfaces*. 8 (34), 22457–22467.	© 2016 American Chemical Society	2017.01.06	Yes	Rightslink® by Copyright Clearance Centre License is granted to use the full article as the author's original work
74	Figure	**Figure 3-20.** Cellular uptake of DOX was quantitatively analyzed by flow cytometry and presented as relative MFI (A) and representative histogram plots (B).	A virus-mimicking, endosomolytic liposomal system for efficient, pH-triggered intracellular drug delivery. *ACS Applied Materials & Interfaces*. 8 (34), 22457–22467.	© 2016 American Chemical Society	2017.01.06	Yes	Rightslink® by Copyright Clearance Centre License is granted to use the full article as the author's original work

77	Figure	**Figure 3-23.** In-vitro cytotoxicity of HeLa cells treated with the liposomes with (close columns) or without (open columns) PP75 at various lipid concentrations for 24 h as determined by (A) Alamar Blue assay and (B) LDH assay.	A virus-mimicking, endosomolytic liposomal system for efficient, pH-triggered intracellular drug delivery. *ACS Applied Materials & Interfaces*. 8 (34), 22457–22467.	© 2016 American Chemical Society	2017.01.06	Yes	Rightslink® by Copyright Clearance Centre License is granted to use the full article as the author's original work
78	Figure	**Figure 3-24.** In-vitro cytotoxicity of free DOX (open columns), DOX-loaded bare liposomes (gray columns), and DOX-loaded virus mimicking liposomes (dark columns) against HeLa cells after treatment for 24 h and further incubated for 24h.	A virus-mimicking, endosomolytic liposomal system for efficient, pH-triggered intracellular drug delivery. *ACS Applied Materials & Interfaces*. 8 (34), 22457–22467.	© 2016 American Chemical Society	2017.01.06	Yes	Rightslink® by Copyright Clearance Centre License is granted to use the full article as the author's original work

82	Figure	**Figure 4-1.** FT-IR spectra of PLP, PLP-HDA 18%, PLP-NDA 18%, PLP-TDA 18% and PLP-ODA 18% in their acid forms	Membrane Anchored, Comb-Like Pseudo-Peptides for Efficient, pH-Mediated Membrane Destabilization and Intracellular Delivery, *ACS Applied Materials & Interfaces*, 2017; 9 (9), 8021–8029.	© 2017 American Chemical Society	2017.03.01	Yes	Rightslink® by Copyright Clearance Centre License is granted to use the full article as the author's original work
82	Figure	**Figure 4-2.** ^{1}H-NMR spectra of PLP, PLP-HDA 18%, PLP-NDA 18%, PLP-TDA 18% and PLP-ODA 18% in their acid forms in d_6-DMSO at room temperature	Membrane Anchored, Comb-Like Pseudo-Peptides for Efficient, pH-Mediated Membrane Destabilization and Intracellular Delivery, *ACS Applied Materials & Interfaces*, 2017; 9 (9), 8021–8029.	© 2017 American Chemical Society	2017.03.01	Yes	Rightslink® by Copyright Clearance Centre License is granted to use the full article as the author's original work
83	Figure	**Figure 4-3.** pH-Dependent transmittance of the aqueous solutions of (A) PLP, (B) PLP-NDA 3%, (C) PLP-NDA 10% and (D) PLP-NDA 18% at 1.0 mg mL^{-1} in 100 mM phosphate or citrate buffer	Membrane Anchored, Comb-Like Pseudo-Peptides for Efficient, pH-Mediated Membrane Destabilization and Intracellular Delivery, *ACS Applied Materials & Interfaces*, 2017; 9 (9), 8021–8029.	© 2017 American Chemical Society	2017.03.01	Yes	Rightslink® by Copyright Clearance Centre License is granted to use the full article as the author's original work

85	Figure	**Figure 4-4.** pH-Dependent I_{338}/I_{333} in the excitation spectra of pyrene dissolved in aqueous solutions of PLP (■), PLP-NDA 3% (●), PLP-NDA 10% (▲) and PLP-NDA 18% (▼) at 0.5 mg mL^{-1}	Membrane Anchored, Comb-Like Pseudo-Peptides for Efficient, pH-Mediated Membrane Destabilization and Intracellular Delivery, *ACS Applied Materials & Interfaces*, 2017; 9 (9), 8021–8029.	© 2017 American Chemical Society	2017.03.01	Yes	Rightslink® by Copyright Clearance Centre License is granted to use the full article as the author's original work
86	Figure	**Figure 4-5.** Concentration-dependent I_{338}/I_{333} in the excitation spectra of pyrene dissolved in aqueous solutions of PLP (■), PLP-NDA 3% (●), PLP-NDA 10% (▲) and PLP-NDA 18% (▼) at pH 7.4	Membrane Anchored, Comb-Like Pseudo-Peptides for Efficient, pH-Mediated Membrane Destabilization and Intracellular Delivery, *ACS Applied Materials & Interfaces*, 2017; 9 (9), 8021–8029.	© 2017 American Chemical Society	2017.03.01	Yes	Rightslink® by Copyright Clearance Centre License is granted to use the full article as the author's original work

86	Table	**Table 4-1.** pH Values at the onset of precipitation (pH_p), pH values at the onset of hydrophobic association (pH_h), and pH ranges for hydrophobic association of PLP and the comb-like polymers at 0.5 mg mL^{-1} and their CACs at pH 7.4	Membrane Anchored, Comb-Like Pseudo-Peptides for Efficient, pH-Mediated Membrane Destabilization and Intracellular Delivery, *ACS Applied Materials & Interfaces*, 2017; 9 (9), 8021–8029.	© 2017 American Chemical Society	2017.03.01	Yes	Rightslink® by Copyright Clearance Centre License is granted to use the full article as the author's original work
87	Table	**Table 4-2.** The mean hydrodynamic diameters of PLP and its derivatives at a concentration of 0.5 mg mL^{-1} at pH 7.4	Membrane Anchored, Comb-Like Pseudo-Peptides for Efficient, pH-Mediated Membrane Destabilization and Intracellular Delivery, *ACS Applied Materials & Interfaces*, 2017; 9 (9), 8021–8029.	© 2017 American Chemical Society	2017.03.01	Yes	Rightslink® by Copyright Clearance Centre License is granted to use the full article as the author's original work

88	Figure	**Figure 4-7.** Particle size distributions of PLP (A) and PLP-NDA 18% (B) at a concentration of 0.5 mg mL^{-1} at pH 7.4 (solid) and pH 5.5 (dash)	Membrane Anchored, Comb-Like Pseudo-Peptides for Efficient, pH-Mediated Membrane Destabilization and Intracellular Delivery, *ACS Applied Materials & Interfaces*, 2017; 9 (9), 8021–8029.	© 2017 American Chemical Society	2017.03.01	Yes	Rightslink® by Copyright Clearance Centre License is granted to use the full article as the author's original work
92	Figure	**Figure 4-10.** pH-Dependent hemolysis of RBCs incubated with PLP (■), PLP-NDA 3% (●), PLP-NDA 10% (▲) and PLP-NDA 18% (▼) at 0.5 mg mL^{-1} for 1h	Membrane Anchored, Comb-Like Pseudo-Peptides for Efficient, pH-Mediated Membrane Destabilization and Intracellular Delivery, *ACS Applied Materials & Interfaces*, 2017; 9 (9), 8021–8029.	© 2017 American Chemical Society	2017.03.01	Yes	Rightslink® by Copyright Clearance Centre License is granted to use the full article as the author's original work
93	Figure	**Figure 4-11A.** Concentration-dependent hemolysis of RBCs incubated with PLP-NDA 18% (A) at pH 7.4 (open columns) and 5.5 (close columns)	Membrane Anchored, Comb-Like Pseudo-Peptides for Efficient, pH-Mediated Membrane Destabilization and Intracellular Delivery, *ACS Applied Materials & Interfaces*, 2017; 9 (9), 8021–8029.	© 2017 American Chemical Society	2017.03.01	Yes	Rightslink® by Copyright Clearance Centre License is granted to use the full article as the author's original work

94	Figure	**Figure 4-12.** Time-dependent hemolysis of RBC incubated with PLP (■), PLP-NDA 3% (●), PLP-NDA 10% (▲), PLP-NDA 18% (▼) at 0.5 mg mL^{-1} at pH 5.5	Membrane Anchored, Comb-Like Pseudo-Peptides for Efficient, pH-Mediated Membrane Destabilization and Intracellular Delivery, *ACS Applied Materials & Interfaces*, 2017; 9 (9), 8021–8029.	© 2017 American Chemical Society	2017.03.01	Yes	Rightslink® by Copyright Clearance Centre License is granted to use the full article as the author's original work
96	Figure	**Figure 4-14.** Confocal microscopy images of RBCs incubated with FITC-dextran (4 kDa) and Texas Red® with or without polymers (0.5 mg mL^{-1}) for 30 min at pH 5.5	Membrane Anchored, Comb-Like Pseudo-Peptides for Efficient, pH-Mediated Membrane Destabilization and Intracellular Delivery, *ACS Applied Materials & Interfaces*, 2017; 9 (9), 8021–8029.	© 2017 American Chemical Society	2017.03.01	Yes	Rightslink® by Copyright Clearance Centre License is granted to use the full article as the author's original work
97	Figure	**Figure 4-15.** Confocal microscopy images of RBCs incubated with FITC-dextran (4 kDa) and Texas Red® with or without polymers (0.5 mg mL^{-1}) for 30 min at pH 7.4	Membrane Anchored, Comb-Like Pseudo-Peptides for Efficient, pH-Mediated Membrane Destabilization and Intracellular Delivery, *ACS Applied Materials & Interfaces*, 2017; 9 (9), 8021–8029.	© 2017 American Chemical Society	2017.03.01	Yes	Rightslink® by Copyright Clearance Centre License is granted to use the full article as the author's original work

98	Figure	**Figure 4-16.** Confocal microscopy images of RBCs incubated with Texas Red® and different molecular weight of FITC-dextran with the presence of 0.5 mg mL^{-1} PLP-NDA 18% for 30 min at pH 5.5	Membrane Anchored, Comb-Like Pseudo-Peptides for Efficient, pH-Mediated Membrane Destabilization and Intracellular Delivery, *ACS Applied Materials & Interfaces*, 2017; 9 (9), 8021–8029.	© 2017 American Chemical Society	2017.03.01	Yes	Rightslink® by Copyright Clearance Centre License is granted to use the full article as the author's original work